Characterization of interactions between energy geostructures within ground water flow

Badr Ouzzine

Thèse présentée pour obtenir le grade de

Docteur de l'Université Gustave Eiffel

Spécialité : Géotechnique

par

Badr OUZZINE

Ecole Doctorale : Sciences, Ingénierie et Environnement

CARACTERISATION OF INTERACTIONS BETWEEN ENERGY STRUCTURES WITHIN GROUND WATER FLOW

Thèse soutenue le 12/10/2023 devant le jury composé de :

Pr. Fleur Loveridge	Rapporteuse	University of Leeds
Pr. Cristina de Hollanda Cavalcanti Tsuha	Rapporteuse	University of Sao Paulo
Dr. Anh Minh Tang	Examinateur	ENPC
Pr. Gopal Madabhushi	Examinateur	University of Cambridge
Pr. Giulia Viggiani	Examinatrice	University of Cambridge
Dr. Philippe Reiffsteck	Directeur de thèse	Université Gustave Eiffel
Dr. Jean de Sauvage	Encadrant	Université Gustave Eiffel
Dr. Sahar Hemmati	Co-encadrante	Université Gustave Eiffel

Acknowledgements

"Recognition is the memory of the heart" wrote Hans Christian Andersen, and it is important for me to express my gratitude to all the individuals who have been by my side throughout this journey. Each of them has played a role, either through their scientific contributions or their personal interactions, in shaping the outcomes of this work.

I would first like to sincerely thank Philippe Reiffsteck, my thesis director. Thank you for his follow up, his confidence, his proofreading and his advice. His door has always been open to any PhD student wishing to draw on his experience or scientific culture.

I would also like to express my entire gratitude to Jean de Sauvage, my main supervisor: firstly for having convinced me to do a PhD, and secondly for having followed and supervised me in the best of ways during these three years. The doctorate, through scientific reflection, collaborations, conferences, the writing of articles and training courses, is an extremely enriching experience on both a personal and professional level, and I will always be grateful to him for having enabled me to do all that, especially the stay in Cambridge. I really enjoyed doing this thesis, and I'm sure that my supervision was one of the main reasons for that. Thank you for the benevolence, motivation and pleasant working atmosphere. Thank you for all the proofreading and the very pertinent advice.

On a similar note, I would like to thank my two other supervisors. Thank you to Sahar Hemmati for her help and enthusiasm, which were both motivating and a driving force. Thanks to Thibault Badinier for his day-to-day help and proofreading. Many thanks for the numerical support and the code that enabled us to run the numerical simulations. Without this work, a large part of this thesis would not have seen the light of day. Thank you also for supporting me in my first experience as a teaching.

The core of my thesis work and one of the most rewarding experiences of my life was my time at Cambridge University. I would therefore like to extend my warmest thanks to the Director of the Schofield Centre, Pr. Gopal Madhabushi, for welcoming me into his laboratory and introducing me to centrifuge testing. I would also like to thank Pr. Giulia Viggiani for welcoming me and supervising me during my stay. I was lucky enough to be supervised by renowned experts, so I would like to thank them for the time they gave me and for sharing their knowledge and experience with me. I would also like to thank the Schofield technicians whose ingenuity and great support enabled my experiments to succeed. I am extremely grateful to them for their availability and patience with my ability to come up with a new problem every day. So, thank you to John Chandler, Chris McGinnie, Kristian Pether, Mark Smith, David Layfield and all the technical staff of the Schofield Centre. I also want to say a huge thank you to Théophile Grappe, with whom I worked on his internship. It was also thanks to him that the tests were able to take place. Finally, my thanks to Cambridge would not be complete without thanking the doctoral students at the Schofield Centre for their welcome, support and discussions. Thanks to Douglas, Diarmid, Carlos, Yazan, Juntae and all the other PhD students. A special mention to Ahmad Alagha, whom I am happy and proud to have met, thank you for everything.

I would also like to thank Thierry Dubreucq and Matthieu Blanc from the CG laboratory in Nantes, with whom I really enjoyed working and sharing knowledge. Thanks to them and to the superb technical team for their availability and their teaching. I would also like to thank Gurvan, with whom I enjoyed working during his internship. His results were very useful.

Thank you to Yvon Delerablée for his willingness to help and his kind advice from the start of my thesis. I would also like to thank Anh Minh Tang for his support and advice and for agreeing to be a member of the jury.

These three years would not have been so great if I had not been lucky enough to share my office with two wonderful people. Thank you to Tyan Yu Wang and Nader Elayni for the support, motivation, discussions and incredible working atmosphere in the office. I wish them all the best for the future. Thanks also to Mara, Marwa, Alessandra, Juba, Thibault, Matthieu and all the other PhD students in the lab with whom I was delighted to share this adventure.

I also wish to extend a special thank you to Mohamed, who encouraged me on the path of the PhD and with whom we spent our student years together. He is much more than a friend, thank you for everything.

Finally, I reserve my deepest thanks to my parents, who have always been my main source of motivation. Thank you to my mother for her unwavering support and unconditional backing. Thank you to my father for always pushing me to study and seek knowledge. No words will ever be enough for the gratitude I owe them.

Résumé

L'évolution des villes et le contexte énergétique et environnemental actuel nécessite de développer encore les énergies renouvelables et de réduire les émissions de gaz à effet de serre. Les géostructures thermiques, qui se développent depuis les années 80, permettent de répondre à ces deux objectifs en utilisant les ouvrages géotechniques comme des échangeurs thermiques, leur donnant ainsi une seconde utilité. Le principe consiste à placer des tubes échangeurs dans les pieux, les parois moulés, ou encore les voussoirs des tunnels pour profiter de la constance de la température dans le sol à partir d'une certaine profondeur et puiser de la chaleur en hiver ou de la fraicheur en été grâce à une pompe à chaleur réversible. Ce faisant, le champ de température est localement modifié dans le sol, et l'on nomme cette modification: anomalie thermique. La présence d'écoulement d'eau souterrain favorise les échanges thermiques et dissipe les anomalies thermiques qui se créent dans le sol en fonction du fonctionnement des géostructures. Cependant, l'écoulement déplace l'anomalie thermique dans l'espace et le panache thermique qui se crée est susceptible d'interférer énergétiquement et mécaniquement avec d'autres ouvrages géotechniques, qu'ils soient géothermiques ou non. L'objectif de cette thèse est de caractériser ces interactions au sein d'une structure ou entre différentes structures. Pour cela, un premier travail expérimental en centrifugeuse sur des modèles réduits a été mené au Schofield Centre, University of Cambridge. L'objectif était de caractériser le transfert thermique dans le sol ainsi que le comportement d'un groupe de pieux géothermique au sein d'un écoulement. Par la suite, l'influence de l'écoulement sur l'efficacité d'un système géothermique a été étudiée numériquement. Enfin, sur la base des résultats expérimentaux, un modèle numérique hydro-thermo-mécanique a été réalisé sur un logiciel de calcul en éléments finis afin d'extrapoler les résultats à différents scénarios.

Abstract

Urban development and the current energy and environmental context require the development of renewable energies and the reduction of greenhouse gas emissions. Energy geostructures, which have been developing since the 1980s, help to achieve these two objectives by using geotechnical structures as heat exchangers, giving them an energetic use in addition to the mechanical one. The principle is to place heat exchanger tubes in the piles, formwork or tunnel segments to exploit the constant temperature of the ground from a certain depth, extracting heat in winter and cooling in summer using a reversible heat pump. The temperature field is locally modified, and this modification is known as a thermal anomaly. The presence of groundwater flow promotes heat exchange and dissipates the thermal anomalies created in the ground by the operation of the geostructures. However, the flow displaces the thermal anomaly in the ground and the resulting thermal plume is likely to interfere energetically and mechanically with other geotechnical structures, whether geothermal or not. The aim of this thesis is to characterise these interactions within a structure or between structures. To achieve this, initial experimental work using a centrifuge on reduced scale models was carried out at the Schofield Centre, University of Cambridge. The aim was to characterise heat transfer in the ground and the behaviour of a group of energy piles in a flow. The influence of flow on the efficiency of a geothermal system was then studied numerically. Finally, based on the experimental results, a hydro-thermo-mechanical numerical model was developed using finite element software to extrapolate the results to different scenarios.

Summary

TABLE OF ABBREVIATIONS

ADEME : French Environment and Energy Management Agency (Agence de l'Environnement et de la Maîtrise de l'Energie)

AFNOR: French Standards Association (Association française de normalisation)

AFPAC: French Association for Heat Pumps (Association française pour les pompes à chaleurs)

ASHP: Air Source Heat Pump

BHE: Borehole heat exchanger

BRGM: Geological and Mining Research Bureau (Bureau de Recherches Géologiques et Minières)

COP: Coefficient of Performance

CFMS: French Soil Mechanics Committee (Comité français de mécanique des sols)

DHW: Domestic Heat Water

GHG: Greenhouse gas

GSE: Geothermal system energy

GSHP: Ground Source Heat Pump

HSM: Hardening Soil Model

MTES : Ministère de la Transition Ecologique et Solidaire (French Ministry for the environment)

RAGE : French programme to support professionals (Règles de l'Art Grenelle Environnement)

SCOP: Heat pump Seasonal coefficient Of Performance

SPF: Seasonal Performance Factor

TAZ: Thermal affected zones

THM: Thermo-hydro-mechanical

TRT: Thermal response test

TABLE OF NOTATIONS

α: Thermal diffusivity (m^2/s)

δ: Skin depth (m)

ε: Mechanical strains ($-$)

λ: Thermal conductivity (W/mK)

μ: Dynamic viscosity ($Pa.s$)

η: Kinematic viscosity (m^2/s)

ρ : Density (kg/m^3)

σ: Mechanical stresses (Pa)

θ_0: Average temperature over a year (°C)

θ: Water content by volume (-)

ω: Thermal wave pulsation (rad/s)

γ: Euler Constant

C: Volumetric heat capacity ($J.m^{-3}.K^{-1}$)

D: Inter-pile distance

g: Gravity (m/s^2)

h_c: Capillary rise

H_b: Height of the box

h_{NC}: Soil height not crossed by water

h_th: Thermal transfer coefficient (W/m^2K)

h: Hydraulic head (m)

i : Hydraulic gradient ($-$)

$\vec{J}$: Thermal flux (W/m^2)

K: Intrinsic permeability (m^2)

k: Soil permeability (m/s)

n: Soil porosity ($-$)

L_b: Length of the box

$\dot{m}$: Mass flow rate (kg/s)

R_{th}: Thermal resistance of the pile ($K.W^{-1}$)

Q_c: Thermal power exchanged at the condenser (W)

Q_e: Thermal power exchanged at the evaporator (W)

Q: Flow rate (m^3/s)

Sr: Soil degree of saturation ($-$)

S: Hydraulic cross surface (m^2)

t: Time (s)

T : Temperature (°C)

V_D: Darcy velocity (m/s)

V_{av}: Average ground water velocity (m/s)

v_φ: Thermal wave velocity (m/s)

W_b: Width of the box

W: Electrical power supplied to heat pump (W)

GENERAL INTRODUCTION

Contemporary urban expansion requires high energy demands, while current energy and environmental imperatives encourage the advancement of renewable energy technologies. Moreover, in line with these motivations, the thermal regulations governing new buildings in France are becoming stricter, with the aim of achieving a policy of exclusively positive-energy buildings, which produce more energy than they consume. To meet these objectives effectively, new buildings must incorporate renewable energy production mechanisms.

Geothermal energy, which developed rapidly during the 20th century, pertains to the harnessing of the heat naturally present in the ground for energy generation. Characterised by its renewable nature, geothermal energy benefits from an intrinsic accessibility that transcends geographical constraints, while wind and solar energy are intermittent and dependent on meteorological dynamics. In today's geopolitical landscape, geothermal energy appears to be a rational and prudent option for reinforcing energy autonomy.

Distinct categories of geothermal energy can be identified, depending on the depth of the ground and the temperature considered. For instance, geothermal techniques that provide access to high-temperature water reservoirs, for purposes ranging from domestic hot water supply to electricity generation, are widespread in the common mind. Notably, a variant within this domain, denoted as very low-energy geothermal energy, exists. It involves exploiting the thermal resources of the initial dozens metres of ground to heating and cooling capabilities to buildings. Various solutions allows exploiting very low-energy geothermal energy, all based on the use of a heat pump. Among these, energy geostructures, which were developed in Austria in the 1980s, have surged as a renewable energy solution, becoming increasingly widespread in Europe and around the world for heating and cooling buildings.

The principle is to add to the geotechnical structures, which have a primary role of mechanical stability and diffusion of forces to the resistant soil layers, a second energetic role of heat exchanger in order to inject heat into the soil in summer to cool the building or extract heat from the soil in winter to heat the building. During their operation, energy geostructures are therefore subject to temperature cycles which induce thermal deformations. However, energy geostructures are not free to deform because they interact with the ground and the structure they support, resulting in thermally induced stresses and strains. The first issue is therefore to assess the mechanical behaviour of energy geostructures. Indeed, the challenges of designing these structures require a precise description of their thermal and mechanical behaviour. In addition, energy geostructures produce a local change in the temperature field in the ground, called thermal anomaly. In the frequent case where the building's demand for cooling and heating is not balanced, a multi-year thermal drift can occur, impacting the energy efficiency of the geothermal system. The second issue therefore concerns the impact of this thermal drift on the system energy efficiency. Finally, the presence of groundwater flow adds a further layer of complexity to the issue. On one hand, it allows the soil to be thermally washed and the thermal anomaly to be dissipated, thereby increasing the efficiency of the system. On the other hand, the flow also creates an advection phenomenon that moves the thermal anomaly and the associated issues downstream. The soil evolves into an arena of diverse

hydrological, thermal and mechanical interplays, leading to a number of questions. The aim of this thesis is to tackle the four following issues:

- What is the impact of water on ground thermal potential?
- How does temperature influence the mechanical response of an energy geostructure?
- What is the impact of water flow on the system energy efficiency?
- How does ground water flow impact the mechanical response?

To address these issues, the work presented in this paper focuses mainly on experimental centrifuge tests carried out at the Schofield Centre, Civil engineering Department, University of Cambridge, and on numerical modelling. The implementation of a water flow in a centrifuge soil model was an innovative aspect in terms of experimental methods. The interactions between the different issues are summed up in Figure 1.

The work is presented in 5 chapters. First, literature review is established in order to present the current state of research on the operation of these energy structures, soil thermics, the impact of underground flow, and the study via centrifuge models. This chapter shows the thermal potential of the ground and how it is enhanced by hydraulics. It also presents the impact of thermal loading on an energy pile. This state of the art shows that the behaviour of a single energy pile is relatively well known, but that this is not yet the case for other types of energy geostructure. It also shows that hydro-thermal interactions are well studied (experimentally and numerically). In particular, the impact of subsurface flow on the temperature field in the ground is well documented. However, the impact of this flow on the mechanical response of an energy geostructure has been little studied. These two scientific gaps, namely the study of the mechanical response of a group of energy piles to thermal loading and the study of the impact of groundwater flow on the mechanical response of this group, constitute the two cornerstones of this thesis. Therefore, the second chapter focuses on the hydro-thermal coupling that takes place within a model energy pile in the ground in order to characterise the energy interactions within a group of piles when seepage is present. Then, the spotlight is on mechanical interactions. Indeed, the third chapter presents scaling laws that theoretically govern the centrifuge testing of model energy piles, before focusing on the group of model piles that was built for experimental purposes. These scaling laws are crucial to carry out centrifuge tests which are presented in Chapter 4 and enable the hydro-thermomechanical (HTM) behaviour of model energy pile group to be assessed. The results of these tests will be used in Chapter V to calibrate a numerical model and analyse typical operating scenarios.

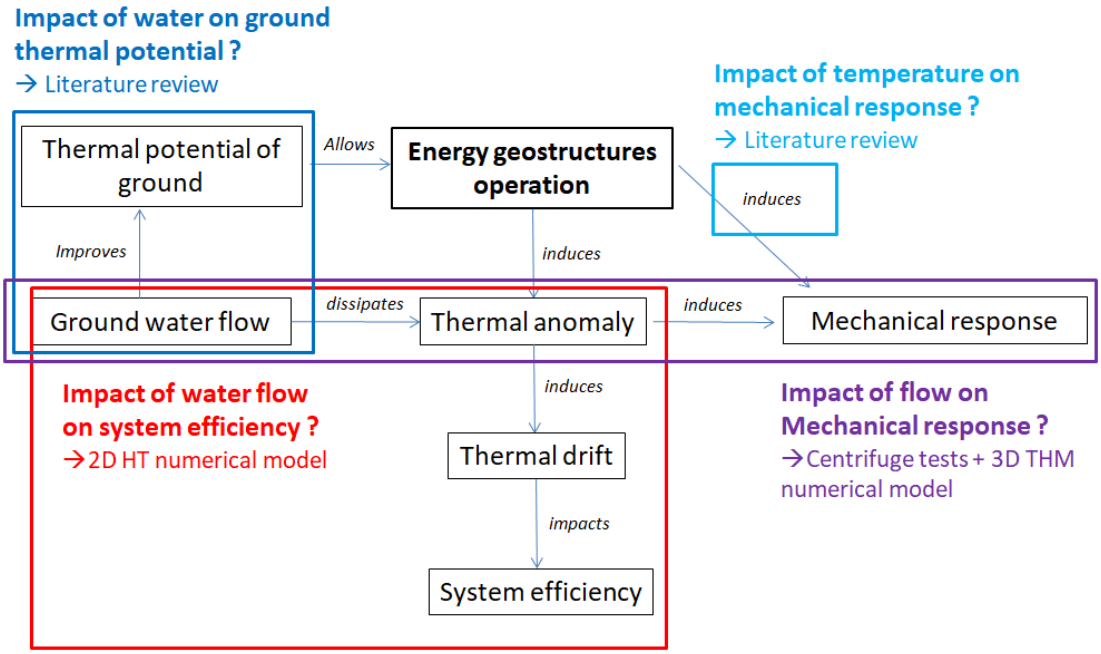

Figure 1 - Representative diagram of the different issues addressed in the thesis

CHAPTER I

LITERATURE REVIEW: GROUND AS HEAT RESERVOIR AND ENERGY GEOSTRUCTURES

« We are dwarfs on the shoulders of giants», Bernard de Chartres (7th Century)

In this first chapter, which is divided into two parts, we first review the state of the art in soil energy potential, energy geostructures and how they work. The various parameters that influence the thermal characterisation of soil are also detailed. The second part reviews the state of the art in the study of the mechanical response of energy piles.

1. Thermal potential of ground for energy geostructures

1.1. Geothermal energy

1.1.1 Place of the geothermal energy in the energy mix

In France, the heating sector represents a significant share of energy consumption and greenhouse gas emissions. Indeed, the building sector is the first energy consuming sector in France, and heating is the first item with more than 80% of building energy consumption. The building sector is also the second most GHG-emitting sector in France after transport (MTES, 2022).

In 2021, heat represented more than 40% of France's final energy consumption (heating of buildings, industry...). This heat is mainly generated using a gas system, accounting for 40% of the total, followed by renewable energies at 19%, and finally, a combination of electricity and coal (MTES, 2022). Under the 2019 energy and climate law, France aims to achieve in 2030 a 33% share of renewable energy in gross final energy consumption. In 2021, this share amounts to 19.3%, more than 10 points below target as shown in Figure I. 1. However, among the renewable energy solutions, geothermal energy represents only 2% of the primary energy consumption (Figure I. 2) and geothermal heat pumps are by far the minority of heat pump solutions (Figure I. 3). Its potential seems to be very little harvested and should therefore be more developed in order to meet the national and European targets.

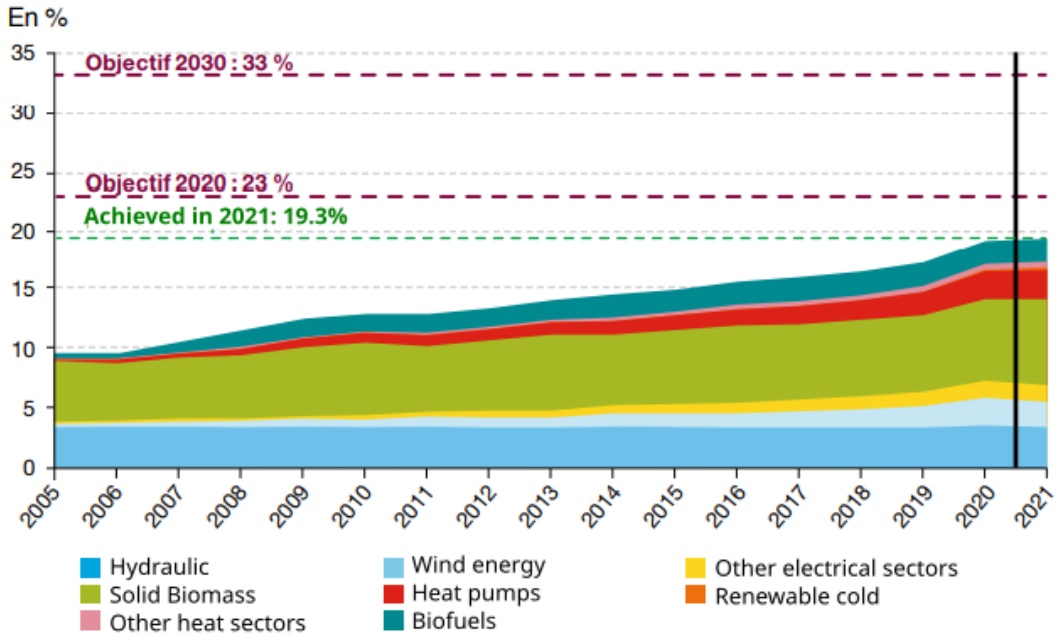

Figure I. 1 - Share of renewable energy in gross final energy consumption by sector in France (MTES, 2022)

Thus, In order to support investment in geothermal energy and in particular in geothermal heating and cooling networks, the French government has set up incentives such as the Heat Fund, which aims to finance heat production projects based on renewable energy. Geothermal energy itself covers a wide variety of technologies, but they all offer several benefits. It is not reliant on weather conditions like sunlight or wind, ensuring uninterrupted energy production. Moreover, it requires less space compared to other renewable installations, making it a viable alternative for energy supply in densely populated urban areas. It is a renewable energy, a source of energy independence and has low greenhouse gas emissions (GHG).

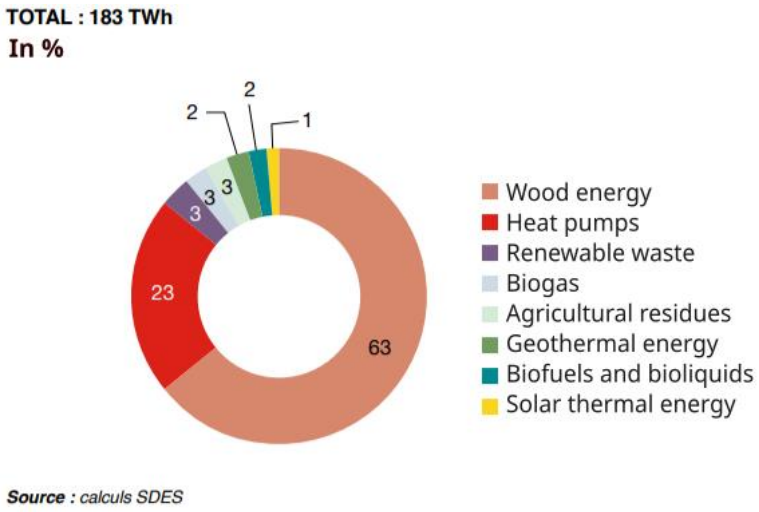

Figure I. 2 - Primary consumption of renewable energy for heat use in 2021 by sector in France

To meet the expectations of the new regulations that impose a positive energy balance for new buildings, the owners have many solutions that they must often combine such as insulation, photovoltaics, double flow ventilation and geothermal energy. The different existing forms of geothermal energy should therefore be detailed.

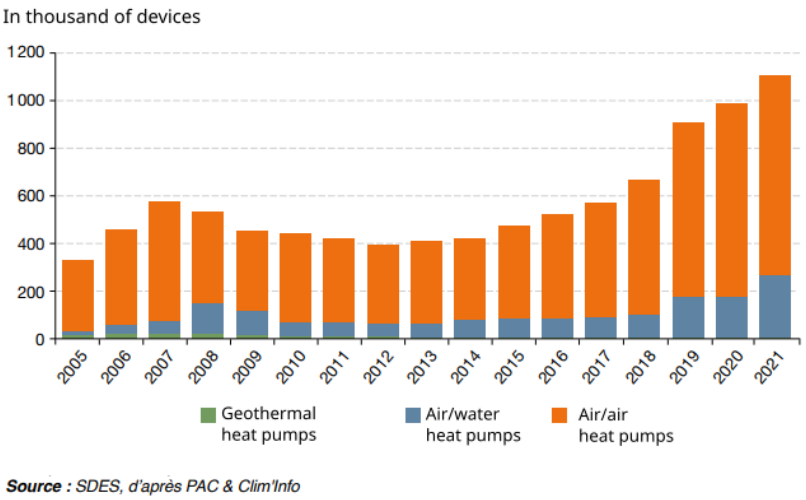

Figure I. 3 - Annual sales of individual heat pumps in France

1.1.2 Different types of geothermal energy

The diverse types of geothermal solutions are differentiated by the depth and therefore the temperature of the subsoil from which heat is drawn. Depending on the calories captured, geothermal systems can be used for heating (or air conditioning) of houses and buildings, for industrial processes or for electricity production. Three major approaches to harnessing geothermal energy are summarised on Figure I. 4 and presented here after:

- High-temperature geothermal energy (also called high enthalpy) concerns cases where heat is extracted from the ground by drawing directly groundwater with temperatures above 150°C. These are produced by drilling generally at a depth of more than 1,500 meters. High-temperature geothermal resources are located in areas with an abnormally high geothermal gradient (up to 30°C per 100 m).
- Low-temperature (or low-enthalpy) geothermal energy exploits the heat of water deposits located at depths of a few hundred meters up to about 2,000 m, for temperatures generally between 30°C and 90°C.
- Superficial geothermal energy, also known as very low temperature geothermal energy or very low enthalpy geothermal energy, exploits the heat of the ground or of the water of the subsoil at depths generally lower than 200 meters, for temperatures lower than 30°C.

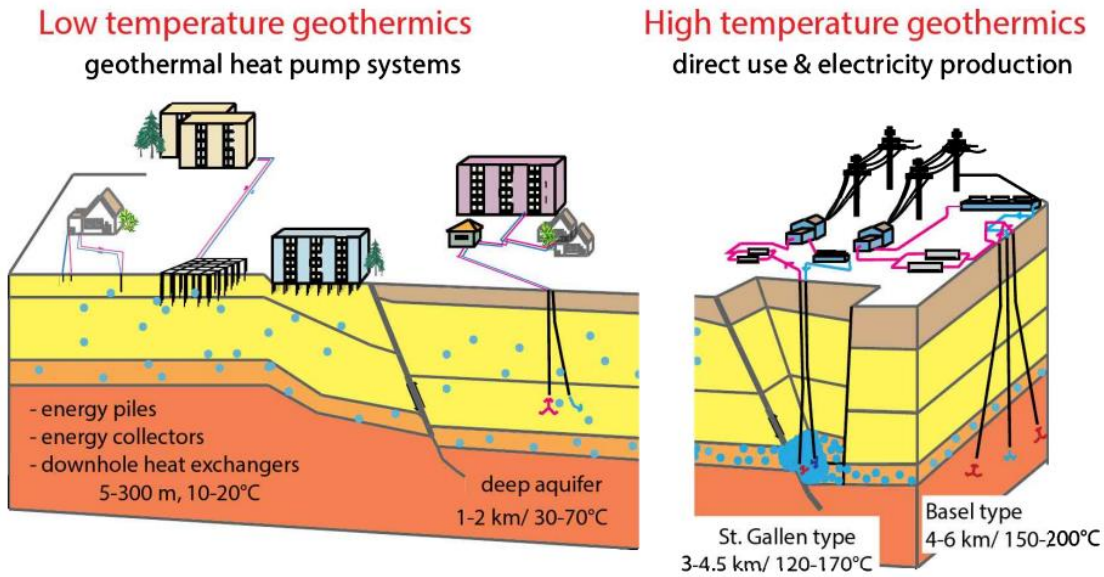

Figure I. 4 - Majors geothermal systems (Hirschberg, 2015)

As Figure I. 4 suggests, the geothermal system can either be in open-loop or in closed-loop. In open-loop geothermal systems, groundwater is directly pumped from a well and used as a heat-source without any heat exchanger system. After being used, groundwater is discharged either to a surface water body (e.g. lake or river) or back to the ground through discharge well. In closed-loop geothermal system a heat exchanger fluid circulates in a network of pipes absorbing geothermal heat from the surrounding soil. Then the heated fluid exchanges its calories with the system one wants to heat before returning to the loop and repeat the process.

As energy geostructures are included in the superficial geothermal energy framework, let us focus now on the latter. This technology uses a heat pump to transfer energy from a cold place (the soil) to

a warm place (the building). Opposing to the second principle of thermodynamics, this heat transfer requires an energy contribution in electricity (see below the functioning of the heat pump). This technology also called Ground Source Heat Pump (GSHP) was already mentioned in 1940 by Robert Webber (Akrouch, 2014). It can take place on aquifer, that is to say that the water of an underground table is pumped via drillings and feeds in calories a heat pump before being reinjected in the aquifer via other drillings. The reinjected water has a lower temperature than the extracted water. This approach has been successfully implemented at various locations, including the L'Oréal site in Caudry, France, where geothermal groundwater is harnessed for both industrial processes and building requirements, resulting in a 50% reduction in CO2 emissions (Lesquel, 2021). Shallow geothermal techniques also encompass the utilization of geothermal boreholes. These involve drilling boreholes of up to 200 meters deep and integrating heat exchanger tubes to supply heating networks. For instance, this method was employed to provide heating and cooling to the Eiffage Immobilier headquarters in Amiens, France, using a configuration of 7 double-U type boreholes exceeding 100 meters (ADEME, 2013). It should be mentioned that the cold production is based on a principle called geo-cooling or free-cooling. It is the direct use of the underground temperature. The naturally present coolness is recovered via the heat exchanger tubes. Only the water circulation pumps are powered by electricity, which makes the system even less energy consuming.

1.1.3 Energy geostructures

Energy geostructures are a specific type of shallow geothermal energy solution whose objective is to combine structural and thermal role by using the geotechnical structure (piles, diaphragm walls, tunnel segments) to exchange energy with the ground. Initially, they were developed in the 80's, in particular in Austria in order to face the oil shocks by developing a renewable, local (thus allowing certain independence) and non-intermittent energy. Today, many projects include them. The Tramways de Tours maintenance centre, for example, is built on 500 piles, 10% of which are geothermal. Many other projects such as Zurich Airport, the Columbus Centre in Vienna or the Norddeutsche Bank building in Hanover are built with this technology (ADEME, 2017). The Figure I. 5 shows that the number of projects incorporating geothermal foundations has risen sharply since the 1990s, thus avoiding a significant amount of CO2 emissions. This figure also shows the preponderance of energy piles over the other energy geostructures.

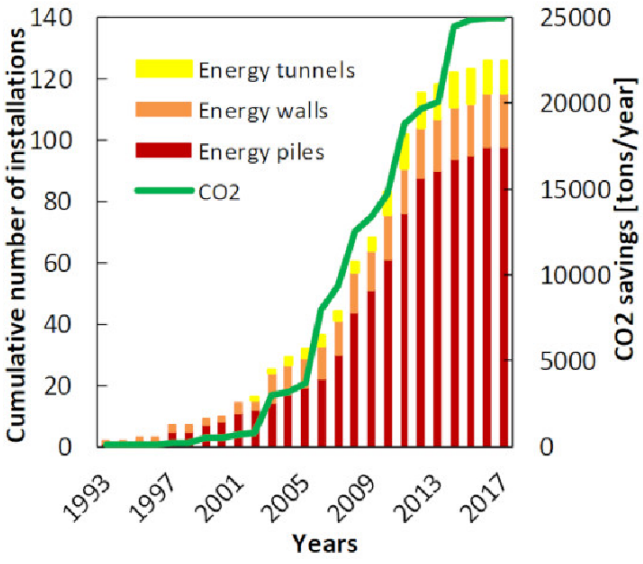

Figure I. 5 - Number of installations and CO2 savings as function of time (Di Donna et al., 2017)

The implementation of this energy system in new buildings is an important tool to meet two objectives that appear in national and international action plans, namely the reduction of CO2 emissions and the construction of positive energy buildings. Using these systems can result in a decrease of approximately 320 kg of CO2 emissions per kilowatt of energy produced in a building (Di Donna, 2017). All the greenhouse gases created by a heat pump actually come from the production of electricity that powers it. According to ADEME (2017), 1 kWh of electricity produces approximately 0.1 kg of CO2eq. The average in Europe is bigger (0.45 kg CO2 eq. per kWh of electricity) because it obviously depends on the production mode (for instance, French nuclear kWh emits less than 4 g CO2 equivalent). Moreover, heating using gas produces 0.2kg of CO2 eq. per kWh. Considering a COP of 3, a heat pump emits 6 times less CO2 than a gas heater in France.

According to the nature and the stake of the project, the owner sets up an energy policy, through which the use of energy geostructures will make it possible to meet entirely or partly the energy need of the building. It can even be surplus and supply energy to neighbouring buildings. The installation of energy geostructures can even be totally dedicated to the provision of energy to third parties. The question of the sustainability of the performance also arises. This type of installation must be designed for the long term by seeking a certain balance between the production of heat and cold in order to avoid a thermal drift of the medium which would alter the performance of the system and which would have negative consequences from an environmental point of view (Cf. Chapter II).

1.2. Ground temperature for shallow energy use

The subsoil holds a vast geothermal energy potential that can be used for heating and cooling purposes. Technological advances in the field of heat pumps make the exploitation of this resource cost-effective from an economic point of view. The basic prerequisite that GSHP take advantage of is the constant temperature in the ground below a few meters deep. In most European climate zones, this temperature varies between 10°C and 15°C, and remains constant down to a depth of around 50 m (Adam, 2009).This temperature corresponds to the annual average of the temperatures recorded at the surface. This is an essential point for the design of thermal probes or energy piles and a significant advantage for this technical solution insofar as energy production is therefore possible everywhere and is not intermittent. However, the temperature of the soil impacts the energy performance which will be better for a warm soil in the case of heat production and inversely in a cold soil.

1.2.1. Constant temperature below a certain depth

The outside temperature, i.e. at the ground surface, can be modelled by the following sinusoidal expression:

$$T(z = 0, t) = \theta_0 + T_0 \cos(\omega t) \quad \text{(I.1)}$$

Where θ_0 is the average temperature over a year and T_0 is the amplitude of the temperature variation over this same period.

When considering the diffusion of heat into the ground from its surface, the evolution of temperature is governed by the heat equation (I.2) which depends only on z:

$$\frac{\partial T}{\partial t} = \alpha \frac{\partial^2 T}{\partial z^2} \quad \text{(I.2)}$$

Where α (W/m^2) is the soil thermal diffusivity.

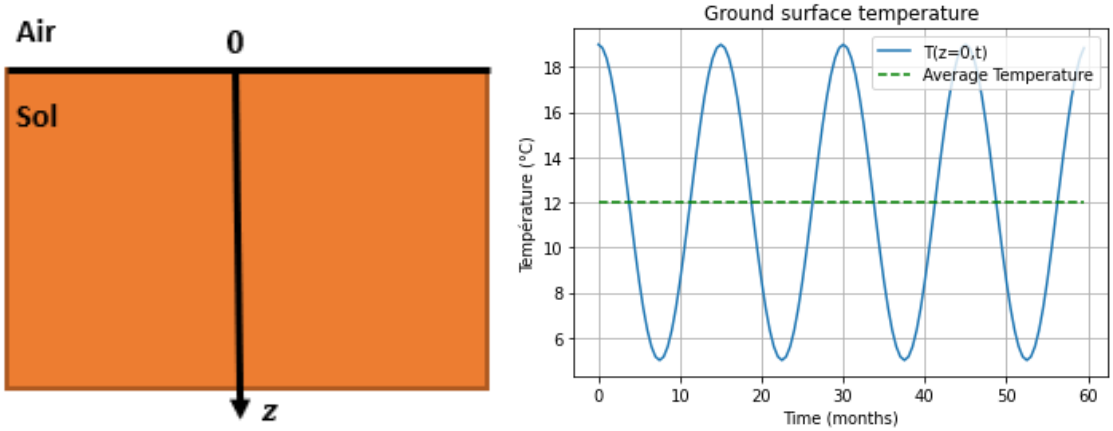

Figure I. 6 - Schematisation of the outside temperature evolution

This equation (I.2) can be solved by taking advantage of the linearity and use complex notation:

$$\underline{T^*(z,t) = \theta_0 + T_0 e^{i(\omega t - k^* z)}} \quad \text{(I.3)}$$

With $k^* = k' + i \times k''$ and one can remind that $T(z,t) = Re(T^*(z,t))$

The solution of the equation (I.3) leads to two families of solutions: thermal waves that will propagate in the direction of increasing z and be attenuated in their direction of propagation and waves that follow the opposite path.

Hence, $k^* = k' + i \times k'' = \pm \frac{1-i}{\delta}$ (I.4)

But the finite character of the solution prevents the development of the second type of waves so that $\mathrm{k}^* = \frac{1-\mathrm{i}}{\delta}$, and

$$T(z,t) = \theta_0 + T_0 e^{-z/\delta} cos(\omega t - z/\delta) \quad \text{(I.5)}$$

Where $\delta = \sqrt{\frac{2\alpha}{\omega}}$ (I.6)

Equation (I.5) governs the evolution of the temperature according to the depth in the ground and the time. Two phenomena coexist: the absorption which results in a decrease of the temperature and the dispersion of this temperature which can be attached to a wave speed $v_\varphi = \frac{\omega}{k'}$

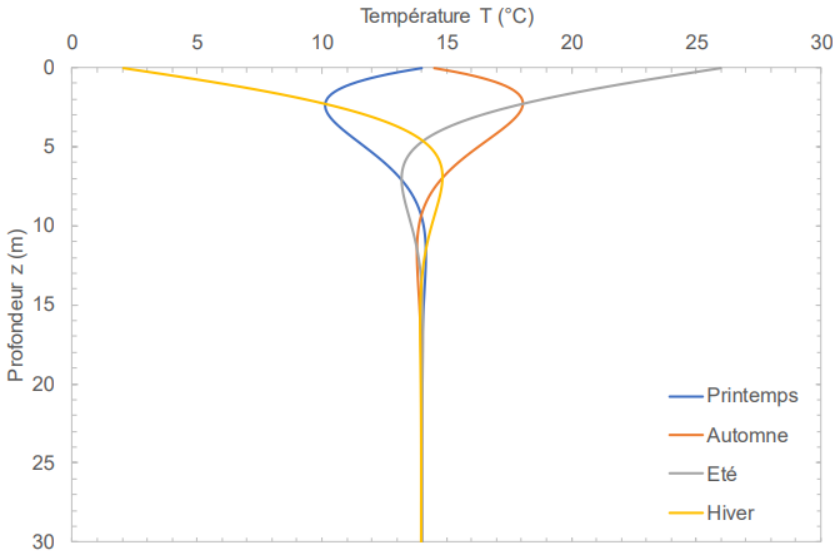

Figure I. 7 - Soil temperature evolution with depth for different seasons (spring in blue, autumn in organe, summer in grey, winter in yellow) (Delerablee, 2019)

Utilizing the expression of this solution (4), it becomes feasible to estimate the depth from which, because of absorption, the temperature variation does not exceed 5% of T_0.

Thus, one is looking for z_e such that $T_0 e^{-z_e/\delta} = 0.05 \times T_0$

$$\text{Hence } z_e = -\delta \times ln(0.05) = -2\sqrt{\frac{2\alpha}{\omega}}\ln(0.05) \quad \text{(I.7)}$$

For a clay soil ($\alpha = 10^{-6}\mathrm{m/s^2}$), and a one year period ($\omega = 2.10^{-7}$ s), it comes $z_e \simeq 6$ m

An interesting remark lies in the fact that δ varies as $\frac{1}{\omega}$. It follows that if the frequency increases (shorter time period), δ decreases. In simpler terms, at a specific depth, annual variations have a more significant impact than daily variations. Alternatively, the effect of daily variations vanishes as one goes deeper; while annual variations remain noticeable. The ground behaves like a low-pass filter, since it blocks high frequencies. This explains why shallow geothermal energy can be considered as non-intermittent.

1.2.2. Heat transfer in soils

Considering a soil assumed to be homogeneous and in which no heat is produced, the equation governing heat transfer is written:

$$C_{tot}\frac{\partial T}{\partial t} + div(\vec{J}) = 0 \quad \text{(I.8)}$$

C_{tot} $(J.m^{-3}.K^{-1})$ is the volumetric heat capacity of the soil. It is considered to be the average of the elements that make up the soil, which is assumed to be saturated with grain (noted with an index gr) and water (noted with an index w).

Thus,

$$C_{tot} = (1-n)C_{gr} + n \times C_w \quad \text{(I.9)}$$

Assuming that the soil is saturated, the thermal flux J can be broken down into two fluxes. The first is a diffusive flow (j_{cond}) which corresponds to the part of the energy transfer that takes place by conduction, i.e. thermal transport without macroscopic displacement of matter. The transfer occurs between warmer and cooler regions through thermal agitation, and it is described by Fourier's law[1] (Fourier J., 1822):

$$\boldsymbol{j_{cond}} = -\lambda_{tot}\boldsymbol{grad}(T) \quad \text{(I.10)}$$

With λ_{tot} (W/mK) the characteristic thermal conductivity of the material in which the heat transfer takes place.

The second flow ($\boldsymbol{j_{adv}}$) is called advective and corresponds to the part of the heat transfer induced by the movement of matter. In the case of heat transfer in the ground, the advective flow comes from the groundwater flow. The expression for the heat flow is therefore as follows:

$$\boldsymbol{J} = \boldsymbol{j_{cond}} + \boldsymbol{j_{adv}} = -\lambda_{tot}\boldsymbol{grad}(T) + C_w V_D \boldsymbol{T} \quad \text{(I.11)}$$

Where V_D (m/s) is the Darcy velocity

In the case of pure diffusion (no groundwater flow), $\boldsymbol{j_{adv}} = 0$ and we find the heat equation similar to (I.2) and the expression for the thermal diffusion coefficient of the soil: $\alpha = \frac{\lambda_{tot}}{C_{tot}}$

The expression of the diffusive energy flux j_{cond} is described by Fourier's law and involves the thermal conductivity of the soil λ_{tot}. In a first approach, this thermal property of the ground is defined by:

$$\lambda_{tot} = \lambda_{gr} + n \times Sr \times \lambda_w \quad \text{(I.12)}$$

Indeed, as soil is a three-phase material, its thermal conductivity can be firstly approximated by a volume average of the property over each of its phases. Equation (I.12) suggests the dependence of the thermal conductivity of soil on the water content. Other parameters also influence the thermal properties of a soil and the estimation of thermal parameters is presented in greater detail in 1.5.2.

1.3. Heat pump

In the winter operating of GSE, the ground from which the heat is going to be extracted is at a lower temperature than the room which will be heated. Thus, the aim here is to transfer heat from a cold source (the soil at about 15°C for example) to a hot source (an office at 20°C for example). The second principle of thermodynamics states that this transfer cannot be done naturally and that additional work is therefore necessary. In the operation of a heat pump, the compressor plays a crucial role. It consumes electrical energy to compress the refrigerant, thereby increasing its temperature and pressure. This additional energy allows the refrigerant to transfer heat from the

[1] Fourier series are also published in the same Traité analytique de la chaleur initially to solve the heat equation.

low-temperature medium (cold source) to the high-temperature medium (hot source), following the principles of thermodynamics. Heat pumps connect therefore energy geostructures or thermal probes in the soil (primary circuit) and the heating/cooling systems of the buildings (secondary circuit).

1.3.1. The principle

To achieve this unnatural thermal exchange, it relies on four basic elements present in any heat pump: the condenser, the compressor, the evaporator and the expansion valve. There are different types of heat pumps that differ in the nature of their cold source and their hot source, i.e. the nature of the entity that will be cooled and the entity that will be heated. For example, air-to-air heat pumps extract heat from the outside air to heat the inside air. In the case of energy structures, the geothermal heat pumps uses ground as a cold source and a water circuit as a hot source. In other words, the calories are drawn from the ground and will heat a water circuit feeding a heating system. It is important to note that the heat pump is reversible and can therefore be used to cool the building. The operating principle can be illustrated as shown in Figure I. 8.

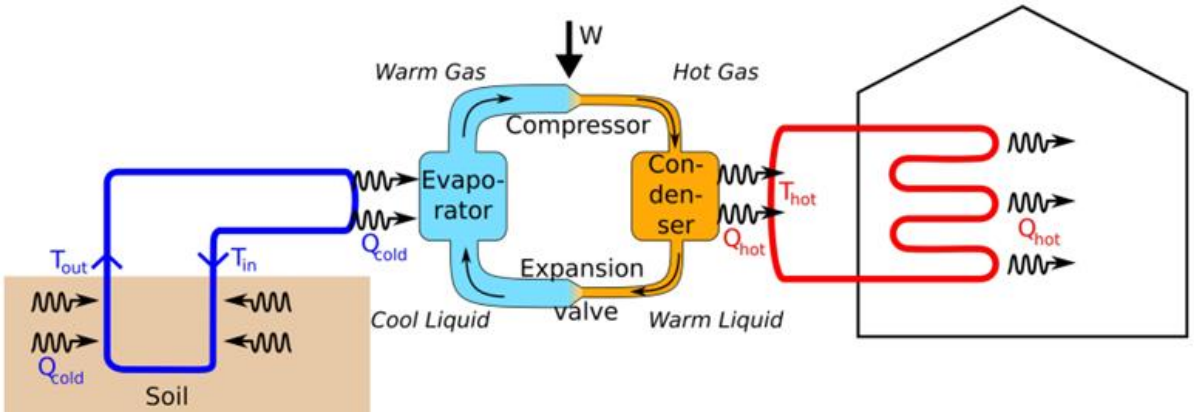

Figure I. 8 - Schematic representation of heat pump operation in a GSHP system

The operation of the heat pump can be summarized in three steps:

- Capture heat from the environment
  The heat transfer fluid that circulates in the tubes of the energy geostructures is always maintained colder than the ground by the heat pump and can therefore capture its heat. The greater the temperature difference between the ground and the fluid, the better the transfer. The heat from this fluid is transmitted through an exchanger to the evaporator of the heat pump, through which a refrigerant fluid circulates and evaporates under the influence of these calories.

- Increase this heat
  The refrigerant leaves the evaporator as a vapour and is directed into a compressor which will increase its pressure and therefore its temperature. The vapour is then hot enough to transfer its heat to the heating system. The fluid is then cooled but is still under high pressure. It finally enters the expansion valve which decreases its pressure and temperature again, the fluid becomes liquid again and the cycle can start again.

- Use this heat in the heating system to heat domestic hot water (DHW) or to supply heat to the heating system.

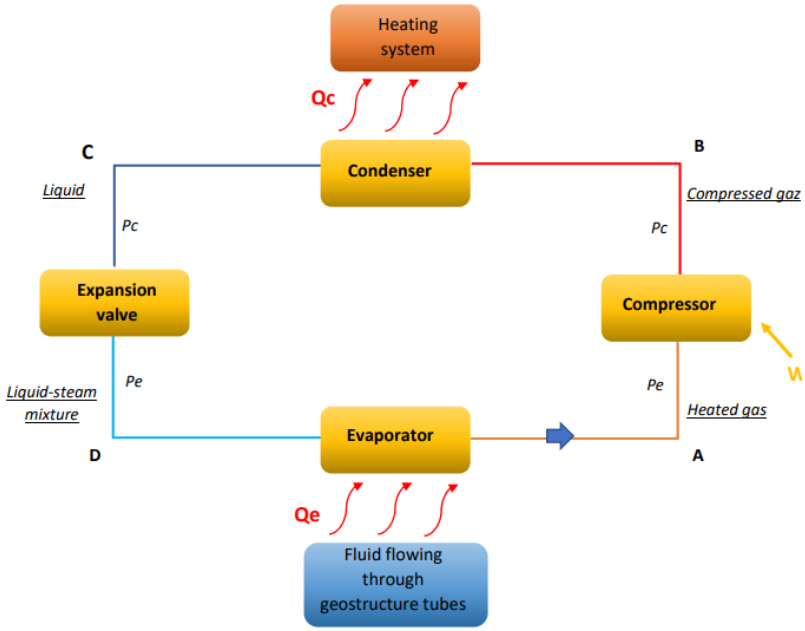

Figure I. 9 - Schematic representation of the thermal balance of GSHP

The refrigerant in the heat pump then undergoes various transformations that can be followed on a Pressure-Enthalpy diagram (Figure I. 10), also called the Mollier diagram, the German physicist who proposed it in 1904.

During the different transformations, the different powers involved are expressed as function of the mass enthalpies (h_A, h_B, h_D) as follows:

- During heat transfer allowing evaporation: $Q_e = \dot{m}(h_A - h_D)$ (I.13a)
- During compression: $W = \dot{m}(h_B - h_A)$ (I.13b)
- During heat transfer inducing condensation $Q_c = W + Q_e = \dot{m}(h_B - h_D)$ (I.13c)

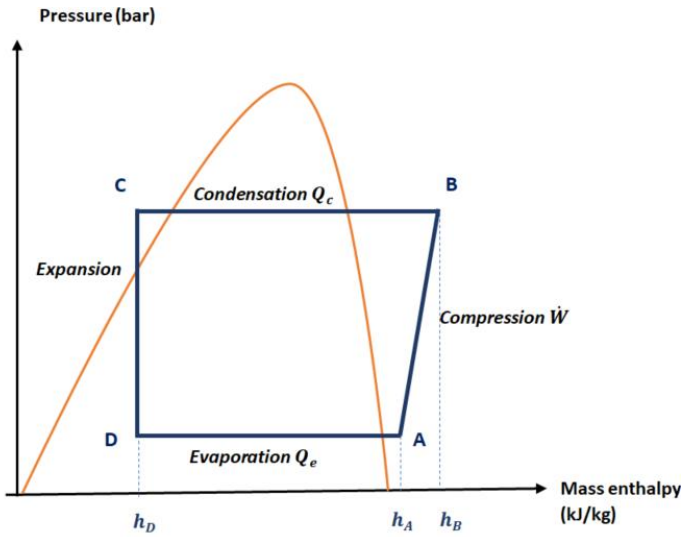

Figure I. 10 - Mollier diagram for GSHP operation

1.3.2. Performance

The efficiency of a heat pump is characterized by the calculation of a coefficient of performance, called COP. It reflects the ratio of heat produced to the energy used to produce it. Geothermal heat pumps generally have a COP of 5, which is about twice as high as that of air-to-water heat pumps. A COP of 5.0 implies that for every 1 kWh of electricity consumed by the heat pump, it can produce 5 kWh of usable heat energy. Out of these 5 kWh, 4 kWh are extracted from the heat source, which is typically the ground in geothermal heat pumps, and the remaining 1 kWh is generated through the heat pump's electrical input. This high COP value indicates the heat pump's efficiency in utilizing the available energy to provide substantial heat output from the heat source.

However, there are different ways of calculating the COP and they depend on the issues one want to consider. The manufacturer COP represents the steady-state of a heat pump under a set of controlled conditions with given input and output temperatures. Manufacturers base their calculations on a ground temperature of 10°C and the COP they calculate does not reflect the real energy savings that a user will make. Thus, it is only a manufacturer's data which makes it possible to compare the machines with each other without taking into account the real efficiency during use. To better appreciate these energy savings, one can calculate the overall COP which takes into account the various energy losses due to the distribution networks. In addition, since 2013, a European directive requires manufacturers to display the SCOP which is the seasonal coefficient of performance. It is a more representative indicator since it takes into account the seasonal temperature variations which influence the temperature of the hot source and therefore the calculation of the efficiency. In the case of thermal geostructures, the ground is assumed to be at a constant temperature because the depths considered are sufficiently great for seasonal temperature variations to be negligible. Finally, the annual COP is the measurement of the pump performance over one year for a given context. It is the most reliable indicator of the savings made by using the heat pump.

Indeed, it is crucial to understand that the Coefficient of Performance (COP) provided by manufacturers is typically based on standardized testing conditions and represents an idealized

scenario. In reality, the performance of a heat pump varies based on the specific environmental conditions in which it operates. Environmental factors such as outdoor temperature, humidity, and the heat load demand of the building can impact the efficiency. As a result, the actual COP experienced during real-world use may differ from the COP advertised by the manufacturer. It is essential for users and installers to consider the specific operating environment and adjust their expectations accordingly, understanding that the heat pump's efficiency may vary based on the actual conditions in which it operates.

Another way to estimate the performance of a heat pump is the Seasonal performance factor (SPF) which represents the average annual performance in a given location, based on the average outdoor temperatures through the year. In addition, when the COP only considers the heat produced and the electricity consumed by the heat pump itself, the SPF takes into account the production and consumption by auxiliary heaters and pumps (to circulate the coolant loop for instance).

It is relevant here to introduce the Carnot cycle. The Carnot cycle describes the most efficient way of transferring thermal energy between a cold source and a hot source by using work. It is a theoretical and idealized scenario, not considering losses during the exchanges. The theoretical COP can be calculated as the maximum COP achievable by a thermal machine in an ideal situation (no losses). However, real thermal machines, including heat pumps, experience energy losses preventing them from reaching the theoretical efficiency of the Carnot cycle. Therefore, the COP of a heat pump is always lower than the theoretical efficiency of the Carnot cycle between the same temperature sources as expressed by the following inequation which refers to Figure I. 10.

$$\mathrm{COP_{real}} = \frac{\dot{Q}_c}{\dot{W}} = \frac{h_B - h_C}{h_B - h_A} < \mathrm{COP_{theoretical}} = \frac{T_2}{T_2 - T_1} \quad (I.14)^2$$

With W the energy transmitted to the fluid (electrical energy-losses), T_2 the temperature at the condenser inlet and T_1 the temperature at the exchanger inlet. It can be noticed that the theoretical COP decreases when the difference between the inlet temperatures of the condenser and the evaporator are close. Thus, to increase the theoretical COP of a heat pump, there are two solutions: increase the temperature of the cold source, which in practice means considering a warmer ground, or decrease the temperature that you wish to reach for the hot source (30°C instead of 35°C in the underfloor heating system, for example). For instance COP drops by between 0.6 and 1 for every 10°C difference, giving 0.6 to 1 kW less heat output per kW of electrical input (Staffell, 2012)

The average annual SPF of the heat pump can be calculated as following:

$$\mathrm{SPF_{HP}} = \frac{\sum_i \mathrm{COP}(\Delta T_i) E_i}{\sum_i E_i} \quad (I.15)$$

Namely, SPF is the average of the COP weighted by the period of time (E_i). Auxiliary systems not considered in the calculation of COP are estimated to lower the SPF by around 10%.

[2] This result is Carnot's theorem for heat pumps. It should be noted that the efficiency of a heat pump is not necessarily less than 1. It is all the greater (and tends towards infinity) the closer the temperatures of the sources are close to each other

Whereas, in winter condition, the soil temperature is always cooler than the target temperature inside the building, the use of heat pump is not systematic in summer condition. Indeed, while the average soil temperature is around 13°C and the coolant fluid target could be set to 15°C the heat transfer will occur naturally without heat pump activation. This condition is called "free-cooling". This effect, will be enhanced if the soil temperature has been cooled. In opposition, if the temperature of the soil exceeds that of the coolant fluid, the heat pump becomes necessary to transfer the heat energy. In such "active cooling" condition, the hot source will be the building and the cold source will be the soil (Pahud and Hubbuch, 2007; Allaerts et al., 2015; Fadejev et al., 2016, 2017). In any case, cooling operation of building will produce heat exhaust in the soil around the energy geostructures, increasing soil temperature, and recharging heat reservoir. Therefore, seasonal use is profitable as it helps to avoid multi-year thermal shift and higher soil temperature will allow heat pumping with higher efficiency (smaller cost).

1.3.3. Design

According to French professional recommendations (AFPAC, 2007), the design of the heat pump requires a preliminary diagnosis that allows the heat needs of the building to be estimated, as well as its losses and its various inputs. To do so, one should take into account indicators such as the geographical location of the building, in particular the basic outdoor temperature according to the area, the surface area of the building and the type of heating system. The losses take into account the air renewal, the losses through the walls, and the infiltrations (joints, doors, windows). It is then necessary to first determine the desired building hourly heating and cooling load with a so-called chronicle of power. The Figure I. 11 gives an example. It should be remembered that in the case of energy geostructures, the geometric design of the structures is based solely on mechanical criteria, which therefore reduces the scope for the energy design of the heat pump. In practice, for example, the size of the energy piles which will be presented afterwards cannot be varied for the sake of energy requirements.

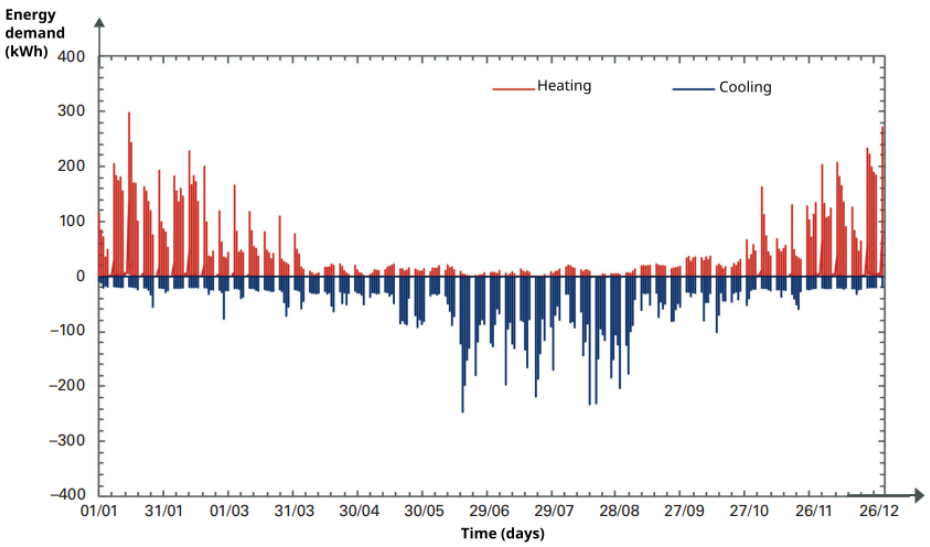

Figure I. 11 - Example of a chronicle of annual power for a tertiary building in France with a net floor area of 2000m² (Delerablée, 2020)

The heat derived from energy geostructures and heat pumps is typically combined with a backup energy source to supplement the energy supply during periods of insufficiency. Consequently, if the geothermal system is linked with renewable electricity generation (such as solar or hydroelectric energy), the entire energy production is considered environmentally friendly. As per the French good practice rules (RAGE, 2015), the combined total capacity of the heat pump and booster system should be sufficient to cover more than 120% of the losses at the standard outdoor temperature. In heating mode, the heat pump is defined by two characteristics: the power dissipated at the condenser and the total power absorbed. In addition, the COP of the heat pump must be higher than a minimum COP imposed by the regulations (AFNOR, 2011). Generally, manufacturers obtain a COP of about 5 for geothermal heat pumps, so it is possible to produce, in theory and for given conditions, 5 kWh of energy for 1 kWh of electricity used. Moreover, the lower the cold source temperature, the poorer the efficiency. There is therefore a limit temperature from which the heat pump cannot be used and where the auxiliary heating alone must operate. In the case of GSHPs, unlike ASHPs, the temperature of the cold source (the ground) is substantially constant over time. Therefore, they theoretically have the advantage of not having to deal with this problem. In the case of an unbalanced demand in an environment where the hydrology does not allow thermal recharge, a solar heat pump solution can allow ground recharging for the next winter in addition to providing hot water. This question will be tackled in a next section (Cf. 1.6 of this Chapter and Chapter III)

1.4. Energy geostructures

As mentioned above, there are different types of energy geostructures even if the most used are the energy piles. In the 1980s, deep foundations were first used for geothermal heat extraction. At first, foundation slabs, then driven precast piles and later bored piles and diaphragm walls were successfully used for heating and cooling purpose (Adam, 2009), and today tunnel segments are also used as heat exchangers. Relying on the widely constant temperature of the ground, the principle of operation is the same: heat exchanger tubes are attached to the reinforcement cages of the in-ground structure (as illustrated Figure I. 12) and a heat transfer fluid circulates inside these tubes to exchange heat with the surrounding soil. It is then possible to draw heat from the ground to heat the building in winter and conversely to inject heat from the building into the ground to cool it in summer. The geotechnical foundations, whose role is to ensure mechanical stability by supporting and diffusing to the ground the load of the superstructure, are thus given a second energy role. It is obvious that the addition of this second role must not be detrimental to the first role which controls the design. In this respect, the number of energy piles, the size of energy walls or the diameter of a tunnel segment is not designed to meet the energy demand but is imposed by mechanical constraints. A designer has to calculate how much energy the structures can exchange with the ground in a sustainable way. Several factors will impact this exchange such as underground temperature and soil thermal properties. The main types of energy geostructures and these different factors will be discussed afterwards.

Figure I. 12 - Illustration of the fixing of HDPE pipes on energy pile reinforcement (geothermie-professionelle)

1.4.1. Energy piles

There are different criteria to classify piles in geotechnical engineering such as the geometry, the method of installation, the mode of construction or the constitutive material. Except for wooden piles, all types of piles can be equipped with heat exchanger tubes and thus become energy piles. Figure I. 13 gives an illustration. Most commonly, energy piles are made of reinforced concrete (Brandl, 2006), but they can also be constituted of steel. For instance, an eco-friendly house at Hokkaido University, Japan was constructed on two energy steel piles to supply the heat and coolness demand. More than 300 buildings have been equipped by this way, since the good results of this experiment (Nagano, 2005). All the techniques of realization of deep foundations, a priori, comply with energy structures. In addition, the installation method (drilling and supporting the soil in the case of bored piles, driving or screwing in the case of soil displacement piles) does not differ from "conventional" piles.

The tubes can be attached to the reinforcement cage before it is placed, or they can be attached to a steel bar that will be lowered into the already poured concrete (Loveridge, 2012). In the latter case, the tubes are placed in the centre of the pile and this implies important differences in heat transfer. In particular, the thermal resistance is higher and heat exchange is not favoured. The recommendations are therefore in favour of the former case.

The heat exchanger pipes also called energy loops can be placed at different locations in the pile and with various configurations. They are made from High-Density Poly-Ethylene/Poly-Propylene (HDPE/HDPP) pipes. The HDPE diameter is in the range between 20 and 44mm. The number of loops will depend mainly on the size of the piles to ensure a minimum spacing between them. Obviously, a longer length of pipe, especially, a large number of loops, means more thermal energy is drawn or exchanged, but also requires more mechanical energy to circulate the fluid in the pipes.

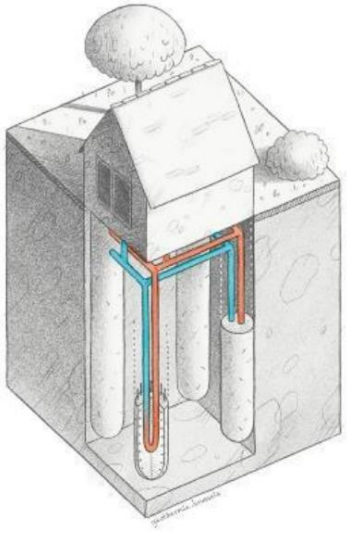

Figure I. 13 - Schematisation of energy piles (Source: Environment Brussels)

The pipes can be installed in various forms within the energy pile. Some common shapes reported are single U-shape, double U-shape, triple U-shape, W-shape, spiral or helical shape, direct double-pipe type and indirect double-pipe type configurations (Sani, 2019). The different typical configurations are shown in Figure I. 14. Generally, the pipes are attached to the inner or outer surface of the steel cage, the length of which dictates the length of the pipes. The installation of the tubes is done under pressure and the follow-up can be done with a manometer to detect any anomaly. It is recommended to equip more piles with energy loops than necessary. On the one hand, this allows anticipating possible defects and on the other hand it leaves the possibility to activate some piles in the future for possible energy needs (CFMS, 2017).

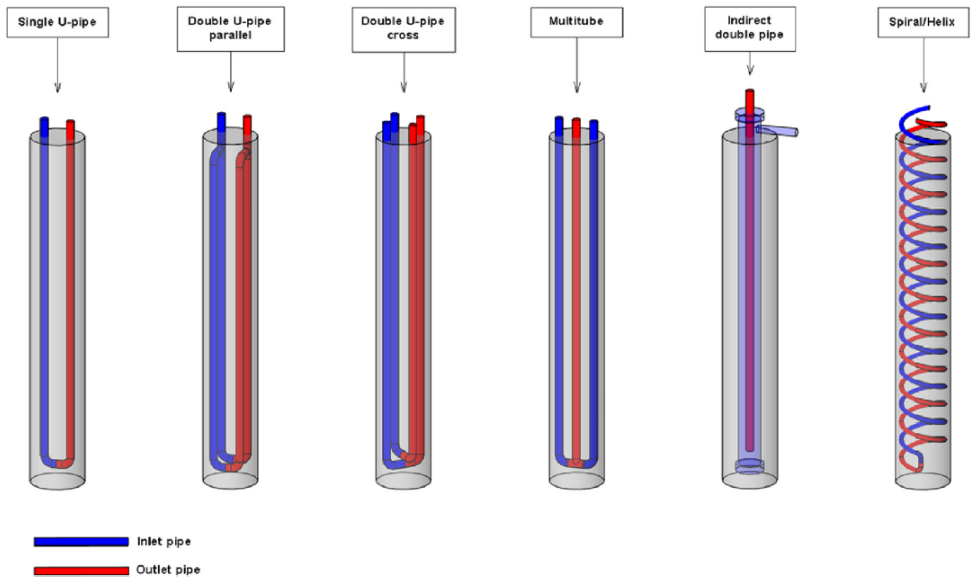

Figure I. 14 - Different configurations of energy loops within an energy pile (Fadejev, 2017)

The heat transfer fluid that circulates within the pipes will allow the heat transfer from the soil to the heat pump or inversely. It can be made of pure water or water plus an antifreeze based solution.

Adding antifreeze to the heat transfer fluid decreases its freezing point, but increases its viscosity which implies higher energy to circulate it.

A study led on a consequent database reports that the heat exchanged by energy piles with ground is generally in the range between 40 and 100 W/m (Di Donna, 2017). The authors attribute the differences to the pile geometry, the hydraulic properties and underground conditions.

The thermal load can be modelled by considering a thermal probe as an element of dimension 1 and infinite length with a constant heat flow q (which in reality varies according to the needs of the building), the (overestimated) thermal response can be simplified to this equation (Carslaw, 1959):

$$\Delta T = \frac{q}{\lambda 4\pi}\left(ln\left(\frac{4\alpha t}{r^2}\right) - \gamma\right) \quad \text{(I.16)}$$

With γ the Euler constant

For small times, this approach underestimates the thermal response because it assumes that the heat source is at the centre and not at the circumference. Thus, if the same approach is considered for piles where the diameter is larger than for geothermal probes, these errors will be even larger and extend over longer periods of time especially if the tubes are placed close to the circumference of the pile (Loveridge, 2014).

The reason behind these errors lies in the distribution of heat within the system. When the heat source is not at the centre, but closer to the edge, the temperature distribution within the pile becomes more complex. This complexity is due to the non-equal heat transfer from the tubes to the surrounding soil or material. As a result, the thermal response of the pile or larger structure will be different from what the simplified centre-assumption model predicts. To obtain a more accurate estimation of the thermal distribution of such systems, one can use more advanced numerical models or analytical approaches that consider the non-uniform heat distribution within the pile. These advanced methods take into account the actual positioning of the tubes and the complex heat transfer processes, thus providing a more precise estimation of the thermal response over time. This is what was done in a study (Maragna, 2019) where “A semi-analytical (SA) model accounting for the pile concrete inertia was developed and validated against a finite-element code”

Although less common than reinforced concrete energy piles, steel energy piles have certain mechanical advantages and are just as suitable for geothermal applications. A building project using steel energy piles is currently underway on the campus of the University of São Paulo, in the city of São Paulo, Brazil. Thermal response tests were carried out on four instrumented piles filled with different materials: water, saturated sand, grout and steel fibre grout. The results showed that thermal performance was comparable, but that the solutions using water or saturated sand were more advantageous from an ecological point of view (Freitas Murari, 2022).

In thermal engineering, and particularly in the building industry, it is often assumed that the temperature is in a state of equilibrium and therefore steady states are considered. It is therefore legitimate to think of thermal resistance in terms of electricity or hydraulics, for example. The thermal resistance of a pile is calculated by taking into account the different thermal resistances in the pipes and in the concrete. The velocity of the fluid in the pipes influences the flow regime and thus changes the heat exchange. In some cases, the convection resistance at the interface and the

conduction resistance in the tubes are negligible, and ultimately the thermal resistance of a pile can be approximated by that of the concrete (Loveridge, 2012).

1.4.2. Diaphragm walls

In a similar way, it is possible to attach heat exchanger tubes to the reinforcement cages of diaphragm walls in order to use them as a heat exchanger system with the ground. These are originally retaining structures used to sustain excavations during constructions of underground stations or parking for instance (See Figure I. 15). Their thickness is typically between 80 and 120cm for depths ranging from 15 and 70 m for the deepest excavations. Because of their large exchange surface with the ground, they have considerable energy potential. Accordingly, these structures are integrated in several large-scale projects like Uniqa Tower in Vienna (7,800 m² of thermoactive walls), the EA General Centre in Vienna (4,200 m² of thermoactive diaphragm walls) or the Columbus Centre in Vienna (12,400 m² of thermoactive cast walls). However, their large exchange surface also makes them very sensitive to the hydrological conditions of the site. It is therefore difficult to generalise about the amount of exchanged energy that one can expect. For existing cases, it can be affirmed that the heat exchange generally varies between 10 and 50 W/m² (Di Donna, 2017).

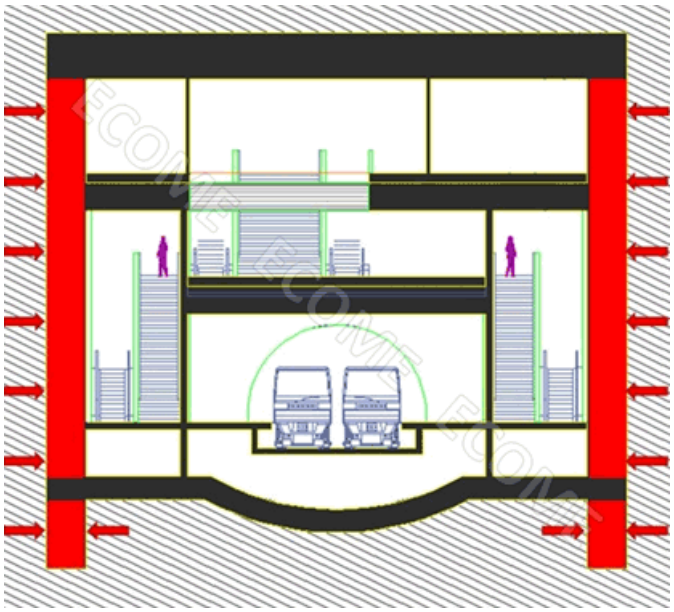

Figure I. 15 - Principle of geothermal energy capture on cast walls (Ecome)

Baralis et al., (2021) instrumented an existing energy wall and collected data from both heating and cooling experimental campaigns in order to highlight the potential of such a technology. The results suggest that an average thermal power of about 17 W per unit area can be exchanged with the ground in heating mode, while an average of 68 W per unit area is exchanged in cooling operations. They also insist on the reduced probability of interferences with other installations in highly urbanized areas insofar that experimental campaign shows that thermal affection of the ground is rather limited in extension and magnitude (surely because the size of the wall means it is in contact with a larger heat reservoir). They also highlighted the easiness of installation and affordable cost.

Due to the large exchange surface of energy walls, the number and the position of the pipes play a key role in the amount of energy exchanged. More generally, for given structure and ground conditions, the energy performance can be enhanced by reducing the thermal disturbances between

the pipes where fluids at different temperatures circulate. Additionally, it is recommended to take advantage from the fact that the fully immersed portions of the wall have both sides into direct contact with ground. Indeed, the boundary condition on the excavation side has the main influence on the temperature of the wall and the circulating fluids (Sterpi, 2018).

1.4.3. Tunnel segments/linings

Today, tunnel boring machines (TBM) offer more safety than sequential tunnelling, especially in groundwater or shallow soft ground. This method is also ideal for geothermal exploitation as it is possible to equip a tunnel with pipes where heat exchanger fluid will circulate to capture the thermal energy of the surrounding soil. Although this technology is much less common than energy piles, it has great potential.

Austria, which can be considered as one the pioneers in the use of energy geostructures, has been testing this technology at real scale in construction lots of the Lainzer tunnel (Adam, 2009). Other real scale devices are also referenced in literature (Moormann et al. 2016, Zhang et al., 2014). Frodl (2010) describes a system designed to provide heating and cooling for a nearby factory, connected to a heat pump system that uses the captured energy to produce hot and cold water. The system was also designed to be flexible and modular, allowing for easy expansion or modification as needed. They suggest that energy tunnel can have lower installation and operating costs compared to other geothermal systems, such as vertical borehole systems. This is due to the fact that the tunnel system can be installed using standard excavation equipment, and requires less drilling and excavation than a vertical borehole system. By arranging the positioning of the tubes, an energy segment (Figure I. 16) was proposed at the Politecnico di Torino to reduce the head losses and also to take advantage of heat exchange by convection (heat exchange with the air and not only with the ground) (Barla & Di Donna, 2018). Moreover, the heat power that can be expected to be exchanged has been studied according to the water flow and the thermal conductivity of the ground and has resulted in charts (Barla & Di Donna, 2018) which are presented afterwards (figure II.26).

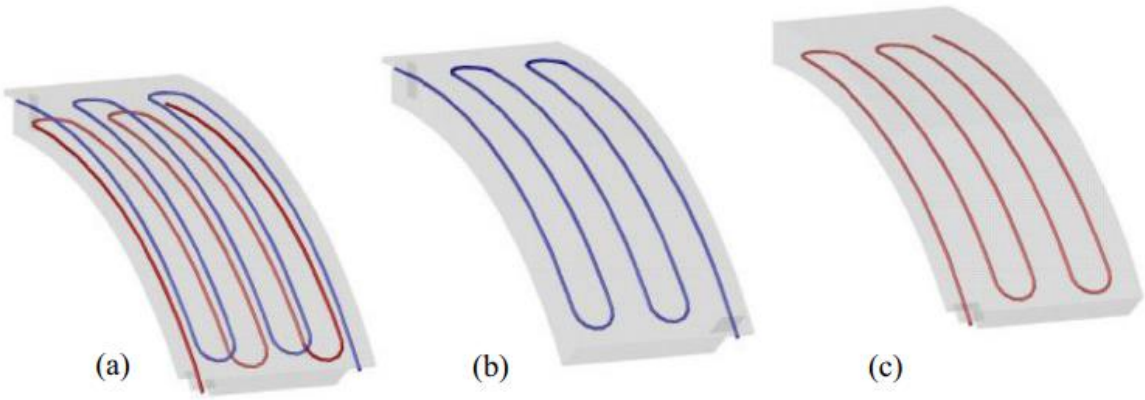

Figure I. 16 - Different configurations of the segmental lining ENERTUN (a) ground&air, (b) ground, (c) air (Barla, 2018)

The main interest is that tunnels present a greater ground contact surface than piles. And in addition to the heat naturally present in the ground, the device take advantage of the heat produced by the passage of trains and more generally by the use of the tunnel. For deep tunnels, this technology can be combined to ventilation system to maintain temperature values at comfortable level. The second interest is that the segments are precast in factory. They are therefore prepared and optimized for

heat exchanged (Barla & Di Donna, 2018). As the tubes are not placed on site, this solution does not require additional time to the placement of conventional tunnel segments. Indeed, the need to adapt site logistics when installing energy piles is a main drawback of this technology.

However, as tunnels are not living places, the heat exchanged by the lining with the surrounding ground is not used to heat the building itself as it is the case when energy piles supply in energy the building that they support. This energy can therefore be used at a district scale to supply the train stations or the buildings at proximity. Therefore, their use in urban areas is more relevant as the exchanged heat can benefit adjacent buildings. It is also possible to use the heat from energy tunnels to deice routes for the sake of safety and durability. For instance, a test campaign carried out on the Nanaori-Toge tunnel in Japan showed good results regarding the possibility of thawing a road using the heat extracted upstream in the tunnel (Islam, 2006). More recently, a study focused on the future Line 2 of the Turin Metro that could provide 18.7 MW of thermal power in winter for the benefit of the city district heating system. According to the hydrological conditions, an exchanged power of 10 to 60 W/m² can be expected (Barla, 2023).

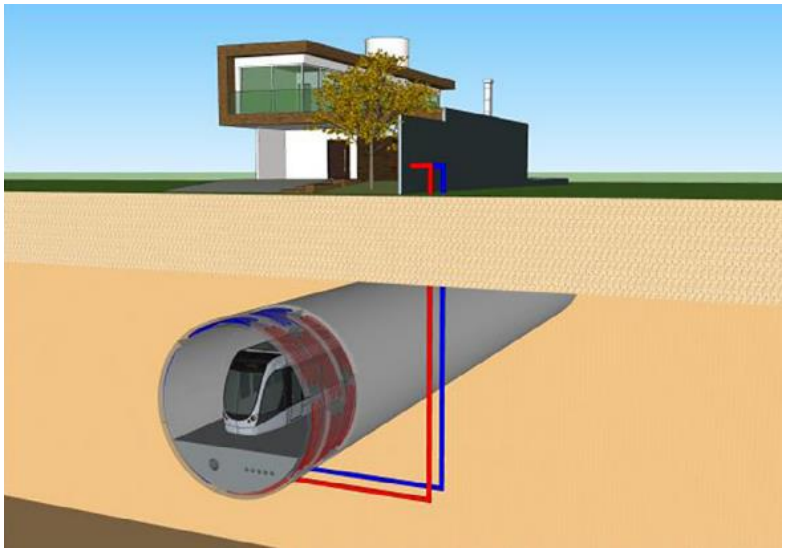

Figure I. 17 - Schematic example of the thermal activation of the tunnel segmental lining (Barla 2018)

1.4.4. Economical aspects

The environmental aspect of energy structures seems obvious, but in order to foster their development, it is crucial to consider also their economical performances.

Using a numerical hydro-thermal model (Barla, 2016), the amount of energy recoverable over the long term from an energy tunnel line in Italy was estimated, enabling the authors to calculate the cost of recovering the same amount of energy using traditional means (gas condensing boiler, oil condensing boiler…). By considering a heat pump COP of 4, they highlighted that traditional heating-cooling plants have annual operating costs of about 75-145% higher than the proposed geothermal system. This calculation was done by taking into consideration the additional cost due to energy equipment and setup. In the case of energy tunnels, the initial investment is usually estimated around 2% of the total cost. They estimated that this additional price has a pay-back-time of 5 years

maximum. Then, compared to the borehole heat exchanger system, this latter is still economically convenient with respect to the energy tunnel system.

Regarding the energy piles, their first economic advantage with respects to BHE is that the drilling cost is not to be considered, as it must be done in all cases to place the piles for structural purposes. The only additional cost would be the raw material cost of pipes, labour cost of workers installing tubes into piles and potential delays in construction (Qi, 2019). Indeed, the economic analysis should include price of the heat pump as first investment, but also operation and maintenance. Heat pumps have a shorter lifespan (around 20 years) than energy foundations, so their replacement should also be included in the financial estimate.

Payback periods of operative energy geostructures are set between 4 to 8 years (SIA, 2005). In their study, Qi et al., (2019) uses three different economic indicators (present worth, annual worth and simple payback period) to compare energy piles system (coupled to GSHP) to traditional way of heating and cooling in Australia (where the energy demand is more balanced as in Europe) and conclude that energy pile GSHP systems are more cost –effective. Likewise, more than 20 years ago, a comparative economic evaluation has been carried out to assess the feasibility of using GSHP in place of conventional heating/cooling systems and air source heat pump. The results indicate that system parameters can have significant effect on performance and that GSHP is economically preferable to conventional system (Healy, 1998). In the same spirit, the Table I. 1 shows that for the same energy demand, the solution based on energy piles is economically advantageous compared with a BHE system.

Table I. 1 - Comparison between cost benefits of boreholes and energy piles (Di Donna et al., 2017)

Item	Option 2 borehole loop	Option 3 thermal pile
Diameter Heat transfer Number of loops Length	0.2 m 35 W/m One 100 m (3500 W)	0.6 m 35 W/m Two 27 m x 2 No (1750 W)
Boring/installation cost	$50/m x 100 = $5000	Pile included anyway Allow 2 hours' attach loops $270/crew time
Thermal grout Pipe – 25 mm ID Spoil removal	$7/m x 100 m = $700 $7/m – 1 loop = $700 $1000	N/A $7 x 2 x (27 m x 2) = $756 Nil
Total installation	**$7400**	**$1026**
Header pipes	$1500/borehole +trenching	$1100 per pile
Grand total for 3500 W	**$8900 + trenching**	**$4,252 (2 piles)**
Construction work	Additional construction time required if under footprint of building	On critical path. Addition of loops in piles adds no additional construction period.

From an economic point of view, although a detailed analysis has to be carried out, taking into account the energy that can be exchanged over the long term and the price of other energies in the region or country concerned, energy structure systems coupled with a GSHP prove to be profitable, at least in the long term. This is mainly due to the drilling work that can be avoided with this technique, and also to the efficiency of heat pumps. A public promoter would therefore probably

have every interest in investing in this system and a private promoter also if he operates on a long-term perspective.

1.5. Characterisation of soil thermal parameters

The energy performance of a an energy geostructure depends not only on the temperature in the subsoil, which is constant from a certain depth as previously presented, but also on the thermal parameters of the soil in which it is placed, namely its thermal conductivity and its thermal capacity. These parameters can be determined in different ways.

1.5.1. Thermal response test (TRT) and thermal conductivity

One of the existing methods for determining the thermal conductivity of soil in situ is the thermal response test (TRT). It consists in realising a geothermal probe, injecting a heated fluid in the probe and measuring the inlet and outlet temperatures of the fluid to reach a constant linear power exchanged $Q\ (W/m)$(See Figure II. 18). This method was initially developed for the thermal design of vertical probe fields, but is equally well suited to energy piles. The advantage of this method is that it avoids the errors due to the sampling of the soil in the case of laboratory tests, but it only provides average and global results without taking into account the stratification of the soil for example.

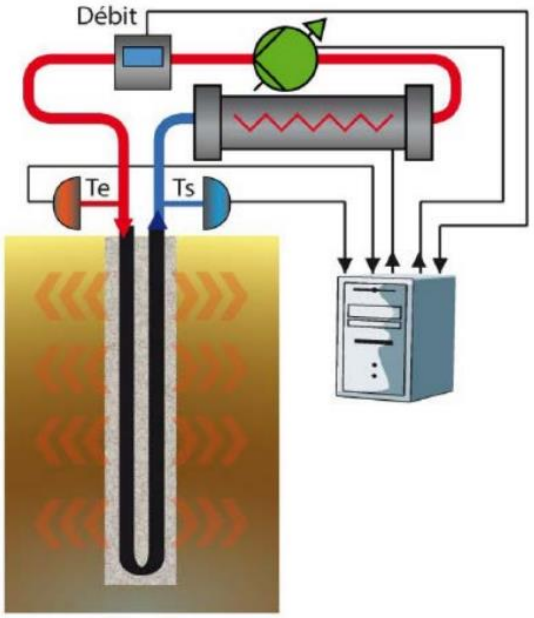

Figure I. 18 - Schema of TRT device (BRGM, 2012)

By defining a curve that best matches the evolution of the fluid temperature as a function of time, the effective thermal conductivity of the soil is determined. Indeed, considering the analytical resolution of the heat diffusion in transient regime from an infinite linear source between two instants t_1 and t_2, the thermal conductivity is written (ASTM, 2022)

$$\lambda = \frac{Q}{4\pi(T_2 - T_1)} ln(t_2 - t_1) \quad (8)$$

However, the results of a thermal response test are sensitive to the conditions of the experiment, and in particular to the fact that the thermal gradient is not perfectly radial. Thus, a minimum duration is recommended and the longer it is, the more negligible the error will be. As for the vertical component of the thermal gradient, it is due to the non-homogeneity of the temperature field in the ground. The longer the probe length, the smaller the induced error.

This method also allows evaluating the thermal resistance of the borehole according to its geometry, the number of pipes and their arrangement, the type of grout, the fluid used and its mass flow. Standard methods of interpreting thermal response tests are based on a curve fit of the average fluid temperature calculated as the average of the inlet and outlet temperatures of the fluid in the pile. The estimation of the average temperature by this simple calculation is based on the assumption that the flow is constant along the borehole. Consequently, it was shown that this assumption leads to an overestimation of the thermal resistance of the borehole (Marcotte, 2008).

In addition, an extended thermal response test (TRT) campaign, supplemented by laboratory experimentation, was undertaken over a four-year timeframe on a tropical soil in Brazil characterized by varying hydric conditions attributed to alternating dry and rainy periods. The outcomes reveal that the thermal behaviour of the investigated energy pile exhibits temporal variations throughout the year. Notably, the thermal conductivity of the soil encompassing the pile experiences a reduction of approximately 32% at the culmination of the dry season. This observation underscores the significance of incorporating seasonal fluctuations in soil thermal properties into the design considerations of ground-source heat pump systems utilizing energy piles within analogous soil and climatic contexts (Morais, 2020).

1.5.2. Role of moisture content in the thermal characteristics of the soil

Heat transfer due to thermal conduction is closely related to the porosity of the soil and its degree of saturation. For instance, as temperature changes the viscosity and density of fluids within the pores, moisture content and drainage conditions can influence thermal expansion making them reversible or not (thermo-elastic behaviour versus thermoplastic) (Goode, 2015). Moreover, soil saturation with water generally promotes heat exchange in that the thermal properties of the soil, including its thermal conductivity and heat capacity, increase with saturation. Empirical methods have, for example, provided orders of magnitude of thermal parameters of several soils depending on their water status (dry or saturated) as in Table I. 2. The main result is that water is a better conductor than air and so the thermal conductivity increase with moisture content.

Table I. 2 - Thermal conductivities and thermal capacities of different soils according to the water content (Fromentin, 1999)

Type of soil	Thermal conductivity $\lambda\ (W/m.K)$		Heat capacity $C_v\ (MJ/m^3.K)$	
	Dry soil	Saturated Soil	Dry soil	Saturated Soil
Clay	$0.2 - 0.3$	$1.1 - 1.6$	$0.3 - 0.6$	$2.1 - 3.2$
Silt	$0.2 - 0.3$	$1.2 - 2.5$	$0.6 - 1.0$	$2.1 - 2.4$
Sand	$0.3 - 0.4$	$1.7 - 3.2$	$1.0 - 1.3$	$2.2 - 2.4$
Gravel	$0.3 - 0.4$	$1.8 - 3.3$	$1.2 - 1.6$	$2.2 - 2.4$

Analytical formulations also account for the increase in the thermal conductivity of a soil by its saturation. One of the best known is the Kersten model, which in 1949 proposed empirical

formulations for fine unfrozen soils and for coarse soils. These formulas allow to estimate the thermal conductivity for any water content and to visualize the evolutions (see Figure I. 19).

$$\lambda_{fin} = 0.1442 \times 0.9 \times (log(w) - 0.2) \times 10^{0,6243\rho_d} \quad \text{(I.17a)}$$

$$\lambda_{sable} = 0.1442 \times 0.7 \times (log(w) + 0.4) \times 10^{0,6243\rho_d} \quad \text{(I.17b)}$$

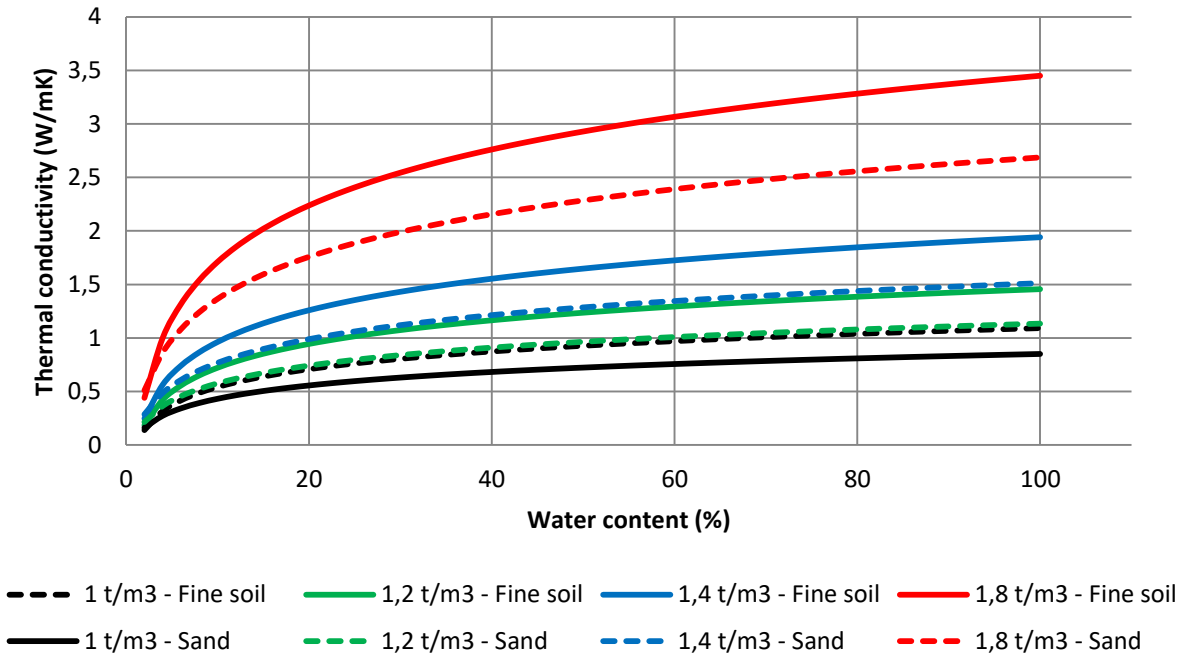

Figure I. 19 - Kersten model thermal conductivities according to water content for fine soils and sands

Since Kersten's equations follow a logarithmic law, it should be noted that for low saturation levels, a small variation in water content implies a large variation in thermal conductivity. Therefore, an error in the estimation of the water content will strongly distort the estimation of the thermal conductivity. Conversely, for high water contents, a small error in the estimation of the degree of saturation will not greatly distort the thermal conductivity calculation. These first models show the importance of the increase of the water content in the estimation of the thermal properties of soils, in particular for weakly saturated soils. Indeed, water adsorbs around soil grains until it forms a thermal bridge between them, since water has a better thermal conductivity than air (Usowicz, 2013). It is then understood that for low water content, these bonds exist little or not at all and the thermal conductivity is low since the air between the individual particles acts as a contact thermal resistance. By increasing the water content and thus creating these thermal bonds, the thermal conductivity of the soil increases significantly. In contrast, for soils already possessing high water content, the bonds almost all already exist, and increasing saturation has little influence on thermal conductivity (Delerablee, 2019). For low-density clays, this critical water content corresponds to the plasticity limit (Salomone, 1984). However, in the case of swelling clays such as Kaolinite, the increase in water content can lead to a decrease in thermal conductivity (Lee, 2011) .

The same reasoning can be made regarding the heat capacity. Indeed, the specific heat of water is about 3 to 5 times higher than that of soils. Thus, the specific heat of a medium depends very

significantly on its water content (Fromentin et al., 1997). Moreover, this variation of the specific heat according to the water content is linear until saturation for sands but it is not the case for clays (Cf. Figure I. 20)

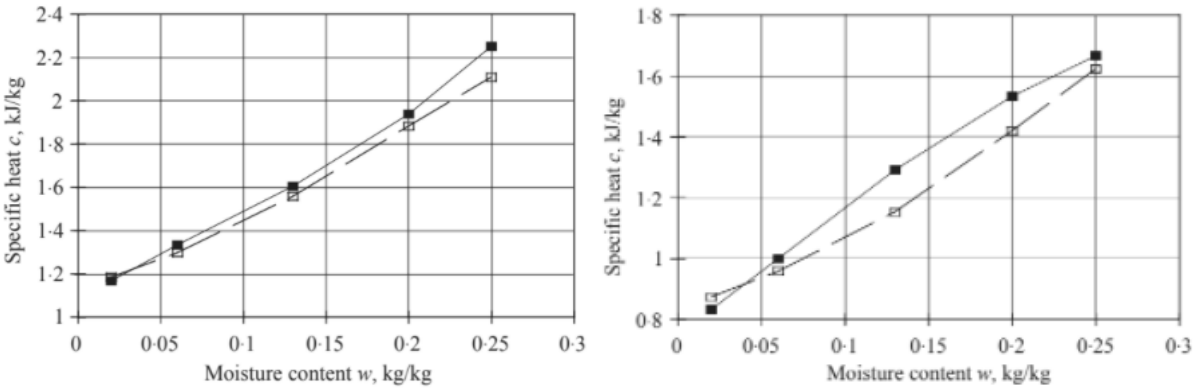

Figure I. 20 - Evolution of the predicted (□) and measured (■) specific heat capacity as a function of water content for clay (left graph) of density 1300 kg/m3 and sand (right graph) of same density (Abu-Hamdeh 2003)

Thus, in the vast majority of cases, the increase in water content leads to an increase in thermal conductivity and specific heat. It seems important to look at the thermal diffusivity which is expressed as the ratio of these two quantities and which characterizes the capacity of the soil to transfer thermal energy. Studies show that, for sands, the thermal diffusivity increases to a maximum value before decreasing and stabilizing on a plateau. In contrast, for clays, thermal diffusivity increases continuously with water content. This difference is explained by the fact that, for sands, the thermal conductivity increases strongly with respect to the specific heat for low values of water content. For clays, on the other hand, specific heat and thermal conductivity increase in the same proportions with water content (Abu-Hamdeh, 2003)

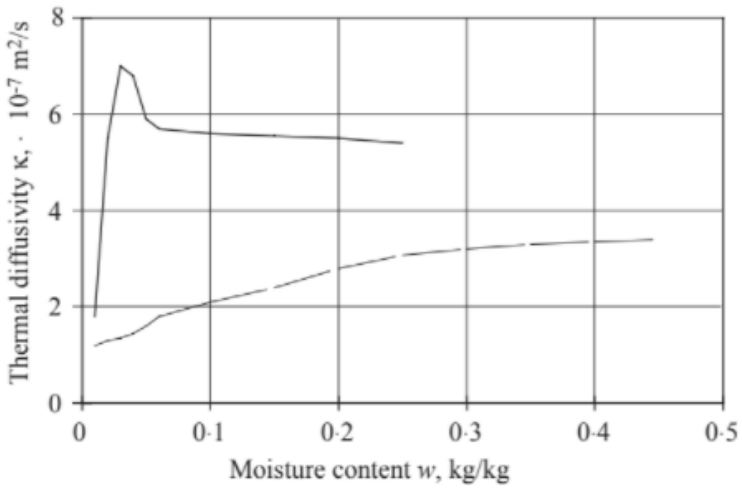

Figure I. 21 - Evolution of thermal diffusivity as a function of water content for sand (solid line on top) and clay (continuous line) - Abu Hamdeh 2003

It is also interesting to note that for the same water content, Kersten's model shows that thermal conductivity increases with dry density. Thus, when energy geostructures are used, they can lead to

localised drying, resulting in a reduction in the thermal conductivity of soils over time and, ultimately, a decrease in pile performance (Behbehani, 2020).

1.5.3. Influence of density

The dry density also influences the thermal conductivity of a soil. Indeed, following the same macroscopic reasoning, an increase in dry density leads to a greater number of soil particles in a unit volume and consequently to a greater number of contact points between grains. This increase in the number of inter-grain contact points results in a larger path for heat flow. In other words, the thermal conductivity of a soil increases with dry density (Salomone L.H., 1989). For sandy soils, the increase in thermal conductivity is almost linear with dry density. In contrast, for clay soils, the curves have an inflection point at a given density (See Figure I. 22).

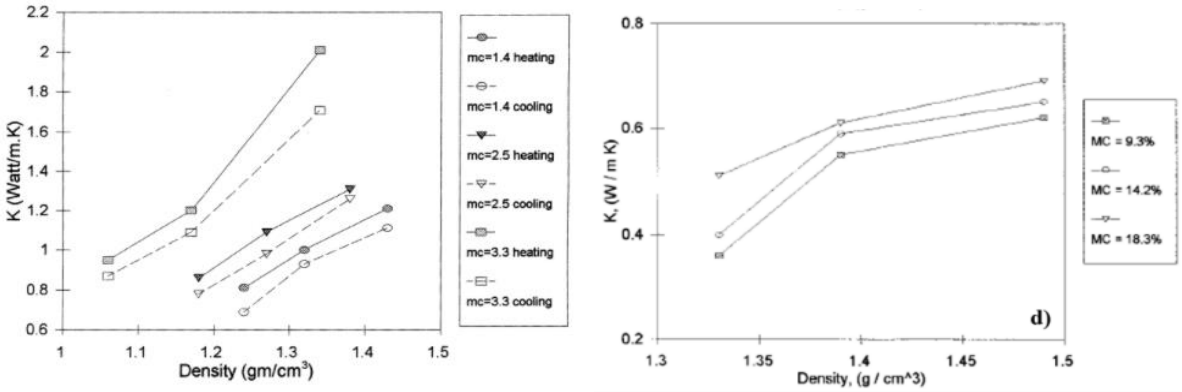

Figure I. 22 - Evolution of thermal conductivity as a function of density for different water contents and for two types of soil (sand on the left and clay on the right) - Abu Hamdeh 2001

The increase in density also increases the volumetric heat capacity of soils. This increase is linear for all types of soil, and is also true for zero moisture content (dry soil) (Abu-Hamdeh, 2003).

1.5.4. Thermal conductivity according to mineralogical composition

There are also approaches in which the thermal conductivity is approximated by averaging the thermal conductivities of the different mineralogical components of the soil. In 1963, De Vries proposed a formulation of the thermal conductivity of a soil as the weighted average of the conductivity of its components (De Vries, 1963):

$$\lambda_{sol} = \frac{\sum_{i=1}^{n} \lambda_i \times F_i \times x_i}{\sum_{i=1}^{n} x_i} \quad \text{(I.18)}$$

Where x_i (-) is the volume fraction of each component (mineral, organic matter, water, air...), F_i the De Vries factor (-), and λ_i the thermal conductivity. According to (Evett et al, 2012), this formulation tends to underestimate the values for soils with low water content. It is therefore advisable to increase the thermal conductivities obtained with this formulation by 25% for dry soils.

Similarly, the model of Brigaud and Vasseur, 1989 is also a model based on the composition of the soil by considering the three phases that are the skeleton, water and air. The formulation of the thermal conductivity of the soil is then:

$$\lambda = {\lambda_w}^{\theta} \times {\lambda_a}^{n-\theta} \times {\lambda_s}^{1-n} \quad \text{(I.19)}$$

With λ_w, λ_a, λ_s are the thermal conductivity of water, air and solid respectively (W/m.K), θ the water content by volume (-) and n the porosity.

Where $\lambda_s = \prod_i \lambda_i^{x_i}$ and x_i is the volume fraction of each mineral component and λ_i its thermal conductivity.

1.5.5. Conclusion

Water content and density to a lesser extent appear to improve the thermal properties of soils. Other parameters, to an even lesser extent, influence the thermal properties of soils. Many models, such as the Johansen model presented above, show the significant role of mineralogical composition on the thermal conductivity of the soil. In particular, quartz content increases thermal conductivity (Tarnawski, 2009). Conversely, an increase in salt and organic matter content decreases thermal conductivity (Abu-Hamdeh, 2000).

Finally, thermal conductivity also increases with temperature (Brandon and Mitchell, 1989), although this influence remains relatively small, especially considering the temperature ranges involved in geothermal energy. This result has also been shown more recently by thermal probe tests (Aljundi, 2020). The authors thus proved that the temperature and the heat flow increase the thermal conductivity as shown in the summary Figure I. 23.

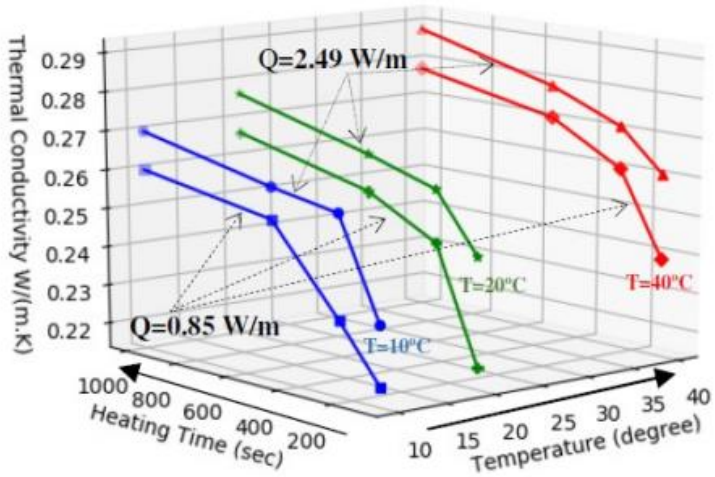

Figure I. 23 - Effect of heating and temperature on thermal conductivity of a specimen under dry conditions

1.6. Influence of groundwater flow

The French Geological and Mining Research Bureau (BRGM) indicates that the speed of groundwater flow in France varies from a few meters per year for low permeability groundwater to several hundred meters per year for the most permeable groundwater. Historically, the majority of towns were built close to watercourses and therefore in places where underground flow is very likely. Obviously, the presence of flow and its velocity depend locally on the fluvial regime and the alluvial stratigraphy. From a general point of view, the presence of groundwater flow induces heat exchanges no longer only by conduction but also by convection. This is energetically beneficial for

heat exchange, but more restrictive for energy storage in the ground. Indeed, the calories could be moved by groundwater whose flow may be modified by in-ground structures.

1.6.1. Dam effect

In a soil, an aquifer will have its flow modified when it runs into geotechnical structures. This change in flow, called the dam effect, depends on the geometry of the construction, the hydrodynamic properties of the aquifer, the angle of incidence and the cut-off height of the water table (Delerablée, 2019).

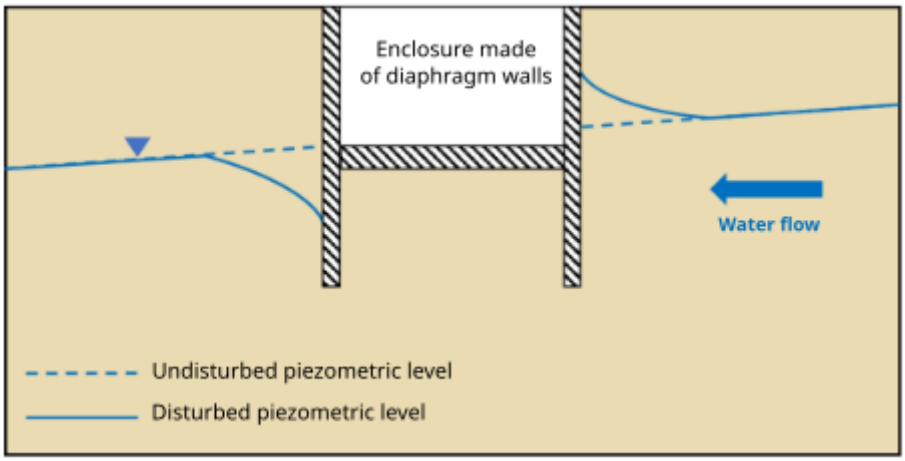

Figure I. 24 - Dam effect for an enclosure made of diaphragm walls (Delerablée, 2019)

The Figure I. 24 shows that the dam effect increases the piezometric level upstream and decreases it downstream, which results in a modification of the water flow velocity in the ground. For instance, in the case of a diaphragm wall box, the downstream velocity can therefore decrease by 100% when an acceleration of 300% can be reached upstream in the angles of the structure (Delerablée, 2019). Obviously, this effect weakly affects the piles but concerns especially the big structures such as the diaphragm walls or the tunnels.

1.6.2. Improvement of heat exchange

Just as the presence of water has previously been shown to improve the thermal conductivity of the ground and therefore decrease its thermal resistivity, the flow of water is considered to improve the apparent thermal conductivity. This assumption is experimentally verified in the in situ tests (TRT) (Fromentin, 1999). In the Figure I. 25, it appears that below a certain velocity ($0.1\ m/day$), the thermal exchanges are weakly affected. Above a value of $10\ m/day$, the benefit reaches a threshold. This result is valid for energy piles because the velocity field surrounding them will be globally homogeneous. For larger structures, the dam effect means that each segment will behave differently.

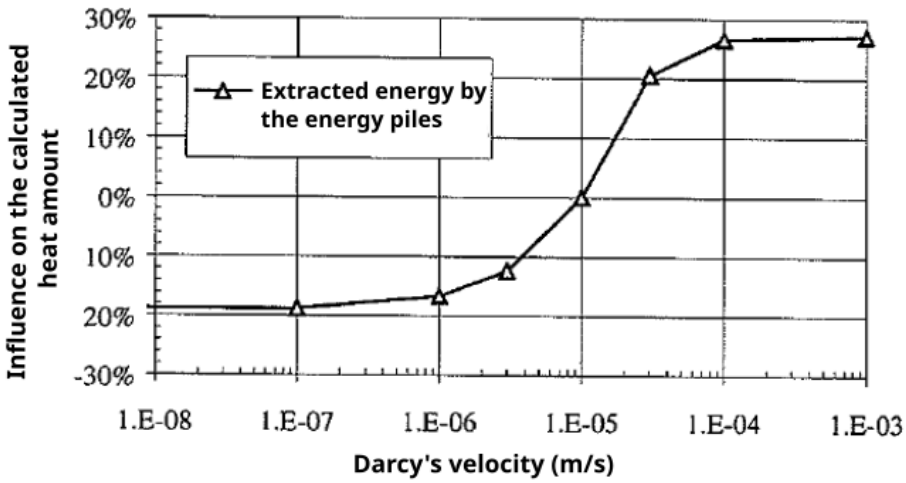

Figure I. 25 - Effect of flow on the amount of heat removed by an energy pile (Fromentin et al, 1999)

Likewise, studies were led for tunnels segments in order to estimate the thermal power that they can exchange with soils (Barla, 2023). These numerical studies also show that the presence of ground water flow leads to greater exchanged thermal powers. They therefore provide charts which give the thermal potential of the ground according to groundwater flow velocity, soil temperature and thermal conductivity (See Figure I. 26).

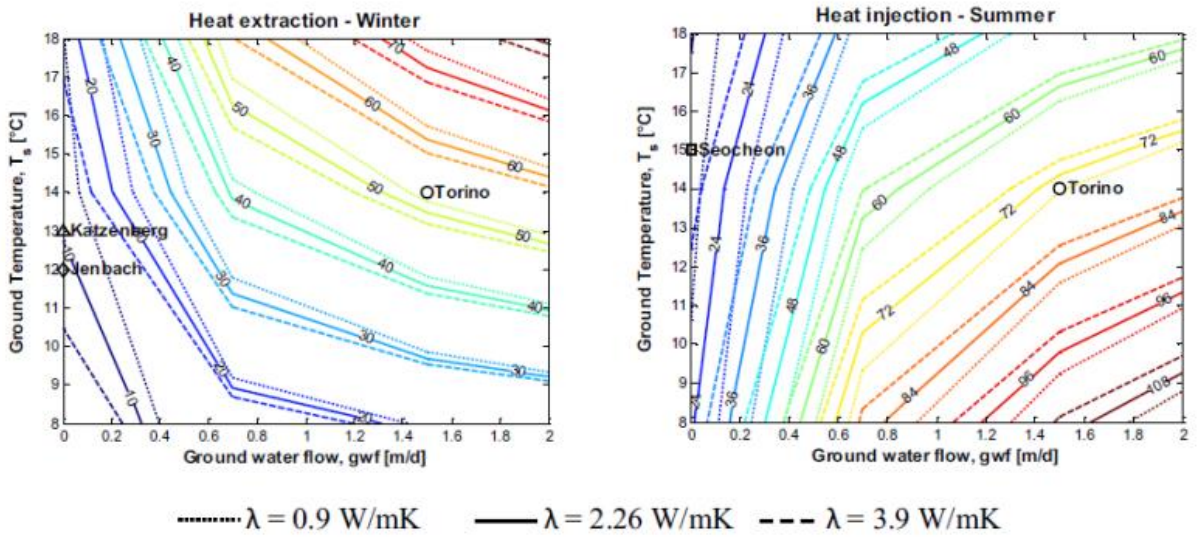

Figure I. 26 - Influence of flow velocity on thermal performances of energy tunnels (Di Donna, 2016)

1.6.3. Soil washing and Thermal affected zones (TAZ)

Without any groundwater flow, an unbalanced need for heating or cooling will lead to a change of soil temperature, called thermal drift. This latter can be multi-year or seasonally established (e.g., injection of heat into the soil during the whole summer) and reduces the energy efficiency of the system. For instance, a study investigated a small-scale experimental model as a method of simulating the behaviour of large-scale unconfined aquifers for thermal storage. Thermal energy was stored by injection to simulate potential large-scale heating and cooling demand scenarios. Thermal efficiency was found to be better with the addition of a storage period (Charlwood & Madabhushi, 2021). Implanting energy geostructures in a soil where groundwater flow is present will have the

effect of thermally washing the soil and thus avoiding thermal drift. In this sense, the presence of flow is beneficial and this benefit will be studied more precisely later in this thesis (Cf. Chapter III.3).

This thermal washing is therefore locally beneficial but, by definition, the advection phenomenon by which it takes place moves the thermal anomaly further downstream. Thus, another area can be affected by this problem and the question regarding the interactions should be taken into consideration. Indeed, local thermal anomalies can lead to a waste of underground energy or affecting the efficiency of other energy geostructures located downstream (Barla et al., 2018; Badinier et al., 2020, 2022; Ouzzine et al., 2022).

In addition, groundwater must be protected and excessive temperatures must be avoided. Geothermal potential maps are tools for land use planning and development at the city or district level. However, few of them take geothermal operations into consideration. A study conducted (Barla et al., 2018) aimed to implement a hydro-thermal model at the scale of a neighbourhood to account for the resulting situation of thermal exploitation of the soil. The findings of this study show that heat plumes are more persistent than cool plumes. Thus, the thermal alteration is more pronounced at the end of the summer. In this study case, there are significant variations throughout the year that can affect the efficiency of the different pumps (open or closed loop). This must be taken into account when designing pumps or when installing a new system.

Thermal variations are mainly limited to the surroundings of the installations. However, over a longer period of time, heat plumes can persist and give rise to heat affected zones called TAZ (Thermal affected zones). Their size and shape depend on the soil permeability and seepage velocity as demonstrated in a numerical study (Pannike, 2006). Indeed Figure I. 26 shows that a low groundwater flow will produce a small and circular plume while a high flow will induce an elongated and narrow plume. Physically, an analogy can be drawn between the shape of the plume and the predominance of advection over conduction. This ratio is expressed in the dimensionless Peclet number. When this number is large, for example, it means that advection prevails, suggesting a long, thin plume (Cf. Chapter II).

Furthermore, energy piles are commonly built in groups for structural purposes; therefore several energy piles might draw their energy from the same thermal reservoir. In such cases, the thermal anomaly of each pile will have a cumulative effect on the global efficiency, decreasing the COP factor. In the case of pile groups, one can expect that the effect of thermal clusters will increase while the piles are built closer to each other (Di Donna et al., 2016; Lou et al., 2021). According to Fujii et al. (2005), the optimal distance between two geothermal sources should be 3 to 6 m. However, according to French and European mechanical design rules (Burlon et al., 2017; Brach et al., 2014), inside pile groups the distance between two pile should be less than 3 diameters, i.e. around 2 m.

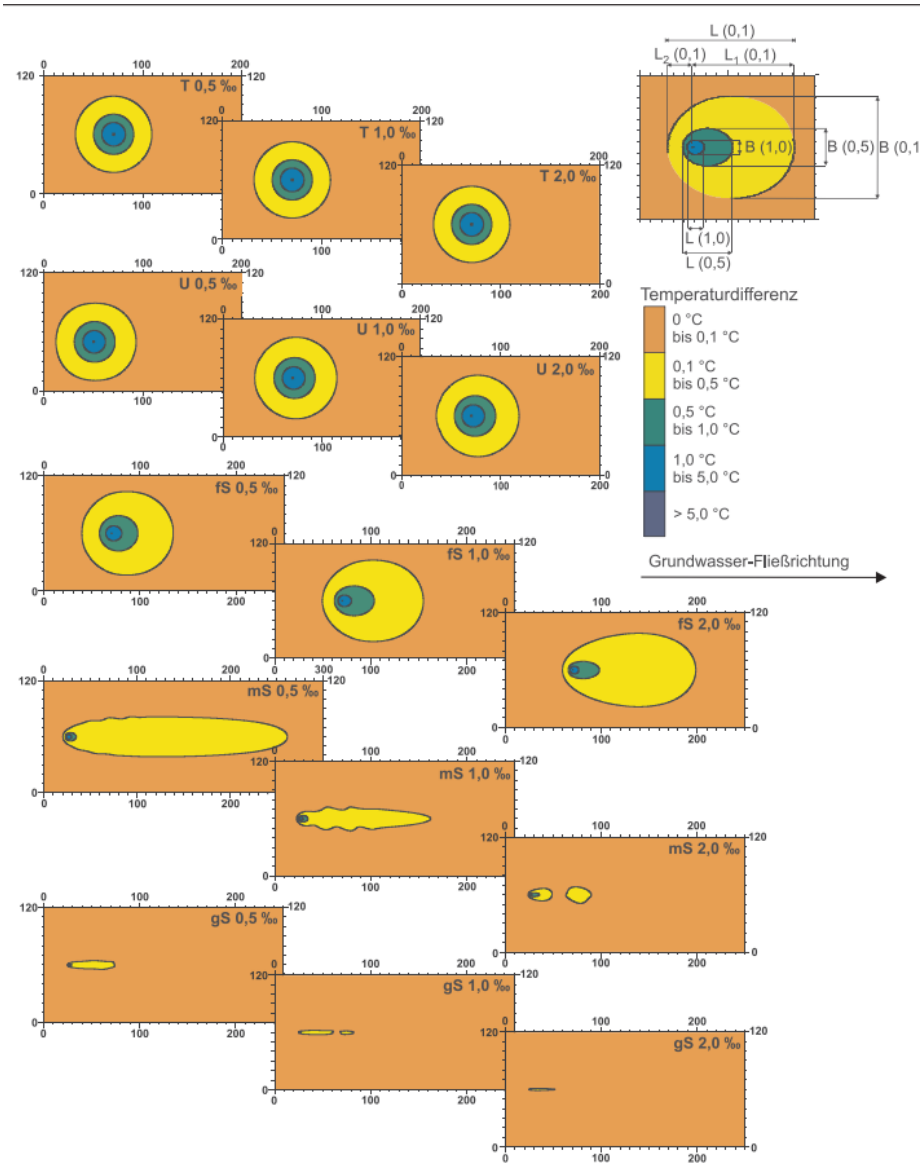

Figure I. 27 - Temperature fields around a vertical geothermal probe at the end of the 30th heating season for five different permeabilities and three hydraulic gradients 0.5%, 1% and 2% (Pannike, 2006)

Taking into account all the aspects previously mentioned, the identification of the TAZ should allow the design or even the authorisation of new installations. Indeed, the thermal variations of a soil must not be excessive and this limits the heat transfers carried out. The model developed by Barla et al. (2018) can be improved by taking into account the geology and hydrology of the city which have been simplified in their approach. Once again, the importance of the existence of data is highlighted. They finally allow the use of shallow geothermal energy in urban areas to be developed. The use of geothermal heat is not strictly framed by law. However, some recommendations have been established within a national framework in Switzerland, France, UK, and Austria for example ((CFMS, 2017), (SIA, 2005)…).

2. Mechanical response of the energy geostructures under thermal loading

In a general way, when an object is heated (or cooled) it expands (or contracts) according to its coefficient of thermal expansion. In the case of an energy geostructure, the latter is not free to deform because it interacts with the soil and the rest of the structure. Thus, the thermal load applied to the structure will induce deformations but also stresses which correspond to the deformations prevented. A study based on a database for energy piles reports that induced stresses are in the range between 50 to $300\ \mathrm{kPa/°C}$ and the thermally induced displacements vary between 0.01 to 0.15 mm/°C (Di Donna, 2017). It corresponds to an additional constraint that is not taken into account in the safety factors at the design stage in standard engineering procedures.

2.1. Impact of temperature on soils

2.1.1. Volume deformation

Temperature exchanges during the use of geostructures can induce soil volume variations. Indeed, studies carried out using thermal oedometers (Di Donna & Laloui, 2015) and triaxial devices Cekerevac & Laloui (2004) have shown that subjecting clay to a temperature increase from 25 to 90°C induces volume variations. It appears that the volume variation depends on the loading history of the clay but is independent of the plasticity index. They also investigated the impact of temperature on the mechanical behaviour of saturated clay. For this purpose, tests were carried out on Kaolin clay in a thermally controlled triaxial apparatus. The temperatures applied vary between 22 and 90°C. The volume deformation is calculated by measuring the volume of water expelled from the sample during a heating test in a drained configuration. It appears that the thermally induced volume strain is dependent on the stress history of the sample (OCR) as shown in Figure I. 28. Heating normally consolidated specimens leads to contraction. Slightly over-consolidated specimens show less contraction during heating. Finally, heavily over-consolidated specimens show expansion on heating. The OCR values for which the soil changes from contracting to expanding behaviour depend on the soil type.

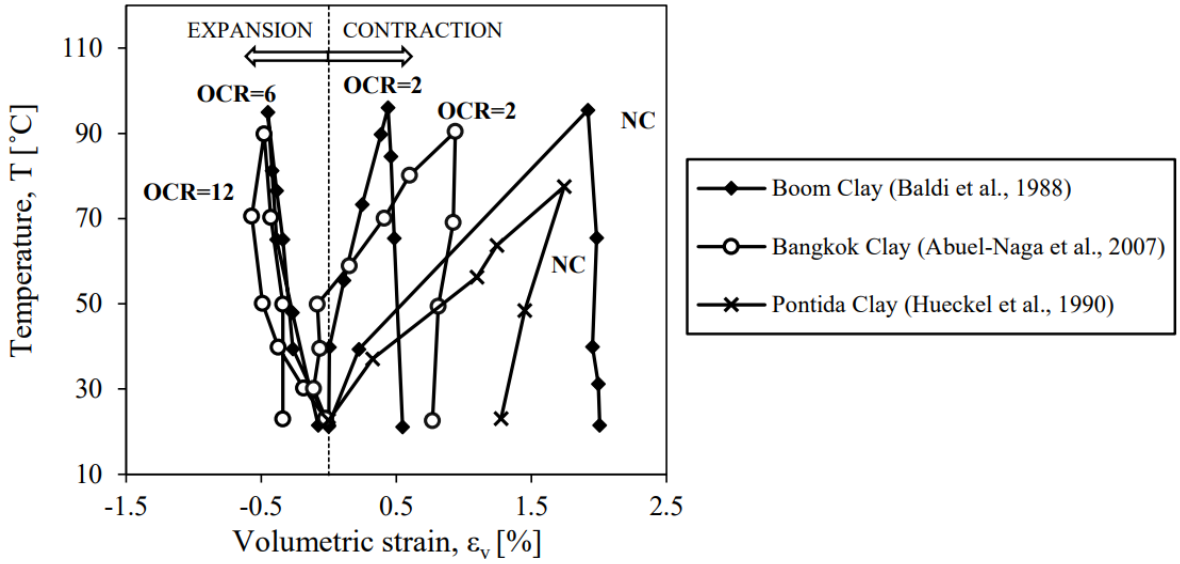

Figure I. 28 - Volumetric behaviour of heated clays (Casarella, 2021)

The volume variations can be explained by the effect of temperature on the electrochemical forces between particles (Abuel-Naga, 2007; Casarella, 2021). Indeed, for over consolidated clay soils, the clay particles are positioned in a face to face configuration. The increase in temperature induces a decrease in the reversible binding forces which therefore creates a thermo-elastic dilatation. In contrast, clay particles in normally consolidated soils are in a face to edge configuration. The increase in temperature induces a rupture of the Coulomb bond and thus a thermo-plastic contraction because it is not reversible (Casarella, 2021). The increase in temperature therefore induces a lowering of the apparent pre-consolidation pressure, which leads to a consolidation mechanism.

Sands are much less sensitive to temperature variations in their volume deformation. Those relatively small variations are attributed, in the temperature range of 20°C-100°C, to the thermal expansion of the individual grains which induce deformation through grain rearrangement and results in irreversible contraction at high relative density (Agar, 1986). However, it happens that reversible expansion is observed under heating for other experiments (Liu, 2018). These differences in behaviour are attributed to transient dynamics of heat diffusion (Coulibaly, 2022). Sand subjected to quasi-static and uniform thermal loading under no experimental conditions expands according to its intrinsic coefficient of thermal expansion. However, in some special cases where the thermal loading is dynamic and the sand is in a loose state, thermal contraction can be observed with relatively small values. In the very likely case where the sand is subjected to cyclic thermal loading, the alternation of contraction and expansion leads to an overall contraction (Ng, 2016).

Temperature also induces a change in pore pressures (Abuel-Naga, 2007). The thermally induced pore pressures depend on the effective stress applied during the heating phase and the loading history during the cooling phases. Indeed, in this study, the authors explain the effects of temperature on pore pressures in Bangkok clay. Firstly, the thermal expansion of the water contained in the clay induces a thermal expansion of the soil, impacting pore pressures in response to the change in soil volume. Secondly, the change in pore size induced by the thermal load leads to a consolidation effect. This diffusion of pore pressures obviously depends on the previous state of consolidation of the clay. Variations in pore pressure therefore depend on both the state of consolidation (i.e. the prior mechanical load) and the thermal load. This study does not mention it,

but we can imagine that the heating rate also plays a role in the sense that a slow thermal load (just like a slow mechanical load) would prevent the creation of pore pressure.

2.1.2. Mechanical properties

The French recommendations (CFMS, 2017) suggest that, given the temperature ranges involved in the use of energy piles (1-35°C), no variation in the mechanical parameters of the soil and the structure is taken into account in the design. For higher temperature ranges (up to 90°C), studies show that the mechanical parameters undergo some variations:

- Pre-consolidation pressure
  It decreases with increasing temperature (Tidfors M, 1989). Indeed, in order to analyse the effect of temperature on the pre-consolidation pressure for Kaolin clay, 4 consolidation tests were carried out for different temperatures.
- Friction angle
  The fiction angle appears to be independent of temperature as demonstrated by studies on thermal shear boxes (Di Donna A., 2016) and triaxial test (Cekerevac, 2004) s
- Cohesion
  It increases with temperature (20-60°C) for Kaolin clay (Maghsoodi, 2020)
- Compressive index C_c and swelling index C_s
  They were shown to be independent of temperature (Lahoori, 2021)
- Elastic modulus
  The elastic modulus appears to increase with temperature (from the deviatoric stress vs. volume deflection curves) (Cekerevac, 2004).
- Ménard modulus E_m and limit pressure p_l
  These design parameters of energy piles are based on the results of Menard pressuremeter tests carried out in situ (AFNOR, 2000). They are widely used in France to design foundations. The variations of these parameters with temperature have been studied in laboratory thanks to a mini pressuremeter, and it appears that the limit pressure decrease when temperature increases, but the pressuremeter modulus remains quite insensitive to these variations. In France, they find extensive application in foundation design. The influence of temperature on these parameters has been investigated in laboratory settings using a mini pressuremeter (Arairo, 2022). The findings indicate that as temperature rises, the limit pressure decreases, but the pressuremeter modulus remains relatively unaffected by these temperature-related changes. Similar results show the decrease of yield limit with temperature with triaxial tests on sand (Lingnau, 1996), and unsaturated silt (Uchaipichat, 2009). These different results converge towards the idea of a thermal softening behaviour of the soils when temperature increases.

2.2. Effects of temperature on full-size structures

2.2.1. Isolated energy piles

2.2.1.1. Theoretical framework

In general, when a pile of length L, totally free to deform, is subjected to a temperature difference ΔT, it undergoes a deformation $\varepsilon_{th} = \alpha \Delta T$. Assuming that this pile is totally constrained (all deformation is prevented), the thermal load induces an axial mechanical stress $\sigma = E\varepsilon_{th} = E\alpha\Delta T$ (with E the Young modulus of the pile). For a pile buried in soil, any thermally induced deformation is partially prevented by mobilising resistance of the soil-pile interface. An end bearing pile is expected to expand upwards when subjected to thermal loading. A floating pile is expected to expand from its centre in both directions (up and down). Thus, a semi-floating pile is assumed to have an intermediate behaviour. The point from which the foundation expands, whose displacement is null, is called the zero point (see Figure I. 29)

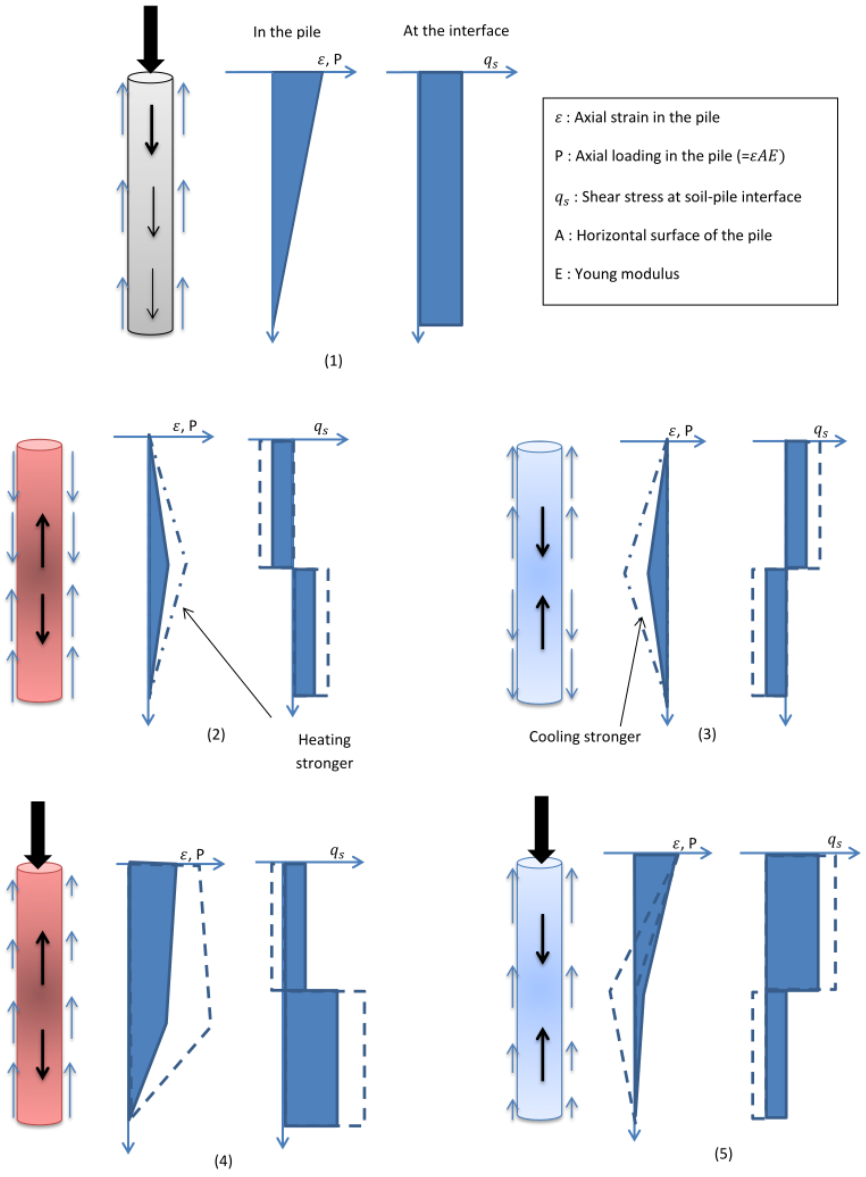

Figure I. 29 - Energy pile response mechanisms (Bourne-Webb, 2009)

The Figure I. 29 presents the different energy pile response mechanisms in the form of 5 main cases:

1. Floating pile subjected to head loading
   In this simple model, the pile is in compression and the mobilised lateral resistance is constant along the pile and therefore the stress decreases from the surface to zero.

2. Floating pile subjected to heating
   The pile will expand on both sides of the zero point which corresponds to the middle of the pile. The upper part tends upwards and the lower part tends downwards. The resistance mobilised opposes these deformations and will therefore be negative on the upper part and positive on the lower part. The pile undergoes compression, and the stress here is also maximum at the zero point and zero at the pile ends.

3. Floating pile subjected to cooling
   This is the opposite of the previous case, the pile contracts and the mobilised friction will act in opposition to the deformation. Thus, the mobilised friction will be positive on the upper part of the pile and negative on the lower part. In the whole pile, a tension will appear which is maximal at the zero point and zero at the ends of the pile.

4. Floating pile submitted to mechanical loading and heating
   This is a combination of cases 1 and 2. Thermal expansion will increase the compression level of the axial load and the lateral resistance mobilised will be lower in the upper part of the pile whereas it will increase in the lower part of the pile.

5. Floating pile submitted to mechanical loading and cooling
   This is a combination of cases 1 and 3. The axial loads become less compressive and more tensile. The mobilised lateral resistance therefore increases at the upper part of the pile and conversely at the lower part. In this case, as in case 4, the zero point is no longer located in the middle of the pile, its position depending on the mechanical load.

2.2.1.2. In situ measures

In 2009, a 23 m energy pile test was carried out at Lambeth college, London (Bourne-Webb, 2009). This energy pile was instrumented with optic fibre in order to measure the axial strain distribution. The pile was in a clay soil and axially loaded. Strain gauges (18 vibrating strings) were used to instrument the pile in order to compare the results with those from the optic fibre. Indeed, two types of optic fibre sensors were used: one to measure deformations, the other to measure temperature. In addition, two methods of placing the optical fibre were used: gluing the fibre along the reinforcement bars and suspending the fibre between the top and bottom of the pile. In both case, the fibre is embedded in the concrete. It was shown that the technique used did not impact the results (Amis et al., 2008). For heating, an 8kW heat pump was used at maximum power in the heating and cooling phases, i.e. an imposed fluid temperature between -6°C and 56°C.

The coefficient of thermal expansion was obtained by studying the evolution of deformations as a function of thermal load at the pile head where friction is assumed to be minimal. A coefficient of $25.10^{-6}\ °C^{-1}$ is obtained. During loading, it is clear that the pile does not behave as a free pile and the impact of the surrounding soil is highlighted. Indeed, only 40% of the theoretical thermal expansion is measured (and respectively 60% of the theoretical contraction) during the heating

phase (respectively during the cooling phase). It is interesting to note here that the subsoil initially had an average temperature of 19°C, which is higher than normal. The authors attribute this observation to the activity of the nearby London underground trains.

Furthermore, differences in measurements were observed between the thermocouples and the optical fibre. The authors attribute this difference to the proximity between the optical fibre and the heat exchanger tubes inside the pile. At a distance of 0.5 m from the pile, the measured temperature variations are already divided by two and at a distance of 2 m, these variations become negligible. From a depth of 5m, the temperature distribution is homogeneous over the depth. The design of a heat pump is based on the assumption that the pile behaves like an infinitely long wire and the symmetry of the temperature field around the pile shows that this is an acceptable simplification. Finally, the thermal conductivity value of $1.5\ W/mK$ frequently used for London clay was confirmed by a thermal response test.

Concerning the deformations measured during the thermomechanical phase. They are observed to be higher at the end of the heating phase than in the mechanical loading phase only (before thermal loading). This suggests that the axial stress supported by the pile is greater than that applied at the head. Temperature changes increase the lateral resistance forces involved. However, it does not seem necessary to take this into account when designing the piles as it is assumed that the safety factor applied is sufficient to ensure that no significant permanent displacement takes place as a result of the thermal load.

In terms of stresses, in accordance with the theoretical framework, during the cooling of the pile, axial tension at the foot is observed. However, given the temperature ranges considered, it is very unlikely that cracks will appear due to thermal loading. Furthermore, the high weight of the building and the rigidity of the soil on which the pile rests explain the increase in axial stresses during the heating phase, as the pile was not allowed to expand. The importance of the floating or non-floating character of the pile is then highlighted.

The results measured during the heating and cooling phases are in agreement with the simple theoretical cases. This confirms the thermo-elastic behaviour of the pile as suggested by a previous study (Laloui, 2006). In other words, the variations observed in the response of an energy pile to thermal loading are purely due to thermal expansion and are reversible. The pile response obviously depends on the head and pile stress conditions. In the case of this study, the geothermal pile tested belongs to a group of mixed foundation piles and is the only pile to be thermally loaded. Therefore, it is very likely that the results are overestimated compared to a case where other piles are active. Especially since the thermal load applied here is higher than would be the case with normal use of the heat pump (for real needs).

Indeed, by testing a 25 m long pile in over-consolidated clay, Laloui et al (2004, 2006) observe increases in axial thermal stress with depth. By heating this pile to 21°C, an upward displacement of the pile head of 4.2 mm takes place. Another instrumented energy pile was installed during the construction of an EPFL building and thermally tested under different mechanical loads corresponding to the construction of the different floors. The axial response was measured with fibre optics, strain gauges and a load cell at the base of the pile. The final mechanical load was 1300 kN and the results show that under this mechanical load, a 15°C increase in the pile almost led to a doubling of the load at the base.

Murphy & McCartney (Murphy, 2014) also conducted in situ tests on the energy performance of two piles in soil consisting of a sand layer underlying a clay layer. These piles were 14.8 m and 13.4 m long and were subjected to temperature variations between 7°C and 35°C for 2 years. A relative displacement of 0.2%D[3] was measured. This low value is explained by the small size of the piles and also by the fact that they were constrained by the clay layer.

McCartney and Murphy also evaluated the stresses and strains induced in a pair of 12.7 m long piles supporting an 8-storey building during heat pump operation (McCartney, 2012). The largest axial compressions (respectively axial tractions) were measured at the pile toe during pile heating (respectively cooling). Later on, in 2015, they characterised the soil-structure interaction by studying three end bearing piles in sand and showed that the heat-induced mechanical effects (stresses and displacements) depend on the conditions at the head of the pile (Wang, 2015).

More recently, a full-scale in situ experimental study on the bearing capacity of energy piles under temperature and multiple load levels was carried out in Shanghai (Wang, 2023). They studied the impact of mechanical load on thermally induced mechanical response of 6 energy piles of 30 m in clay soil and found out that a larger mechanical load leads to a lower influence of temperature on settlement and axial force variations. Indeed, a heating load creates thermal expansion which induces negative skin friction. And, the greater the head load, the greater this negative friction is compensated (by head settlement). Likewise, during a cooling stage, the thermal shrink induces greater positive skin friction the higher the head load. Namely, by increasing the mechanical load level, the impact of heating or cooling on the axial force of the pile is reduced. This comes from a decrease in the negative skin friction induced by heating and an increase in the positive skin friction caused by cooling. They also found out that the temperature change did not create excess pore water pressure.

2.2.2. Group of piles

Within a pile group, the thermal expansions induced by the activation of one or more energy piles are not only constrained by the interaction with the soil as it is in the case of an energy pile alone. In a pile group, the structure that connects the piles together will affect the behaviour of the group. Indeed, it will constrain thermal expansion or even diffuse it from an energy pile to a non-energy one. Therefore, depending on its stiffness, the number and the configuration of the thermally active piles, the behaviour of the group is likely to change.

The Sept-Sorts wastewater treatment plant represents one of the rare examples of a real case study in France (Borely, 2017). The study of a building resting on 102 piles, half of which are equipped with heat exchangers, was carried out using three different methods:

- The first method consisted in considering piles with springs at their head with certain rigidity, reflecting the fact that the pile is embedded in the supported structure. This is equivalent to considering each of the piles independently, as if there is no group effect and that each of the piles were isolated.
- The second method is to represent the pile group by a stiffness matrix obtained from a finite element model of the structure. This time there is a dependency and therefore mechanical interactions between the different piles via the stiffness matrix that represents the structure.

[3] 0.2 percent of the diameter

- The third model is similar to the previous one, but the stiffness matrix is obtained from an equivalent plate model. This last matrix, a priori less precise, is much easier to access.

The soil/pile interaction has been taken into account with a "t-z" type law allowing taking into account the thermal loading cycles. It also appears that non-energy piles are also indirectly thermally loaded because of their connection to the group and that the interaction is complex when there is a strong contrast in stiffness between the pile and the floor. Figure I. 30 illustrates this phenomenon.

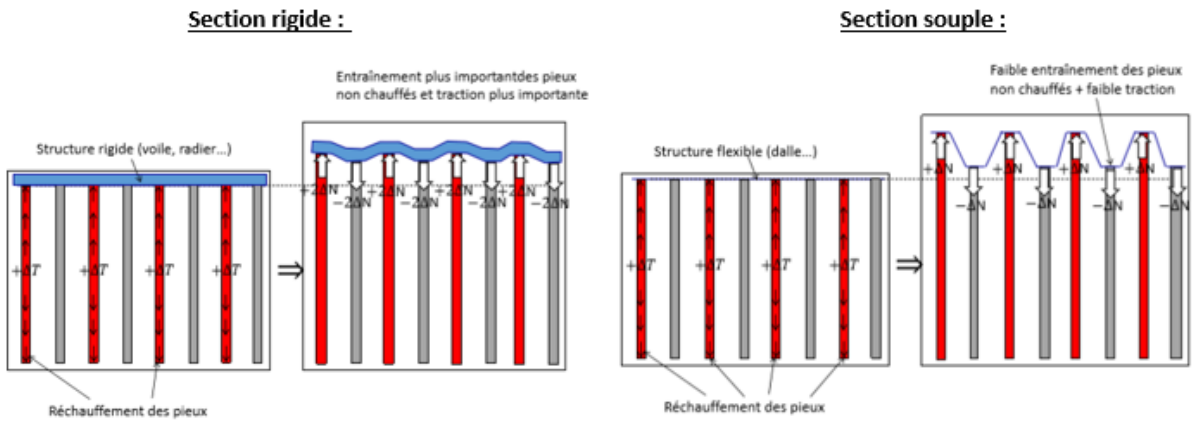

Figure I. 30 - Relationship between the stiffness of the structure supported by energy piles and the traction induced in non-energy piles

In addition, the instrumentation of this wastewater treatment plant over two years: one year before the piles were activated and one year afterwards, led to the conclusion that the thermally induced deformations were not as high as in the case of the were activated and one year after, concluded that thermally induced deformations remained in the elastic range of concrete (Vasilescu, 2019). Indeed, to understand better the impact of cyclic thermal loads on energy foundations, an experimental campaign was carried out to measure deformation and temperature under real conditions. In this project, 45 of the 100 foundation piles were fitted with heat exchanger tubes to meet 100% of the building's energy demand. The temperature and deformation trends of three piles were monitored for 18 months. The results show that the thermally induced deformations are small, in the same order of magnitude as those caused by seasonal variations (Vasilescu, 2020)

Finally, a study case should be mentioned here insofar as it presents the particularity of working on a group of four energy piles on which a crane stands (Fang, 2022). In reality, such a small group is rarely encountered, whereas in the study of a reduced model, and for the sake of technical ease, this is much more frequent. It is very interesting to note that comparable results emerge from this study on real-size energy piles with the studies on reduced scale models. These results notably include the observation of ratcheting settlement (expressed as ratcheting compressive stress “due to drag-down effect of the surrounding soil on the energy piles”) during thermal cycles. The phenomenon is more pronounced in compressible soils. The authors also identify group tilting caused by the non-symmetry of the thermal loading.

2.2.3. Numerical Hydro-thermo-mechanical (HTM) models

The results and methods presented in the previous sections provide information on the design of simple energy geostructures. For more complex ones or if one wants to study more detailed phenomena, it is often crucial to use adapted numerical models.

To the current research, a large number of works have been carried out, notably to focus on the energetic aspect of the energy geostructures; they have made it possible to obtain long-term energy efficiency or feasibility results. They, for example, allow:

- Evaluating the influence of design and operating parameters such as concrete thermal conductivity, pile diameter, and flow rate on the energy piles thermal performance (Carotenuto, 2017)
- Analysing the thermal resistances of piles and obtaining an empirical relationship for its calculation ((Loveridge, 2014)
- Simulating circulating fluid in order to study the sustainability and efficiency of energy tunnels in long term (Barla, 2016) and suggest that the influence of energy tunnels on the ground is limited if the system is used both in winter and summer (Barla, 2016)

The study of mechanical behaviour by numerical modelling is less widespread although very useful for studying THM models complex in terms of geometry, loadings or couplings they involve. Thus, studies focused on the thermomechanical response of energy geostructures during the continuous and cyclic extraction or injection of heat from or into the ground and including the different technologies such as energy piles (Laloui, 2006) (Salciarini, 2013), (Batini, 2015), (Bourne-Webb, 2009)), energy tunnels ((Barla & Di Donna, 2018)) and energy diaphragm walls ((Dong, 2019), (Makasis, 2020)). They use different modelling approaches in which the behaviour models or interface models can vary. In general, and justifying this by the fact that the temperature ranges are small enough not to create large deformations or plastic deformations in the soil or structure, the various materials are assumed to be isotropic, elastic and linear ((Dong, 2019) (Salciarini, 2013)). Moreover, no specific interactions are considered between the in-ground structure and the soil ((Batini, 2015) (Salciarini, 2013)). The numerical model can also be used to confirm certain mechanism such as the soil-pile interaction during thermal cycles on energy piles (Nguyen VT, 2020). Moreover, some notable studies are presented below.

i) Through a 3-D THM finite element simulation, it was shown that the mechanics of tunnels operating as heat exchangers is governed by the internal airflow conditions of such structures, the air tunnel-soil temperature differential and the tunnel-soil stiffness ratio (Rotta Loria, 2022). In this case, the modelling allows simulating the complex phenomenon that is the dynamics of airflows which characterizes the underground built environment.
ii) Another three-dimensional numerical model allowed capturing the various aspects of transient heat transfer, and to assess the transient and steady-state behaviour of energy piles in a number of design situations. This has made it possible to understand the role of interaction between pipes, which cannot be studied systematically using standard methods (Loveridge, 2016).
iii) A four energy piles group model subjected to cyclic non-symmetrical thermal loading in soft clay has been studied through 3D numerical parametric study. The aim was to investigate the influence of pile head restraint due to cap rigidity on the behaviour of the group settlement

and cap tilting, redistribution of axial load and bending moment along piles. The main results are the followings (Farivar, 2023). First, the greater the number of thermally active piles, the greater the induced settlements (all other things being equal). Secondly, the tilting between active and non-active piles is greater the softer the raft connecting the piles. The maximum tilting is reached when two piles are active and with the softer cap. Finally, the authors' conclude that the induced tensions along the energy pile should be considered during design.

2.3. EXPERIMENTAL MODELLING OF ENERGY PILES IN CENTRIFUGE

Centrifuge testing is a complementary method to in situ testing, with the advantage of being faster, less costly (although requiring access to a centrifuge), allowing tests until failure, and with better control of the parameters. As a result, a significant number of results in the literature come from centrifuge studies, which have also been used to validate numerical models. As shown in Figure I. 31, centrifuge tests are used in geotechnical engineering to understand certain failure phenomena when the mechanical behaviour of the soil is not very well known or when the complexity of the structure requires a comparison of experimental and numerical results. Among the advantages that centrifuge modelling brings to geotechnical engineering (Madabhushi, 2015), the main one in the study of energy constructions is that it makes possible to create accurate models and carry out repeatable tests to increase confidence in the results obtained and the behaviour observed.

To work with centrifuges in geotechnical engineering and interpret observations correctly, particular attention must be paid to the scaling laws. These will be presented in detail in Chapter II. In this section, we simply look at the various centrifuge studies regarding energy geostructures and present the main results.

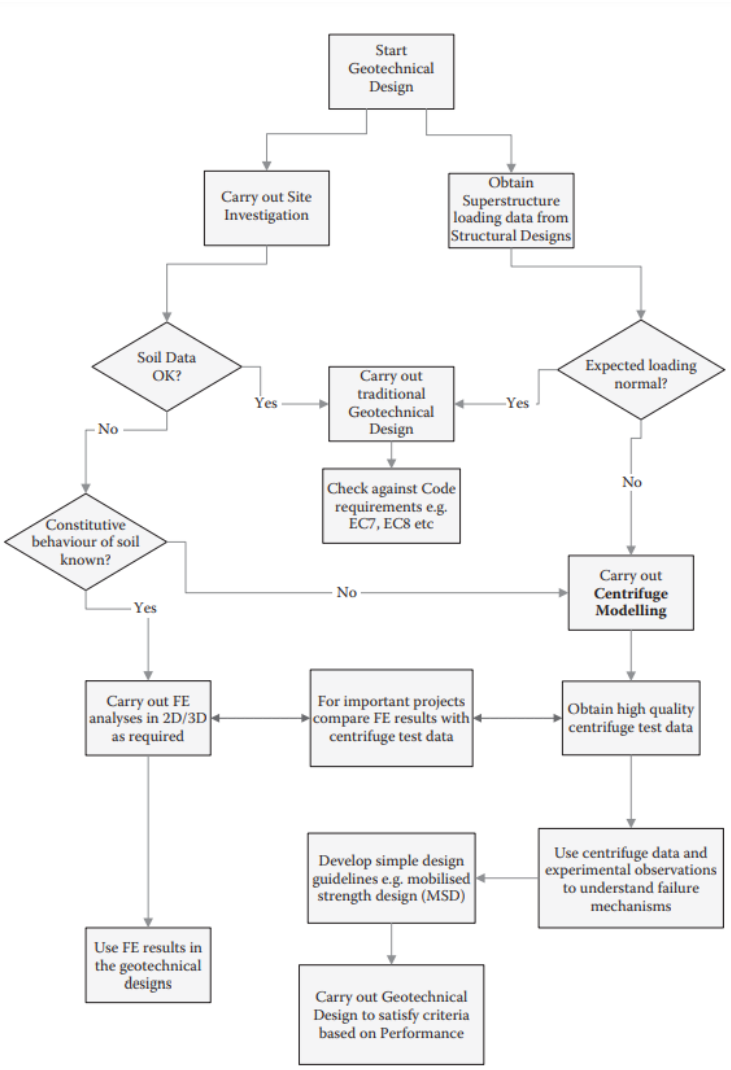

Figure I. 31 - Simplified flow chart for geotechnical design (Madabhushi 2015)

2.3.1. Model selection

First of all, it is interesting to note that among the different types of thermal geostructures presented above (piles, tunnel segments and retaining walls), only piles have been studied in centrifuge. This is because energy piles are probably the first and most studied energy geostructures, due to their geometric proximity with geothermal probes, which are more commonly used in the construction industry. Staying on the geometric issue, one of the advantages of centrifuge modelling is that one can choose and control the geometry of the model. The main criterion for the pile geometry is the acceleration that will be imposed in the centrifuge. Indeed, by applying a centrifugal acceleration of $\mathrm{N} \times g$, the reduced size model pile simulates a full-scale structure whose dimensions are N times larger according to the scaling laws (see chapter II). The slenderness of the model pile is therefore preserved. For example, by imposing a centrifugal acceleration of $24g$, on model piles of $63.5\ mm$ diameter and length of $343\ mm$, Goode & McCartney (2014) modelled piles of $1.5\ m$ diameter for length of $8.2\ m$. This model pile diameter is larger than the pile used in previous experiments in order to increase the space around the on-board instrumentation although $1.5\ m$ diameter piles are not common in Europe (Reiffsteck, 2023). Mechanical and thermal interactions should also be taken into consideration. Obviously it depends on the loadings, but a sufficient distance between the pile and the side edges (more than 4 diameters) and between the bottom of the pile and the bottom of

the box (8 diameters) should be respected (Zhao et al., 2020). Indeed, the thermal interaction between the box containing the model and the exterior is an important element taken into account in most studies of geostructures in centrifuges. Thus, metal boxes can be thermally insulated beforehand (Goode & McCartney, 2015; Ng, 2014) to minimise heat transfer with the exterior.

Secondly, another of the advantages of centrifugal modelling is the possibility of imposing and therefore controlling the soil and construction materials. There are two main families of materials used for model piles. The piles made with metal (usually aluminium in centrifuge modelling) and cement-based piles. As the majority of energy piles installed worldwide is made of reinforced concrete, this latter model appears to be more faithful to reality. In general, these models are prefabricated in cardboard moulds to ensure good construction quality, particularly with regard to the existing instrumentations. It is then possible to test the model outside the ground and the centrifuge to determine its mechanical and thermal characteristics. The reinforcing cage is simulated with a welded steel fabric and the mixture used is as close as possible (mechanically and thermally) to that used in reality. In the interests of respecting the scaling laws (Cf. chapter II), it is aimed for the model piles to get as close as possible to the prototype material in thermal and mechanical terms. However, for feasibility reasons and ease of installation, the materials used in the model piles are generally different from those used in geotechnical engineering for the construction of full-scale structures. Model piles are generally made of an aluminium alloy or a cement mixture (the gravel constituting the concrete being too large to ensure the homogeneity of a model pile).

Concerning the soil used in the centrifuge, it is possible to reproduce the actual stratification of a site or to impose the type of soil in order, for example, to carry out a comparative study. Most centrifuge tests on energy piles have been carried out in clay or sand (dry or saturated). In the case of tests in silt or clay, it is common for the soil to be compacted prior to centrifuge flight in order to reduce the test time. Here the advantage is that the consolidation rate can be chosen and controlled. In their work, Goode & McCartney (2015) also perform models set in Bonny silt. This soil was compacted prior to testing and consolidation is completed under macro gravity in order to make the model preparation time faster (Ng, 2014). Just as the relative density of the model is a study parameter in a granular soil, the consolidation rate is one for fine soils. The latter will logically depend on the load and the consolidation time. Once the soil model is ready, the piles are placed in pre-excavated holes with a placement frame to ensure verticality of the operation. Likewise, two types of configurations can be implemented: end-bearing piles and floating (or semi-floating) piles. The results of the centrifuge tests will show the importance of the configuration case.

Thirdly, it was seen earlier that all methods of pile implementation are compatible with the fact that the piles to be energetically equipped, although most energy piles are bored piles. With a centrifuge, it is possible to model piles taking into account the way of installation. To model drilled piles, soil is placed by sand pouring after placement of the model pile (Goode & McCartney, 2015) or by pre-excavation in clay (Ng, 2014). This is done under normal gravity and is referred to as "wished-in-place conditions" because the installation was carried out under low gravity. When the model piles are placed before sand pouring, there is a risk of having a lower soil density in the vicinity of the piles. This risk remains negligible in the case where a single pile is modelled, but it becomes more worrying in the case of rainfall around a group of piles. This is because the density between the piles is likely to be relatively lower, and it is therefore relevant to measure this density at the end of the test. Piles can be placed on a first layer of sand (Goode & McCartney, 2015) or kept suspended during sand

pouring (Zhao et al., 2020).. To simulate a pile driven in a centrifuge, it is driven into the box already containing the soil at high gravity high (when the centrifuge is running). In all cases, the method used to place the soil in the model should enable homogeneity and density to be controlled.

Fourthly, in the study of energy geostructures by means of reduced scale models, a system for applying a thermal load must be considered. A hydraulic system is often used to keep in line with the prototypes in which it is indeed circulating glycol water that allows heat exchange. Thus, the model piles are equipped with tubes, usually made of steel or copper, to allow for thermal loading. Water, whose temperature has been previously modified by a heating (or cooling) system, circulates through these tubes by means of a pump. The heating system, the flow rate (especially in macro gravity) and the hydraulic circuit in general must be designed before the test. A Peltier system can be used to form a cooling unit through which a tube passes and in which the heat exchange fluid circulates, which can reach temperatures ranging from 3 to 90°C (Ng, 2014). Similarly, a water bath can be used following the same principle (Zhao, 2020).

Lastly, centrifuge modelling allows advanced instrumentation of the model. Since the hydro-thermo-mechanical behaviour is the subject of these centrifuge studies, accurate, relevant and as unobtrusive as possible instrumentation dedicated to these different aspects is necessary in order to provide the data from which conclusions can be drawn. Temperature sensors are required and may be in the form of thermocouples or resistors. Depending on the study, these may be used to measure the temperature of the fluid, the temperature of the pile or the temperature of the soil surrounding the structure.

To deal with the mechanical behaviour, strain and displacements should be measured. To this purpose, strain gauges can be glued to steel plates to facilitate calibration (Goode, 2015). Indeed, placing the temperature sensors on the same steel plate as the strain gauges is very useful in terms of calibrating the latter and avoiding thermal interferences. To do so and to protect the instrumentation, epoxy is often used and the question of its intrusiveness in experimentation arises. However, Ramadan et al. (2013) found that the interaction between epoxy and sand is of the same order of magnitude that the concrete and sand one. Likewise, Zhao et al. (2020) consider that the use of 3 mm strain gauges glued to model pile does not significantly alter the interaction between the two materials.

The mechanical loading is generally implemented statically via a dead weight or a remotely controlled actuator. Finally, from a soil hydraulic point of view, pore pressure sensors are most often used to monitor the variation of water levels or overpressures due to various loads (thermal and mechanical).

2.3.2. Results from centrifuge test

Thermal cycles lead to expansion/contraction cycles of the pile itself. This subsequently leads to irreversible settlement if the pile is subjected to a significant head load. These results are in line with other observations from full-scale in situ tests or numerical/theoretical calculations. (Stewart & McCartney, 2013; Ng, 2013; Zhao et al., 2020). The main results obtained in centrifuges are detailed afterwards and summarised in the Table I. 3.

2.3.2.1 Impact of soil consolidation

The impact of fine soil consolidation on the general behaviour of ratchetting settlement was investigated by subjecting energy piles to mechanical loading a safety factor of 2.5, followed by 5 thermal cycles (Ng, 2014). In the slightly consolidated soil, it was observed that during the heating and cooling phases, pore pressures increased and decreased by $1\ kPa$, respectively. These variations were approximately three times higher in the over-consolidated soil. The authors attribute this observation to consolidation-induced lower pore pressures in the lightly consolidated soil. Additionally, average pore pressure increases were observed over the 5 cycles, indicating ongoing settlement of both the model energy pile and the soil due to consolidation.

The measurement of soil settlement allowed the calculation of net displacements of the pile. When the mechanical load was applied, the net displacement was 0.65% of the diameter, and during the heating cycle, a peak uplift of 0.4%D was measured. This uplift was 27% lower than what would have been obtained under free moving conditions (pile without any interaction). During the cooling phase, a settlement of 1.5%D was measured. Over the total period of 5 thermal loading cycles, a settlement of 3.8%D was observed at a decreasing rate. This continued settlement is attributed to a reduction in confining pressure induced by thermal contraction of the slightly consolidated clay (Campanella and Mitchell, 1968) and to enhanced plasticity due to extension/contraction alternation (Pasten et al., 2014). The progressive settlement is less intense in the case of strongly consolidated clay, which is attributed to the less contractile character of the strongly consolidated clay.

2.3.2.2 Influence of the type of soil

In their study, Goode & McCartney (2015) focus on the differences in energy pile behaviour when subjected to cyclic thermal loads. It is observed that, unlike the experiments conducted in sand, both the soil and the pile continue to settle under their own weight in silt. However, the thermally-induced effects are still evident. Foundations in silt exhibit a higher thermally-induced axial stress compared to those in sand. This difference is attributed to the stronger soil-structure interaction caused by compaction in silt. In dry sand, it appears that the load-settlement curves are similar for different thermal loads. This suggests that temperature plays a negligible role in the load-settlement curve. In silt, temperature seems to increase the bearing capacity of the pile. This difference can be explained by the fact that radial stresses are initially higher in silt (which has been compacted) than in sand which has been setup by sand pouring. Another explanation is that the thermally induced water flow affects the loading-settlement curve. A high thermal loading intensity may lead to drying of the silt in the vicinity of the pile and thus to an increase in the effective stress at the interface. The complexity of interpreting tests in partially saturated soils becomes apparent here.

According to (Ng, 2014), the response of a floating energy pile in clay can be complicated by thermally induced consolidation which could accelerate creep and promote plasticisation and settlements. Two tests were then carried out in a lightly consolidated clay (OCR=1.7) and a strongly consolidated clay (OCR=4.7) and the aim was to study the dilatant behaviour of the over-consolidated clay in contrast to the contracting behaviour of the normally consolidated clay (Laloui & Cekerevac, 2008). To do so, two control piles are in the consolidated clays and are loaded at ambient temperature to failure. The two model energy piles, on the other hand, are tested with mechanical working loading (half the failure load) and then with thermal loading for 5 cycles over a range of 13°C

to 36°C. It therefore appears a higher settlement for slightly consolidated clay (3.8% versus $2.1\ \%D$ for heavily consolidated clay)

2.3.2.3 Influence of limit conditions

Similar to soil stiffness, the displacement conditions at the head and toe of the pile can significantly influence the thermomechanical response. For instance, centrifuge tests performed on an end-bearing energy pile in unsaturated silt demonstrates thermo-elastic behaviour over 4 heating cycles over a range with a maximum uplift of 1.4 mm, while ratchetting settlement would be observed in floating conditions (Stewart & McCartney, 2014). In addition, in the head-locked condition, the axial stresses are logically higher. In other respects, the deformation measured for semi-floating or end-bearing piles are close to the deformation under free conditions. The authors attribute this result to the thermal expansion value of the pile. The greater the thermal expansion, the closer the deformation measured during the tests will be to those obtained in free conditions.

2.3.2.4 Concordance with 1g experimentation

Finally, even if they are not carried out in centrifuge, some studies are also performed on reduced-scale models with a gravity acceleration of 1g and give interesting results in line with the one presented previously. For instance, in the study conducted by Zhao et al. (2020), different axial load increments are applied along with thermal load cycles to a model pile under normal gravity acceleration. When there is no mechanical loading, the pile demonstrates fully reversible behaviour during thermal cycling: the head displacement is positive (upward) when the pile is heated and vice versa when it is cooled. However, once the pile is axially loaded, the thermal cycles result in irreversible settlement at a progressively reduced rate. This same phenomenon was observed by (Ng et al., 2015). Monitoring the evolution of deformations over time when thermal cycles are imposed on the model pile for different head loads again shows the reversible and therefore thermoplastic behaviour of the interface between the model pile and the soil. Likewise, the increase of the irreversible settlement of the pile head with pile head axial load is also observed after heating/cooling cycle in dry sand (Nguyen et al., 2017) and saturated clay (Yavari et al., 2016).

Table I. 3 - Main results of centrifuge tests on energy piles

Test	Pile type & Prototype size	Gravity	Type of soil	Mechanical load (prototype scale)	Thermal load	Main Results
Stewart & McCartney (2013)	Pre-cast $12.8\ m$ x $1.22\ m$ End-bearing Cement pile	24g	Unsaturated silt from Bonny Dam	443 kN (384 kPa)	4 cycles $\Delta T_{hot} = 19°C$ $\Delta T_{cold} = 9°C$	• Impact of end-bearing boundary conditions and side-shear resistance: Maximum axial stress occurs near the base due to the increase in side shear resistance with depth • Ratchetting settlement due to change in stiffness of the unsaturated soil
Ng et al., (2014)	Aluminum Cylindrical $0.9 \times 17\ m$	40g	Kaolin clay slightly and heavily consolidated	$192\ kN$ (constant load)	5 cycles between 9 and $38°C$	• Ratchetting settlement with thermal cycles • Higher settlement for slightly consolidated clay (3.8% vs $2.1\%D$ for heavily consolidated clay) • Decrease of stress due to plastic contraction of clay and creep accelerated by heat at the interface
Ng, Farivar, Gomaa et al., (2015)	2x2 floating pile group	40g	Clay (OCR = 1.7)	Dead weight (FoS=2)	$\Delta T = \pm 14°C$	• Ratchetting settlement of piled raft less than one of elevated group • Ratchetting irreversible cap/raft tilting • Negative skin friction due to soil consolidation, pile thermal expansion, and cap tilting are the three phenomena involved in the complexity of load distribution
Goode and McCartney (2015)	Cement mixture Cylindrical $8\ m$ and $12\ m$ length with $1.5\ m$ diameter	24g	Nevada dry sand Non-saturated silt	$197\ kPa$ $1310\ kPa$	$\Delta T = +7°$, $+12$, $+18\ °C$ (30 min)	• Head displacement of $0.001 \times D$ • Axial stresses higher for pile in silt • Axial stresses twice greater for end-bearing piles • Bearing capacity increase during heating for piles in silt but not for piles in dry sand

Ng (2016)	Same as 2014	40g	Saturated Toyoura sand	Constant axial load	5 thermal cycles $(7 - 32°C)$	• The importance of pile installation is highlighted: the bored pile is subject to ratchetting settlement, whereas the driven pile is subject to slight uplift due to the densification of the soil during installation. The latter reduces the contraction of the soil, and the horizontal stresses therefore prevent settlement.
Ng and Ma (2019)	Group of four piles	40g	Saturated Toyoura sand	Constant load of 2.64kN (FoS=2)	10 cycles ($\Delta T = 7°C$) of 96 min	• Thermal cycles lead to head load redistribution (until 30% of charge load variation for one pile) and cap tilting but acceptable according to Chinese regulations.
Zhao et al., 2020	Rectangular $0.63 \times 0.63 \times 10.5\ m$	35g	Congleton HST95 silica sand	Vertical working load equal to 0%, 13%, 15%, 51% and 89% of ultimate capacity	4 cycles $\Delta T_{in} = 45 - 12°C$	• Ratchetting settlement increase with vertical load

Chapter II

ENERGY INTERACTIONS WITHIN A PILE GROUP

"It is impossible to perform a transformation whose sole result is the transfer of heat from a colder body to a hotter body without the contribution of external work" (1854) Rudolf Clausius

The first chapter has pointed out that the ground has great energy potential, even at shallow depths, and that energy geostructures can take advantage of this potential. This potential depends in particular on hydrology, which has a decisive impact. The use of these geothermal solutions does, however, have an impact on the mechanics of the structure, and this impact has been studied in particular for single energy piles through in situ and centrifuge tests. Nonetheless, the impact of groundwater flow is almost never considered in spite of its major role.

In this second chapter, the objective is to first focus on the hydro-thermal coupling in order to characterize the energetic interactions. This chapter is then divided into 4 parts. Firstly, the model energy pile, which is the central element of the experiments in this thesis, is presented and the energy exchanges and resulting temperature distribution are characterised. Secondly, the implementation of a water flow (or seepage) on a reduced soil model is introduced. Thirdly, heat transfer between the model pile and the soil is studied for three hydric states: dry soil, saturated soil and soil with water flow. Finally, the fourth part presents a numerical model that investigates the impact of flow on the energetic efficiency of a group of energy piles.

1. Characterisation of temperature and heat flux distribution along the pile

To have a better understanding of the heat transfer from the heating system to the soil through the cement pile, an experiment consisting in putting a reduced-scale energy pile within saturated sand was carried out, and thermal sensors were used to observe the temperature distribution along the pile and in the soil. The experiments presented in this part were carried out in Schofield Centre, University of Cambridge in collaboration with Théophile Grappe an undergraduate student as part of his internship.

1.1 Description of the model

The various experimental tests carried out as part of this thesis were carried out on model piles built beforehand. It was verified that these model piles complied with the scaling laws and these verifications will be presented in more detail in Chapter III. But to give an initial description of these piles, they are 300 mm long and 20 mm in diameter, made a mixture of cement, water and copper powder. The mass ratio is $water/cement = 0.5$ and the copper powder represents 6% of the total weight as suggested in recent study (Leung, 2019). A copper U-shape tube serves as heat exchanger tube in which hot (or cool) water will circulate to heat (or cool) the model pile. Its internal diameter is 2 mm and its thickness of 0.5 mm, giving an external diameter of 3 mm. Once cast in the mould and solidified, the piles are left in water for cement setting in order to avoid cracks.

In this experiment, a model energy pile is equipped with 6 thermal sensors (Pt100) fixed with aluminium tape all along. In Figure II.1, the pile is seen before and after being equipped with the sensors. The upper sensor was judged irrelevant regarding its position and was then removed. The pile is therefore well equipped with 6 Pt100s during the experiment.

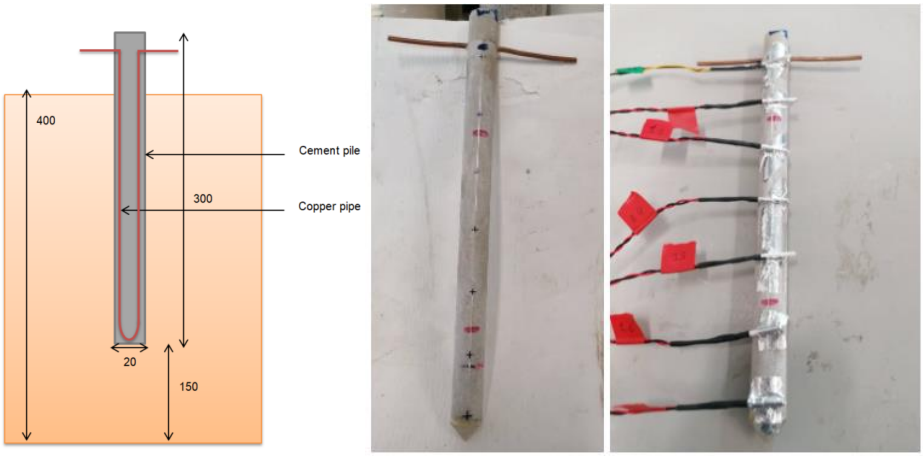

Figure II. 1 - Schematic representation and Picture of the model energy pile with and without thermal sensors

Three sensors were also placed at 50 mm from the centre of the pile at three different heights, resulting in nine sensors in the soil as one can see in the Figure II.2.

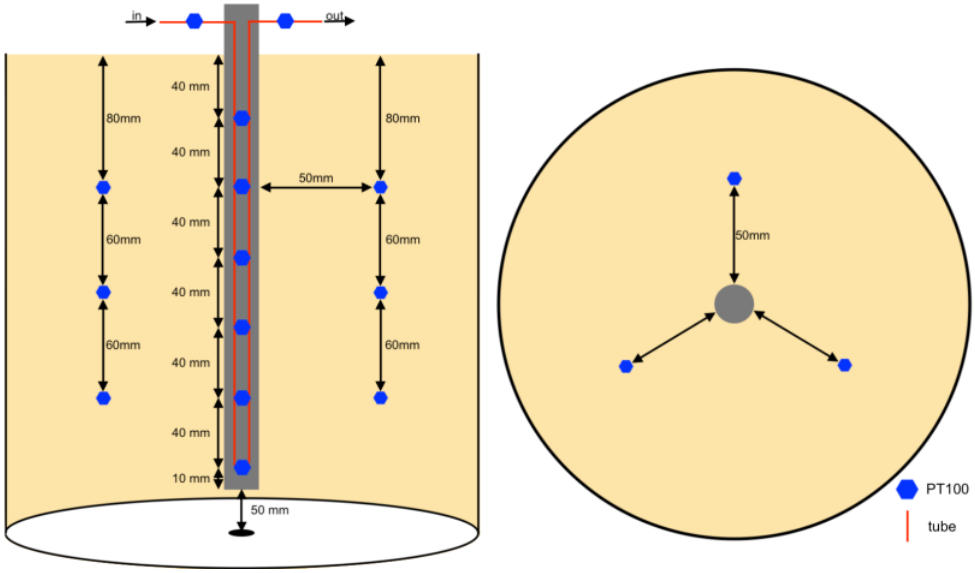

Figure II. 2 - Position of the sensors on and around the model energy pile

To make sure that the sensors are aligned according to the depth, they have been taped to a plastic stick. The thermal conductivity of the plastic is lower than the sand one, which allows assuming that the stick will not diffuse the heat. The objective is to better understand the distribution of temperature all along the pile's length and around the pile at different depths. Thus, Pt100s are taped to the pile and around at multiple heights, and also for the water inflow and outflow of the pile. , As it appears in Figure II.2, in order to measure the inlet and outlet temperature, two Pt100s are taped to the copper tube. An error could result from the thermal resistance of the copper. However, this thermal resistance is assumed weak (as the thermal conductivity is high) and the fundamental point is the difference between the inlet and outlet temperatures. Thus, as the copper tube creates the same thermal resistance, the temperature difference should be the same. In spite of this point, it was verified that the temperatures measured in the surface of the tube are very close to the corresponding water temperature.

To guarantee the saturation, a plastic tube (Figure II.3a) as previously been placed to be able to inject water at the bottom of the box and the saturation has been carried out with a flow of 200 ml/min assumed sufficiently low to reach an entire saturation. In total $7\mathrm{l}$ of water were used to complete the saturation. The top of the box is not covered by water to avoid creating a thermal bridge around the head pile. Indeed the presence of water in surface could generate a thermal flux likely to disturb the temperature distribution. The sand pouring has been done by hand and the soil density state is assumed loose. The volume of sand is around $20.5\mathrm{l}$ for a weight of sand of $28.7\ \mathrm{kg}$. That corresponds to a density of 1400 kg/m3 and to a relative density of 31 %.

The thermal conductivity of Hostun sand was determined in a thermal laboratory using 3 different methods for dry and saturated water conditions. The methods gave relatively the same results. A conductivity of between 0.28 and $0.34\ W/mK$ for dry sand and between 2.5 and 3 for saturated sand. The thermal conductivity of the cement grout was estimated at $1\ W/mK$.

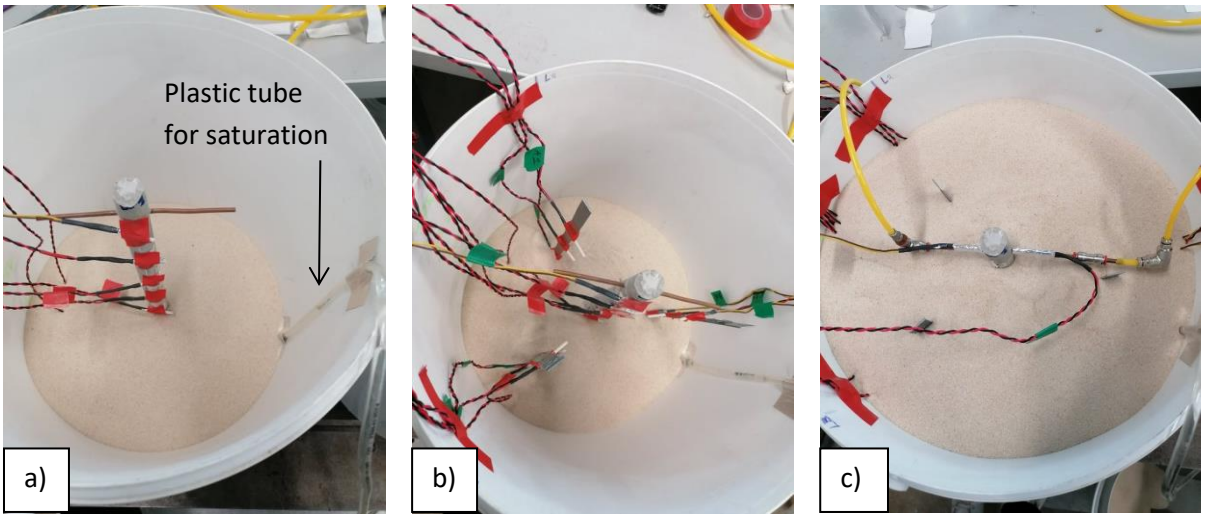

Figure II. 3 - Pictures of the setting up of the energy pile in bucket experiment: positioning of temperature sensors a) on the pile, b) in the sand, c) on the fluid inlet and outlet tubes

1.2 Calibration of the thermal sensors

The principle of a Pt100 thermal sensor is relatively simple. It consists of a platinum (Pt) resistor with a resistance of 100 Ohm at 0°C. The value of this resistance changes quasi linearly with temperature. It is the most popular example of Resistance Temperature Detectors (RTD), based on the fact that electrical resistance changed with temperature. An electrical circuit based on a Wheatstone bridge can be used to estimate precisely the value of this resistance and therefore the temperature. All the Pt100 are related to a junction box calibrated beforehand to have the right corresponding gain and to acquire the good voltage range for each sensor. This junction box has 24 independent channels and can therefore be connected with as many sensors. This latter is connected to the computer and the processing is done by the DASYLab 9.0 software.

In practice, the following work was carried out to calibrate the temperature sensors. A container of water was thermally insulated in its entirety, with 5 holes at the top for a digital thermometer and 4 thermal sensors. By varying the temperature of the water between 10°C and 60°C, and by reading

the voltage read by the data logger for each sensor, it is possible to determine the linear relationship between voltage and temperature for each sensor to an accuracy of around 0.1°C.

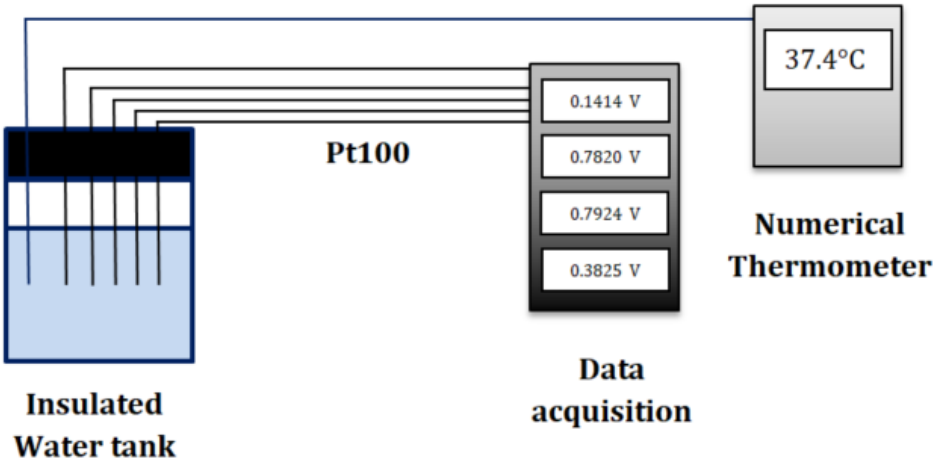

Figure II. 4 - Schematic representation of the Pt100 calibration device

1.3 Heating system and Protocol

The heating system is built around a Peltier system based on the eponymous physical principle (discovered by Jean-Charles-Athanase Peltier in 1834): when an electric current passes through a junction of two semiconductors, heating and cooling are produced on opposite surfaces. The system allows heating (or cooling) the water that will then circulate in the tube inside the pile by means of a peristaltic pump. The choice of a peltier for the heating system is explained by its technical proximity to reality. In both cases, the thermal load is provided by a flow of water in the tube, reproducing the phenomena of thermal convection. Using thermal resistance would have been simpler but less realistic from this point of view. Thus, the water circulates through the pile exchanging energy with it before being evacuated from the model (in open loop case) or reinjected in the loop (in closed loop case). In practice, in the open-loop[4] heating system which is used in this experiment, there is a tank of water at a constant temperature from which water is pumped to the Peltier module at a certain flow to be warmed up. Then, the hot water will cross the pile by circulating in a U copper tube inside the model pile. The water is finally run off out of the system so that the inlet water temperature remains constant once the steady state reached. By calibrating the pump and the Peltier module, it is thus possible to evaluate the inlet water temperature as a function of the voltage supplied to the Peltier module and the fluid flow in the circuit (Figure II. 1). The two different heating systems (open and closed loop) are schematized in Figure II. 6.

[4] This term was also introduced in Chapter I to refer to a type of geothermal energy. However, here, the term open-loop refers only to the heating system used to apply a thermal load to the model pile.

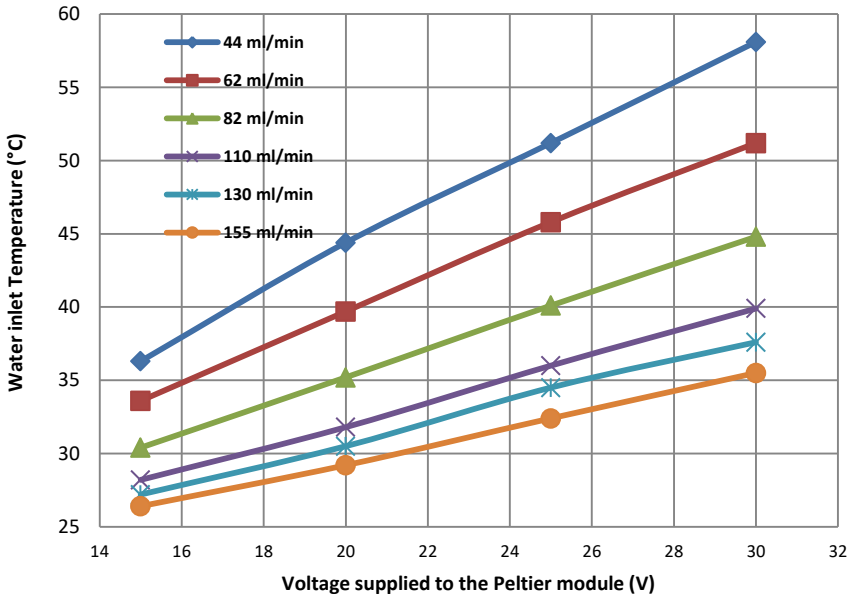

Figure II. 5 - Open loop heating system calibration parameters

Moreover, by measuring the water temperatures at the inlet and outlet of the energy pile, we can assess the thermal power, P exchanged between the pile and the ground by knowing the pump mass flow, q and the thermal capacity of the water, C_v using the following equation:

$$P = C_v . q . \Delta T \quad \text{(II.1)}$$

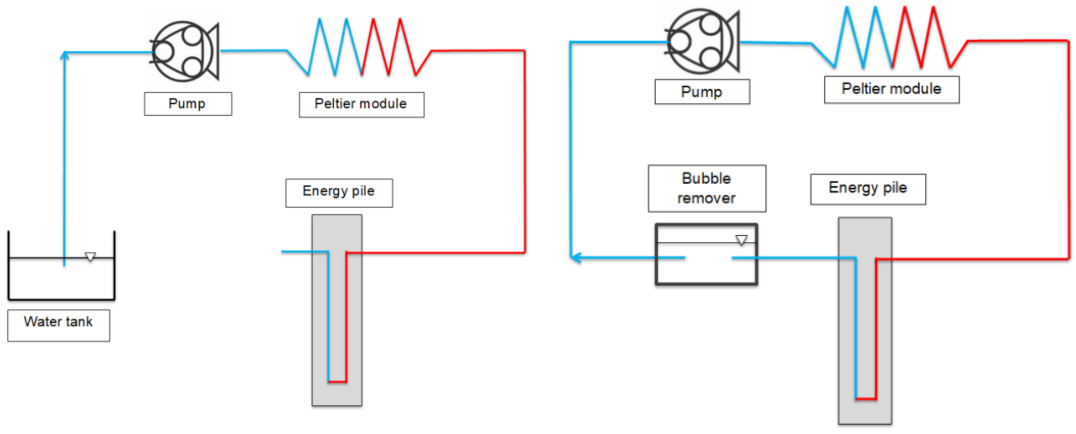

Figure II. 6 - Schema of heating system in a) open loop and b) closed loop

Regarding the protocol of this experiment, three experiments are carried out with the same voltage for the Peltier module. Namely, the electrical power used to heat the pile is the same. Only the water flow was changed in order to evaluate the impact of the water flow on the heating system. However, as the water flow in the system is different, the inlet water temperature is not the same for each experiment. The parameters of the three experiments are presented in Table II.1.

Table II. 1- Characteristic input parameters for the three experiments

Experiment	1	2	3
Pump flow (ml/min)	**78**	**150**	**60**
Pile inlet temperature (°C)	**45**	**39**	**52**
Peltier parameters :			
Voltage (V)	30	30	30
Amperage (A)	4.4	4.4	4.4
Power (W)	132	132	132

1.4 Results

1.4.1 Exchanged power

In Figure II.7, the evolution of the temperature recorded by all the sensors during the first experiment is presented. Three curves group are clearly distinguishable: the water outlet and inlet temperatures, the temperature of the sensors stuck to the pile and the sensors in the sand. First, it appears the inlet and outlet water temperature become quickly almost constants which means that the heating system reached a steady state but not the whole system as some sensor still record temperature variation. To confirm this, it is necessary to look at the difference between these two temperatures and verify that it becomes constant. One can then be sure that the heating system is providing constant power as required.

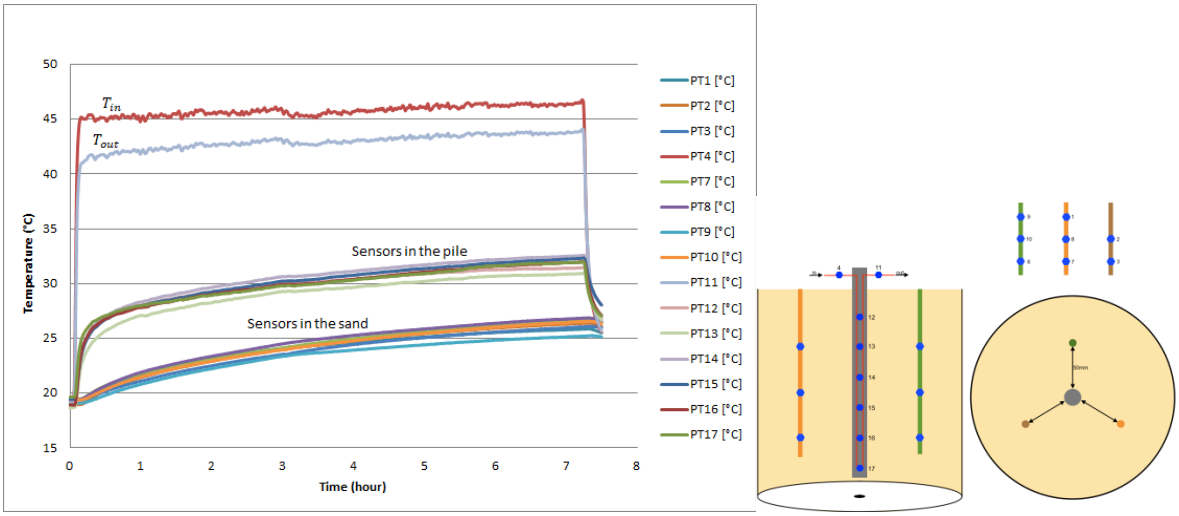

Figure II. 7 - Temperature evolution of the sensors in Experiment 1

The results confirm this hypothesis, as Figure II. 8 shows where the difference between inlet and outlet temperatures is plot for three different water flows. The important point is that the temperature difference ends to be constant which means the steady state is quickly reached. Consequently, the thermal exchanged power between the water in the pile and the rest of the system becomes quickly constant and it appears that when the flow decreases, the temperature difference increases.

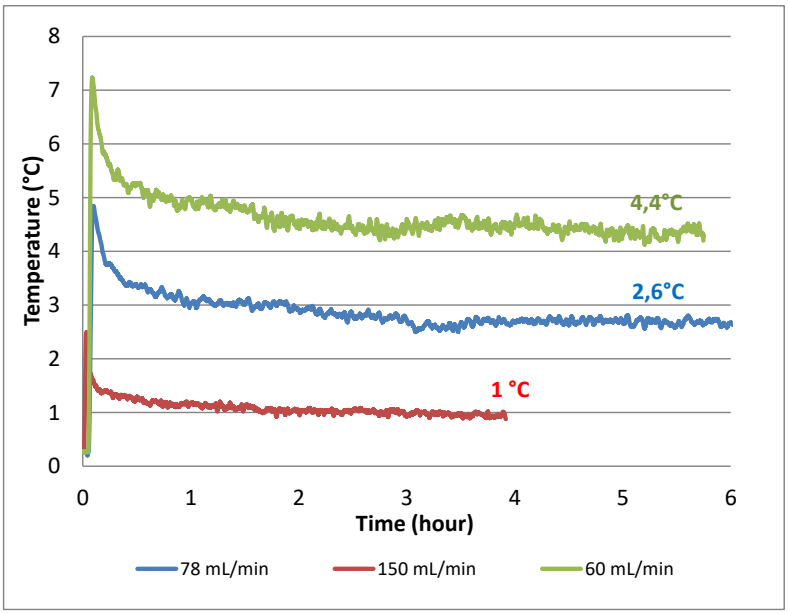

Figure II. 8 - Evolution of temperature difference between the water entering and leaving the pile for a same Peltier voltage

In other words, for a given and constant electrical power input in the Peltier system, changing the water flow leads to different temperature differences between the inlet temperature in the pile and the outlet one (Figure II. 8). It appears clearly that when the flow -and therefore the fluid velocity- decreases, then the temperature difference increases (Figure II. 9). Indeed, the water has more time to exchange heat with the energy pile. That is what appears when one calculates the exchanged thermal power as in Table II.2.

Table II. 2 - Energetic parameters and exchanged thermal power for experiments 1, 2 and 3

Experiment	Flow (ml/min)	Inlet temperature in the pile (°C)	Thermal capacity (J/kg.K)	Delta T (°C)	Exchanged thermal power (W)
1	60	52	4185	4.4	18.4
2	78	45	4185	2.6	14.1
3	150	36	4185	1	10.4

Accordingly, changing the fluid velocity also changes the inlet water temperature because of our heating system design. To tackle this point and in order to make a more relevant comparative study where only one parameter evolves (the flow), new experiments campaign is led. This time, the inlet temperature is kept constant and only the flow is varying according to the heating system calibration presented previously (Figure II. 5). The aim is to have different flows for the same inlet water temperatures of 45°C and 35°C. As data for a flow of 78ml/min are already available, the point is now to do so with a flow of 60ml/min and then 40ml/min. All the experiments carried out are resumed in Table II.3.

Table II. 3 - Energetic parameters of experiments for two water inlet temperature in the pile

Water inlet temperature in the pile (°C)	45			35			
Flow (ml/min)	40	60	78	88	120	150	200
Reynolds number (-)	424	637	828	934	1273	1592	3032
Voltage Peltier (V)	20	25	30	20	25	27.5	34
Delta T - last 4 hours average (°C)	5.9	3	2.6	1.7	0.9	1.3	0.9
Thermal power (W)	**16.5**	**12.6**	**14.7**	**10.4**	**7.5**	**13.6**	**12.6**

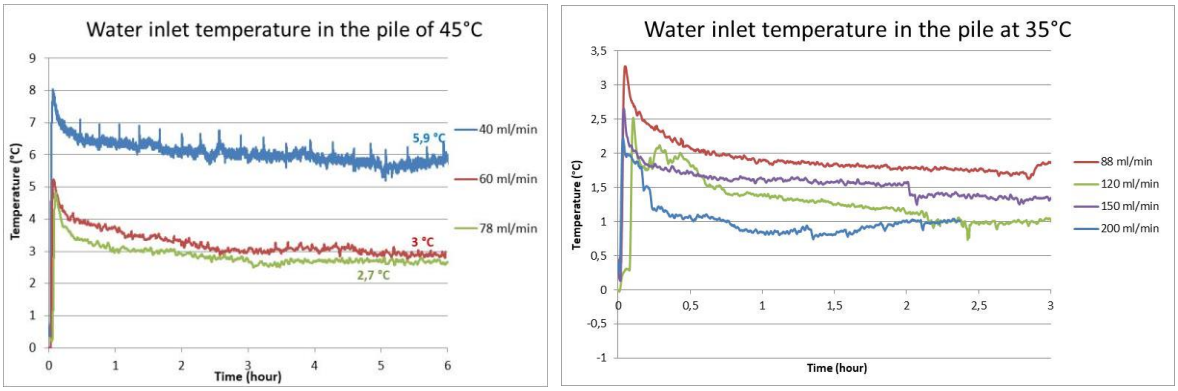

Figure II. 9 - Evolution of the water temperature difference as a function of the time

These experiments were carried out to characterise the heating system and the exchange of energy between the model pile and the ground. In addition, it appears that the thermal power exchanged per linear meter between this reduced model and the soil is of the order of magnitude of those of the real energy piles, even if they are close to the low end of the range (Di Donna et al., 2020). Indeed literature gives values between 20 and 80 W/ml and the results found here are between 10 and 16 W/ml.

1.4.2 Temperature distribution and diffusion

Regarding the temperature distribution along the pile, it appears that the sensors are not all at the same temperature and that the temperature is non constant with depth (Figure II. 10). This non-homogeneity can arise either from the heating system or from thermal interactions with the outside of the system. Indeed, our heating system, and especially the heat exchanger, is not homogeneous, and as the sandbox is not thermally insulated. It is difficult to know which part of the temperature evolution is due to the insulation and which one is due to the non-homogeneous heating system. Nonetheless, the differences between the sensors along the model pile are relatively low (2°C for the bigger gap) and also real piles do not have a constant temperature distribution with depth. To better see the evolution of the vertical temperature along the pile, the temperature distributions have been plotted for different heating times: 1 hour, 3 hours, and 7 hours. It appears first that the curves have the same shape at each time and that the bigger the heating time, the hotter the pile. However, the fact that the sensor 13 (second one from the top) was colder than the first one seems illogical. It is also possible that the sensor 12 (on the top of the pile) is too hot. This irregularity could be explained by the fact that one of those sensors is not perfectly taped to the pile, by the calibration, or by a discontinuity in the pile.

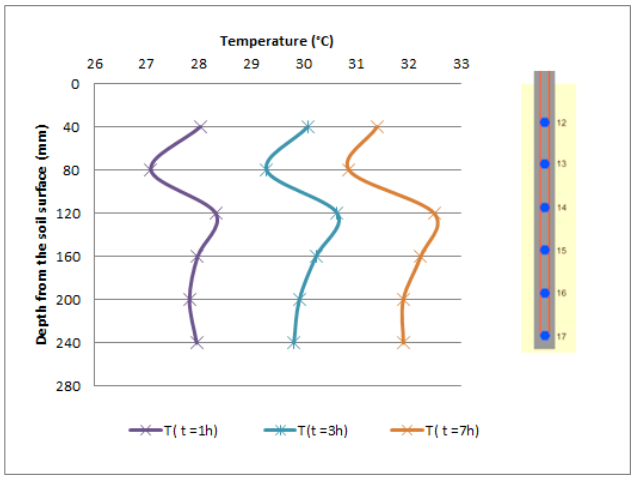

Figure II. 10 - Temperature distribution along the pile at different heating time (Experiment 1)

Three points stand out:

1. The radial heat transfer is indeed isotropic: the maximum difference between two sensors at the same depth and at the same distance from the pile is 0.4°C (i.e. around 5% of the thermal variation). We can therefore confirm that the heat transfer evolves at the same velocity in all the directions in a horizontal plan which was predictable in homogenous sand.
2. The temperature distribution along the pile length is not perfectly constant: a slight temperature difference (i.e. around 10% of the thermal variation for the bigger gap) between the sensors along the pile appears as the extremities are colder if one considers that one of the two top sensors malfunctioned. The most plausible explanation is the energy exchange with the ambient air because of the boundary conditions. Indeed, the sandbox was not insulated. In addition, certain heterogeneities can disrupt heat diffusion and, consequently, the temperature field. Specifically, the distance between the heat exchanger tube and the pile wall is not perfectly constant due to the fabrication process. Regardless, assuming the temperature at the middle of the pile as representative of the temperature throughout the entire pile is a reasonable approximation.
3. After 5 hours of heating, as the Figure II. 11 shows, the difference of temperature between the heating pile and the sensors far apart of 50 mm (line 1, 2 and 3) independent of depth. That result confirms the purely radial aspect of heat transfer in the ground and suggests that vertical heat transfer is negligible.

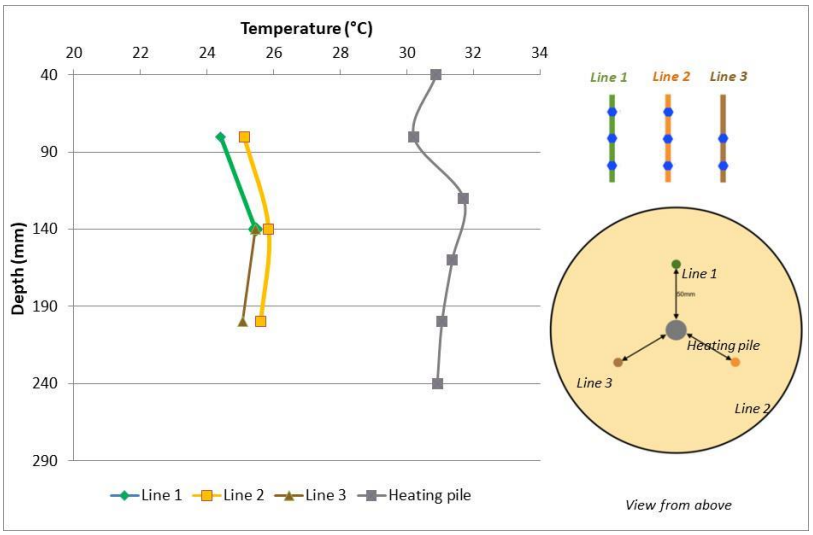

Figure II. 11 - Temperature of the sensors located in the sand after 5 hours of heating (Experiment 1)

1.4.3 Comparisons

Figure II. 12 focuses on the temperature distribution along the pile and compare the results for different inlet water temperature and water flow. The first remark is that the temperature along the pile seems quite constant and keeps the same shape with the time. However, even if the variation is very weak, the shape does not seem coherent because the temperature is bigger up the pile for instance. Then, for a given heating time, when the flow decreases, the temperature of the water entering in the pipe increases and understandably the temperature along the pile too. It means that the water has more time to exchange heat with its environment as the flow is lower. Finally, with a bigger flow, the increase of temperature along the pile for a heating pile of 3 hours is lower than for a smaller flow (the distance between two curves with same flow is bigger for the smaller flow).

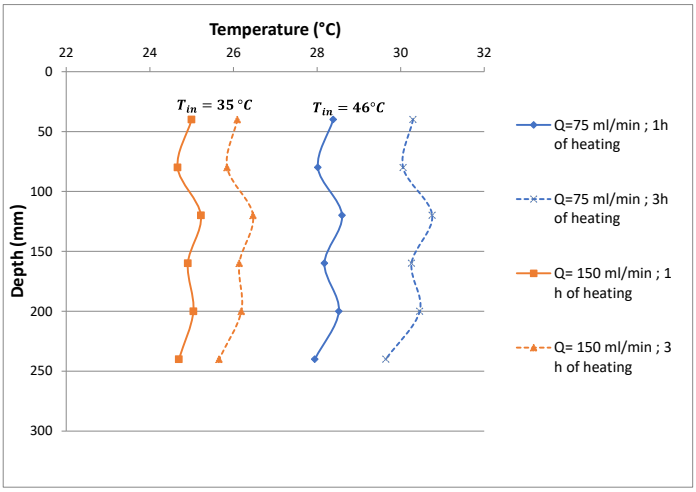

Figure II. 12 - Temperature along the energy pile for different flows and heating times

1.5 Conclusions

To sum up this part, the model energy pile and the heating system has been presented. The exchanged thermal powers are of the same order of magnitude as the real exchanged powers for instrumented prototype piles (in W/ml). Then, with that heating system, the temperature

distribution along the model energy pile can be assumed constant. Moreover, the difference of temperature between the water entering and the water leaving the pile is increasing when the fluid flow is decreasing. However, an increase of fluid flow does not imply an increase of heat exchanged power in our experiments. In the numerical experiment one can find in literature, they focus on the fluid flow whereas it could be more relevant to focus on the Reynolds number if one wants to compare different results. Thus, it seems that in a majority of our experiments, the flow is laminar whereas it is often considered turbulent in numerical models.

2. Establishment of seepage in reduced scale model

To impose a groundwater flow in a reduced scale model, the simplest method consists in imposing a hydraulic head difference between the two extremities of a sandbox. The flow created this way is characterised hereafter.

2.1 Presentation and set up

To realise the first model, a sand box is separated in three parts by geotextile like in the Figure II.13. The two parts on the sides are filled with gravel and the middle part is filled with Hostun sand. The sand has been placed by hand trying to maintain a constant drop height, targeting a loose state but a relative density of 85% was calculated.

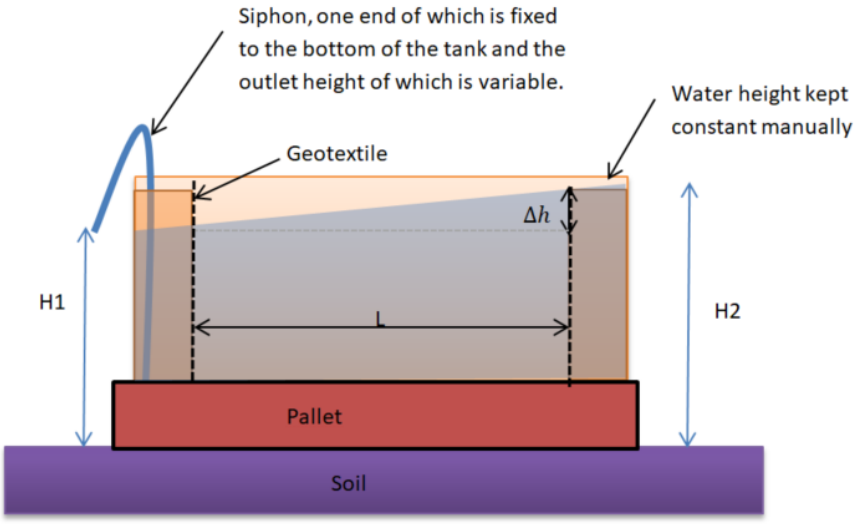

Figure II. 13 - Photo of the device completely finished with numbering of the piezometers

Geotextile allows the water passing through but not the sand and the system is then saturated by introducing water from the upstream side (Figure II. 14). In the initial transient phase, water passes through the geotextile and migrates in the sand. On Figure II.14, it appears that water migration front is quite aligned and perpendicular to the box sides. It shows therefore that the sand is rather homogeneous. This figure shows the presence of model piezometers, which will be presented in more detail below (2.1.3).

Figure II. 14 - Photo of the device during water saturation

Once the system is saturated, the gravel reservoirs represent equipotential regarding the hydraulic head because of the high permeability of gravel compared to sand. The water level upstream is manually kept constant by adding water when the level begins to drop. On the downstream side, the water is evacuated using a siphon system. Indeed, a tube is fixed by one of its ends to the bottom of the gravel and the other end of the tube is kept outside at an adjustable height. Thus, it is possible to choose which hydraulic head difference H2-H1 one wants to apply (Figure II.13). By doing so, seepage is setting up in the sand following the Darcy's Law (Darcy, 1856):

$$Q = k.i.S = k.\frac{\Delta h}{L}.S \quad \text{(II.2)}$$

Where $Q\ (m^3/s)$ is the flow rate, $i\ (-)$ is the hydraulic gradient, $k\ (m/s)$, is the soil permeability, and $S\ (m^2)$ is the hydraulic surface.

2.1.2 Horizontal seepages for different hydraulic heads

Different tests where then carried out where the upstream water height was kept constant (H2= 0, 42 m) for the different cases. Only the positioning of the siphon outlet changed so as to vary the hydraulic head differences.

A first head hydraulic difference of 0.09 m was imposed and the outlet flow was measured at several times by weighting the water released in one minute. The results are presented in the Table II. 4.

Table II. 4 - Outlet flow measured for the first experimentation

Measure n°	**1**	**2**	**3**	**4**	**5**	**6**	**7**	**8**	**9**	**Average**	**Standard deviation**
Outlet flow (mL/min)	790	775	778	779	776	780	790	788	785	**782.3**	5.3

The standard deviation is very low compared with the measured values; so it can be assumed that a hydraulic steady state is reached. It is then possible to calculate the permeability of the soil with Darcy's formula than links the flow rate to the hydraulic head difference. To do this, the surface area through which the flow passes is calculated, and the length over which the flow takes place is already known (See L in Figure II.13). The surface area is calculated as the average of the two water heights

at the ends of the model multiplied by the width of the model (constant). Thus, the Darcy's equation gives allows here to calculate a soil permeability of $0.0008\ m/s$

Afterwards, the syphon that forms the downstream water evacuation system has been completely lowered so that all the water in the model soil can be evacuated. This dewatering stage possibly increased the sand density. New experimentations were then carried out, this time for several hydraulic head differences. Figure II. 15 shows the evolution of seepage flow as a function of hydraulic head difference. The coloured point corresponds to the data obtained before dewatering and then probably in looser sand. However, as the Figure II. 15 shows the evolution of the flow is quite linear and the dewatering seems to not have a considerable effect on the results.

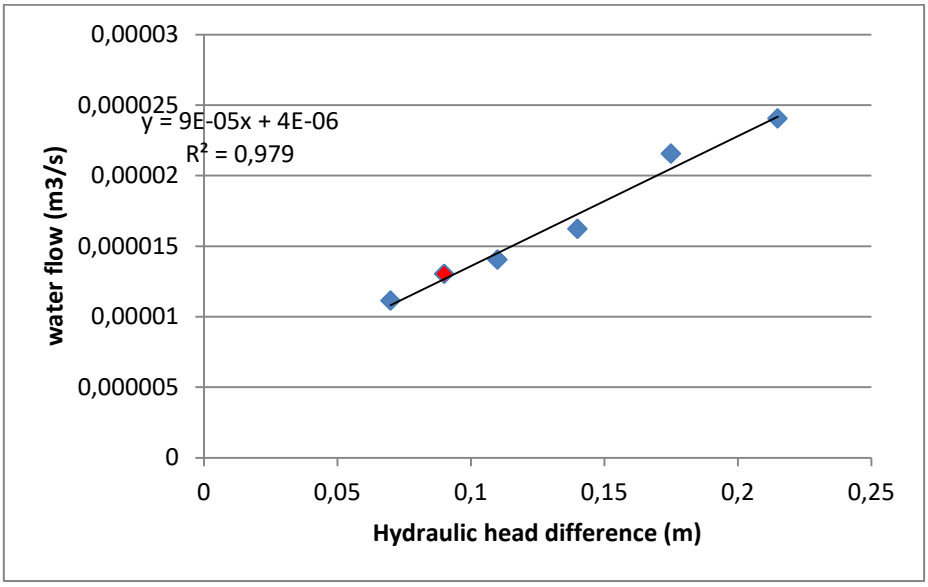

Figure II. 15 - Evolution of the flow with the hydraulic head difference

2.1.3 Homogeneity of the groundwater flow

In order to evaluate the homogeneity of the seepage and its velocity, nine piezometers were put in place in the sand. These piezometers were fabricated with perforated tubes, rolled up in geotextile to protect them from the sand. A polystyrene pad connected to a graduated rod allows the water level to be measured (Figure II. 16).

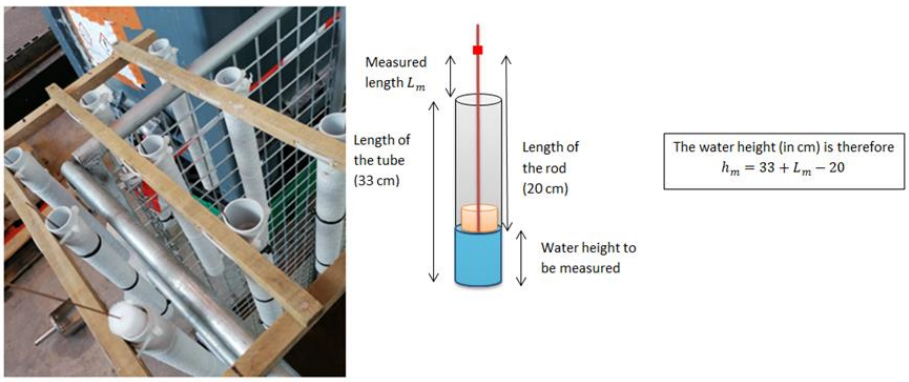

Figure II. 16 - Photo and schema of the piezometer system and schema of a piezometer

First, the results seem to show that there is no side effect. Indeed, the three lines of piezometers (piezometers (1, 2, 3), (4, 5, 6) and (7, 8, 9), see Figure II. 14) present almost the same results. For instance, with a hydraulic head difference of 0.09 m, the water heights for the different piezometers were as follows in Table II. 5:

Table II. 5 - Water heights measured for a hydraulic head difference of 0.09 m

Delta h (m)		**0,09**	
Line 1 (piezometers 1,2,3), water height (cm)	21	22	23
Line 2 (piezometers 4, 5, 6), water height (cm)	21.5	23	24
Line 3 (piezometers 7, 8, 9), water height (cm)	22	23	25

Moreover, it also appears that the roof of the water table presents a slope of about 0.04 is present between the piezometers 1, 2, 3 and 4, 5, 6. Indeed, this phenomenon is linked to the fact that the piezometers are not perfectly but the error can be considered negligible (2% of measured heights).

In order to verify that this system of piezometers was not too intrusive, the same experimentation has been carried out without the system and the water flows measured were the same. Moreover, same experiments were also carried out after dewatering, as the phenomenon is likely to change the density of the sand and the results were also identical.

For each hydraulic head difference, the flow is almost constant with time, but as the water height is not constant all along the box (the water table is not a horizontal plan), the speed varies along the sandbox. Obviously, the water level is low downstream and therefore the seepage is faster. Using the piezometers (only presents in the gravels this time in order to know the water level in the extremities), a water height and therefore a wet surface (surface crossed by the flow) are obtained as in 2.1.2. This allows calculating the associated seepage velocity. For instance, the water heights are given in the Table II.6 with the different associated results. The resulting soil permeability value is very close to the one calculated in 2.1.2 and that proves that the piezometers system was not too intrusive.

Table II. 6 - Water heights and associated values for a hydraulic head difference of 0.09 m

Hydraulic Head difference (m)	**0,09**		
h_m for piezometers 1, 2, 3	8	9	10
h_m for piezometers 4, 5, 6	8,5	10	11
h_m for piezometers 7, 8, 9	9	10	12
Average h_m	**8,5**	**9,7**	**11,0**
Water height (cm)	**21,5**	**22,7**	**24,0**
Wet surface (m²)	**0.118**	**0.125**	**0.132**
Seepage velocity (m/day)	**9.5**	**9**	**8.5**
Average flow	$1{,}3.\,10^{-5}$		
Average wet surface (m²)	0.125		
Hydraulic conductivity (m/s)	**0.0007**		

The same work was done for the different hydraulic head differences and the results are summarized in the Table II. 7.

Table II. 7 - Table summarizing the principle values for the different hydraulic head differences

DeltaH	0.07	0.09	0.11	0.14	0.175	0.215
Average seepage flow (m3/s)	1,11E-05	1,3E-05	1,4E-05	1,6E-05	2,15E-05	2,4E-05
Average seepage velocity (m/d)	8.2	9	11.3	14.2	18.7	22.7
Average wet Surface (m²)	0.117	0.125	0.109	0.101	0.103	0.097
Hydraulic conductivity (m/s)	**0.0007**	**0.0008**	**0.0007**	**0.0007**	**0.0007**	**0.0007**

The average hydraulic conductivity obtained by calculation is 7.10^{-4} m/s which is not far from the permeability of the Hostun evaluated as 10^{-3} m/s by a falling-head test (Haigh, 2012). Moreover the obtained results are very similar for the different hydraulic head differences and that proves the homogeneity of the seepage set up in the model box. However, this quantity depends –even to a small extent- on the density of the sand. Indeed, after considering a porous material as an assembly of capillary tubes for which the equation of Navier-Stokes is valid, the hydraulic conductivity can be expressed as a function of the void ratio, the specific surface (m²/kg), and a factor that takes into account the shape and tortuosity of channels. It appears therefore a relationship between the hydraulic conductivity and the void ratio, and so the density. Therefore, these experiments effectively confirm the order of magnitude of the permeability of the soil under study.

2.1.4. Verifications

Firstly, the presence of gravel and geotextile at both ends of the sand block could lead to a discontinuity in the hydraulic head. It was possible to verify this aspect by measuring the hydraulic gradient between two piezometers and between the two gravel sections, and to check that there was no drop in load between the gravel and the sand. Finally, as the measurements of hydraulic loads in the sand are in line with those measured in the gravel, it appears that the presence of geotextile and gravel does not induce an error in the hydraulic gradient.

Secondly, a part of the soil is not crossed by the flow on a depth named h_{NC} (see Figure II.17) and its saturation should be checked.

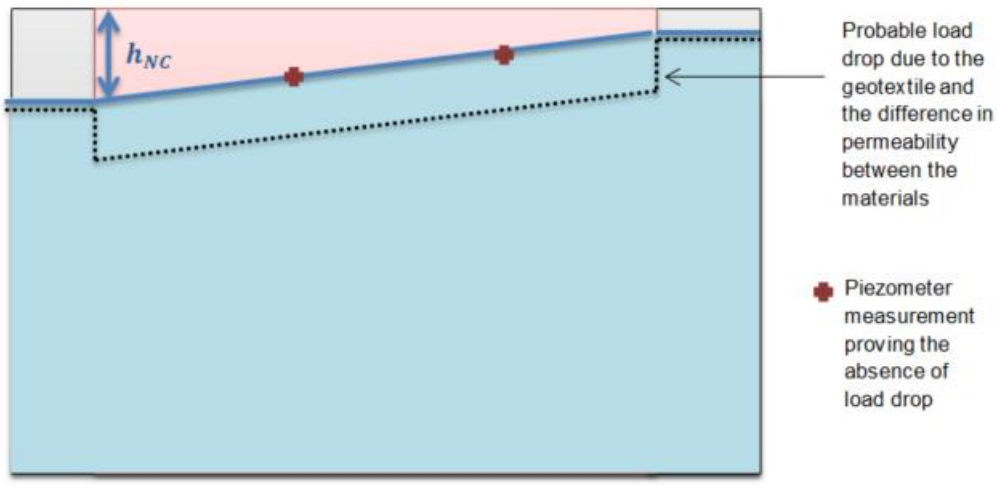

Figure II. 17 - Sandbox side cut to schematize the capillary rise and check of load drop absence

Different formulations exist to calculate the height of capillary rise h_c. This calculation allows determinig the height at which soil saturation can be achieved by capillary rise. A well-known equation, analogous to the Jurin's law which measures the height of capillary water in a tube, is:

$$h_c = \frac{2\sigma \cos(\lambda)}{\rho_w g R} \quad \text{(I.20)}$$

Where σ is the surface tension of the fluid, λ the contact angle of the fluid meniscus with the capillary tube wall (degrees), ρ_w the density of the fluid, g the acceleration of gravity. Applying this formulation to estimate capillary rise reveals that it is relatively low in comparison to h_{NC}, suggesting that the portions of the model not traversed by water flow will not be fully saturated.

3. Effect of saturation and groundwater flow on the heat exchange between energy pile and soil

The previous sections characterised the heat exchange between the heating system and the model pile as well as the groundwater flow imposed on reduced scale models. The heat generated in the pile is transferred to the soil by conduction and/or advection in the case where a flow is present. In this section, the heat transfer is characterised in the reduced model studied for cases where the soil (Hostun sand) is dry, saturated or crossed by water flow. The evolution of the temperature field is appreciated thanks to thermal sensors (Pt100), all placed in the same plan (at a constant depth at the middle of the piles height). This arrangement of sensors is made possible by the homogeneity of the temperature field demonstrated in the first section. The measurement of the heat transfer is done before the saturation in order to compare the thermal wave velocity in dry sand and saturated sand.

3.1. Model presentation

The model is made in a box whose dimensions are $L_b \times W_b \times H_b = 790 \times 200 \times 500\ mm^3$. One side of the box is made of Perspex. The box was not thermally insulated as it was assumed that the thermal gradient between the box and the exterior was negligible. Moreover, by insulating the edges, one creates the risk of accumulating heat which would not happen in the reality of a semi-infinite soil. In line with what has been done previously, the box is also divided lengthwise into three parts in order to establish a water flow in this sandbox. The two ends, each 85 mm long, are filled with gravel and the central part is filled by hand with Hostun sand trying to keep the same height drop in order to get a homogeneous model and Geotextile also separates the three parts. A relative density of 65% was calculated for the sand.

In this experiment a group of four energy piles is placed in the sand box and, the open loop heating system is used to heat one of the four piles. For measuring the temperature field in the soil, eleven Pt100 are used. They are placed at 135 mm deep on the piles in the soil. Thus, the sand has been poured handily until 265 mm height from the bottom of the sandbox. Then, the sensors have been put in place and the rest of the sand has been poured until 40 cm height (Figure II. 18).

In this part, in the figures, letter and number are for the link between the sensors and the junction box, to remember exactly where the sensors are in order to interpret correctly the data. However, the reader will only be interested in the number of the sensors.

Once all the system was installed, it appeared that one Pt100 was not functional. This is B3 placed on the energy pile. A digital thermometer was then placed on the surface of the heating pile to measure its temperature as a function of the time. The digital probe is not exactly at the same depth as the other sensors, but the experiments presented in the previous part allow considering the temperature

distribution along the pile as homogeneous. Figure II. 18 shows the installation of the thermal sensors and the pile group. The Peltier module also appears in this figure. The sand pouring was hand-done trying to keep the same height drop in order to get a homogeneous model.

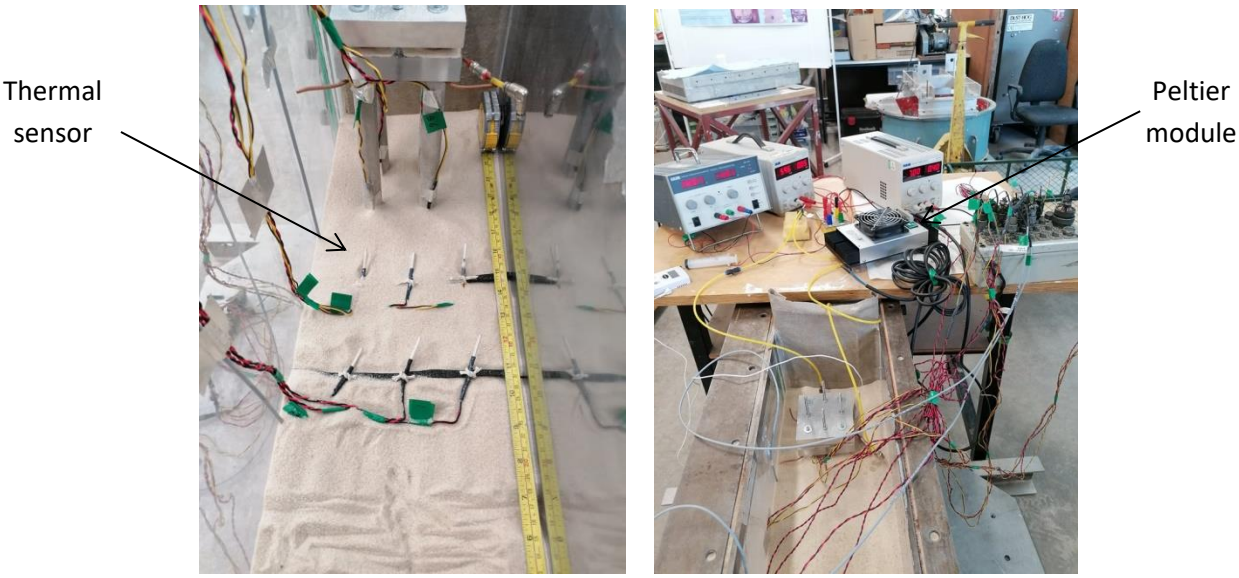

Figure II. 18 - Pictures of the setting up and during the test

For this experiment and based on previous calibrations of the heating system, a temperature of around 40°C is targeted for the water entering the pile. However, only the temperature at the surface of the pile is monitored and allows us following the experiment.

3.2. Presentation of the test campaign

As a reminder, the objective is to characterize heat transfer in the whole model for dry, saturated and seepage conditions. The test campaign was conducted as follows. Two experiments were carried out in dry sand. In the first, the thermal load did not last long enough to spread the heat far enough. This also raised the question of the impact of external temperature variations on the model. So, in the second experiment in dry sand, the thermal load was applied for longer and the data recorded over several days after the end of heating to assess the impact of external temperature variations. Subsequently, the model soil was saturated with water and again one of the four piles in the group was heated and the induced temperature field measured. Finally, a water flow is set up in the model, and then same protocol of heating is followed.

For the different experiments in dry and saturated sand, the inputs data are summarised in Table II. 8. These values are not useful for the interpretation of the results but are needed for anyone wishing to reproduce the test under the same conditions.

Table II. 8 - Characteristics of the experiment “Dry sand 1”

Experiment	Dry sand 1	Dry sand 2	Saturated
Water inlet temperature (°C)	15.4	21.3 and then 16.9	19
Initial temperature in the model (°C)	22.7	22.7	23

Duration of the heating	2h36	6h50	7h

Principle of seepage set up is identical to the one presented in the previous section and is reminded Figure II. 19 where the position of the thermal sensors are also indicated. The only difference is that this time the flow in the model soil is controlled by a pump whose flow rate is known and can be varied.

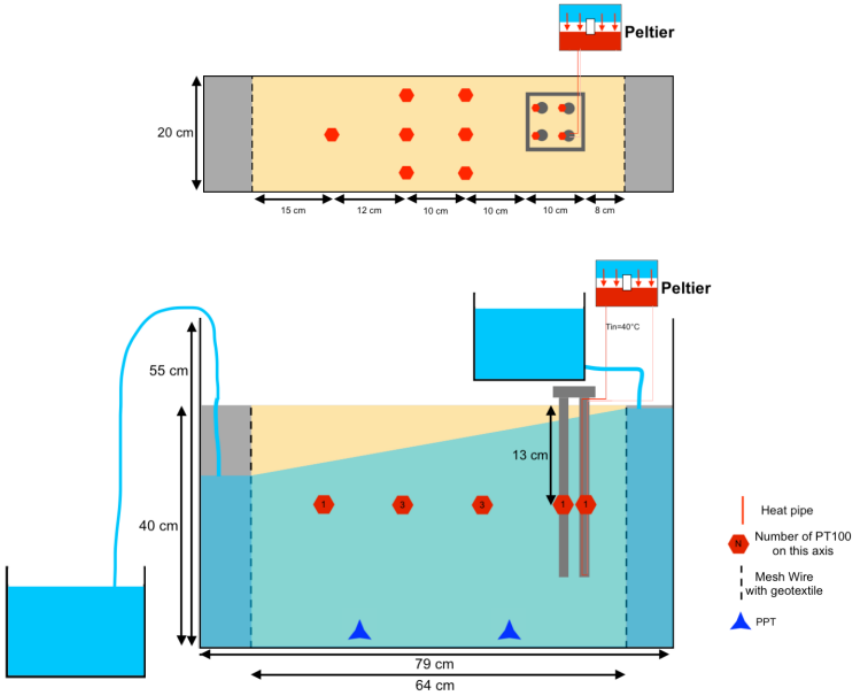

Figure II. 19 - Schema of the experiment with the seepage, from above (up), and side (down)

For different water levels, by measuring water flow and by using Darcy's law, it is possible to calculate the seepage velocity and then the hydraulic conductivity of the soil also called permeability. A mean permeability of $\mathbf{1,5.10^{-3}\ m.s^{-1}}$ is obtained and corresponds well to the order of magnitude found in literature (See Table II. 9).

Table II. 9 - Calculation of the model soil permeability

Upstream water level (cm)	Downstream water level (cm)	Δh (cm)	Hydraulic gradient (-)	Real flow (ml/min)	Wet surface (m²)	Seepage velocity (m/day)	Permeability (m/s)
32	29	3	0,046	311	0,0610	7,3	0,00184
33	28	5	0,077	400	0,0610	9,4	0,00142
32,5	27	5,5	0,085	420	0,0595	10,2	0,00139
33,5	27,5	6	0,092	460	0,0610	10,9	0,00136
34	27,5	6,5	0,100	575	0,0615	13,5	0,00156
36,5	27,5	9	0,138	800	0,0640	18,0	0,00150
36	25	11	0,169	1090	0,0610	25,7	0,00176
						Mean	**0.0015**
						Standard	**0.0002**

	deviation

The evolution of the water flow as a function of the difference of water is thus plotted on the Figure II.20.

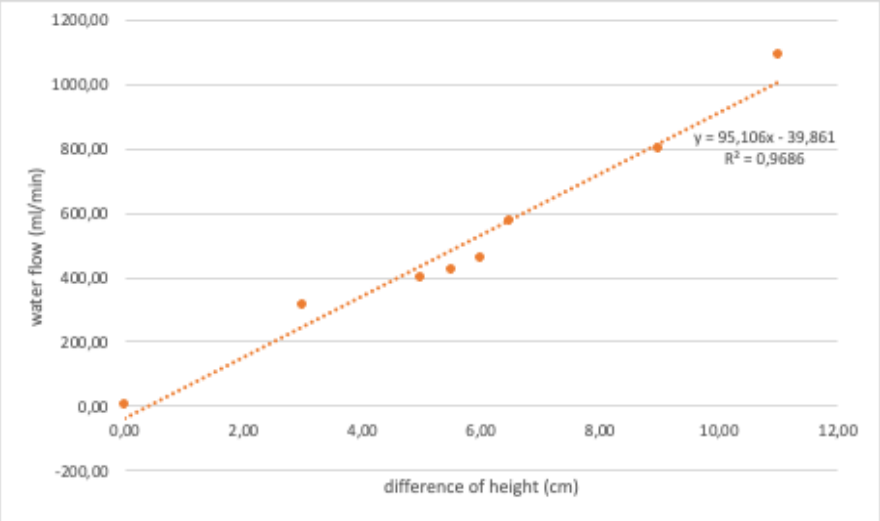

Figure II. 20 - Graphic of the evolution of the water flow for different height of water

An obvious linear correlation exists between these two variables. We now have a relation between the water flow imposed by the pump realizing seepage and the water height difference in our system. Each water level difference is also related to a seepage velocity.

The inputs data for the experiment in seepage are presented

Table II. 10

Table II. 10 - Seepage experiment inputs data

Water flow crossing the soil	**500 ml/min**
Water level difference	0.085 m
Seepage velocity	10 m/day
Initial temperature of the pile	22.1 °C
Water inlet temperature	20.6°C
Duration on the experiment	3h39min (13140 s)

3.3. Results

3.3.1. Dry sand 1

Figure II. 21 shows the evolution of temperature of sensors with time. The start and the end of heating are clearly visible. Indeed, the moment when the heated model energy pile curve ends corresponds to the end of heating and the temperature decrease is clearly observable from this point.

The sensors placed on the piles feel quickly the temperature increase, even if it is at a smaller level. This can be asserted by focusing on the three first curves (PT4, PT5 and PT6) which are represented with also the energy pile temperature evolution in Figure II. 21.

The first column of sensors (Pt9, Pt10 and Pt11), located at around 20 cm, have such a small variation (less than one degree) that it is difficult to attribute it to heat transfer from the energy pile or to the ambient temperature variation as the sandbox is not insulated. It can be assumed that after more than 4 hours of heating, the thermal anomaly has not spread to these sensors. Translated on a prototype scale (50 times bigger), this means that after more than one year of pile heating, piles located 10 m away from the heat source (the energy pile) and situated in dry sand, would not be affected by the thermal anomaly. Obviously, this is a "textbook case" in that a single pile is the source of the heat, and this heat source does not correspond to any real need (which would create a heat source that varies in intensity and time).

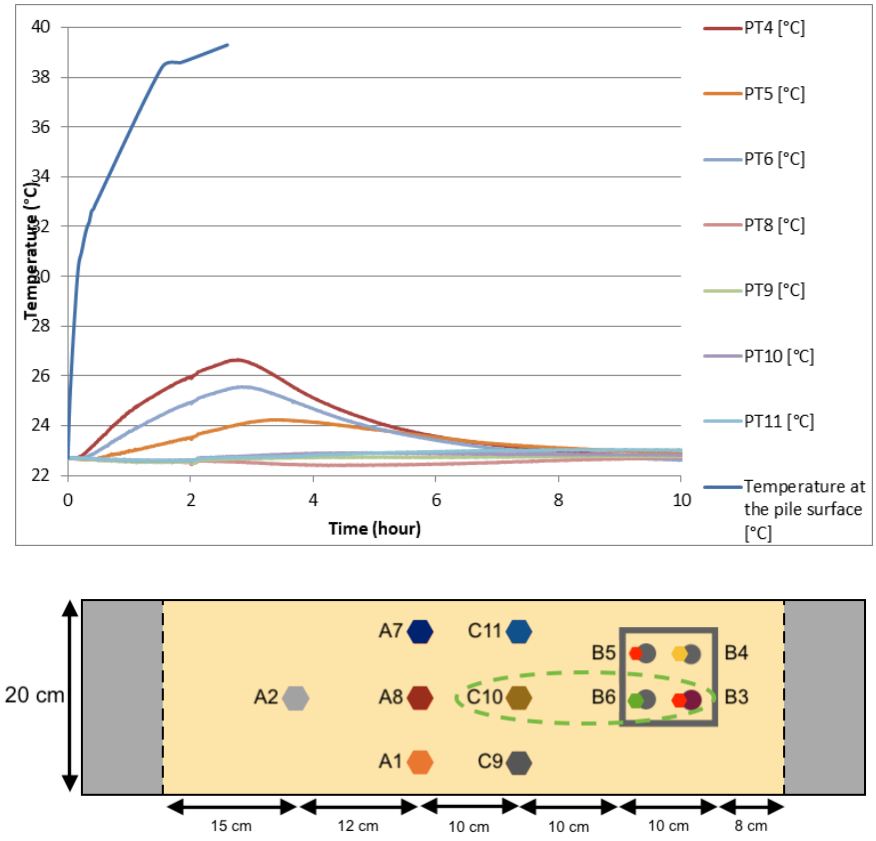

Figure II. 21 - Temperature evolution recorded by the thermal sensors with time and their Position in the model

Two questions have to be tackled and lead to two more experiments in dry sand:

- Does ambient temperature evolution affect the experiment?
- At which moment the sensors in first column will be affected by the thermal anomaly?

3.3.2. Dry sand 2

For this second experiment in dry sand, the aim is to run the same experiment and record data during three days after the end of the heating phase in order to observe the outside temperature evolution impact.

In Figure II. 22, it appears quite clearly that the evolution of the temperature after the heating period is a periodic function of the time. One can determine that the period corresponds obviously to one day. Considering that the model we are working on is reduced 50 times, the similitude law allows us asserting that it would correspond to a period of 6.8 years at the prototype scale (see Chapter III). Thus, it will not be right to take into consideration these variations and one should free himself from it. Indeed, by comparing the temperature peaks outside the model with those inside, it is possible to characterise the thermal inertia of the model with dry sand. It has been calculated that it takes an average of 8.5 hours for a daily temperature variation to spread to the centre of the model (located at a known distance. It is therefore possible to estimate the thermal diffusivity of this soil model by considering the ratio of the squared of the distance (0.1^2m) on the characteristic time (8.5 hours): $\alpha = \frac{0.1^2}{8.5 \times 3600} \approx 10^{-7} m^2/s$. The order of magnitude of sand thermal diffusivity is found identical to the one present in literature (Cf. Figure I. 21)

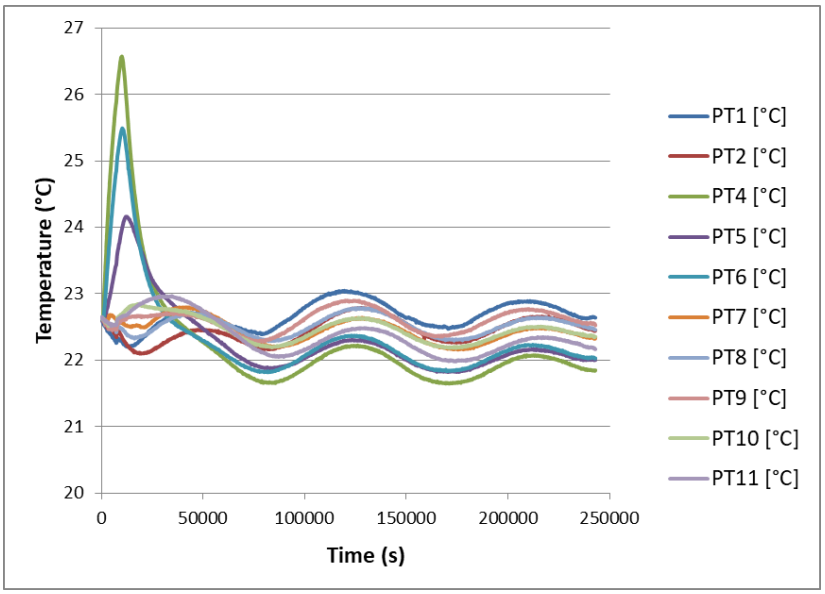

Figure II. 22 - Graph of the PT100's temperature on time in the dry experiment (full)

The fact that the box is not insulated subjects the model to temperature variations in the room with a certain degree of intertia. So if the temperature variation in the room is of the same order of magnitude as what one wants to observe, this becomes problematic. However, this is only really a problem if the inertia of the walls of the box allows the heat to be transferred quickly enough for the duration of the experiment. So, the order of magnitude of the temperature variation and the inertia are the two points to consider. However, insulating the box is not a relevant solution if the temperature variations reach the wall. In all cases, the ideal is to carry out the test with a sufficiently low temperature range and a sufficiently low duration to remain sufficiently far from the walls so that they have no influence.

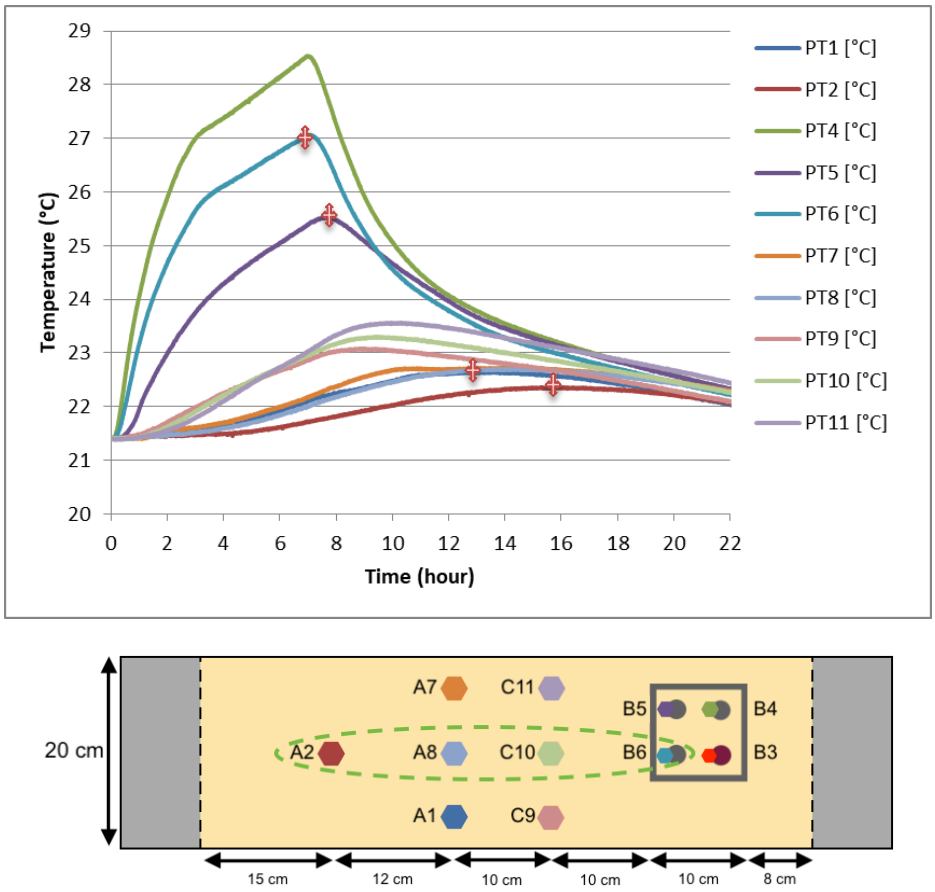

Figure II. 23 - Graph of the evolution of the temperature as a function of the time in the dry sand

For this second experiment in dry sand, since the heating time was longer (than experiment named Dry sand 1), all the sensors felt the temperature increase even the farthest one (Pt2). In Figure II. 23, it also appears that the further the sensor is from the heating pile, the lower the temperature increase is.

In addition, it is also possible to plot the evolution of the temperature as a function of the distance to the heating pile for several times (Figure II. 24). In all cases, it appears that the temperature decreases quite quickly as soon as the heating system is switched off, to reach the initial temperature. It is important to notice that the temperature drops highly near the heat source. It means that for energy piles close to each other a small distance variation can induce a much bigger thermal anomaly. But far from the energy pile (4 diameters), thermal anomalies have low impact.

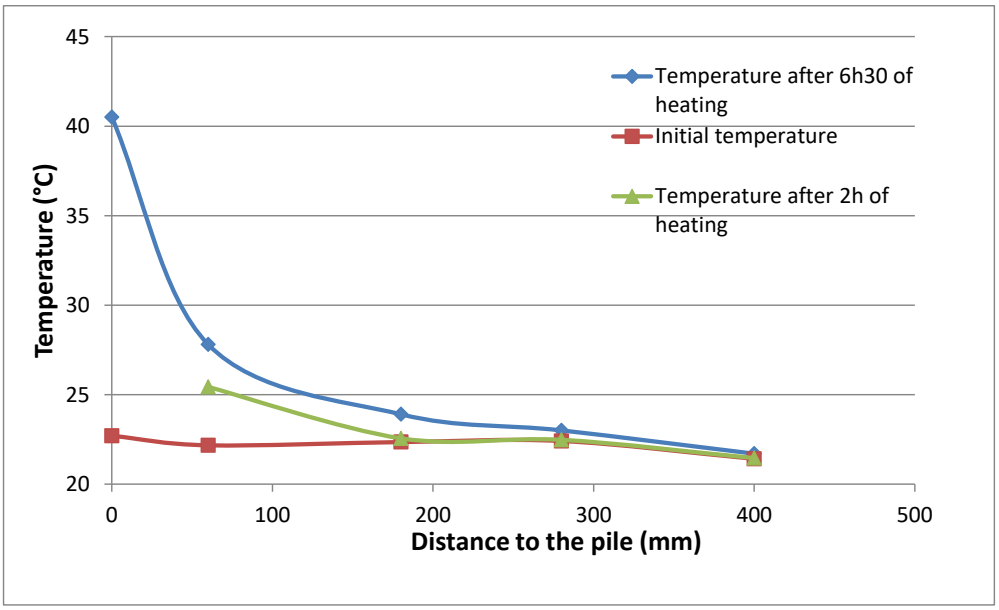

Figure II. 24 - Graph of the evolution of the temperature as a function of the distance to the energy pile

3.3.3. Heat transfer in saturated sand and with seepage

The sandbox model was saturated by adding water at a low flow rate to one end of the box. As this end is made up of gravel (with a high permeability), the water ends up at the bottom of the model and will move upwards over time. Saturation from the bottom and at low flow rates has the same objective of saturating the model as much as possible. In addition, saturation is monitored using two PPTs placed at the bottom of the model.

Once the model has been fully saturated, the model energy pile has been heated with the same power as for the dry case for almost 7 hours. The evolution of the temperature as a function of time is plotted for all the sensors in Figure II. 25

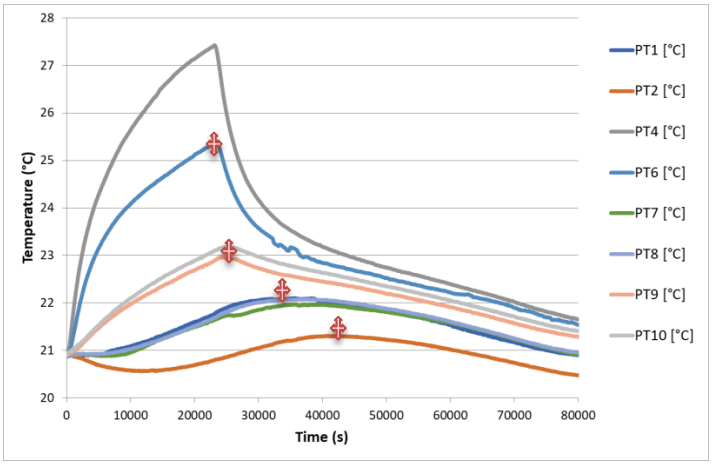

Figure II. 25 - Graph of the evolution of the temperature as a function of the time in the saturated sand

Once again, it appears that the temperature increases first very quickly before moving towards a steady state which is illustrated by the fact that the water entering and leaving the pile are constant. The farthest sensor from the heating pile (Pt2) feels a relatively small temperature increase (less than 1°C) around 2 hours after the end of heating. It can correspond to the heat wave, but it is more probable to be related to the change of the ambient temperature phase-shifted by the inertia of the sandbox, that would be this time around 6 hours. It corresponds to a phase-shift twice smaller than

the case where the sand is dry. It seems logical because the saturated sand has a bigger diffusivity; the velocity at which the heat moves on is therefore bigger.

Figure II. 26 shows the thermal measurements evolutions in seepage case. Globally, it appears that the temperature first increases very quickly for all the sensors and then the temperature increases less quickly until the end of the heating. The shape of this thermal load is determined by the heating system.

Among the interesting points raised, we can see that, contrary to the cases without seepage, the three hottest sensors are in the ascending order: Pt6, Pt8 and then Pt1. The two firsts ones are along the heating pile in the seepage direction. In the cases without water flow in the soil, the hottest sensor was the one on the side of the heating pile. Thus, the impact of the heating plume clearly appears as it is this time the sensors at the middle of the box (centre of the plume) that heat the most. The heat moves in the same direction as the water with a relatively narrow plume due to the quite big seepage velocity.

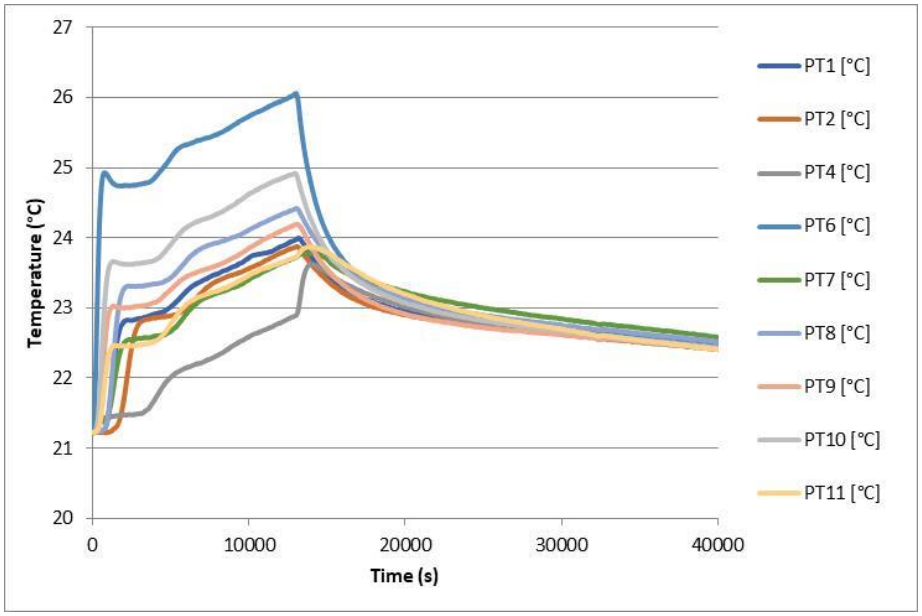

Figure II. 26 - Graph of the evolution of the temperature as a function of the time in the saturated sand with a constant seepage

The evolution of the temperature with the distance from the heating pile is also plotted in Figure II. 27 for several heating times.

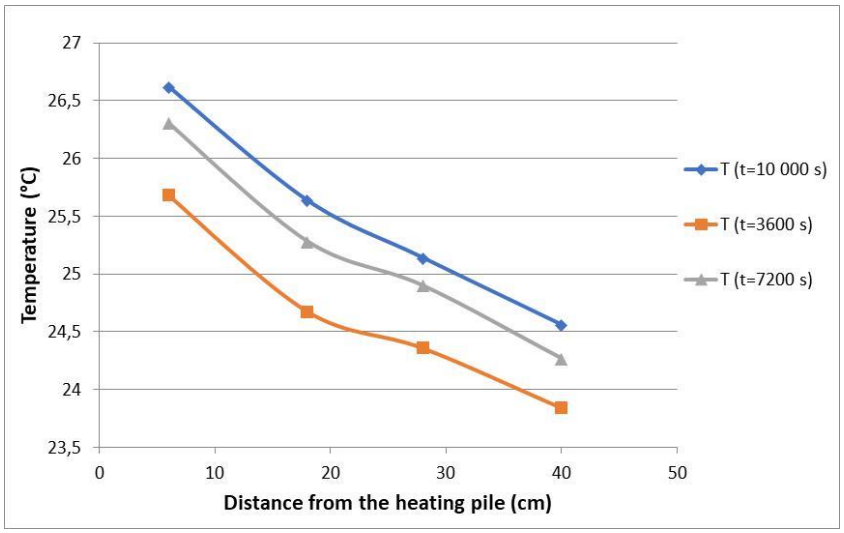

Figure II. 27 - Graph of the evolution of the temperature as a function of the distance with a seepage at different times

The evolutions seem to be every time linear confirming that the advection phenomenon is dominant.

3.3.4 Heat wave velocity

For each case, by focusing on the sensors aligned to the heating pile (Pt6, Pt10, Pt8 and Pt2), heat transfer velocity could be estimated. Indeed, the delay between the sensors appears clearly. The moment when the Pt6 curve stops increasing, nearly corresponds to the end of heating. Then, as several temperature sensors are aligned along the length of the box, it is possible to focus on the additional time required for a sensor or a fictive pile that would be in place of the sensor to reach peak temperature compared with pile 6 investigated. A plot can then be made of the distance between piles as a function of the delay in reaching peak temperature. From a theoretical point of view, in the case of pure diffusion, the curve should be logarithmic: the further the thermal wave wants to spread, the longer it needs to travel (the speed of the wave therefore varies). In the case of pure advection, the evolution is linear: the wave travels at constant speed. In that latter case, the slope of the plot corresponds to this heat wave velocity. In an intermediate case where both advection and conduction are present, the plot should be between the two curves. The points from which these curves were drawn have been highlighted on the corresponding graphs and the results are summarized in Figure II. 28 where a comparison between dry, saturated and seepage cases is made. At each time, the slope of the trend line gives an estimation of the heat front wave velocity.

Following this protocol, a velocity value of 1.3 m/day was found for the dry case. In saturated case, the heat should move on faster and this assumption was verified in the same way as described above for dry sand. In saturated sand, a heat wave “velocity” of 1.5 m/day has been found. It is around 1.2 times faster than in the dry sand. Finally, a thermal wave front velocity of 2,6 m/day is calculated for the seepage case. It is twice quicker than the heat wave front velocity in dry it is 1.7 times than the saturated case. In addition, it can be observed that water flow leads to a reduction in the thermal anomaly. Because of seepage, the thermal anomaly is certainly moved faster (or further, depending on how you look at it), but above all it is weaker at a given point and time. For example, for the same thermal load, sensor 10 goes from 20 to 25°C in 10 000s in the saturated case (25% increase) whereas it goes from 21 to 24°C in the flowing case for the same time (+7%). The water flow therefore has the effect of reducing the intensity of the thermal anomaly.

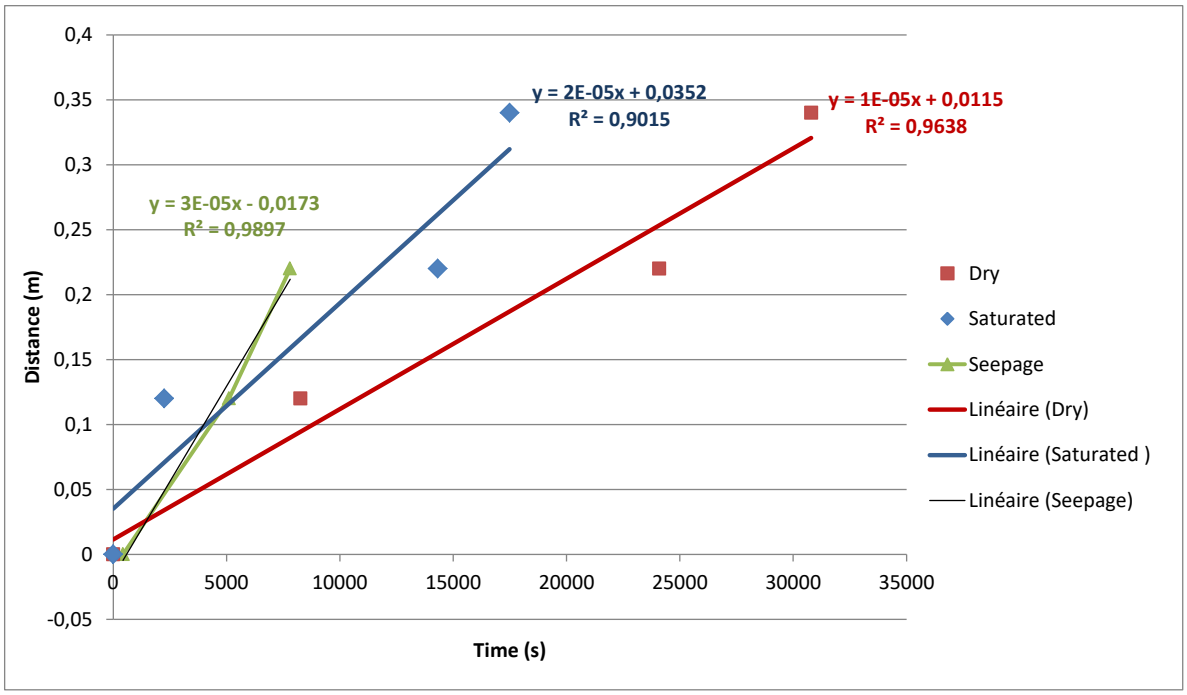

Figure II. 28 - Time taken to reach peak temperature as a function of distance

In this section, the thermal transfer was characterised for the model and studied for different hydric state and in particular within seepage. Indeed, in this particular case the thermal anomaly is moved downstream by advection. This particular way of heat transfer depending on the hydrologic state will influence the mechanical behaviour of the energy structure but could also affect the energetic efficiency of the system and the ones located downstream. Thus, and in order to keep with the thermal and energetic questions, the next part will present a numerical study about the impact of groundwater flow on energy structures system efficiency.

4. Evaluation of heat pump efficiency for energy piles group within seepage

The previous section showed that for a constant heating power, seepage allows decreasing the energy pile temperature and obtaining therefore a temperature field with smaller temperatures. This modification of the temperature field will impact the efficiency of an energy structure system. The question tackled in this section deals with this efficiency of such a system but with a most realistic size and thermal power demand. The piles group size and the complexity of the demand drive us to tackle this question numerically. Indeed, in this section, a project carried out in collaboration with Dr Thibault Badinier and Dr Jean de Sauvage, which will result in a journal article, is presented. The creation of the numerical model was not carried out by myself and is therefore presented only briefly. My work consisted creating a python code that can simulate the behaviour of a heat pump for both operating modes (summer and winter) and integrate it into the code, carry out the various studies, process and analyse the results.

4.1. Cluster effect and thermal anomaly washing

As explained in chapter I, energy piles operation benefits from the relative constant temperature in the soil below a certain depth. According to the first law of thermodynamics, heat naturally transfers from hotter regions to colder regions. Consequently, in order to transfer heat from the ground (approximately 13°C) to a building's heating system (around 35°C); electrical energy is required, which is facilitated by a heat pump. The ratio between the heat power provided to the building (noted $\mathrm{Q_{hot}}$) and the electric power consumed (noted W) defines the performance factor of the system (noted COP) (Equation II.4.1a). It is worth noticing that according to the first law of thermodynamics, the heat power is the sum of the power drained from soil (noted Q_{cold}) and the electrical power transformed into heat (Equation II.4.1b).

$$COP = \frac{Qhot}{W} \qquad \text{(II.4.1a)}$$

$$Qhot = Q_{cold} + W \qquad \text{(II.4.1b)}$$

As explained in Chapter I:

- Seasonal use is profitable as it helps to avoid multi-year thermal shift and higher soil temperature will allow heat pumping with higher efficiency (I.1.3.2).
- The effect of thermal clusters will increase while the piles are built closer to each other (I.1.6.3)
- Ground water flow will thermally recharge the ground by replenishing the thermal energy surrounding energy geostructures, resulting in a thermal washing effect (I.1.6.3)

Therefore, the tackled problem can be summarised as follows. On one hand, by drawing heat from the ground, the group of energy piles leads to a decrease in soil temperature, which has the

consequence of reducing the efficiency of the heat pump system (COP factor). This effect might depend on the geometry of the group, particularly on the distance between the piles. On the other hand, the groundwater flow might create a thermal washing effect, reducing the thermal anomaly and restoring efficiency of the heat pump system. This phenomenon becomes greater as seepage velocity is high. Finally, in summer mode, the heat evacuation in the soil will restore the thermal reservoir, providing heat energy for winter season at higher temperature which will increase COP factor.

In the following study, thermal efficiency questions are tackled by studying the theoretical efficiency of the heat pump system depending on the geometry of the pile group, on the underground water flow conditions and on the season heating and cooling cycles. For this purpose, numerical models using the FEM software CESAR-LCPC are built in order to simulate this problem of hydro-thermal coupling. The objective of this section is to study numerically the thermal and energy interactions within a group of piles. It aims to present the measurable impact of heat clustering and thermal washing.

4.2. Numerical model

The study is carried out with CESAR-LCPC, a finite element modelling (FEM) software continuously developed by the University Gustave Eiffel. This software is dedicated to civil engineering problems such as foundations, embankments, concrete structures, etc. (Humbert et al. (2005)). In particular, it has the ability to deal with transitive diffusion problems like thermal and hydraulic problems. It makes it possible to study geothermal problems taking into account the groundwater flow conditions. Moreover, the CESAR-LCPC software can be used with a Python script and the dedicated Python module called "Pilote CESAR"[5]. With this tool, it is possible to describe model geometry, meshing, boundary conditions and loading, run the computation and analyse the resulting data. Other Python module can also be used within the script. Therefore, it allows easy parametric study even regarding geometrical aspect.

4.2.1. Numerical problems and equations

The main objective is to solve simultaneously the hydraulic problem, i.e. seepage velocities, and the thermal problem, i.e. the temperatures field.

It is supposed that the hydraulic problem consists in water flow in fully saturated soils. The governing equation is then the classical Darcy equation:

$$\overrightarrow{V_D} = -k.\overrightarrow{grad}h \qquad \text{and} \qquad div\,\overrightarrow{V_D} = 0 \qquad \text{(II.4.2)}$$

Where $\overrightarrow{v}$ is the Darcy water velocity in $m \cdot s^{-1}$, k is the water permeability in $m \cdot s^{-1}$ and h is the hydraulic load in m. The thermal problem is governed by the thermal equation:

$$C_v \frac{dT}{dt} + div\,\vec{j} = 0 \qquad \text{(II.4.3)}$$

Where T the temperature in K, t is the time in s, $\vec{j}$ is the total heat flux in W and C_v is the volumic thermal capacity in $J \cdot m^{-3}.K^{-1}$ (Cf. Chapter I, 1.5). In underground condition, the heat flux is the sum of two fluxes, each corresponding to a distinct physical phenomenon. First, the conductive flux,

[5] Cf. https://cesar.univ-gustave-eiffel.fr/exemples

noted $\overrightarrow{J_{cond}}$, is due to natural thermal conduction and computed according to Fourier Law, considering λ the thermal conductivity in $W.m^{-1}.K^{-1}$, and the temperature gradient:

$$\overrightarrow{J_{cond}} = -\lambda \overrightarrow{grad}\, T \qquad \text{(II.4.4)}$$

Secondly, the advection flux, is noted $\overrightarrow{J_{cond}}$, and corresponds to the movement of underground water with its stored energy. It is computed, considering underground water flow velocity $\overrightarrow{V_D}$ according to Darcy's equation (II.4.2), the water volume heat capacity noted C_w, and T the temperature:

$$\overrightarrow{J_{adv}} = \overrightarrow{V_D}\,.C_w\,.T \qquad \text{(II.4.5)}$$

Therefore, the thermal problem depends on the hydraulic results. The global problem is then considered as coupled. However, the variation of temperature is assumed not sufficient to change significantly the water viscosity or to freeze the soil. Then, the effect of temperature on hydraulic problem is supposedly negligible and not considered in the numerical process.

4.2.2. Variable heat loading

The principle of the heat pump was explained and schematized in Chapter I. As a reminder, in winter mode, the system pumps a quantity of heat energy Q_{cold} in the cold source (here the soil), and gives a quantity of heat energy Q_{hot} to the building, while consuming a quantity W of electric power. To do so, a fluid, of volumetric thermal capacity $C_{v,f}$ is pumped in the piles heat exchangers at a pumping rate of q ($m^3.s^{-1}$), resulting in a temperature difference between the inlet and outlet fluid (T_{in} and T_{out}). Overall, it produces heating fluid at temperature T_{hot}. A schematic representation of the whole system with the different exchanges and the associated equations is proposed Figure II. 29

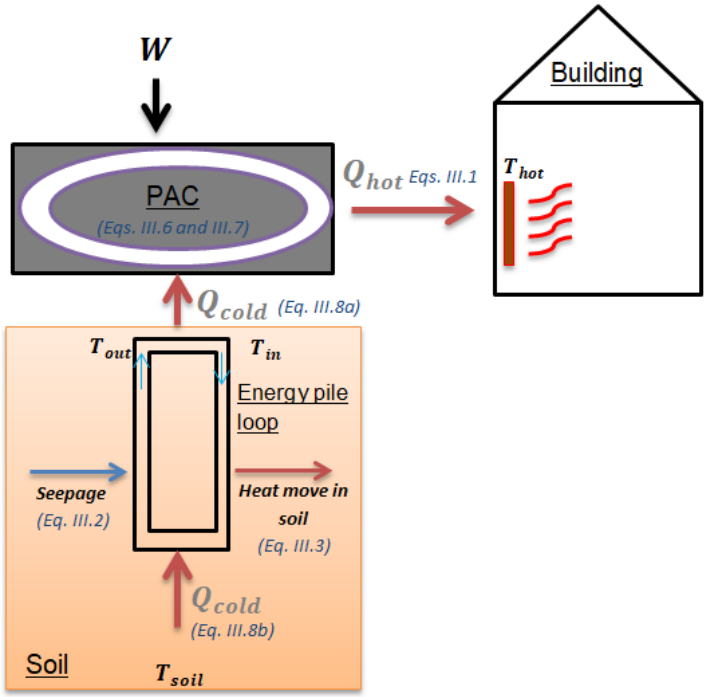

Figure II. 29 - Schematic representation of the whole system with different exchanges and associated equations

As already explained, the relation between Q_{cold}, Q_{hot}, and W is given by the first law of thermodynamics (see equation (II.4.1b)) and the heat pump efficiency is defined by the COP factor (see equation (II.4.1a)). Hence, taking into account that the required heat power for the building (Q_{hot}) is already known, the heat load imposed on the model (Q_{cold}) should be calculated using equation (II.4.6):

$$Q_{cold} = Q_{hot}\left(1 - \frac{1}{COP}\right) \qquad \text{(II.4.6)}$$

However, according to manufacturer's data, the heat pump efficiency will decrease while the temperature gap between cold and hot source increase. Based on their benchmarking work (see Figure II. 30) (Staffell et al., 2012) propose the equation II.4.7 to compute the COP factor depending on the difference between the temperature T_{hot} of hot source (underfloor heating) and the temperature T_{cold} of cold source (the heat exchanger fluid), expressed in K :

$$COP = 8.77 - 0.150\,(T_{hot} - T_{cold}) + 0.000734\,(T_{hot} - T_{cold})^2 \qquad \text{(II.4.7)}$$

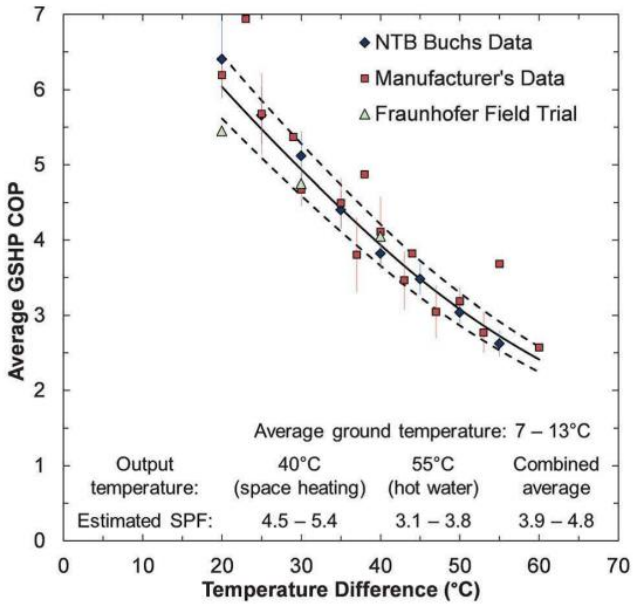

Figure II. 30 - Benchmarked COP factor regarding temperature difference between hot and cold sources for ground sourced heat pumps (Staffell et al., 2012)

While the hot source temperature is a given data according to the building heating system (around $35°C$), the cold source temperature depends on the soil temperature T_{soil}), on the exchanged power inside the soil Q_{cold}, on the geostructure fluid pumping rate q (in $m^3.s^{-1}$), and on this fluid volume heat capacity C_{fl}. Indeed, to exchange Q_{cold} with the soil, the heat pump circulates the geostructure's fluid with a difference between the inlet temperature T_{in} and the outlet temperature $\mathrm{T_{out}}$. $\mathrm{Q_{cold}}$ is then computed with equation (II.4.8a). We consider that the same amount of energy is extracted from soil through the pile, and is then computed according to a simple thermal resistive equation (see equation (II.4.8b)). Where $\mathrm{T_{fl}}$ is the average fluid temperature computed with equation (II.4.8c) and $\mathrm{R_{th}}$ is the thermal resistance of the pile in $\mathrm{K.W^{-1}}$ (evaluated numerically, see section 3.4.1).

$$Q_{cold} = C_{fl}.q_{pump}.(T_{out} - T_{in}) \qquad \text{(II.4.8a)}$$

$$Q_{cold} = \frac{T_{soil} - T_{fl}}{Rth} \qquad \text{(II.4.8b)}$$

$$T_{fl} = \frac{T_{in} + T_{out}}{2} \qquad \text{(II.4.8c)}$$

Combining equations (II.4.8a), (III.8b) and (II.4.8c), and assuming that the temperature of the cold source is equal to T_{in} will lead to the following equation:

$$T_{cold} = T_{in} = T_{soil} - Q_{cold}.R_{th} - \frac{C_{cold}}{2C_{fl}.q_{pump}} \text{ (II.4.9)}$$

Finally, combining equations (II.4.9), (II.4.7) and (II.4.6) lead to the following equation:

$$COP = 8.77 - 0.150\left(T_{hot} - T_{soil} + Q_{hot}\left(1 - \frac{1}{COP}\right)\left(R_{th} - \frac{1}{2C_{fl}.q_{pump}}\right)\right)$$

$$+0.000734\left(T_{hot} - T_{soil} + Q_{hot}\left(1 - \frac{1}{COP}\right)\left(R_{th} - \frac{1}{2C_{fl}.q_{pump}}\right)\right)^2 \qquad \text{(II.4.10)}$$

Finally, considering T_{hot}, C_{fl} , q_{pump}, and R_{th} as constants of the system and Q_{hot} as an input data, the COP factor is the solution of a third degree polynomial equation, depending only on soil temperature (T_{soil}).

4.2.3. Summer mode heat pump

In summer mode, the behaviour of the system is reversed. Therefore, the heat pump aims at moving calories from the cold source (now the building) to the hot source (now the soil). The efficiency of the heat pump in summer mode, noted COP_S is then measured as the ratio between the heat evacuated from the building Q_{cold} and the consumed electric power W. Considering equation (II.4.1b), (II.4.1a) and (II.4.7):

$$COP_S = \frac{Q_{cold_S}}{W} = \frac{Q_{hot_S} - W}{W} = COP_W - 1 = 7.77 - 0.150\left(T_{hot_S} - T_{cold_S}\right) + 0.000734(T_{hot_S} - T_{cold_S})^2 \text{ (II.4.11)}$$

However, in case of free cooling, the difference between T_{hot_S} and T_{cold_S} could be small or even negative which is outside the Staffell et al. (2012) dataset. Nevertheless, for this study it is assumed that this equation remains valid even for negative temperature gap for three main reasons:

- It allows the numerical continuity of the computing process during summer period modelling.
- The COPS remains defined because electrical work is always present to ensure that the heat pump maintains fluid circulation (even though the compressor is no longer in use).
- At such temperature gaps the efficiency of the heat pump is high enough to consider the error on W estimation as negligible.

Eventually, in summer mode, the imposed heat to the soil is then Q_{hot_S} computed with equation (II.4.12).

$$Q_{hot_S} = Q_{cold_S}\left(1 + \frac{1}{COP_S}\right) \qquad \text{(II.4.12)}$$

4.3. Global computation process

The global computation process is described below and can be summarized with the Schematization of the program process in Figure II. 31, where the blue frame corresponds to the hydraulic calculation made using finite element software, the red frame contains the thermal calculations (made using finite element software) and energy calculations (COP calculated using the Python program), and the green frame corresponds to the results also calculated using Python.

First, the hydraulic problem is described, with geometry, parameters, boundary condition and loadings. The computation is conducted in order to get a steady state solution with the DTNL (Diffusive Transient, Non Linear) solver from CESAR-LCPC (Piau et al., 2005). The results are stored and will be used in the thermal computations.

Secondly, the thermal problem is described with geometry, parameters and boundary conditions. The computation will be conducted as transient evolution on successive time steps (t) with the DTNL solver from CESAR-LCPC. In Transient mode this solver uses implicit Eulerian integration, which ensures stability of the results, independently of the time step. The initial temperature of the entire system is supposed to be homogeneous at $13°C$. At each computation step, the thermal loading imposed to the model Q_{cold} is modulated according to the COP factor computed through equation (II.4.10) considering the current soil temperature.

In particular, for the first step, the COP factor is computed based on the initial temperature solving equation (III.10). Then the thermal loading is determined based on equation (II.4.6) and the values of $Q_{hot}(t)$ given as input data of the problem. After step $t = i$, the average soil temperature around the piles is determined from the temperature results. The $COP(i)$ at time $t = i$ is then computed. This value is then used to compute the $Q_{cold}(i + 1)$, the thermal loading imposed to the model between step i and $i + 1$. The computation between step $t = i$ and step $t = i + 1$ then proceeds. The computation process continues like this until the defined time $t = N$.

At the end of the process, the successive values of $COP(t)$, $T_{soil}(t)$ and Q_{cold} are stored in a .txt file, and temperature field evolution can be observed and studied with CESAR-LCPC tools. In cases of seasonal summer and winter solicitation, the program is able to switch from winter COP computation to summer COP_S computation. Therefore, in summer mode the values of imposed heat to the building $Q\_hot(t)$ is then negative and the sign of the heat loading Q_{cold} imposed to the model also changes (corresponding respectively to Q_{cold_S} and Q_{hot_S} from equation (II.4.12).

4.4. Study case description

For the purpose of this study, we produce models based on the case of a fictive building of $1000\ m2$ needing a peak heating power of $15\ 500\ W$. The building is therefore built on a group of 20 energy piles, each being $12\ m$ long. Those values have been established based on the example of an energy-neutral building in Gonesse, France (Bernard, 2022)

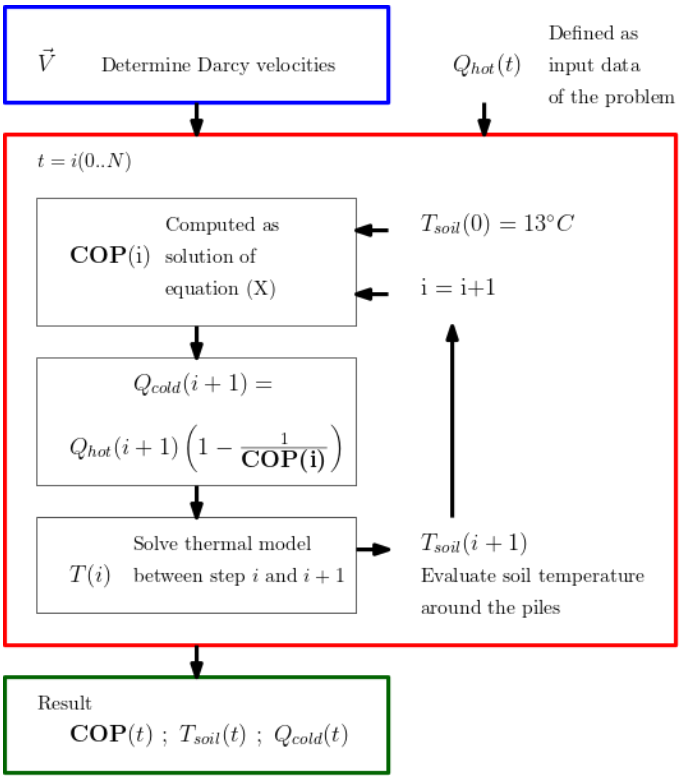

Figure II. 31 - Schematization of the program process

4.4.1. Geometry

According to section 2.1, heat transfers to depth are negligible and one can reasonably work in 2D. The distance between the piles will be part of the parametric study varying from 1 diameter to 10 diameters. The global size of the model is six times longer than the pile group (at least 20 m long), and 3 three times larger (at least 10 m wide). The pile group is in the middle of the left half of the model and the underground flow goes from left to right. Those geometric conditions have been chosen in order to limit interaction between the group and the boundary conditions, including the thermal plume formation. The principles of these models are shown on Figure II. 32 and it appears that the distance between the pile group and the edge is at least once the pile group size.

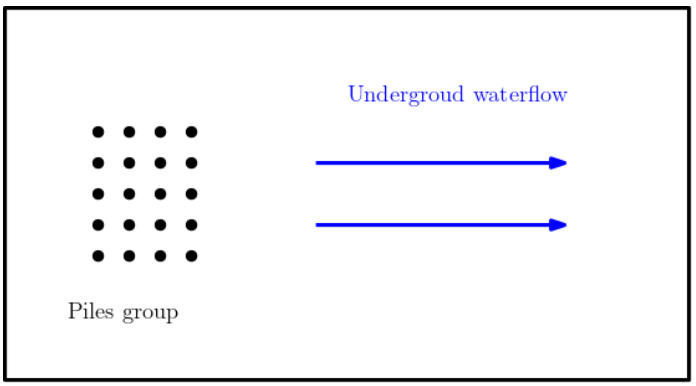

Figure II. 32 - Geometrical model principles

Each pile is supposed to have a diameter $D = 0.60\ m$, and to be equipped with four heat exchanger tubes attached to the reinforcement cage on the side of the pile. In order to spare computation time, such a level of detail is simplified using a unique central heat exchanger tube of greater diameter (as

shown on Figure II. 33. Such simplified geometry is commonly used as it exposes similar macroscopic thermal behaviour. The radius of equivalent tube is set to expose the same permanent thermal resistance as the realistic geometry (Cecinato and Loveridge, 2015). In the study case, this equivalent radius has been numerically estimated to $0.19\ m$. This estimation process consists in imposing a heat flux between tube and soil on a geometrically detailed pile with constant soil temperature. The temperature gap between soil and tube is used to compute the thermal resistance and then the equivalent tube radius.

4.4.2. Parameters

For simplification reasons, the materials are considered homogeneous and isotropic. All parameters are summed up in Table II. 11. For the hydraulic models, parameters are set to represent permeable soil and impermeable structures. Exact values do not impact the results as boundary conditions are set to obtain the targeted average Darcy velocities (see 3.4.3). The thermal parameters of the materials are taken from Delerablee (2019), these values were evaluated on the experimental site of ESense City with a thermal probe test.

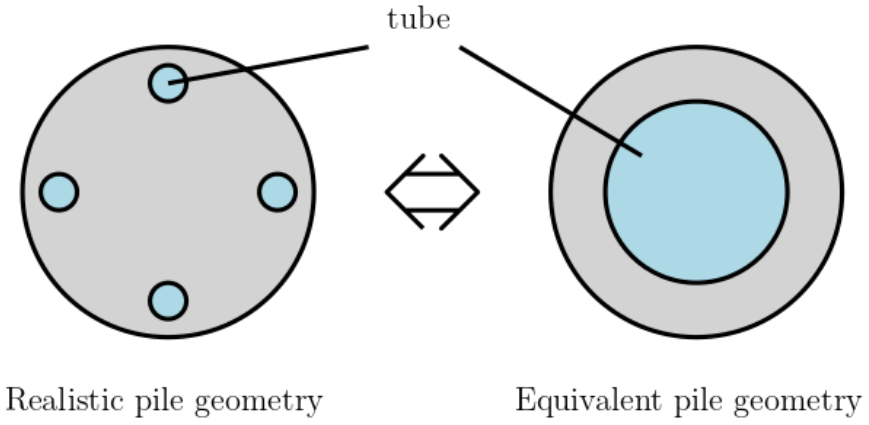

Figure II. 33 - Pile simplified geometry

As a particularity, the thermal conductivities of the tube are extremely high in order to represent moving and turbulent fluid which will impose homogeneous temperature. However, its thermal capacity is set equal to the concrete to keep the global thermal capacity of pile constant.

Table II. 11 - Numerical models parameters

	Thermal conductivity (W/mK)	Volumetric thermal capacity (J/m^3K)	Water permeability (m/s)
Soil	3.0	$1.8.10^6$	10^{-4}
Concrete	1.8	$1.8.10^6$	0
Tube	10^{10}	$1.8.10^6$	0

The other parameters including heat pump parameters are listed below:

- Water volume thermal capacity: $C_w = 4{,}20.10^6$
- Fluid volume thermal capacity: $C_{fl} = 3.60.10^6$
- Fluid pumping rate: $q_{pump} = 3\ m^3.h^{-1}$
- Winter hot source temperature: $T_{hot} = 40\ °C$

- Summer cold source temperature: $T_{cold_S} = 11\ °C$
- Initial model temperature: $T_{init} = 13\ °C$

4.4.3. Boundary conditions

4.4.3.1. Hydraulic model

The hydraulic model is set to impose an average groundwater velocity V_{av} parallel to the model axis. Therefore, upstream and downstream boundary conditions are set with imposed hydraulic charge. On the two other edges of the models, the boundary conditions are set to impose water velocities parallel to the models edge. The difference between h_{max} and h_{min} is then computed according to equation (II.4.13) with L the length of the model. The hydraulic model boundary conditions can be summarized on Figure II. 34.

$$h_{max} - h_{min} = \frac{V_{av}L}{k.} \qquad \text{(II.4.13)}$$

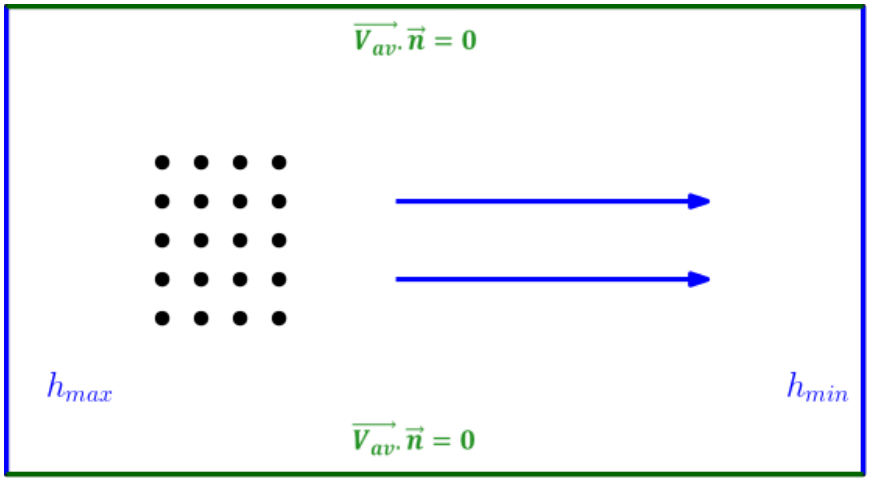

Figure II. 34 - Hydrological boundary condition

4.4.3.2. Thermal model

The thermal boundary conditions are set to represent soil temperature away from the thermal anomaly induced by the system. Therefore, the edge temperature is set to $13\ °C$ which is also the initial model temperature. The thermal loading is set as a cooling power (or heating during summer) imposed inside the tubes by the heat pump system. Its value is variable during the computation, as explained in section 3.2.2. The imposed thermal load is computed to match the global heating need of the building, and is equally shared between each pile and along the pile. This is equivalent to considering that the thermal load is applied in series. This is much simpler to simulate numerically and is also consistent with practice, although real system are generally a mix of parallel and series. The thermal model boundary conditions can be summarized in Figure II. 35.

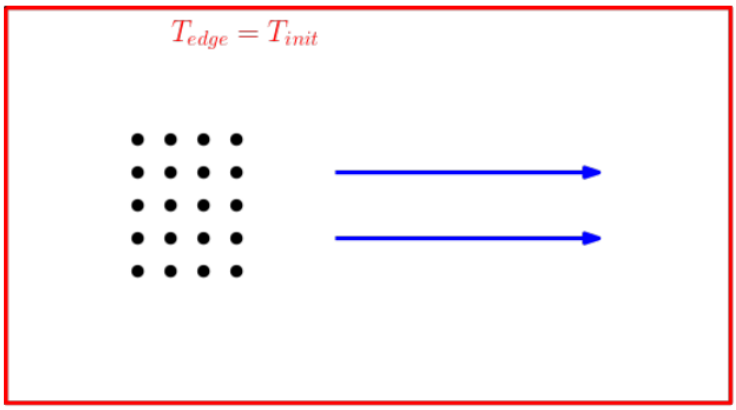

Figure II. 35 - Thermal boundary conditions

4.5. Parametric study and results

In this section, several parametric studies with diverse scenarios are exposed in order to show different behaviours of the system. The first scenario simulates one month's operation of the heat pump and looks at the evolution of the COP for different flow speeds and distances between the piles.

4.5.1. Group of pile under one month of peak use

For these first models, the scenario is one-month winter solicitation at the peak maximal heating power of $15.5\ kW$ with a daily activation pattern consisting in $12\ h$ heat pump activation and $12\ h$ rest ($0\ W$ heating). The computation process uses 336 steps of $2\ hours$ (28 days total), which allows a detailed description of the heat pump behaviour within each day. This hypothetical heating scenario was selected because it allowed highlighting the behaviour of our heat pump model while keeping the temperature and COP values in a realistic range.

4.5.1.1. Influence of seepage water velocities

The first study aims to observe the COP evolution over 28 days of intensive use with different seepage velocities. For this case, the inter-pile distance is constant and equal to 3 diameters. The velocities range is then set between $0\ m/day$ and $2.0\ m/day$. Such range has already been proved to be wide enough to observe various behaviours (Badinier et al., 2023). As preliminary results, one can observe final temperature fields with two different values of seepage velocities (Figure II. 36). For null seepage velocity, the thermal anomaly is concentrated on the piles group. In opposition, a relatively fast seepage will result in a thermal plume and smaller temperature decrease overall.

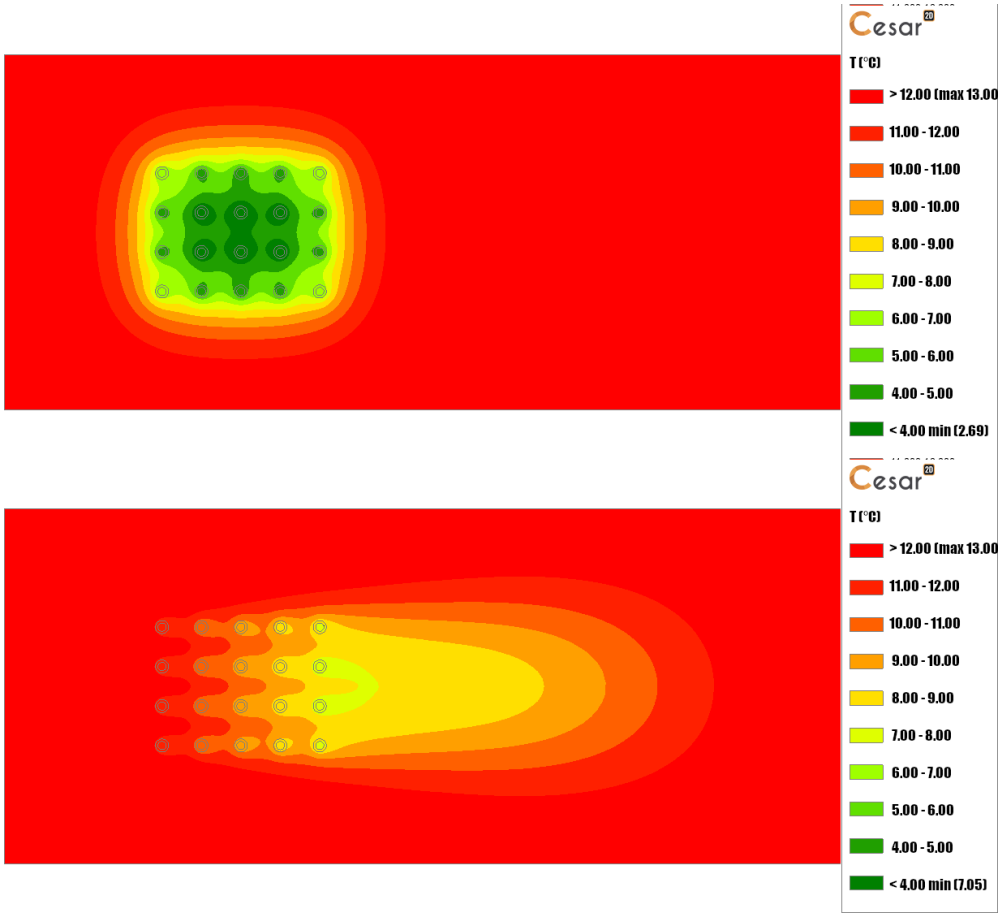

Figure II. 36 - Temperature fields for a) seepage velocity of 0 m/day and b) seepage velocity of 0.3 m/day and inter-pile distance of 1.2m

Figure II. 37 shows the COP evolution over the 28 days resulting from the computation process. As expected, the COP factor decreases over the period. However, the intermittency in the heat demand generates the particular wavelet shape of the curve, with decreasing values in activation periods and an increase of the COP during the resting period. The observation of the soil temperature data will lead to the same observation. Indeed, according to equation (II.4.10), these data are strongly linked. As an information and, for example, in case of average velocities of $0.3\,m.day^{-1}$, the soil temperature decreases over the month from $13\,°C$ to $9.9\,°C$ while with null seepage velocity, the average soil temperature will reach a minimum value of $4.5\,°C$ (Figure II. 37) There is a clear correlation between COP and ground temperature

As expected the higher the water velocity, the higher the COP value. For relatively low seepage velocities ($0m.day^{-1}$ to $0.1\,m.day^{-1}$) the COP does not stabilize and should tend to 1 for hypothetical infinite simulation. On the contrary, above a certain seepage velocity, the COP stabilizes around an acceptable value. This phenomenon can easily be explained by the equilibrium between the input heat power by the inflow and the heat power drained by the heat pump system. The soil surrounding the energy piles is therefore maintained at a certain temperature that allows acceptable efficiency of the heat pump.

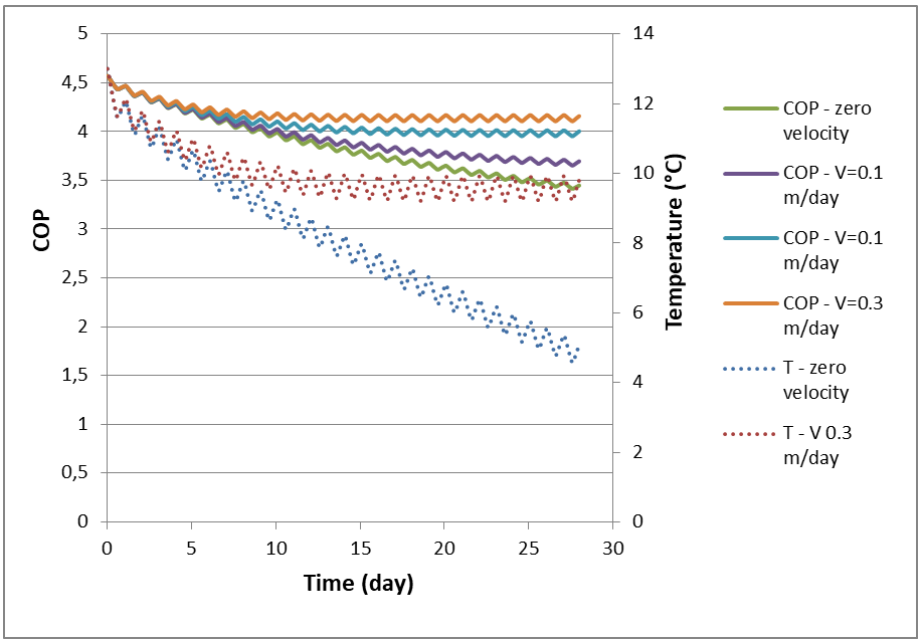

Figure II. 37 - COP and soil temperature evolutions for different seepage velocities

The conclusion of this first study is consistent with our previous work (Badinier et al., 2023) and with literature.

4.5.1.2. Influence of the inter-pile distance

The second study aims to observe the COP evolution over the same period of time with different distance between the piles. The inter-pile distance is then set between 2 diameters and 10 diameters. The seepage velocity is set to a constant value of $0.2\ m.day^{-1}$.

Figure II. 38 shows the COP evolution for the different inter-pile distance. Results tend to demonstrate the existence of a cluster effect. If multiple energy piles are close enough, they will all drain energy from the same soil area and the thermal anomalies will demonstrate a cumulative effect. As a result, the COP remains at higher values for larger distances between the piles.

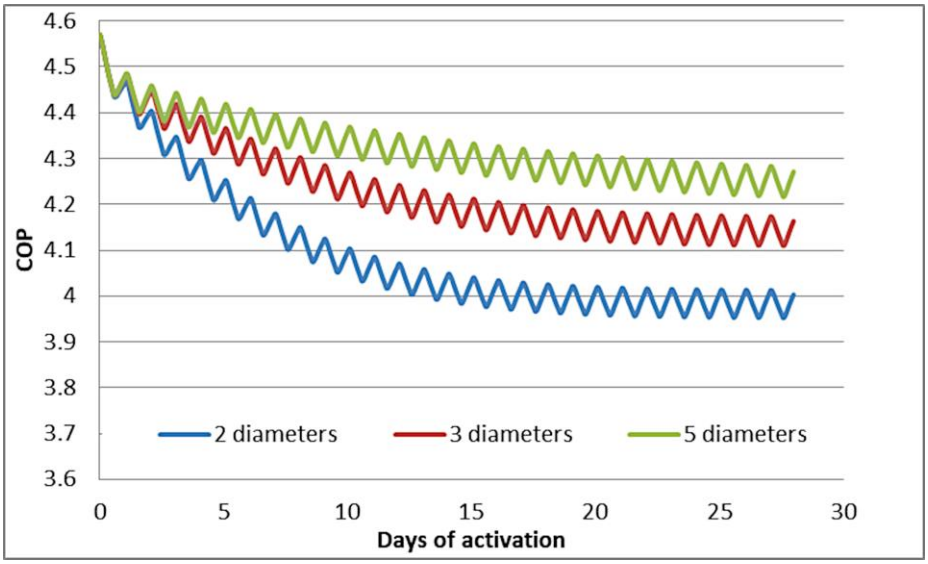

Figure II. 38 - COP evolution for diverse inter-pile distances

4.5.1.3. Overall study and results

Finally, with this heating scenario, all cases with different inter-pile distances and seepage velocities are carried out. Then COP values after the 28 days are compared as an indicator of the residual efficiency of the system in these cases. It is important to mention that the COP value obtained does not always correspond to a stable behaviour, especially when dealing with lower seepage velocities. The results are shown in

Figure II. 39. This figure shows the combined effect of both seepage and inter-pile distance. As previously observed, for the same inter-piles distance, the efficiency will grow with the seepage velocities. This effect is observed for each value of inter-pile distance, but is stronger for smaller distances. Consistently, for the same seepage velocity, a greater distance will allow greater final value of the COP. However, for seepage velocities over $0.5\ m.day^{-1}$, the effect of the distance is almost negligible. The same conclusion could be exposed with summer mode. The final COP_S values after 28 day of activation are shown on

Figure II. 39c.

Based on the obtained COP and COP_S data, the equation (II.4.14) is proposed to evaluate the COP and COP_S depending on the inter-pile distance D (in m) and seepage velocity V_D (in $m.day^{-1}$):

$$COP(D,V_D) = COP_{max}(1 - \frac{0.3}{D}(1 - \exp(-3.8V_D)) \qquad \text{(II.4.14)}$$

The comparison between data and formula are exposed in Figure II. 39b and Figure II. 39d. We were able to fit the same equation to both scenarios, only changing the target COP value with $COP_{max} = 4.50$ and $COP_{S,max} = 7.13$. This might indicate that this formula is applicable on this system whatever the solicitation scenario is. However, further study should be conducted to confirm the applicability of the heat pump simulation on other system configuration (others power demands and sizes of piles group).

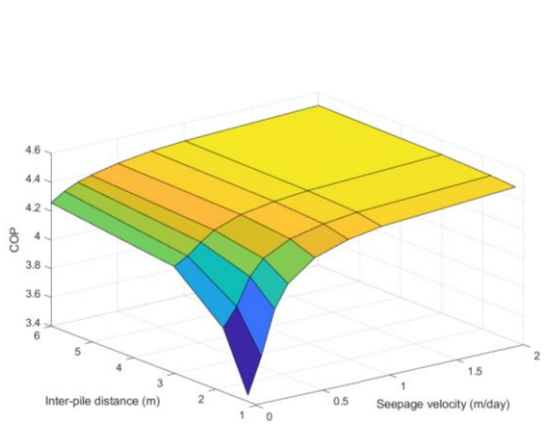

a) COP after 28 days on winter mode, depending on inter-pile distance and seepage velocities

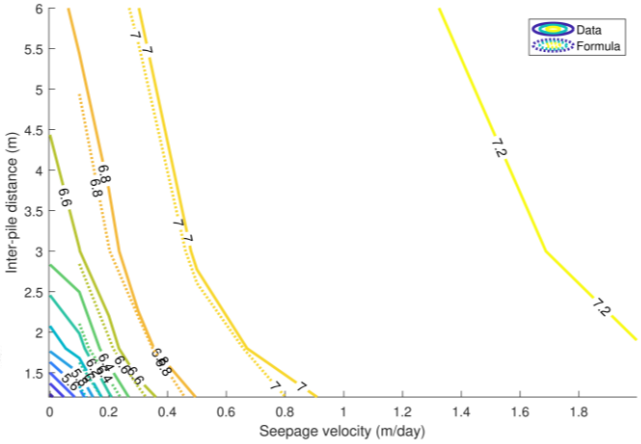

b) Comparison between COP and evaluated COP with proposed formula

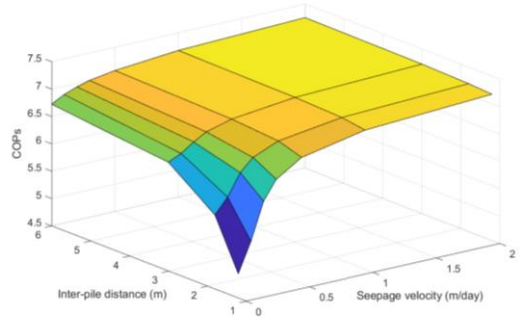

a) COP_S after 28 days on winter mode, depending on inter-pile distance and seepage velocities

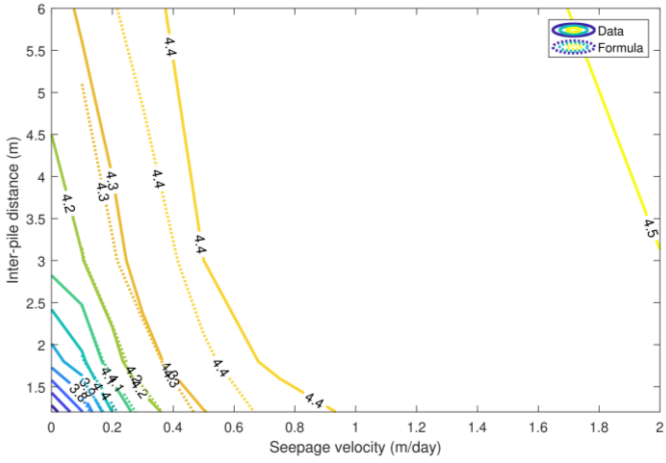

b) Comparison between COP_S and evaluated COP_S with proposed formula

Figure II. 39 - Evolution of COP and COPs as a function of inter-pile distance and seepage velocities

Finally, it can be inferred that distance between the piles and seepage velocity are favourable parameters for the heat pump efficiency. Therefore, each one of these parameters could be used to impact the COP factor. As an example, in a case where the seepage velocity is small, the heat cluster effect can be tampered by increasing the inter-pile distance. Additionally, it is observed that the influence of seepage velocity is exponential. Since this parameter is measured with a high variability on real sites, a great caution should be used in the design phase.

4.5.2. Multi-year seasonal behaviour

For this second model, the geometry is set to an inter-pile distance of $1.2\ m$ (2 diameters), the total size of the model is increased to twice the original size, to ensure correct behaviour at the model boundary for longer solicitation. The computation is set on 3649 steps of$12\ h$, which represents a total of 5 year of use. The thermal solicitation is set to represent seasonal heating and cooling demand with sinusoidal variation. The peak heating demand is set to 15.5 kW and the cooling depend on the case study, varying from 0 % of the peak heating (only heating scenario) to 100% (symmetrical demand). The heating and cooling demand scenarios are presented on Figure II. 40. In each case, the heating scenario uses a daily activation pattern of $12\ h$ and $12\ h$ rest. Two seepage conditions are compared: $0\ m.day^{-1}$ and $0.4\ m.day^{-1}$. For these models, the aim is to observe the

behaviour of the system through multiple years with various seasonal activation patterns and different seepage conditions.

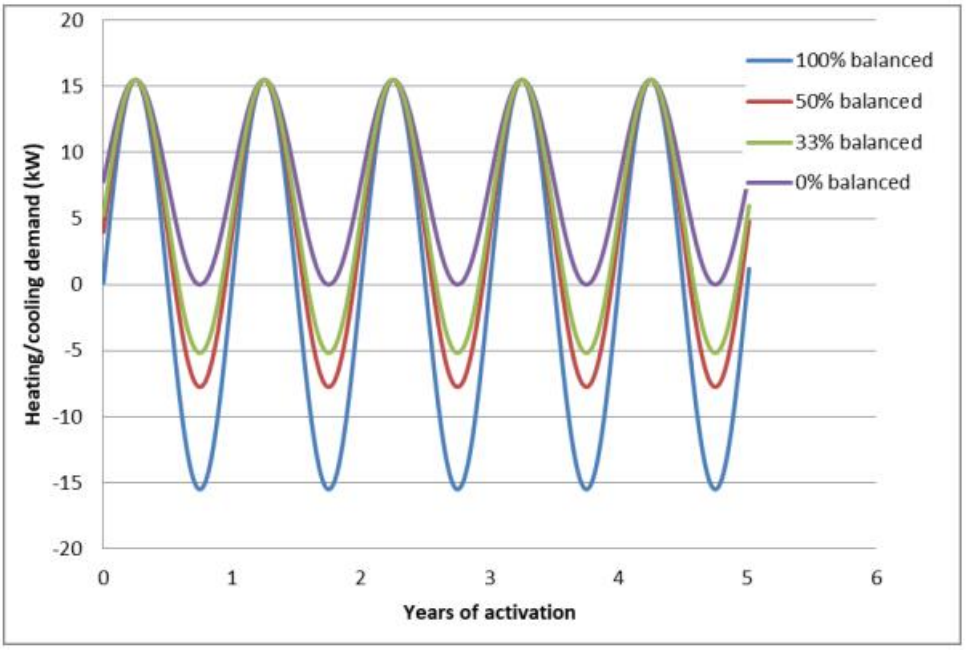

Figure II. 40 - Heating/cooling seasonal scenarios

Results of COP and COP_S values without seepage are presented on Figure II.41. Note that discontinuities of the COP values are due to the shifts between summer and winter mode. With these results, multiple aspects of multiyear use of energy geostructures and heat pump can be observed.

- First, in case of totally unbalanced heating demand (0% building cooling) classical thermal drift behaviour appears (as introduced in Chapter I). Moreover, the COP values decrease up to 2.34, which is extremely low and unrealistic. For the three other scenarios, the induced heat in the soil, during building cooling period, will help to prevent such behaviour.
- Second, the COP and COP_S variation are extremely important. The importance of heat recharge of the soils during summer is then highlighted. Indeed, greater building cooling demand will lead to increase the soil temperature which will provide easier exploitation of heat power during winter, i.e. higher COP value. However, even for high thermal recharge of the soil, heat exploitation will lead to rapidly decrease soil temperature and therefore decrease the COP values.

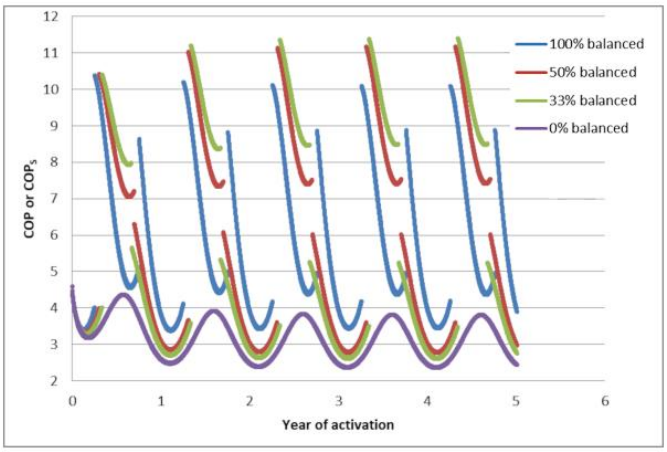

Figure II. 41 - COP and COPS value for different scenarios and 0 m · day−1 seepage

Results of COP and COP_S values with $0.4\ m.day^{-1}$ seepage are presented on Figure II. 42. On this figure, we can observe a totally different behaviour. Indeed, the systems expose similar behaviour in each case.

During summer, the cooling system exposes almost constant COP_S value around 8.6. And during winter, the COP factor varies from 4.2 to 5.2. Moreover, as expected, no scenario exposes multiyear thermal shift. These results could easily be explained by the thermal washing effect. Indeed, seepage phenomenon will tend to cancel thermal anomalies and impose an almost constant soil temperature around the energy piles, therefore the COP and COP_S variation are mainly related to the variation of heating and cooling demand.

Finally, the Table II. 12 presents the average COP value computed for each scenario during the winter period. As expected, the unbalanced scenario without seepage presents the lower average COP. In opposition, the fully balanced scenario without seepage shows the maximal average COP (higher than seepage cases). This shows the beneficial aspect of heat storage mechanism during summer. However, this high average COP conclusion should be mitigated by the important COP variation observed. Scenario with seepage will not benefit from heat storage effect. However, the thermal washing effect will guaranty constant and identical efficiency through multi-year activation independently of balance in heating and cooling cycles. For a 50% balanced scenario, the average COP is already better in the seepage case.

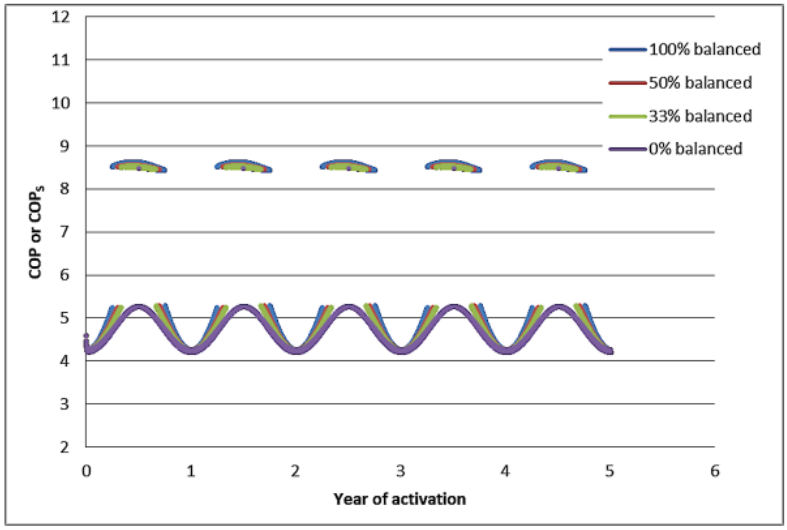

Figure II. 42 - COP and COPS value for different scenarios and 0.4 m/day seepage speed

Table II. 12 - Average COP during winter period for different scenarios 6

Seepage	100% balanced	50% balanced	33% balanced	0% balanced
$0\ m.day^{-1}$	4.79	3.62	3.34	3.03
$0.4\ m.day^{-1}$	4.57	4.59	4.60	4.73

4.6. Conclusion, discussion and perspective

In this study, a dedicated numerical modelling process has been developed for the purpose of representing the energetic behaviour of energy piles group and analysing the effects of seepage velocities and heating/cooling loads on heat pump efficiency. This process allows computing soil and system temperatures, COP and COP_S factor variation depending on seepage conditions, geometrical aspect and various heating/cooling scenarios.

With a first model, the energetic response of a realistic energy pile group during one month of peak use (winter and summer) is showcased for various seepage conditions and various inter-pile distances. As a result, in any case, the COP (or COP_S) decreases during this month with soil temperature variation. However, the minimal value widely varies on the seepage condition and geometry. On one hand, the seepage condition has the most important effect on the COP (or COP_S). It allows thermal washing and balance between energy inflow by advection effect and energy drained by the heat pump system. Therefore, seepage will conduct to a quick stabilization of the behaviour, while slow or absent seepage will lead to continuous decreasing of COP factor. On the other hand, the inter-pile distance also influences the COP values, as greater inter-piles distance increases the heat reservoir size and reduces the cluster effect. Finally, as both parameters impact the COP factor, i.e. the system efficiency, an expression of COP as a function of inter-pile distance and ground water flow velocity is proposed (Equation II.4.14).

With a second model, the same system is studied through a multi-year solicitation with heating and cooling cycles, balanced and unbalanced, and two different seepage velocities. Again, the results show the importance of seepage conditions. It allows the stabilization of the behaviour independently of the heating/cooling balance at reasonable efficiency level, but does not allow heat storage. In opposition, without seepage, the thermal recharge and heat storage (with building

cooling for example) is particularly important in order to avoid the multi-year thermal shift and to increase the overall efficiency of the system. Accepting strong temperature variations in the soil, the average COP in cases with important heat storage could even be greater than cases with important seepage velocities condition.

These results are promising, and the process can easily be applied to various other cases. However, the heating/cooling scenario should be selected with care. Indeed, some purely hypothetical scenarios presented in this work will lead to soil temperature so low that the realistic heat pump would turn off for safety reason. Therefore, it is evident that the presented process can still be further improved. For example, emergency case should be introduced to mitigate the use of heat-pump in cases of overconsumption of soil energy. In a similar way, model description could also be improved, with more detailed interactions at model boundary or with thermal boundary conditions depending on depth. In the future, the possibility offered by this model should be used at larger scale with more diverse scenarios. The integration of other energy geostructures such as tunnels or walls and conventional geothermal system (open loop, borehole, etc.) could also be considerate.

This second chapter focused on the thermal study of the model pile that will later be used for centrifuge experiments. It showed that the temperature distribution along the pile was relatively constant and that it was therefore possible to work on a 2D horizontal plane. Based on this result, numerical work was able to show that the distance between piles and the underground flow velocity were two parameters that favoured the energy efficiency of an energy pile group system Figure II.39 and equation II.4.14 provide a clear picture of the impact of flow velocity and inter-pile distance on the COP of a heat pump.

Chapter III

CENTRIFUGE MODELLING OF ENERGY PILE GROUPS

"Clearly if then one wishes to maintain in a great giant the same proportion of limb as that found in an ordinary man he must either find a harder and stronger material for making the bones, or he must admit a diminution of strength in comparison with men of medium stature; for if his height be increased inordinately he will fall and be crushed under his own weight. ***Whereas, if the size of a body be diminished, the strength of that body is not diminished in the same proportion; indeed the smaller the body the greater its relative strength.*** *Thus a small dog could probably carry on his back two or three dogs of his own size; but I believe that a horse could not carry even one of his own size.*"

Discorsi e dimostrazioni matematiche, intorno a due nuove scienze, (1638) Galileo Galilei (1564-1642)

Introduction to centrifuge tests and scaling laws

In the previous chapter, the focus was on the hydro-thermic interactions. This chapter will focus on the mechanical aspects which lead to place the reduced scale model in a centrifuge. Indeed, the study of mechanical structures can be tackled through three global ways:

The study of mechanical structures can be tackled through three main ways:

- The study of full-scale structures, which requires the construction of these structures, access to them and the ability to instrument them accurately. These studies therefore require time and money, and the range of parameters that can be controlled/imposed is small.
- Numerical modelling, which makes it possible to control the parameters and even to make them the subject of parametric studies. However, parametric studies are hardly sufficient on their own without comparison with reality. In addition, initial parameters are always necessary and often require initial experimental evaluations.
- The study on reduced scale models also allows controlling the parameters and drawing direct conclusions about the full-size structure, provided that certain similarities are respected. Indeed, even if the geometry is the same, the ratio of sizes cannot be extrapolated to the ratios of observed physical phenomena. To use Galileo's example, this would be like saying that a bone N times as big would support a weight N times as great, whereas this latter would break under that weight. Thus, working on reduced-scale models raises the question of similarity with realty. As shown below, centrifugation can provide answers.

The present section focuses on the latter aspect, and more specifically on the similarities between the reduced scale energy piles and their (sometimes hypothetical) real scale equivalent, called prototype.

Similarities are mainly approached by two concepts which are mathematically equivalent. One way to check if they are respected is to use dimensionless numbers. Equality of meaningful dimensionless numbers then ensures similarity between model and prototype. It is known, for example, that in a hydraulic duct or during wind tunnel testing, the Reynolds number must remain identical between an object and its reduced model. The second way is the scaling laws: namely ratios between corresponding values in the model and in the prototype are used to account for the evolution of certain properties or behaviours with the change in size. Using the same example as above, this is like asking how much more load a bone can support if it is N times larger.

One of the first references to studies of centrifuges for scale models was made in 1869 (Phillips, 1869), who wrote: "But I show further how, by bringing in inertial forces and particularly centrifugal force into play, it can be made possible that, for the system of small dimensions, the force acting on the whole mass and referred to the unit of mass is very much greater than gravity and equal to the value we wish to give it". In the 1950s, reduced scale models technique were widely used in fields such as hydraulics and aeronautics, but its application in soil mechanics did not really develop in the western countries until the 1960s and thanks to scientific cooperation with the USSR, which was

already centrifuging mechanical models in 1932 (Pilot, 1975). The use of centrifuge modelling in geotechnical engineering was truly developed in Western Europe in the 1980s and made it possible to study the behaviour of geotechnical structures with reduced scale models while keeping the same materials (soil and pile) and the same mechanical stress field. Since the behaviour of soils is complex and becomes quickly nonlinear, keeping the same materials and the same stress field helps to ensure the similarity between a reduced model and the prototype (Garnier, 2007). Because of same reasons (non-linearity, complexity,…), temperature is kept unchanged between the prototype and the model. On top of the usual benefits of centrifuge modelling (cost-effectiveness, mastering of boundary conditions and study parameters, possibility to reach failure), a new advantage appears when it comes to the study of diffusion phenomena (such as heat diffusion): the characteristic times are highly reduced and a year of exploitation can be modelled in a few hours, as it will be demonstrated below.

The ratio between the reduced scale characteristic time and the prototype one is an example of scaling laws. The idea is that the model and the prototype undergo the same physical phenomena. The similarity of behaviour between the model and the full-scale structure implies that there are constant ratios called scale factors x^* between the variables, x^m representing the reduced model and the variables x^p describing the prototype. The scaling laws will finally be expressed as relations between the scale factors x^*. Some of these scaling factors can be chosen arbitrarily, others are set by equations linking the scaling factors.

A classic way of introducing scaling laws is to consider the fundamental law of equilibrium in continuum mechanics. The latter reflects the phenomenon mentioned above by E. Philippes (i.e the need to increase the acceleration of gravity for a scale model to keep the constraints).

$$\frac{\partial \sigma_{ij}{}^p}{\partial x_j^p} + \rho^p \left(g_i^p - \frac{d^2 \varepsilon_i^p}{dt} \right) = 0 \quad \text{(III.1a)}$$

If we want the reduced scale model to undergo the same phenomena, this equation should also be verified for the model variables

$$\frac{\partial \sigma_{ij}{}^m}{\partial x_j^m} + \rho^m \left(g_i^m - \frac{d^2 \varepsilon_i^m}{dt} \right) = 0 \quad \text{(III.1b)}$$

By introducing the different scaling factors, we get:

$$\frac{\partial \sigma_{ij}{}^p}{\partial x_j^p} . \frac{\sigma^*}{x^*} + \rho^p \rho^* \left(g_i^p g^* - \frac{d^2 \varepsilon_i^p}{dt} \varepsilon^* \right) = 0 \quad \text{(III.1c)}$$

The equation remains true provided that $g^* = \frac{\varepsilon^*}{t^{*2}}$ and $\frac{\sigma^*}{x^*} = \rho^* . g^*$. Now considering that in soil mechanics, the material are the same ($\rho^* = 1$), and that the levels of constraints too ($\sigma^* = 1$), the resulting equation is:

$$\sigma^* = g^* \; ; \; x^* = 1 \quad \text{(III.2)}$$

This equation translates as follows: similarity can be obtained by increasing the mass forces in the inverse ratio to the length scale (Pilot, 1975). The most common way to achieve this is through centrifugal acceleration. Thus, by spinning the model at a velocity which imposes a centrifuge

acceleration of $N \times g$, the model which is N times smaller will finally undergo the same mechanical stresses (see Figure III. 1). The scaling law regarding the acceleration of gravity is then denoted

$$g^* = \frac{g^m}{g^p} = N \quad \text{(III.3)}$$

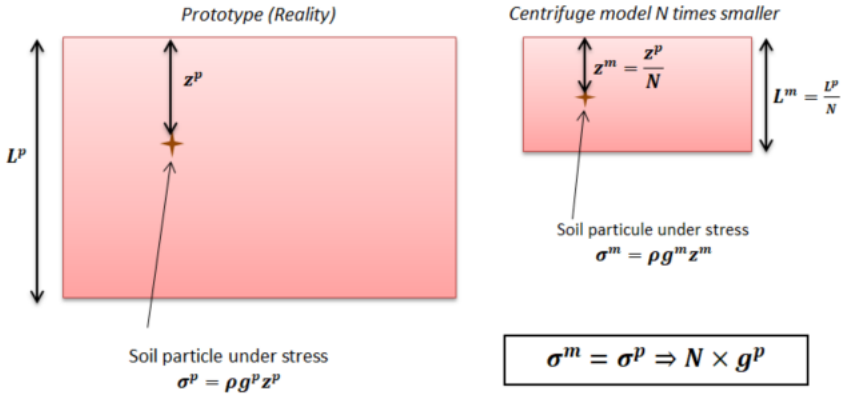

Figure III. 1 - Schematisation of the acceleration scaling law

1. Principle of centrifuge modelling and scaling laws for energy pile model

1.1 Presentation of the different thermal phenomena involved

In the case of use in summer mode, the heat is transferred from the building to the soil while during a winter mode, it is the contrary. Thus, the fluid which circulates in the thermal exchanger tube is hotter than the ground in summer and cooler in winter, and the first law of the thermodynamics reminds that the heat transfer occurs from hot to cold. However, in any case, once an energy pile is activated the heat flux crosses the tube, the pile and the soil through several thermal phenomena. They are presented here along with the corresponding equations and the dimensionless numbers involved in the establishment of the scaling laws.

1.1.1 Thermal phenomena

The Figure III.2 schematizes the different thermal phenomena existing when an energy pile is activated in summer case. They are detailed below:

- ***Natural convection***

The natural convection is the thermal transfer where the energy is transmitted by the displacement of the fluid due to the difference in density. Indeed, a hot fluid is less dense than a cold fluid and therefore rises to the surface.

- ***Thermal transfer between a fluid and a wall – forced convection***

There is also a thermal transfer where the energy is transmitted by the displacement of the fluid, which is, however, set in motion mechanically (by a pump for example). In this case, the heat flow transmitted is defined by the Newton law according to Equation III.4 where T_f is the temperature of the fluid (away from the heat source), T_w the temperature of the wall and h_{th} is the thermal transfer coefficient which depends on the nature of the fluid, its temperature and its flow rate or velocity (Lagrée, 2010)

$$j_{conv} = h_{th} (T_f - T_w) \quad \text{(III.4)}$$

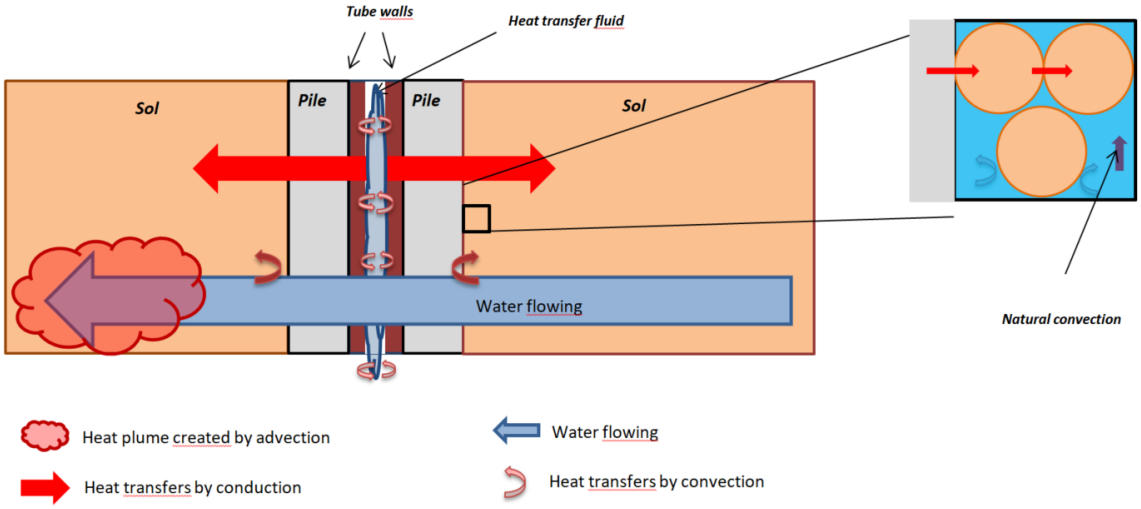

Figure III. 2 - Schematic representation of the thermal phenomena involved in energy pile use

- ***Conduction in solids*** *(introduced in Chapter I, 1.2.2)*

Conduction is the heat transfer in a media, without moving matter, and under the influence of a temperature difference. The propagation takes place through the vibration of atoms and is transmitted by free electrons. This phenomenon is the only diffusive phenomenon considered in this document. Thus, the thermal conduction is also called diffusion.

- ***Advection*** *(introduced in Chapter I, 1.2.2)*

In the case of moving matter, the displacement of material causes a displacement of heat from upstream to downstream. This phenomenon is called advection, and it creates a temperature plume. In the situations with groundwater flow, the temperature variation induced by energy piles, and called thermal anomaly, appears in the soil and is transferred trough the soil. It differs from convection (natural or forced) which takes place at an interface between two media and not in the medium.

1.1.2 Heat equation in the overall case

In order to consider a general case, one can focus on a system constituted by a saturated soil where an energy pile is heated without other heat source. Heat transfer is then governed by Equation III.5.

$$C_{tot}\frac{\partial T}{\partial t} + \mathrm{div}(j) = 0 \quad \text{(III.5)}$$

C_{tot} is given by Equation III.6 where the index gr refers to grains and the index w to water.

$$C_{tot} = (1-n)C_{gr} + nC_w = C_{soil} + nC_w \quad \text{(III.6)}$$

Determining the thermal parameters of a soil can be more complex and is presented in Chapter I. Here, these equations assume that the soil is saturated and can be assimilated to an equivalent monophasic medium. It means that the heat transfer between the water and the grains is assumed sufficiently fast to consider that both constituents have always the same temperature. This assumption can be made since the conductive characteristic time inside a grain of sand is much smaller than the conductive characteristic time in the macroscopic model. Indeed, on one hand, considering a grain of sand entirely drowned in water, the characteristic time necessary for the whole grain to be at a homogeneous temperature is given by equation III.7 where $\alpha = \frac{\lambda}{C_{tot}}$ is the thermal diffusivity and r the characteristic length equal to the grain radius in this case. With the usual thermal properties of a grain of sand, one finds $\tau_{grain} \approx 10$ s

$$\tau_{grain} = \frac{r^2}{\alpha_{grain}} \quad \text{(III.7)}$$

On the other hand, if one focuses on the conduction in the sand as a monophasic media with a characteristic length equal to a pile diameter (1 m for instance), the characteristic time will be 10000 times bigger in order of magnitude. This allows considering the media as monophasic and using the Darcy's model in particular.

The heat flow j breaks down into two flows (see Equation III.8), a diffusive flow j_{diff} and an advective flow j_{adv}. In soil, the diffusive heat flow passes through the grains which are in contact with each other. Water saturation improves this contact by forming thermal bridges. The advective flow will spread thanks to the movement of water through the connected pores (Usowicz, 2013).

$$j = j_{diff} + j_{adv} = -\lambda \mathrm{grad}(T) + \rho_W c_w V_D T \quad \text{(III.8)}$$

In the case of pure diffusion $j_{adv} = 0$, and one finds the classic heat equation in the conduction case (see Equation III.9).

$$\frac{\partial T}{\partial t} = \alpha . \Delta(T) \quad \text{(III.9)}$$

1.1.3 Dimensionless numbers

In thermal studies, as in other areas of physics, dimensionless numbers have been defined. They often represent the ratio between two physical phenomena of the same nature that occur simultaneously in order to be able to decide on the predominance of one of them (eg: diffusion over advection). The consistence of centrifuge modelling often requires to maintain the ratio between two phenomena, which means keeping the dimensionless number constant between prototype and reduced scale model. Some of the scaling laws presented in this document are derived in this way

and it seems necessary to first present some important dimensionless number in thermal studies. In appendix A is a detailed derivation of some of these numbers.

1.1.3.1 Reynolds number (Re)

The Reynolds number is given by Equation III.10

$$\mathrm{Re} = \frac{\mathrm{D} \times \mathrm{V}}{\nu} \quad \text{(III.10)}$$

Depending on the geometry of the system, the Reynolds number reflects the transition between a laminar flow and a turbulent one. For instance, in a tube, the transition is assumed to occur for Re≈2400. When Re is less than this value, the flow is called laminar, if not it is turbulent. Indeed, in this case the transition is quite brutal but, for example, for a flow perpendicular to a cylinder, it would be laminar for Re<5, and will go through several stages before being completely turbulent.

1.1.3.2 Nusselt number (Nu)

The Nusselt number is given by Equation III.11.

$$\mathrm{Nu} = \frac{\mathrm{h} \times \mathrm{L_c}}{\lambda_{\mathrm{fl}}} \quad \text{(III.11)}$$

The heat transfer between a fluid and a wall combines two main mechanisms, conduction in the fluid and convection on the wall. The Nusselt number is the ratio of convective to conductive heat transfer at a boundary in a fluid. A Nusselt number of value 0 represents heat transfer by pure conduction. Indeed, in case of no fluid movement, there is still the heat transfer by conduction due to the thermal gradient. A larger Nusselt number corresponds to more active convection, with turbulent flow. The literature presents a lot of correlations between Nu, Re and Pr (introduced below). This allows to determine Nu and eventually h (Jannot, 2012)

1.1.3.3 Prandtl number (Pr)

It represents the ratio between momentum diffusivity and thermal diffusivity (see Equation III.12).

$$\mathrm{Pr} = \frac{\nu}{\alpha} \quad \text{(III.12)}$$

Small values of the Prandtl number (Pr<<1) mean that thermal diffusivity is predominant. While with large values, momentum diffusivity dominates the behaviour. Compared to the Reynolds number, the Prandtl number depends only on the fluid and its state. Air and water at 20 °C have respectively a Prandtl number of 0.7 and 7.

1.1.3.4 Péclet number (Pe)

The Péclet number, product of the Reynolds number and the Prandtl number (see Equation III.13) represents the ratio between the transfer by advection and the diffusion. When Pe>>1, then diffusive effects dominates over convective transport.

$$\mathrm{Pe} = \mathrm{Pr} \times \mathrm{Re} = \frac{L_c \times V}{\alpha} \quad \text{(III.13)}$$

1.1.3.5 Rayleigh number (Ra)

The Rayleigh number is the product of two numbers, Grashof number (noted Gr) and Prandtl number (Pr). It characterizes the relative "efficiency" of convection and conduction as a mode of thermal transfer and is given by Equation III.14.

$$\mathrm{Ra} = \mathrm{Gr} \times \mathrm{Pr} = \frac{\beta.\Delta T.g.L_c^3}{\lambda.\nu} \quad \text{(III.14)}$$

The Grashof number is the ratio of gravity forces to the viscous forces: it quantifies the heat transfer by displacement of matter. The higher it is, the more convection is "efficient". Empirically, by studying various real systems, a critical value of Ra beyond which the system evacuates its heat by convection and no longer by conduction has been determined. This value is 1700.

1.2 Scaling laws for the thermal phenomena involved

Having presented the different thermal phenomena involved during the activation of an energy pile, we now focus on establishing or reminding the scaling laws related to these phenomena. The case of a homogenous soil crossed by seepage is considered and the different phenomena will be taken into account chronologically: from the conduction in the pile to the advection in the soil. An additional phenomenon is considered: the heat transfer by convection inside the heat exchanger pipe.

1.2.1 Conduction in the tube, in the pile and in the ground

Once the fluid exchanged thermal power with the pipe tubes, a conduction phenomenon occurs: the heat flux crosses radially the pipe, the pile and the soil (see Figure III.3)

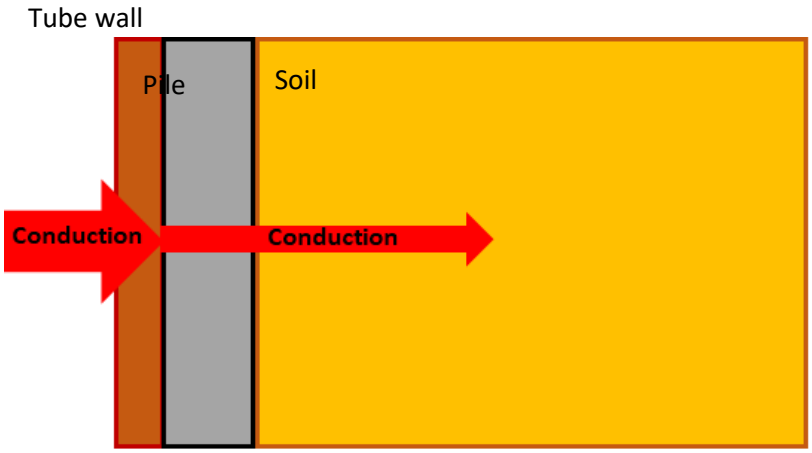

Figure III. 3 - Schematic representation of the thermal conduction in energy pile system

It is assumed that the tube/pile and pile/soil contacts are perfect, that is, it is assumed that there is continuity of temperature and heat flow at the interfaces. A recent study shows (Joao Diogo, 2020), thanks to experimental works, that "in dry sand, the impact of contact thermal resistance on energy geostructure operation and behaviour would be small". Obviously, it depends on the density of the soil and its water saturation, as explained in introduction. When one creates a model energy pile in order to carry out centrifuge tests, the tubes are often made of metal (in aluminium or copper in particular) for the sake of ease of construction. Thus, as the thermal conductivity of the copper is bigger than others (pile and soil), the heat is transferred faster in the tube. And as the pile and the soil have almost the same thermal conductivity, the heat transfer velocity is pretty equal in these two materials.

It is assumed that the only phenomenon governing heat transfer is conduction, and that there is no heat production in the system. The heat flow is therefore given by Equation III.15 and the heat equation becomes Equation III.16.

$$j_{cond} = -\lambda . \mathrm{grad}(T) \quad \text{(III.15)}$$

$$\frac{\partial T}{\partial t} - \alpha . \Delta T = 0 \quad \text{(III.16)}$$

Here, in order to make the demonstration more intelligible, a simple case of a 1D system with Cartesian coordinates is considered but, the demonstration would be similar in the other different cases. Using the scale factors x^* between the variables x^m representing the reduced model and the variables x^p describing the prototype, the heat equation in the prototype is written as Equation III.17.

$$\frac{\partial T^p}{\partial t^p} - \alpha^p \frac{\partial^2 T^p}{\partial^2 x^p} = 0 \quad \text{(III.17)}$$

The scale of the model imposes $x^* = \frac{1}{N}$ and, since the same soil is used, $\alpha^m = \alpha^p$ et $\alpha^* = 1$. Furthermore, temperature is kept identical between the prototype and the model to avoid any misinterpretation of the thermal behavior of soil, Therefore T*=1 and Equation III.17 becomes Equation III.18.

$$t^* \frac{\partial T^m}{\partial t^m} - \alpha \frac{\partial^2 T^m}{\partial^2 x^m} X^{*2} = 0 \quad \text{(III.18)}$$

As the behaviours of the model and the prototype are similar if and only if the equations keep the same shape when changing units, t* is given by Equation III.19.

$$t^*_{cond} = X^{*2} = \frac{1}{N^2} \quad \text{(III.19)}$$

This result could also be found by considering the dimensions of the heat equation terms ($\frac{[\text{Temperature}]}{[\text{time}]} = \frac{[\alpha][\text{Temperature}]}{[\text{Length}]^2}$). One can identify the characteristic time $\tau = \frac{L_c^2}{\alpha}$ (with Lc the characteristic length) and one finds again the fact that if we divide the length of the system by N, we also divide the characteristic time by N^2 (the diffusion is faster in the model). Finally, this result is also listed in the Garnier's catalogue. An important point to notice here is that this scaling law only comes from the fact that the model is N times smaller. Indeed, the scaling laws in centrifuge come from two distinct phenomena: the increase of the gravity and the decrease of the dimensions. Here, only size reduction matters.

In view of the size of the physical model and the fact that it must be made by a continuous material, it cannot be made with the same concrete as in the prototype. Then, a question appears regarding the thermal conductivity of the model which has to be the same as in the prototype. It has been shown (Leung, 2019) that adding some copper powder to the model mixture allows enhancing the mix's thermal properties. Indeed, without the addition of copper, the thermal conductivity of their mixture is only 0.38 W/mK. With a copper content of 6% and 12% by volume, the thermal conductivity increases to 0.7 and 0.94 W/mK respectively. Single compression tests and four-point tests were carried out and they show that the addition of copper powder in controlled amounts (6%) does not significantly affect the compressive strength or the modulus of elasticity.

1.2.2 Natural convection in the soil near the pile

Once in the soil, the thermal power can create natural convection (see Figure III.4). Namely, because of the density difference between hot and cold fluid, this latter can move and move thermal energy with it.

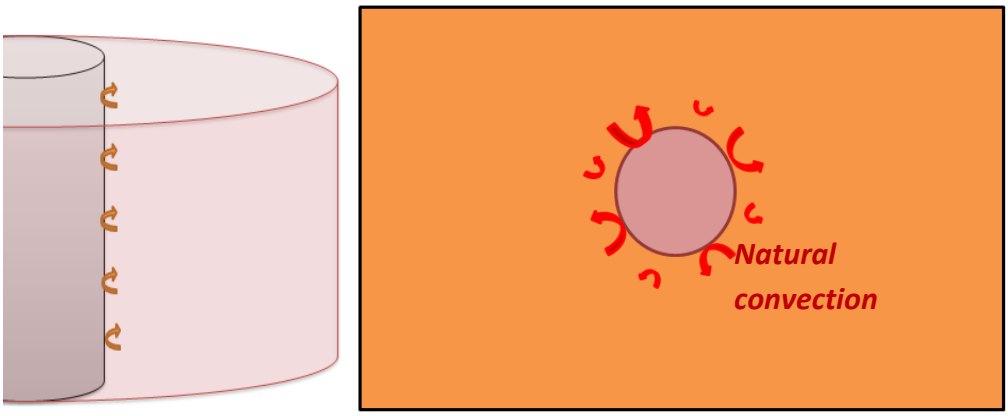

Figure III. 4 - Schematic representation of natural convection at the interface between energy pile and soil

To study the predominance of conduction or natural convection, the Rayleigh number is used, keeping in mind that if Ra<1700, the conduction is dominant. Table 1 presents usual values for a 1/25 centrifuge model of energy piles (the characteristic length, corresponding to the width affected by the convection, is taken in the same order as the pile diameter). It clearly appears that Ra remains well below 1700 so it can be concluded that in the centrifuge model, as in the prototype, natural convection remains negligible compared to conduction in the soil.

Table III. 1 - Transfers mode in model and prototype energy pile

N=	**25**							
	g	**β**	**DeltaT**	**L_c**	**ν**	**α**	**Ra**	**Transfer mode**
Prototype	10	10^{-4}	15	2	10^{-6}	$6{,}8.10^{5}$	0.176	Conduction
Model	250	10^{-4}	15	0,08	10^{-6}	$6{,}8.10^{5}$	$2{,}8.10^{-4}$	Conduction
Ratio m/p	25	1	1	0,04	1	1	$1{,}6.10^{-3}$	

1.2.3 Thermal heat transfer by forced extern convection at the soil/pile interface

At the interface between the pile and the soil, seepage may create a forced convection phenomenon (see Figure III.5). Depending on the speed of the flow, this forced convection may not be negligible.

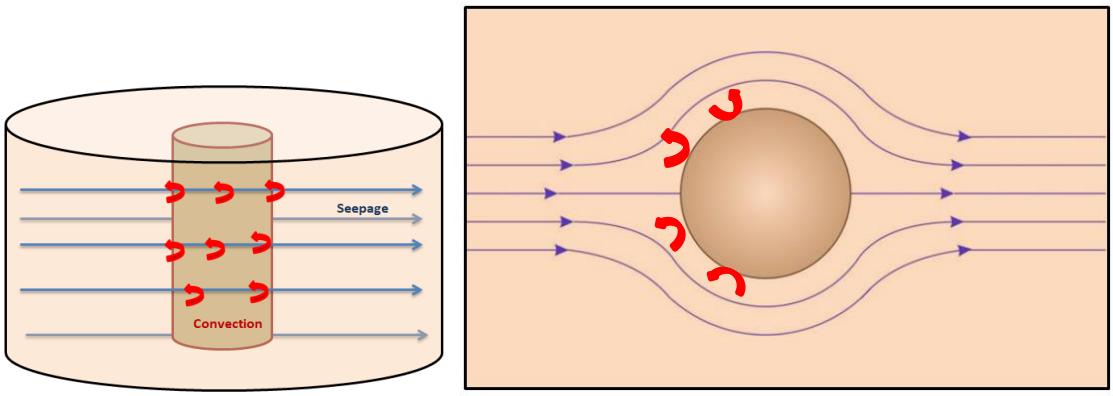

Figure III. 5 - Schematic representation of forced convection at the interface between energy pile and soil

In this case, the key dimensionless number is the Nusselt number because it reflects the ratio between convection and conduction. Considering that the study system can be represented by a flow perpendicular to a cylinder, the empirical expression of the Nusselt number which depends in particular on the Reynolds numbers is given by Equation III.20 (Jeannot, 2012). The parameters for this equation are given in Table III.2.

$$\mathrm{Nu} = \mathrm{C} \times \mathrm{Re}^{\mathrm{n}} \times \mathrm{Pr}^{\frac{1}{3}} \quad \text{(III.20)}$$

Table III. 2 - Parameters for the Nusselt number equation (Jannot, 2012)

Re	C	n
0.4 – 4	0.989	0.330
4 - 40	0.911	0.385
40 - 4000	0.683	0.466
4000 – 40000	0.193	0.618

As an illustration, one can consider a seepage velocity of 1 m/day and a characteristic length equal to the diameter of the pile (taken equal to 1 m). Then $\mathrm{Re} = \frac{\mathrm{VD}}{\nu} = \frac{1*1}{86400*10^{-6}} \approx 10$ and $\mathrm{Pr} \approx 7$. So $\mathrm{Nu} = 0.911 * 10^{0.385} * 7^{\frac{1}{3}} \approx 4.2$. Therefore $\mathrm{h_{th}} = \frac{\mathrm{Nu}*\lambda}{\mathrm{L_c}} \approx 10\ \mathrm{W.m^{-2}.K^{-1}}$ and $\mathrm{j_{conv}} = \mathrm{h_{th}} \times \Delta\mathrm{T} \approx 100\ \mathrm{W/m^2}$. As the diameter of the pile is relatively small, it is more relevant to consider the power exchanged by unit length. In general, depending on the fines content of the soil, an energy pile exchanges between 20 and 100 W/mL (Di Donna, 2021). It corresponds well to the obtained result in the previous approximation, which indicates that the forced extern convection cannot be considered negligible.

Therefore, the point is to keep Nusselt number equal between the model and the prototype. Since the groundwater has the same viscosity in model and prototype, it is necessary to multiply the

Darcy's velocity by N when we reduce the size by the same ratio. The scaling law is given by Equation III.21.

$$V_D^* = N \quad \text{(III.21)}$$

1.2.4 Advection in the soil

Once the heat flux crossed all the pile and is in the ground, a ground water flow can move this thermal power downstream by an advection phenomenon (see Figure III.6). The relative predominance between this advection and the conduction in the soil must be kept between the prototype and the model. This can be checked by calculating the Peclet number (see Equation III.13) and see how seepage velocity impacts it. For this, let's consider that advection dominates when Pe>1 and that conduction dominates when Pe<1. Obviously, the more we get far from this limit value (Pe=1), the more the phenomenon is dominant.

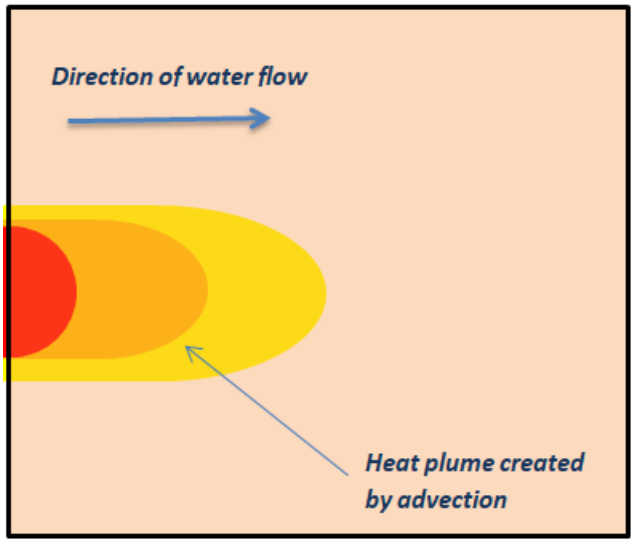

Figure III. 6 - Schematic representation of advection phenomenon in the energy pile system

The advective heat flux is defined by Equation III.22.

$$j_{adv} = \rho_w c_w V_D T \quad \text{(III.22)}$$

V_D is the Darcy's velocity which follows from the Darcy's law describing the fluid flow through a porous media (soil in this case). This law establishes a proportional relation between the hydraulic gradient and fluid flow and remains valid as long as the flow is laminar.

Thus, in soils, when seepage is present at a certain velocity, the dominant thermal phenomenon could be advection. The predominance of this phenomenon is reflected by a high Peclet number. For

instance, by considering saturated sand, a characteristic length of 1 m, which corresponds to the pile diameter, and a velocity of 1 m/day, we obtain Pe≈10

In order to maintain the relative predominance of diffusion or advection, the Peclet number must be kept constant. Thus, as the size of the system is divided by N and the thermal diffusivity is unchanged, it is necessary to multiply the velocity by N. It means the water flowing velocity has to be N times higher in the reduced scale model. The scaling laws are given by Equation III.23.

$$t^*_{adv} = \frac{1}{N^2} \text{ and } V^*_D = N \quad \text{(III.23)}$$

This result is in accordance with the Garnier's catalogue (Garnier, 2007) which reports results from (Nakajima, 1998).The fact that this scaling law matches the ones regarding conduction and forced extern convection allows to consider centrifuge modelling of energy piles in a groundwater flow without any discrepancy or time distortion.

According to Khalifa, (Khalifa, 2000), the hydraulic conductivity is N times higher in a model than in its prototype. This result comes from the fact that the hydraulic conductivity depends on the gravity acceleration. In other words, when by working on a reduced scale model, the gravity increase is enough to induce the velocity increase. Equation III.23 means that if we consider seepage velocity N times higher in a model N times smaller, the heat advection will be N^2 times faster in the model. This scaling law is identical to the thermal diffusion one. So there will be no problem of interpretation of the centrifuge test results as the two thermal phenomena (diffusion and advection) responsible of the heat transfer evolve according to the same scaling law. As an illustration, two models where created in finite elements model (FEM) software. One is 50 times smaller with seepage velocity 50 times higher. And it appears that the isotherms are perfectly confused when one considers a 50 times shorter timescale for the reduced scale model as shown in the Figure III.7.

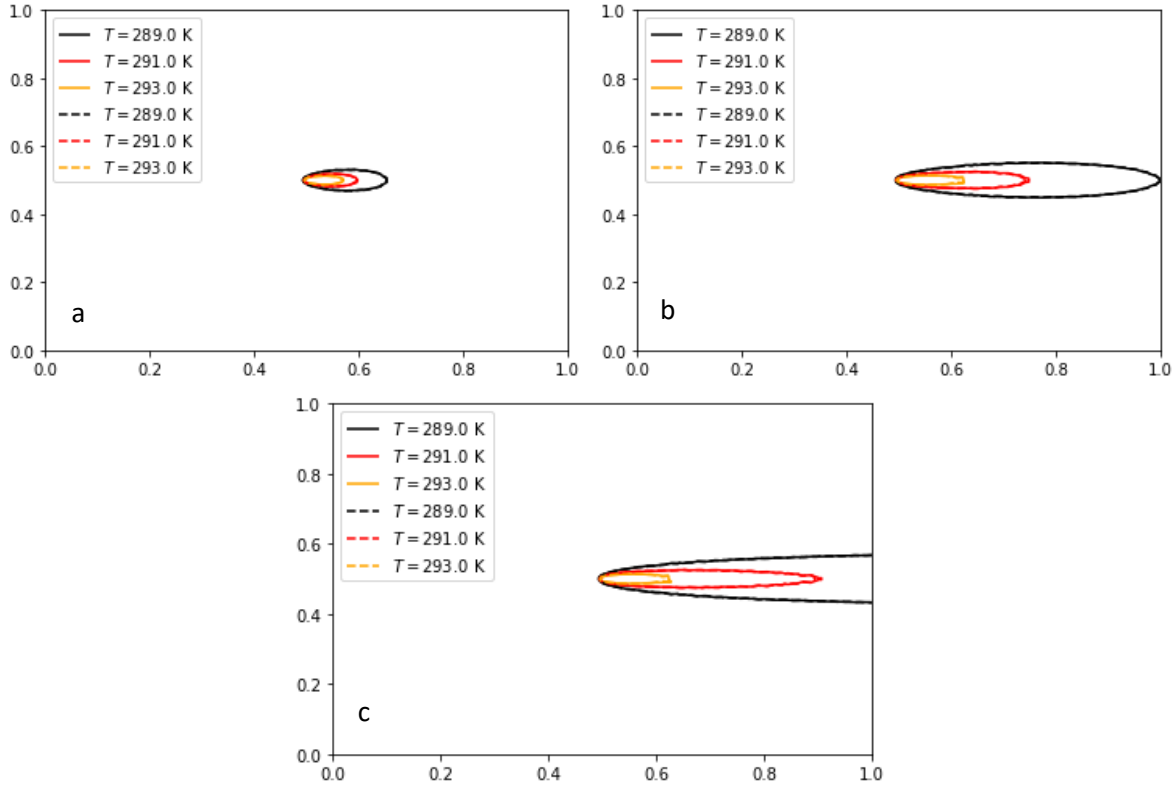

Figure III. 7 - Isotherms obtained after a) one week, b) one month, c) three months for reduced scale (dotted lines) and prototype (full line) numerical models with same materials and seepage

1.2.5 Forced intern convection between the heat transfer fluid and the tube wall

The first step in the heat transfer from the building to the soil is the thermal exchange between the heat carrier fluid and the PEHD pipes. Since the heat carrier fluid is set in motion by a pump, this phenomenon is forced convection (see Figure III.8).

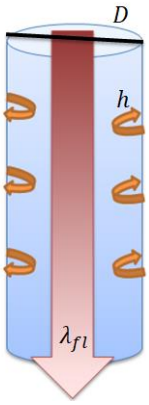

Figure III. 8 - Schema of the thermal convection induced by a fluid circulating in a tube

By definition, $X^* = \frac{1}{N}$ and, as shown previously, $t^* = \frac{1}{N^2}$. Then Equation III.5 gives $j^* = \frac{X^*}{t^*} = N$ for all particles submitted to heat flux, no matter the nature of the flux. In the particular case considered

here, the thermal flux is convective and given by the Newton equation (Equation III.4). Thus one can deduce the scaling law given by Equation III.24.

$$h^* = N \quad \text{(III.24)}$$

It is worth noticing that if Equation III.24 is fulfilled and the fluid is identical ($\lambda_{fl}^* = 1$), then the Nusselt number, given by Equation III.11, is kept constant. The relations Nu = f (Re, Pr) suggest that an increase of the fluid velocity in the pipes can help fulfilling the scaling laws. Indeed, several empirical formulation exist to define Nu as a function of Re and Pr, depending on the flow regime. For instance, the empirical formula for a turbulent flow of a fluid (hotter than the pipe walls) in a cylindrical pipe (Jannot, 2012) is the formula of Dittus-Boelter (Equation II.1.22) valid for Re > 5000 and while the Prandtl number stands between 0.6 and 1000 (so it suits for water).

$$Nu = 0.023 Re^{0.8} Pr^{0.3} \quad \text{(III.25)}$$

As it is assumed that the fluid is identical between the prototype and the model, the Prandtl number remains the same and only the Reynolds number is likely to change. Therefore, to conserve Nu, one has to conserve Re. And according to the definition of Re, it is necessary to multiply the fluid velocity by N in order to keep Re, as the lengths are divided by N. However, in practice, the flow regime is not always turbulent (Gehlin, 2015) and so the Nusselt formulation is not anymore the same. It is then advised to do again this reasoning to check how keeping Nu constant between the model and the prototype.

Furthermore, in centrifuge models, the heat exchanger tubes are often constituted with another material than the one used in prototype. Therefore, the temperature field in the model is likely to differ from the prototype one. To check this assumption, a finite element model was made on COMSOL. It consists in a 3D soil domain of saturated sand crossed through its middle by a water flow inside a tube. Two numerical models were constituted: the prototype one and the reduced scale model one. The prototype one is 10 times bigger than the second model, the tube is in PEHD and the fluid velocity is around 0.137 m/day (which corresponds to a reasonable flow for a heat pump). In the centrifuge model, the tube is in copper and the fluid velocity is 10 times higher. The equations used are presented in Appendix B. The point is to compare the isotherms at several dates as presented in Figure III.9. As imposed by the scaling law for heat diffusion in soil, the timescale was divided by 10^2=100 in the reduced scale model. In this figure, it appears that the isotherms are not exactly confused but remain very close. Indeed, as the copper has a 100 time higher thermal conductivity than PEHD, the heat flux coming from the pile crosses the system quicker for the reduced scale

numerical model than for the prototype numerical model, and so the isotherms are further from centre.

If the material were the same, the prototype and the reduced scale numerical models would have the same isotherms. Therefore, one can conclude that, if the reduced model is made with more conductive materials, the fluid velocity can be lower according to the definition of Nusselt number. To proof this idea, the reduced scale model was numerically run with a fluid velocity three times faster than the prototype one, rather than a fluid velocity 10 times higher. It appears in Figure III.9 (b) that the isotherms overlapped this time. Therefore, by using a more conductive material (thermally speaking), it is not necessary to increase the fluid velocity in the pipe by N, a weaker increase would be enough depending on the material used.

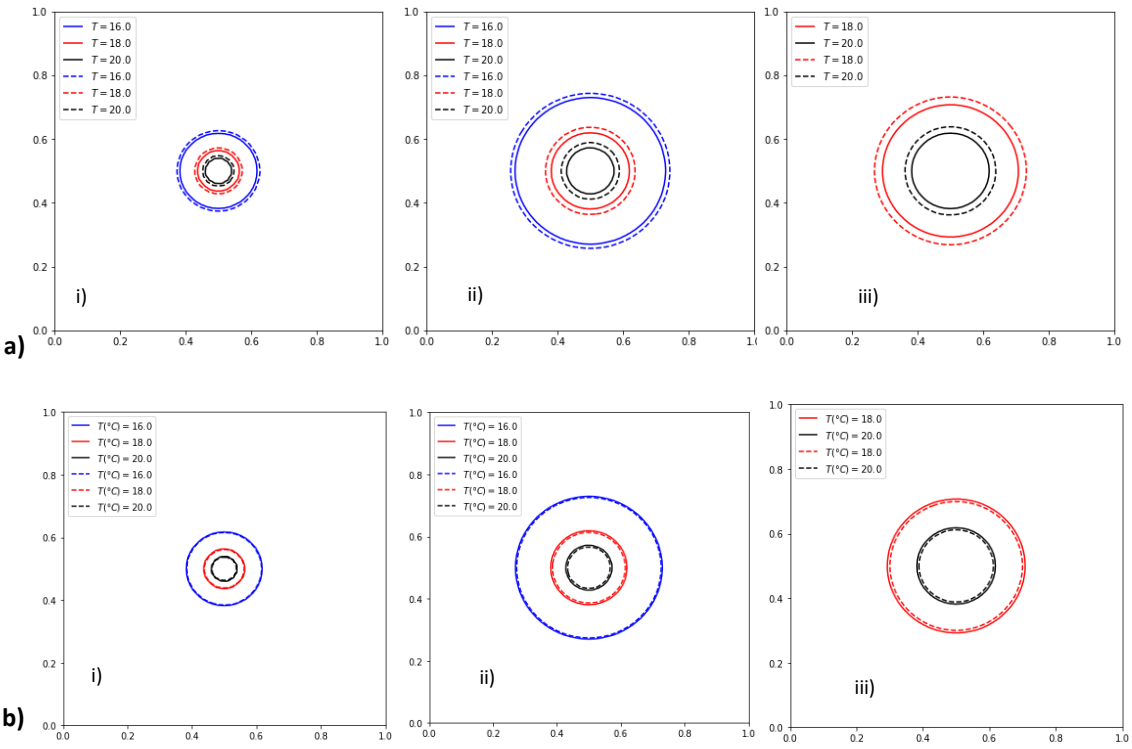

Figure III. 9 - Isotherms obtained after i) one week, ii) one month, iii) three months for reduced scale (dotted lines) and prototype (full line) numerical models for a fluid velocity 3 times (a) and 10 times (b) higher than the prototype one

1.3 Mechanical scaling laws

The scaling laws mentioned earlier are crucial to ensure that the thermal loadings generated by the use of energy structures are correctly modelled. To allow the study of the mechanical behaviour induced by these loadings, some mechanical scaling laws must be fulfilled.

1.3.1 Geometry of the energy pile and size of the sand particles

First, even if this parameter does not depend on the thermal loadings; the geometry of the pile is one of the more basic scaling laws and depends directly on the acceleration imposed in the centrifuge. Indeed, by applying a centrifugal acceleration of $N \times g$, the model pile of reduced size simulates a prototype pile (of real size) whose dimensions are N times higher in accordance with the scaling laws. The slenderness of the model pile is therefore kept in relation to a prototype pile and must therefore be respected. Since the soil is kept unchanged between the prototype and the model, the ratio of the pile diameter to the average diameter of the soil particles (D/d50) is modified and one can wonder if it has an impact on the behaviour of energy pile.

According to Professor Madabhushi (2015), scaling down particles of soil would be a mistake and "will lead to a totally different soil mechanics" notably because that means "ignoring the mineralogy of the soil particles and their affinity to water retention". Moreover, "In order to capture the true behaviour of the soil in the prototype we need to use the same soil as the prototype, which has the same stress-strain relationship. This enables us to observe the correct deformations as the soil mobilises appropriate stiffness for the strains induced". Also in this sense, in 2019, an experimental study (Ng, 2019) showed that "the scaling effects due to particle size on the centrifuge modelling of floating energy piles with a ratio of D/d50 larger than 92 can be ignored." To reach this conclusion, they carried out centrifuge experimentation where they thermally loaded two energy model piles. These two models were of different size but the acceleration was adapted so that each model ultimately represented the same and unique prototype. They then observed that the two models experienced the same normalised pile head settlements (almost 1.3%D) and thermally induced axial load.

1.3.2 Mechanical aspects

Secondly, one of the challenges to be able to interpret the results of centrifuge tests without error is to create models that respect both the thermal and mechanical scaling laws of the foundation. Model piles are generally made of an aluminium alloy or a mixture of cement. The scaling laws are based on the fact that the materials are identical. Since, it's not exactly true, some points have to be tackled with attention. Indeed, as the material that constitutes the model changes, one has to make sure that the thermal expansion coefficient and resistance remain the same as in the prototype. The response of a soil-structure system is mainly influenced by the relative soil-structure flexibility and reduced-scale models of piles are often designed to have correctly scaled bending stiffness $EI^* = \frac{1}{N^4}$ and bending moment $M^* = \frac{1}{N^3}$ (Knappett, 2011). However, for practical issues, model piles are often made from materials differing from real practices like aluminium for instance (Ng, 2019) and the section should therefore be modified to respect the scaling law.

Recent works (Zhao, 2020) present results of thermal expansion tests realised in order to determine the coefficient of thermal expansion of their model energy piles. Each model pile was supported by two stainless steel rollers, so the pile was allowed to expand and contract freely upon heating-cooling cycles. Thermocouples and strain gauges were used to measure the temperature and deformations. By calculating the slope of the linear curves describing the evolution of the deformations as a function of temperature, a coefficient of thermal expansion of 8.9 με/°C is obtained (Zhao, 2020). This result is close to the coefficient of thermal expansion of concrete of 8.5 - 10 με/°C determined by Bourne-Webb (Bourne-Webb, 2009). It was also shown that the behaviour of the model pile was thermo-elastic.

When reduced scale model made with the same aggregate as the prototype are mechanically tested, overstrength appears for failure beams in flexure and increase with the scaling factor. A power law was proposed and it suggests that the overstrength increases as N0.1 (Knappett, 2011). The authors attribute this phenomenon to the fact that the model is smaller in size while the mixture is constituted by the same aggregates. According to this law, as the scaling factor is at less 20 in a geotechnical centrifuge test, the overstrength will be at less around 130%. As an example, in order to make concrete structural elements for use in geotechnical centrifuge, a model concrete consisting of plaster, water and fine sand that can produce a range of model concretes with cube compressive strengths between 25-80 MPa has been created (Knappett, 2011). Reinforcement is modelled using a steel wire of 0.26 mm (10.4 mm in prototype scale) and with a steel wire of 0.58 mm (23.2 mm in prototype scale). Thus, it appears that beams without reinforcement present a shear failure while beams with reinforcement fail in flexural bending. Therefore, it is shown that load capacity, bending stiffness, and ductility were appropriately scaled over a range of scaling factors appropriate for geotechnical centrifuge testing.

Another study shows, by different methods of thermal conductivity estimation, that the model pile have worst thermal properties when it is constituted by simple mortar (cement and water). For instance the thermal conductivity can be three times lower. However, this mixture shows compression characteristics (Young modulus in compression) close to the concrete used for prototype energy piles (Guenneau, 2022).

1.3.3 Pile-soil interaction

Finally, the interaction between the pile and the ground could also be submitted to scaling laws. In the design of energy piles, thermal loading can induce a cyclic mechanical mobilization of shear stresses at the interface and thus modify its behaviour. A paper published in 2015 (Di Donna, 2015) presented a mechanical shear box set up to test the interfaces between different materials. This

work shows that temperature does not influence the interaction between concrete and sand at an interface and confirms the thermo-elastic character of sandy soils. On the other hand, the resistance at the clay-concrete interface increases with temperature. Except for high temperatures, it appears that the friction angle at the interface between concrete and clay increases with temperature so ignoring it goes in the direction of safety. A study shows that the interaction between epoxy and sand is of the same order of magnitude as the one between sand and concrete (Ramadan, 2013). Finally, Zhao et al. consider that the use of three 3 mm strain gauges glued to a 300 mm long model pile does not significantly modify the interaction between the two materials (Zhao, 2020).

1.4 Overview of the scaling laws

This first section of Chapter II derived and presented all the scaling laws and attention points to keep in mind when centrifuge modelling energy geostructures and especially energy piles:

1. The advection characteristic time has the same scale factor than the conductive one ($1/N^2$). Therefore, both phenomena can be observed at the same time.
2. The important conduction phenomena are in the pile and in the soil, one has to make sure that the thermal properties of the model and the prototype are identical.
3. To correctly model the interface transfer between the pile and the soil, the point is to keep the Nusselt number constant by considering seepage velocity N times bigger in the model. Nonetheless one has to make sure to stay in the Darcy's domain.
4. The natural convection can be neglected.
5. Regarding the forced convection in the tube, the ratio between convection and conduction is conserved when h*=N. However, as the tube in the reduce scale model is often made with a more conductive material, the heating fluid velocity should not be multiplied automatically.
6. The thermal expansion coefficient should be the same as the prototype's one
7. The addition of reinforcement should allow fulfilling the mechanical scaling laws regarding bending stiffness and bending moment which are respectively 1/N4 and 1/N3
8. The angle of friction is not affected by the temperature but a question remains regarding the displacement necessary to obtain the friction. Indeed, as the model is by definition smaller than the prototype, the displacements will be smaller as well. It has been proved that the temperature does not affect the angle of friction but not that the displacements thermally induced on the model are enough to generate friction.

2. Presentation of the reduced-scale model

The previous section highlighted the reasons, the advantages, and the points of vigilance regarding the use of centrifuge modelling to study the hydro-thermo-mechanical behaviour of an energy pile group. This section introduces the model used for the centrifuge tests carried out. It consists of a group of four energy piles, connected between them by a header, that will be mechanically loaded with a dead weight (or merely by the mass of the header) and subjected to a non-symmetric thermal load, where only one (or two) of the four piles is/are heated or cooled.

2.1 The centrifuge beam

The geotechnical beam centrifuge is located in the Schofield Centre which is part of the Engineering department of the Cambridge University and consists in a rotor arm of 10 m (with a working radius of 4.125 m) in a 2 m high chamber located underground. Its rotation velocity can reach 180 rpm, which corresponds to an acceleration of 125g. The model is prepared outside and a control room allows supervising the experience. In particular, it is from this room that the speed of rotation of the centrifuge is imposed. Once the model is ready, it has to be placed in one of the two extremities of the rotor arm depending on the type of test (static or dynamic). The other extremity should be loaded with counterweights in order to balance the weight of the model during the spin. The details of the centrifuge and its operations are described in (Schoflied, 1980).

Figure III. 10 - Photography of the centrifuge used for the tests (T. Grappe)

2.2 The model box

The model is built in the box presented in II.2.1 and with the same gravel reservoirs. The central part is filled with dense Hostun sand on a height of 400mm with a relative density Dr ≅ 90%. The choice of working in sand is explained by the two advantages that the latter brings and which are due to its

relatively high permeability. In fact, sand allows relatively rapid flows to pass through it and does not present any problems linked to consolidation, unlike fine soils. In order to have a homogeneous soil, the model was prepared using a mechanical system of automated sand pourer (See Figure III. 11) present at the Schofield Centre (Madabhushi et al., 2006). This allows to obtain the target relative density of the soil, by adjusting the height of fall, the size of the slot through which the sand flows and the speed of movement.

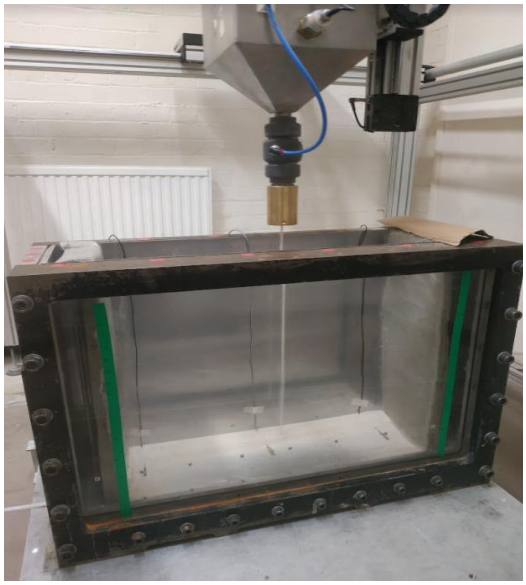

Figure III. 11 - Photography of the box during sand pouring

In geotechnical engineering, there are two main ways of placing piles: by driving or by drilling. In this study model, since driving is technically difficult, the piles are placed before sand pouring, simulating cast in situ piles. The sand pouring was run without the presence of the raft in order to ensure good homogeneity.

2.3 Macro gravity adaptation and mechanical considerations

The piles group model is made up of four piles connected together by an aluminium header. The piles -300mm long and 20mm in diameter are realised in the same way as the ones presented in chapter II.-. Although only one or two of the four piles that make up the group are thermally active, all the piles are equipped with a copper tube so that they all have the same mechanical characteristics such as axial and flexural stiffness's. Indeed, no model reinforcement is placed inside the piles but the copper tube also plays this role. The piles were coated in glue and sand in order to make them rougher and to better simulate bored piles as they are put in place before the sand pouring.

As mentioned, no reinforcement cage is modelled and the copper tube acts as reinforcement. However, as it appears in the state of the art, geotechnical model piles are sometimes fitted with a model reinforcement cage. As part of an internship in which I was part of the supervisory team,

Gurvan Guenneau produced a model energy pile that was more complex. This model pile is only 1:20 scale, but this makes it possible to add reinforcement in the form of a galvanised metal mesh that surrounds the heat exchanger tube, as shown in the Figure III. 12. Unfortunately, it could not be used in our 50g experiment.

Figure III. 12 - Photo of the reinforcement cage of the energy pile model (Geunneau, 2022)

2.4 Thermal and mechanical characterisation of materials

For both numerical modelling and centrifuge modelling, knowledge of the thermal and mechanical parameters of the materials used is crucial. In soil mechanics, when modelling with a centrifuge, the scaling laws are based on the assumption that the materials between the prototype and the model are identical. However, cement (used for the model) is not reinforced concrete (used for real piles). For numerical models, the choice of parameters will logically influence the results obtained, which is why parametric studies are carried out. As these parameters are multiple and interdependent, the different combinations of parameters lead to just as many results, making analysis of the influence of a single parameter of little relevance. So the greater the number of fixed parameters, the more relevant the study will be. Knowledge of the actual parameters is therefore just as important in numerical modelling as it is in centrifuge modelling.

The cement grout Young's modulus has been estimated to be 12.5 GPa. This value was obtained from three compression tests carried out on cylindrical specimens 28 days after the cement was poured into the moulds, as recommended by the test standards.

It is interesting to note here, although it might be expected, that Young's modulus is about 2 or even 3 times smaller than that of reinforced concrete, and that this therefore has an impact on compliance with the laws of similitude and hence on the interpretation of experimental results.

It is interesting to note here, although it might be expected, that Young's modulus is about 2 or even 3 times smaller than that of reinforced concrete, and that this therefore has an impact on compliance with the laws of similitude and hence on the interpretation of experimental results.

2.5 Pile group and loadings

The model energy piles and their thermal and mechanical parameters were presented. As a reminder, the system studied (which will be placed in a centrifuge) is a group of four piles linked together by an aluminum header. The connection between the piles and the header is made via load cells (see next section 2.7) but the important point to note here is that a ball-and-socket joint exists between the piles and the header. This header will act as a mechanical load during the first test campaign and additional weights will be added during subsequent campaigns (Cf. Chapter IV). In the second and third campaigns tests, a dead weight of 1.6kg is placed above the header in addition to its proper weight. Thus, the total mass applied to the piles group is 2.040 kg. It corresponds to half of the maximal load capacity of the piles group calculated as suggested in (Viggiani, 2011), assuming the group effect is negligible. The details of this calculation are given in Appendix A.

Regarding the thermal loading, only the first campaign test was carried out with an open loop heating system. The point was to work with a constant inlet water temperature over the experiment. But, then for the two other campaigns, it was chosen to work in closed loop to optimize the heating system.

During the first test, it was observed that the pile did not heat as much as expected although the temperature of water entering the pile was high enough. It was then assumed that the flow inside the circuit was not fast enough to heat the pile. Indeed, under the effect of the centrifugal force, the calibrations which were carried out at 1g were no longer valid. As one can see in Figure III. 13, the pump has to draw water from a tank located at a lower altitude. This altitude difference is negligible at 1g, but is not anymore at 50g insofar as prototype lengths are multiplied by 50. The energy needed to draw the water is therefore much higher than at 1g and the pump is not able to draw as much water as required. This leads to a smaller water flow than in 50g and so to a different performance of the heating system. It is advised to consider a heating system where the pump and the water reservoir are at the same height for future experimentations. A floater device was developed in order to measure the pump flow during the flight. It consists of a LVDT linked to a floater put in a bucket in which the water leaving the system was collected (See Figure III. 14). The goal is to measure the increase in the water level in the bucket over time to calculate the flow rate of the pump. Finally, an actual flow rate of 20 ml/min was determined inflight using this system and this was the flow rate achieved by the pump. This resulted in lower thermal loads than expected.

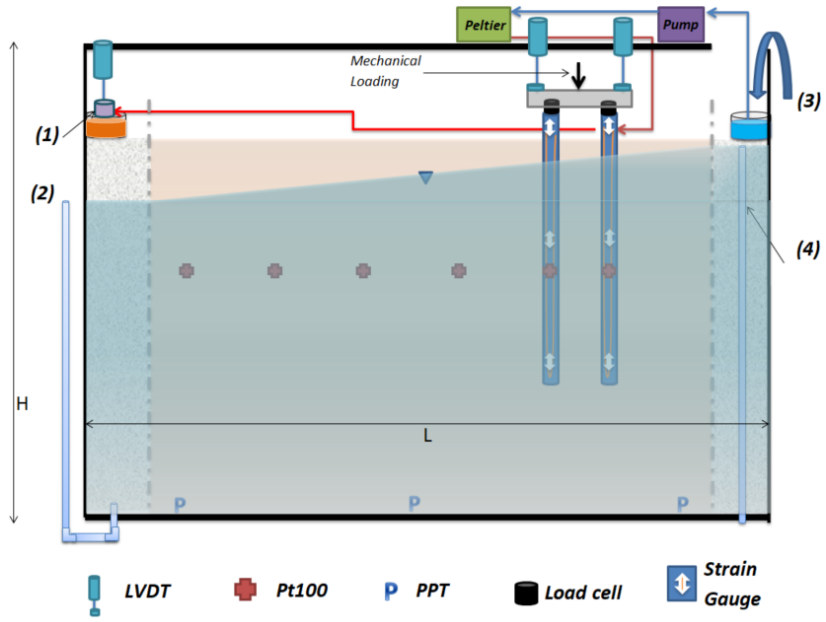

Figure III. 13 - Schematic representation of the model used during the first campaign test: (1) floater system allowing measuring the flow rate of the pump, (2) syphon system, (3) running water supplying the system, (4) tube evacuating the water at the upstream side

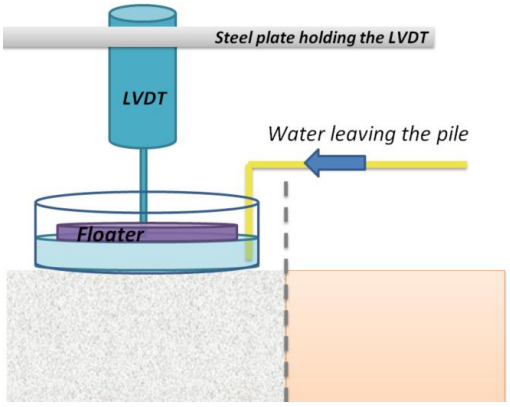

Figure III. 14 - Schema of the floater device used to measure pump flow

2.6 Sensors

To measure the load carried by each pile, a load cell is screwed at the head of each pile and fixed to the raft with a nut. The raft also rests on four nuts so that all its weight is transferred to the piles through the load cells (Figure III. 17). Furthermore, to measure the displacement of the group during the experiment, displacement transducers (LVDTs) are positioned at the four corners of the raft. They have an accuracy of 0.1% of measuring range which is 50mm. These sensors allow characterizing the mechanical response of the pile group. All this sensors allowing measuring the mechanical behaviour of the energy piles group are represented in Figure III. 15. This figure also presents strain gauges but as they did not function during the tests, their results were not exploited.

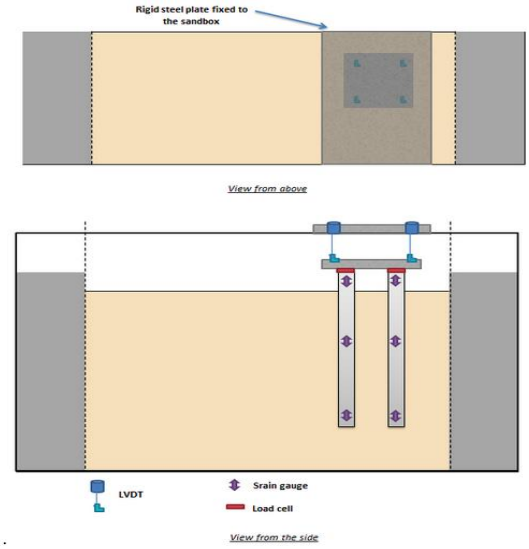

Figure III. 15 - Schematic representation of the model box with mechanical sensors

In order to monitor the lateral ground water flow in the model, seven pore pressure transducers (PPTs) are placed at the bottom of the model along the box (Figure III. 16). Finally, to measure the heat transfer in the model, temperature sensors are placed on a horizontal plane at a depth of 130 mm from the model surface, as well as on each of the piles (same configuration as for the hydro-thermal characterisation in Chapter II).

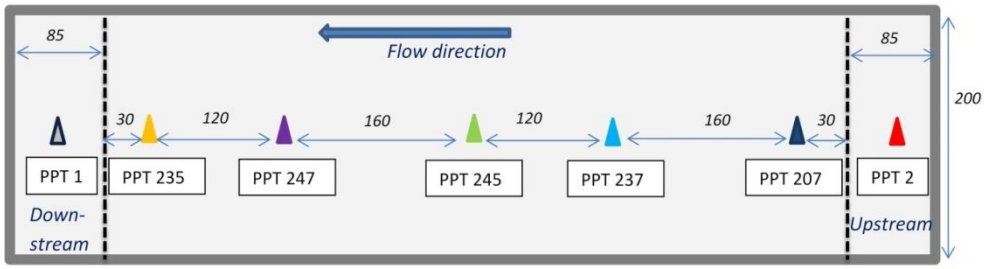

Figure III. 16 - Implementation of the Pore Pressure Transducers (PPTs) in the bottom of the box

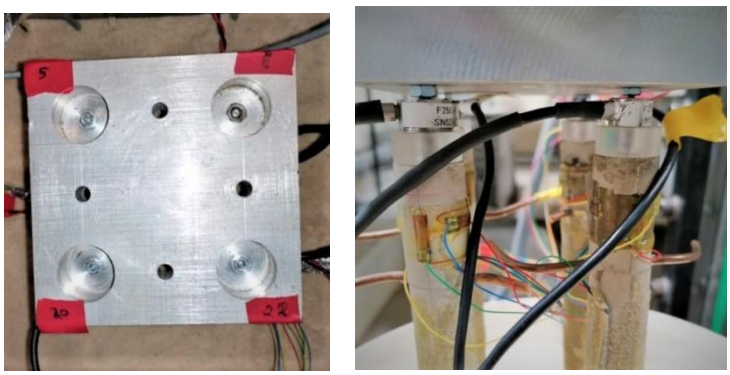

Figure III. 17 - Photography of the header (a) and the piles connected to the header by screwed load cells (b)

2.7 Seepage set up under macro-gravity

2.7.1 Seepage establishment

Once over the sand pouring was competed, the load cells were screwed on the top of each pile and the raft was fixed at the end. With the sand and gravel in place, saturation of the model was carried out by injecting water from the bottom of the model at a low flow rate. The degree of saturation is assumed to be satisfactory for this study. The formulation for calculating the height of capillary rise presented in the previous chapter suggests that the gravity reduces capillary rise. As the latter was already too low to saturate the slice of soil not crossed by the flow in 1g, it is even lower in a centrifuge.

The permeability difference between the gravel and the sand allows maintaining two different water levels in the gravels. Thus, a groundwater flow is established according to Darcy's equation remind here (already presented Chapter III):

$$Q = k.i.S \quad \text{(III.26)}$$

where $Q\ (m^3/s)$ is the flow rate, $i\ (-)$ is the hydraulic gradient, $k\ (m/s)$, is the soil permeability, and $S\ (m^2)$ is the hydraulic surface. The principle is therefore the same as in 1g (Cf. Chapter II), except that in centrifuge, a fluid slip ring is used to supply the model with water inflight. This water supply is controlled to give the required flow rate and once the flow in the model reaches a steady state, the water height upstream remains constant. To impose a constant water height downstream, a siphon system is set up by creating a hole in the bottom and connecting it to a standpipe outside the box. Thus, the water height in the gravels downstream cannot be higher than the siphon height. It is supposed that the running water is at a constant temperature during the test.

The centrifuge acceleration will impose a macro gravity which induces an increase in seepage velocity as highlighted by the scaling laws. Namely, at Ng, seepage velocity will be N times bigger.

2.7.2 Belonging to Darcy's domain

In geotechnical engineering, because of low hydraulic gradient values, the flow velocity is slow enough to apply the Darcy's law. However, on reduced scale model, due to the previously presented scaling laws, seepage velocities are bigger and it becomes necessary to check that Darcy's law is still valid and therefore can be used.

Within the Darcy's domain, the Darcy's law can be written as in Equation III.27.

$$V_D = -\frac{K}{\eta}\nabla P \quad \text{(III.27)}$$

P, the pressure can also be expressed as $P = \rho gh$ according to Bernoulli's equation and the assumptions made (low seepage velocity and incompressible fluid). Darcy's law therefore becomes Equation III.3.8

$$V_D = -\frac{K}{\eta}\nabla(\rho gh) = -\frac{K\rho g}{\eta}\nabla h = k * i \quad \text{(III.28)}$$

Equation 24 introduces the hydraulic conductivity which is expressed through Equation III.3.9.

$$k = \frac{K\rho g}{\eta} = \frac{Kg}{\mu} \quad \text{(III.29)}$$

Another formulation of the Darcy's law exists where the hydraulic head is expressed as a pressure (Khalifa, 2000). This leads to another formulation of scaling laws but, in the present document, the fist formulation will be used. The corresponding scaling laws are listed in Table III. 3 (Khalifa, 2000) and are consistent with the scaling laws section.

Table III. 3 - Usual scaling laws regarding groundwater flow

Acceleration (m/s^2)	Hydraulic gradient (-)	Fluid velocity (m/s)	Hydraulic conductivity (m/s)	Permeability (m^2)
$\mathbf{g^* = N}$	$i^* = 1$	$V^* = N$	$k^* = N$	$K^* = 1$

Darcy's law expresses a linear relationship between the flow velocity and the hydraulic gradient. This relationship remains true as long as the inertial forces are negligible compared to viscous friction (A. Khalifa, 2000). When it is not any longer the case, it becomes more relevant to use the Forcheimer formula (Equation 26) in which the relationship is not anymore linear (Forchheimer, 1901).

$$i = av + bv^2 \quad \text{(III.30)}$$

It is sometimes considered that the Darcy's domain of application corresponds to the range in which the flow has a laminar regime, namely above Reynolds number equal to 10 (Magnan, 2008). However, this cannot be enough to determinate the Darcy's domain validity as it has also been demonstrated that the non-linearity of the relation between hydraulic gradient and seepage velocity appears before the flow stops being laminar (Schneebeli, 1966). In other words, the inertial forces stop being negligible before the flow regime stop being laminar.

To estimate the domain of validity of the Darcy's law, flow rate was measured in centrifuge (macro gravity) for different hydraulic heads and for different type of sands (Khalifa, 2000), aiming at the evaluation of a and b (Equation 26). More precisely, they assessed the linear relationship between

two physical quantities: the friction factor (Ff) and the Reynolds number (Re) whose analytical formulas are given by Equations 27 and 28 where g is the acceleration of gravity, v the average fluid velocity in the soil (Darcy's velocity), n the porosity of the medium, τ the tortuosity, and d_{eq} the equivalent diameter of grains.

$$\mathrm{Ff_{pore}} = \frac{\mathrm{ign^3 d_{eq}}}{\mathrm{3V^2\tau^3(1-n)}} \quad \text{(III.31)}$$

$$\mathrm{Re_{pore}} = \frac{\mathrm{2\rho\tau V d_{eq}}}{\mathrm{3\mu(1-n)}} \quad \text{(III.32)}$$

These numbers originate from the fact that when a flow is considered in a pipe, the shear stress at the pipe wall is equal to $\frac{1}{2}\mathrm{c_f\rho u_m^2}$ with $\mathrm{u_m}$ the mean velocity, and cf the skin friction coefficient depending on the Reynolds number and the roughness of the pipe walls. Inspired by this result, and considering the sand pores as small pipes, this pore Reynolds number was established in order to determine the Darcy's domain limit (Comiti, 2000).

Plotting the evolution of $\mathrm{Ff_{pore}}$ as a function of $\mathrm{Re_{pore}}$, the linear part of the curve corresponds to the range in which Darcy's law is valid. Indeed, the Darcy's law is valid as long as inertial forces are negligible. A limit Reynolds number $\mathrm{Re_{pore_{limite}}} = 4{,}9$ -- valid for all five sands studied -- was deduced. It is therefore possible to estimate limit hydraulic gradient and so the limit acceleration during the centrifuge test.

To support and illustrate this result, a numerical model has been realised on the finite elements software COMSOL. In practice, two 2D-models were realised in order to simulate an energy pile heated in a sandy saturated soil. The parameters and equations of the model are presented in appendix B with also the details of the model. One can focus here on the results (see Figure III. 18) in which it appears that the isotherms calculated with the Darcy's equation and the Forcheimer's equation are superimposed after several times. These calculations have been done for the same hydraulic head difference submitted to macro gravity equal to 50g. In the case where the Darcy's equation has been used, the head hydraulic was calculated in order to get a seepage velocity equal to 40 m/day. According to the scaling laws, that would correspond to groundwater flow velocity equal to 0.8 m/day in prototype. In conclusion, Darcy's law is suitable for both prototype and centrifuge models.

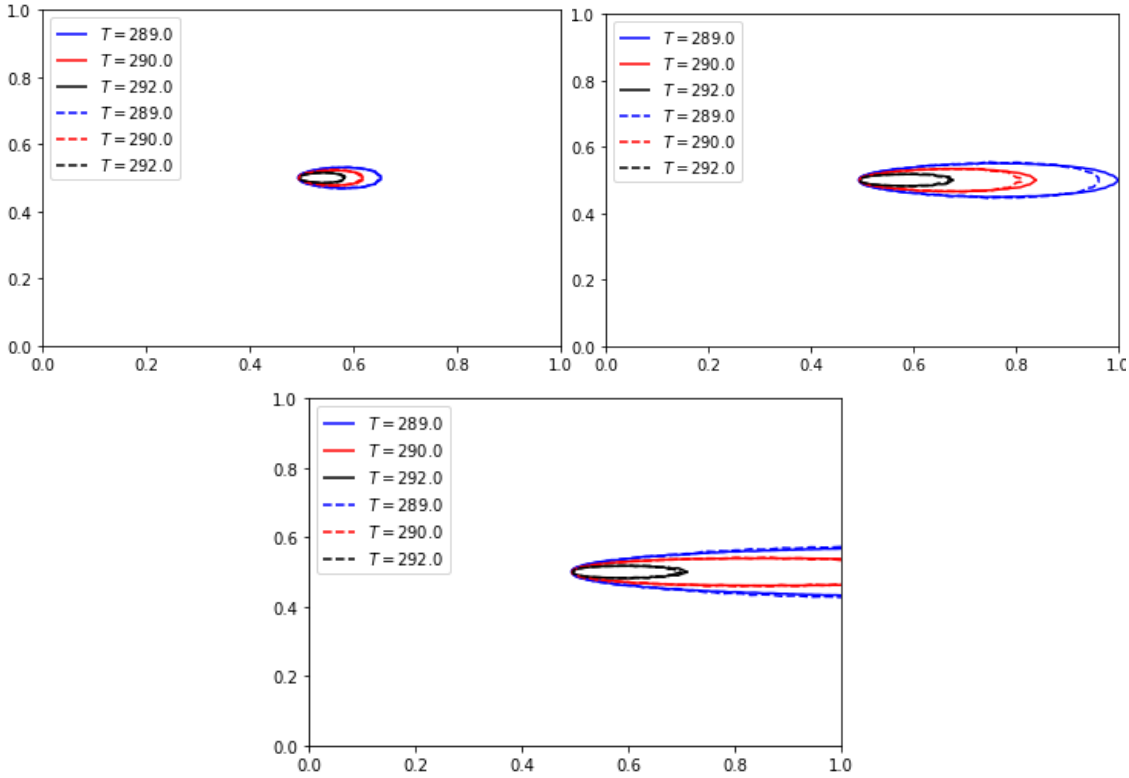

Figure III. 18 - Comparison of three isotherms obtained with Darcy (full line) and Forcheimer (dotted line) after a) one week, b) one month, c) 3 months

In summary, this section describes how groundwater flow is simulated in a centrifuge reduced soil model. One can remind that it was first checked at 1g with piezometers that the top of the water table was linear, thus confirming the use of Darcy's law to assume the flow and calculate seepage velocity. It was then checked that hydraulic scaling laws were respected and that therefore the measurements can be interpreted correctly. Finally, a theoretical and numerical study showed that the flow velocities still allowed the problem to be placed in Darcy's domain.

Chapter IV

HYDRO THERMO-MECHANICAL BEHAVIOUR - CENTRIFUGE TESTS

"Experiment is the interpreter of nature. It never deceives; it is we who deceive ourselves because we expect results other than those which nature gives us." - Leonardo da Vinci

The two previous chapters focused respectively on the hydro-thermal behaviour and the scaling laws regarding the physical phenomena involved in the study of reduced scale model of energy piles group, especially in centrifuge. This chapter is dealing with the study of the mechanical behaviour of such models in reduced scale model, especially at macro gravity level. The aim is to characterise the thermo-mechanical behaviour of a group of energetic piles and the impact of underground water flow on the latter using centrifuge tests. Three test campaigns were then carried out. During the first one, only one of the four piles was heated. In the second, for the sake of technical simplicity and because it is the most unfavourable case mechanically speaking, only one of the 4 piles is subjected to thermal loading, this time cyclic. Finally, the last test campaign aims to thermally load two piles in order to obtain an additional case study.

Introduction and 1g experiment

By investigating the head displacement and the mobilised skin friction of a model energy pile under thermal cycles, it was shown that heating under low axial load induced heave and cooling induced settlement (Yavari, 2013), (Nguyen, 2017). This study also shows that for high axial loads, the pile temperature-displacement curve did not suggest any longer a reversible behaviour as irreversible settlement was observed.

Using the setup presented in II.1.1, these results were confirmed through similar experiments. Indeed, the impact of soil density on the behaviour of an energy pile heated was studied at 1g. The literature review showed that the settlement of an energy pile occurs especially when the soil is loose (Cf. chapter I). This point is studied experimentally at normal level of gravity (1g), and although quantitative results would be unsuitable to deal with, the overall qualitative behaviour remains interesting and relevant to study. To do this, the model energy pile was placed in a soil consisting of dry Hostun sand in a loose state and then in a dense state. A weight of 2kg was imposed at the head and a displacement sensor measured the settlement of the pile at the head during mechanical loading. The pile was then heated for over an hour and the displacement was recorded. It can be seen (Figure IV. 1) that once the settlement induced by the mechanical load is stable (very quickly in the case of dry sand), the thermal load induces heave at the head of the pile, which tends to dissipate over time even though the temperature of the pile does not fall. This effect may be due to heat diffusion in the soil, which attenuates the initial heave. This effect appears for both density state of soil but is more marked in the case of loose sand. Finally, the pile is cooled and its thermal contraction causes a clearly observable settlement. Unfortunately, as the temperature of the energy pile is not the same in dense and loose state, it is not relevant to compare the relative displacement. But, in both case, after a first lifting, a rebalancing is observed. In Figure IV.1, where the sand is dense, at around 2000s there is a new heave in the pile, which occurs just as the pile was beginning to settle gently after the initial heave. This is due to the fact that at this point the power of the heating system was increased. The temperature curve bears witness to this and is consistent with the initial observations.

Finally, when heated, the model energy pile lifts as expected, but tends to settle again and in a greater extent when the sand is loose and this confirm the results present in literature review.

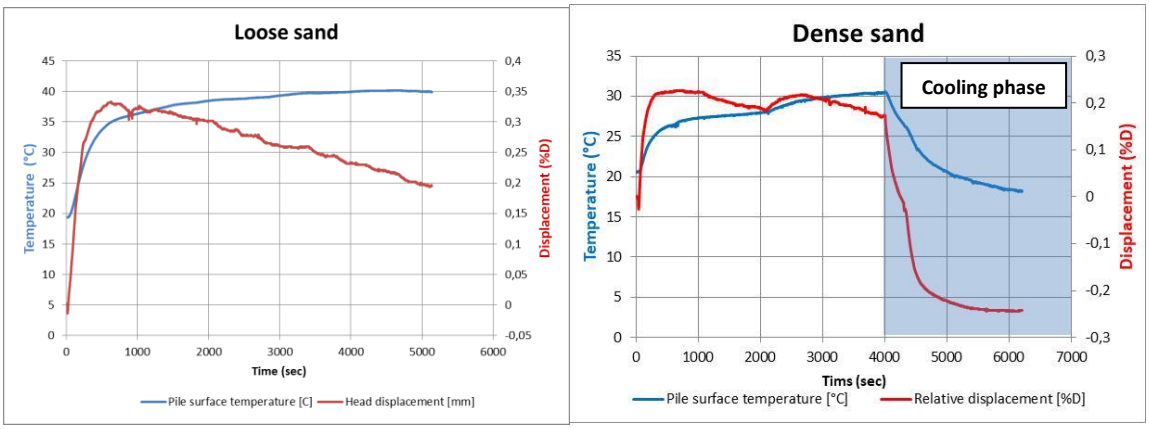

Figure IV. 1 - Head displacement and temperature evolution of heated energy pile in loose and dense sand

However, 1g-tests are carried out in low stress levels and the generalisation of the results for prototypes remains thorny. Beam centrifuge modelling is based on more scaling laws, which makes it easier to interpret the results. In particular, the geostatic stress is the same in the model as in prototype. These advantages, in addition to those already mentioned and specific to reduced-scale studies, lead to a significant increase in centrifuge tests, including heat exchanger structures. Different aspects of energy structures have been studied in geotechnical centrifuge. First, studies have been led in order to correctly model an energy pile employed for centrifuge modelling (Knappett, 2011). The point was to insure the ability to accurately model soil-structure interaction behaviour in centrifuge. Secondly, the attention is logically focused on the thermo-mechanical behaviour of a single energy pile. By investigating the effects of the thermal loading cycles on the thermo-mechanical behaviour of a single energy pile, it was shown that this leads to greater or lesser ratcheting settlement depending on the soil in which the study was carried out (Stewart, 2013), (Ng, 2014). The end restraint effect on soil-structure interaction has also been characterized in dry sand and unsaturated silt with results confirming in-situ observation (Goode, 2015). Likewise, the effect of the pile placing on the thermos-mechanical behaviour of a single energy pile has been tackled. By comparing the response to thermal cycles of a wished-in-place energy pile and a jacked in high gravity one, it turned out that the first one underwent a ratcheting settlement when the second showed a slight heave (Ng., 2016). Finally, the thermo-mechanical behaviour is studied at the scale of a non-symmetrically thermally loaded group (Ng, 2019).

However, as reported in hydrological journals, many deep foundations are located within a flowing water table (Ding, 2008). In the case of energy structures, the hydrology of the terrain will therefore impact the thermic of the studied system and consequently its mechanics via thermally induced phenomena like thermal expansion for instance. Moreover, thermal transfer by advection (displacement of the heat due to water displacement) creates a thermal plume likely to affect the behaviour of other downstream structures (Delerablee, 2020). In order to henceforth take into account this fundamental aspect in the study of a heat exchanger foundations, centrifuge studies were carried out with a flow modelling the movement of a water table. Indeed, the behaviour of foundations like pile groups remains weakly investigated, especially when the thermal loading is not symmetrical and when soil contains a groundwater flow. These two criteria are however frequent and significant. Their study in a geotechnical centrifuge is a technical progress allowing reaching knowledge regarding typical configurations.

Three test campaigns are carried out on the four energy piles group presented in chapter II, but for different thermal loadings. In the first test, only one model pile is heated. In the second one, the thermal load is this time cyclic. In, the third one, two piles are active (submitted to thermal load) in a cyclic way. In each case, the test is conducted with no water flow and in a configuration where water flow modelling the movement of a water table is present. The main aim is to study the impact of groundwater flow on the thermos-mechanical behaviour of model of four piles group in saturated Hostun sand. All the experiments presented in this document were carried out at 50g. According to the scaling laws, the dimensions of the model represent a real structure, called prototype, whose dimensions are 50 bigger.

1. First centrifuge test

The first centrifuge test takes place as follows: the group of piles is subjected to a centrifugal acceleration of 50g, and then one of the piles is heated in saturated sand. The same experiment is afterwards carried out but in soil where seepage is present this time. Seen from above, the piles are located as below:

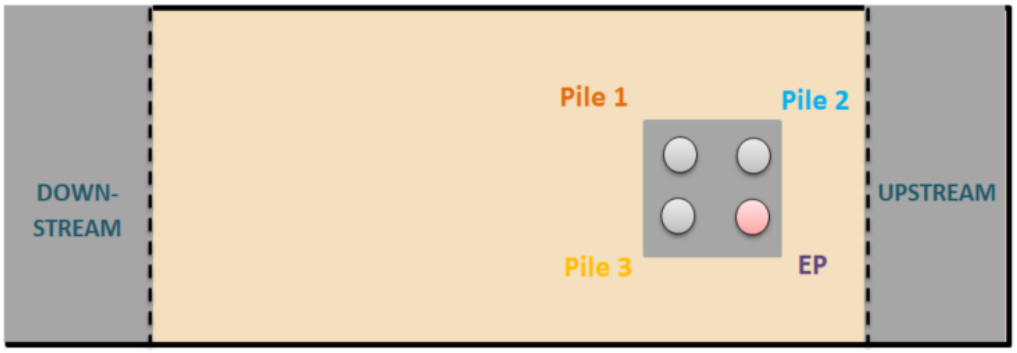

Figure IV. 2 - Top view representation of the model box for the first test campaign

For this first test, the mechanical loading only comes from the header self-weight. This aluminium piece is clear of the ground surface, so that the entire load is transferred to pile heads. An elevated piles group is modelled. Once the model subjected to a centrifugal acceleration of $50\mathrm{g}$, this raft imposes a vertical load of $\mathrm{V} = \mathrm{m} \times \mathrm{N} \times \mathrm{g} = 215\ \mathrm{N}$ on the four piles. By assuming that this load is held by the four model piles which each have a cross section $\mathrm{S^m} = \pi \times {\mathrm{r_{pile}}}^2 = 3.14 * 10^{-4}\ \mathrm{m^2}$, each pile will hold an axial stress

$$\sigma_{\mathrm{ax\_m}} = \frac{\mathrm{V}}{4 \times \mathrm{S^m}} = \frac{215}{4 * 3.14 * 10^{-4}} = 172\ \mathrm{kPa} \quad \text{(IV.1)}$$

As the stresses are conserved in centrifuge, this value is also true in prototype scale. The bearing capacity of this group of model piles has not been previously determined.

However, one can calculate the bearing capacity of a single pile according to the Eurocode 7 (CEN, 2003). For that, a single pile of category 6 (drilled, hollow auger, single or double rotation) in sand is considered with the dimension of the prototype ($\mathrm{D^p} = 1\ \mathrm{m}$ of diameter and $\mathrm{L^p} = 15\ \mathrm{m}$ of length).

The ultimate bearing capacity of the single prototype pile is defined as following:

$$\mathrm{Q_u} = \mathrm{Q_{up}} + \mathrm{Q_{us}}\ (\mathrm{kN}) \quad \text{(IV.2)}$$

With $\mathrm{Q_{up}}$ and $\mathrm{Q_{us}}$ the ultimate bearing capacities of respectively the base and the shaft of the pile.

$$\mathrm{Q_{up}} = \mathrm{S^p} * (\mathrm{L} * 20 + \mathrm{k_p}(\mathrm{p_l} * 1000)) \quad \text{(IV.3)}$$

Where k_p (-) is determined with a table taking into consideration the type of soil and the type of test used to know the resistance parameters of the soil. In this case, a pressuremeter test has been run in a soil identical[6] to the one used in the centrifuge test. Therefore, Eurocode 7 gives a k_p value of 1.65.

p_l is the limit pressure obtained by the pressuremeter test. Here the value obtained is $p_l = 0.05$ Mpa

$$Q_{us} = \sum_i Q_{us_i} = \sum_i h_i . q_s . p_l . 1000 = h . q_s . p_l . 1000 \text{ (Homogeneous soil considerate)} \quad \text{(IV.4)}$$

Where i is the portion of pile, h_i (m) the length of this portion and q_s the ultimate skin friction (MPa) depending on p_l and the type of soil. In this case, the abacus of Eurocode 7 gives $q_s = 0.006$ MPa.

Finally, a value of $Q_u = 600$ kN is obtained. That corresponds to an axial stress of $\sigma_{a\_x_p} = \frac{Q_u}{S^p} = \frac{600}{0.785} = 764$ kPa

Therefore, the axial stress imposed to the model piles corresponds to $\frac{\sigma_{a\_x_m}}{\sigma_{a\_x_p}} = \frac{172}{764} = 22\ \%$ of the bearing capacity of the prototype. As the distances between the model piles are at least equal to 3 diameters (from centre to centre), it can be assumed that there is no effect of the pile group interaction.

1.1 Swing up

During the initial swing-up phase, the model is progressively accelerated until it reaches 50g, in five 10g increments. During this stage, monitoring of the load and pore pressure sensors gives a good account of the rise in acceleration. Indeed, it appears that there is an increase in the pile loads and pore pressures at each step (Figure IV. 3, prototype scale). All the graphs are plotted at the prototype scale and the model pile submitted to the thermal load is named EP (energy pile) in the figures. As it appears in Figure IV.3, at the end of the swing up, the total load is not equally divided between the four piles. However, it is important to notice here that at the end of the last stage, the total force reach a constant value as well as the different pore pressures. This allows us to consider the next evolutions - once the heating system is activated - as being induced by the thermal load. This is also the case for the displacement measurements: during swing-up, a settlement of the raft is observed induced by the increase in centrifugal acceleration. This settlement was not perfectly uniform and a small rotation was observed. However, at the end of the last stage, no more displacement is observed and we can consider that the next displacements will be due to the thermal load.

[6] The real scale experiment was carried out in the same soil (Hostun sand) at a corresponding depth regarding the scaling laws, but there is no information regarding the soil density.

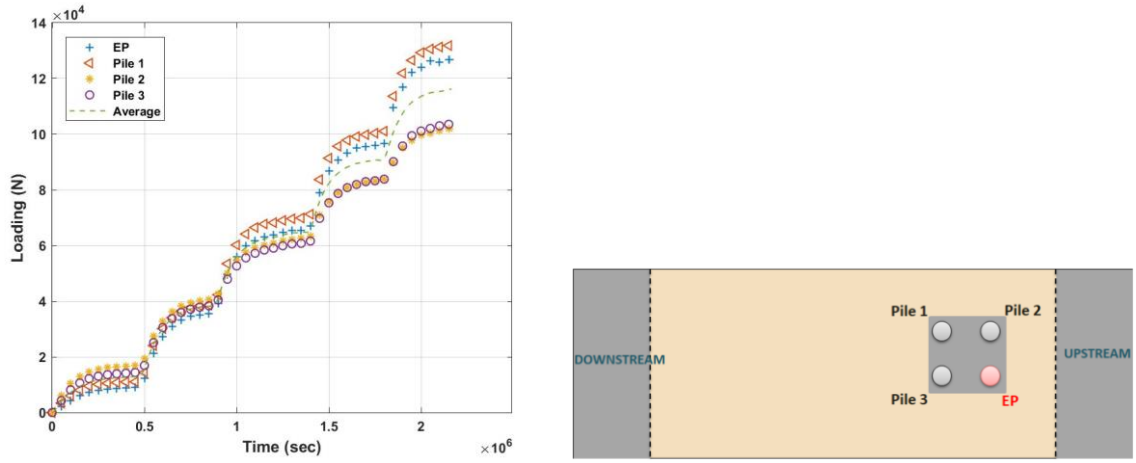

Figure IV. 3 - Augmentation of pile head as a function of time during the swing up (a) and top view schema of the location of the piles (b)

1.2 Thermal loading in a saturated model

Once the centrifugal acceleration reaches the target value of 50g and monitored values stabilise, the heating system is activated by switching on the pump and the Peltier system. Figure IV.5a shows the measures of temperature done by a thermal sensor attached to the surface of the pile. To maintain the thermal load, an increase in Peltier module power was applied at around 1700 s and is shown in the figure by an increase in temperature. In these figures, EP means energy pile and corresponds to the pile which undergoes the thermal loading. It appears that the temperature of the energy pile surface increases quickly but was not as high as expected. This is most likely due to flow rate of the pump that was not large enough because of the centrifugal acceleration. The tests carried out during this study aim at an inlet temperature in the pile of 45°C with a flow rate of 40 ml/min for the pump. However, as mentioned in III.2.5, this target was not reached and the actual flow rate was 20 ml/min.

Nonetheless, the effects induced by the increase in temperature are still observable. The displacement sensor above the energy pile records heave while the opposite pile experiences settlement. These results correspond to a rotation of the raft in the direction of the energy pile towards the opposite pile. The tilting, which is calculated by taking the ratio of the differential settlement to the distance between the centre of two piles, is approximately 10^{-4} in order of magnitude which is very acceptable and comparable to the results of Ng et al. (2019). When the pile is heated, the head load of the model energy pile increases. Indeed, the thermal load induces the thermal expansion of the pile. But the energy pile is not free to expand especially because of the weight applied by the raft. The thermal expansion is therefore constrained by the raft, which leads to an increase in the head load. In parallel, the model pile located opposite on the diagonal also undergoes an increase in head load. This time, as the raft (assumed totally rigid) lifts above the energy pile, it sags at the pile located on the diagonal, which leads to an increase on head load. These increases in the load at the top of these two piles are compensated by a reduction in the load carried by the other two piles. In fact, the total sum of the loads taken by the four piles remains constant during the experiment, as required to satisfy vertical equilibrium.

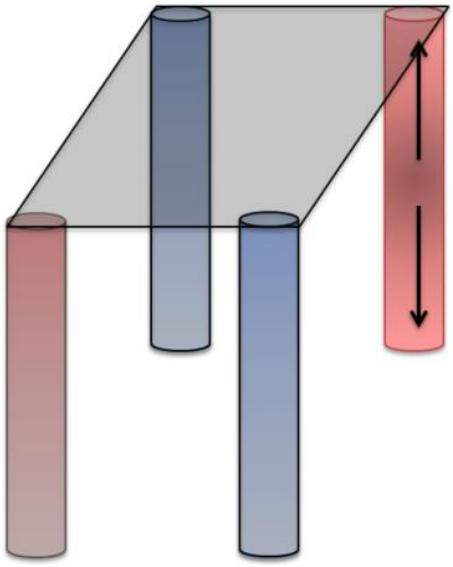

Figure IV. 4 – Head compression (in blue) and traction (in red) induced by group tilting

The measured loads and displacements tend to redistribute after the initial sudden changes, even if heating continues. This could be explained by the fact that the temperature diffused in the soil from the energy pile to the other ones which are then subjected to thermal expansion too. That tends to equilibrate the thermal expansions and the induced effects.

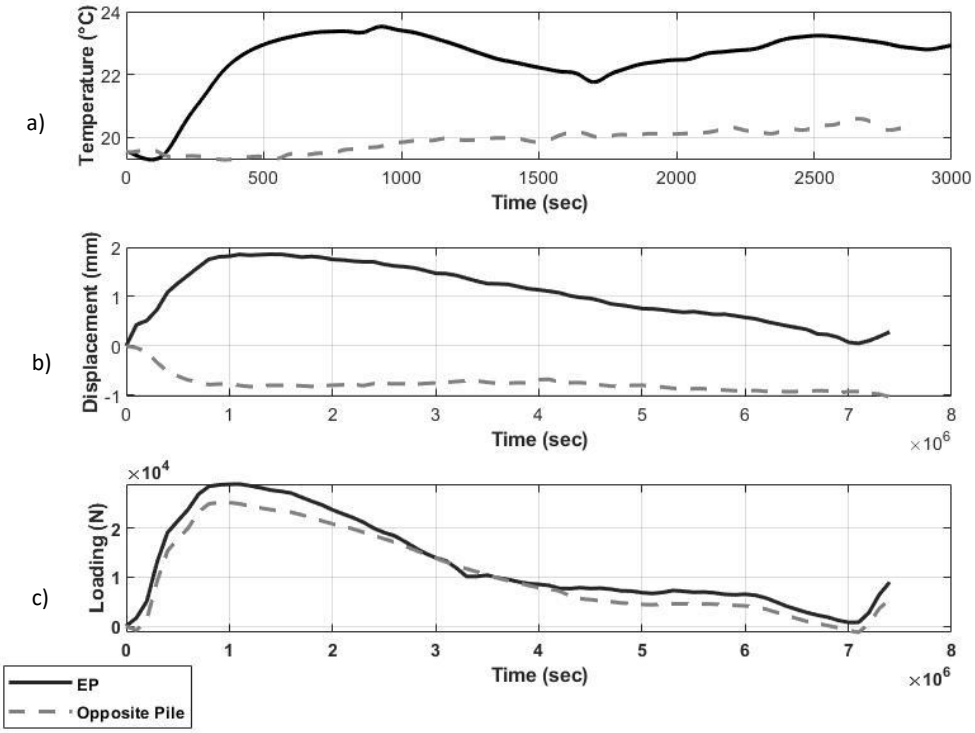

Figure IV. 5 - Evolution of pile surface temperature (a), head load (b) and displacement (c) of the heated pile and the opposite pile as a function of time - case without flow (Prototype scale)

1.3 Thermal loading in a model with ground water flow

After heating the model energy pile for about one hour (around 3 months at the prototype scale), the heating system is turned off and the model seepage is activated with a flow rate of about 2 l/min upstream. This is a cooling phase, in which the water flow controls (reduces) the temperature in the model. In the model, once the soil is at a constant ambient temperature, the groundwater flow is maintained and the heating system is turned on again. The system enters in a new heating phase for the energy pile but this time with a groundwater flow. The electrical powers, supplied to the Peltier system and the pump, are identical to those of the first heating phase. In other words, for the sake of comparison of results, the temperature of the water entering the pile is identical: around 39°C. During all these steps, the centrifuge is still spinning, the two study cases (without and with seepage) are therefore tackled in the same box without reconducting the soil preparation, or stopping the centrifuge.

In the case with seepage, the same phenomenon as before was observed for the case without seepage. The model energy pile rises when it is heated and the pile located opposite on the raft undergoes the opposite effect. Moreover, these two piles register an increase in the head load. Again, the total load is constant throughout the experiment and the increase in the load on the energy pile and the pile opposite on the diagonal is compensated by a loss of head load for the other two piles.

The PPTs which made it possible to monitor the water levels during swing up also give the shape of the water table during the cooling phase. Indeed, thanks to the measures done by the PPTs, it is possible to calculate the water level at different points of the model box as shown in Figure IV.6. These levels have been maintained constant until the end of the centrifuge test, including the phase of thermal load with seepage.

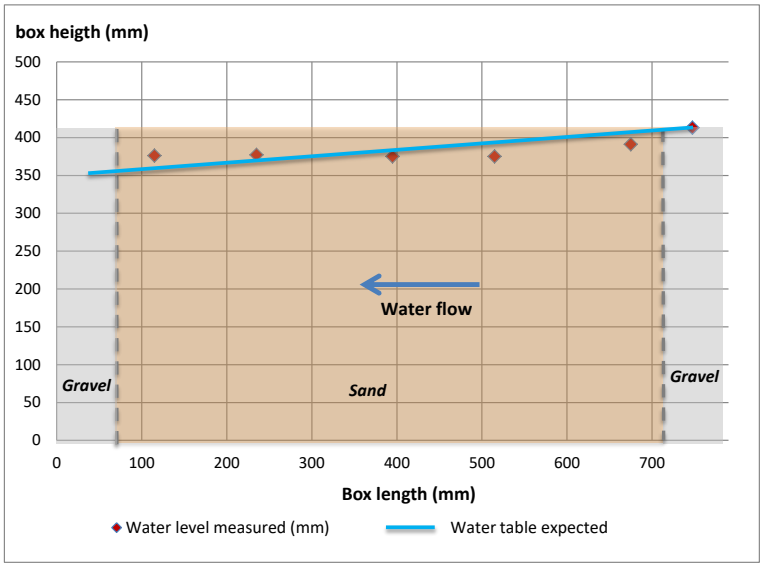

Figure IV. 6 - Water level measured

As it appears in the Figure IV. 6, the PPT 1 (at the upstream side in gravel, Cf. figure III.17) which should measure the water level downstream did not work. However, it can be assumed that the downstream water height was 350 mm as imposed by the syphon. In addition, the effect of the centrifuge acceleration on the water level appears thanks to the circular shape of the water table. In Figure IV. 6, the expected water level corresponds to water level which would have been obtained at a normal g-level (1g) with an entering water flow high enough to reach it. But it was predictable that the water level would be circular due to the centrifugal acceleration which is created by spinning at high velocity the model. Thus, the water flow velocity calculated in this chapter was calculated with

the measured values and not the “expected” values, and result is in line with the inlet water flow imposed. Namely, the velocity calculated as the flow rate (well-known) divided by the surface area is the same as that obtained using Darcy's law and the measurements made by the PPTs. Those measures allow calculating a Darcy’s velocity of approximately 40 m/day. That corresponds to a Darcy’s velocity of 0.8 m/day at the prototype scale, which matches with the order of magnitude of the groundwater flow encountered in reality.

Finally, from a thermal point of view, as seepage is present in the model, a convective phenomenon is involved and it is possible to measure a thermal wave front velocity. For that, the thermal sensors aligned along the bow in the flow direction are considered (Figure II. 23, thermal sensors 6, 10, 8 and 2). The curves of the evolution of the temperature with time have the same shape for all the thermal sensors, but shifted in time. Thus, by considering the required time for each sensor to reach the first pic of temperature the thermal wave front velocity is calculated as explained in II3.3.4. The Figure IV. 7 reproduces these results and the slope of the line is considered as the envisaged value. A thermal wave front velocity of 0.22 mm/s is calculated which corresponds to 19 m/day. This value has to be compared to the seepage velocity. As a reminder, the SIA report (2005) announces a theoretical ratio value of 1.7 between the seepage velocity and the thermal wave velocity. This results originates from the ratio between the heat capacities of the fluid and the soil. In this study the ratio value is closed to 2 and the theoretical outcome is encountered.

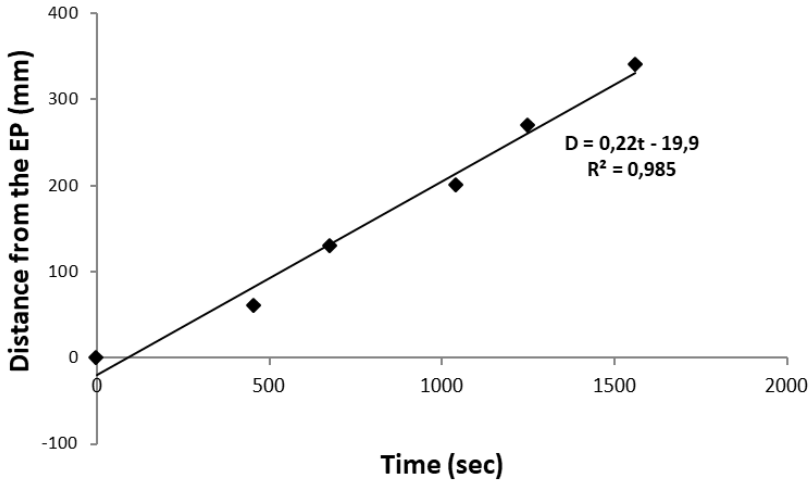

Figure IV. 7 - Relation between distance run by the thermal wave and time

1.4 Impact of the flow on the thermomechanical interaction

In Figure IV. 8, the head load variation of each pile is plotted with Time for the two study cases (presence of seepage and absence of seepage) at prototype scale. For each case, the head load variation of each pile was explained in the previous chapter and the point is here to compare the two cases between them. When ground water flow is present in the model, the thermal convection phenomenon limits the thermal expansion and thus the pile heave and the increase of its head load, which are induced effects. Namely, the water flow around the model energy pile limits the temperature augmentation, in comparison to the case without water flow. By reducing the temperature of the pile, the water flow also limits the thermal expansion of the pile and therefore the induced load variation. This result appears on Figure IV. 9 when one focuses on the mean settlement of the raft (average of the displacements measured by the 4 LVDTs). Indeed, the raft heave is less in the case where a flow dissipates the thermal anomaly although. Similarly, and logically, the head load variations are lower in the case with ground water flow as shown in Figure IV. 8.

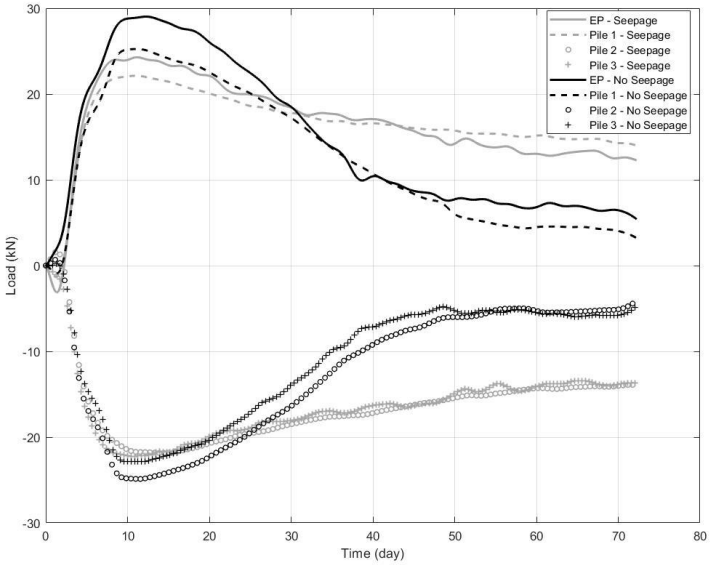

Figure IV. 8 - Variation of the head load of each pile as a function of time for the two configuration cases (Prototype scale)

Regarding the average settlement of the raft calculated by taking the mean of the four displacements recorded by the LVDTs, it appears that the heating of one pile induces first uplift then a rebalancing. Moreover, this effect is globally weaker when seepage is present (Figure IV. 8).

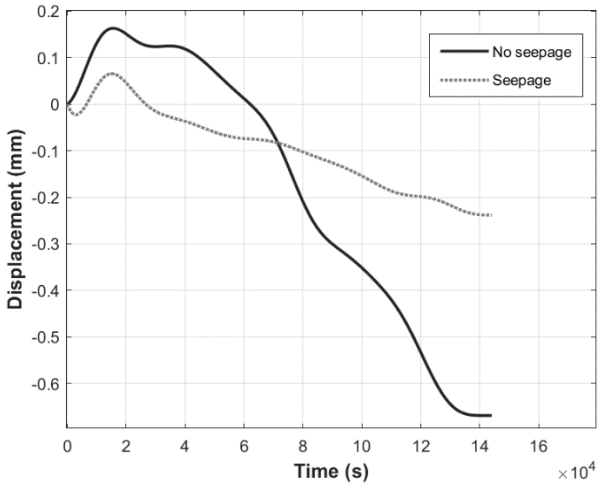

Figure IV. 9 - Mean displacement of the raft during the heating time (Prototype scale)

Indeed, in the Figure IV. 9, the average settlement of the pile group is plotted as a function of the heating time at prototype scale for the two different cases: without seepage (saturated sand) and with seepage. At the beginning of the heating time, both curves describe uplift before the settlement. However, for the seepage case, the variations are smaller and the final settlement is for instance 3.5 times less than the final settlement for no seepage case. In both cases the displacements remain very small and therefore acceptable from a normative point of view (AFNOR, 2012). In addition, if one goes to the end of the test (2000s for instance) without observing the history of variations, it seems that the variation is greater for the seepage case than for the no-seepage case. This is counter-intuitive, but can be explained by the fact that the case with seepage was carried out after the case without flow and on the same soil model, which had therefore already stiffened.

1.5 First conclusions

The study of the thermomechanical behaviour of the pile group shows a heave of the raft above the heated pile at the beginning of the heating period. However, the foundation suffers a global settlement. During uplift caused by thermal expansion of the heated pile, an increase in the head load occurs on the latter. This increase is also seen on the diagonally opposite pile. As the total load remains constant, the other two piles in the group undergo a decrease in the head load. All these variations tend to re-equilibrate over time although the thermal load is maintained. The main innovative aspect of this research was to establish a ground water flow through the model. It was found that the thermomechanical impact is significantly mitigated with ground water flow. However, these results should be viewed with caution since the cyclic aspect of thermal loading is also responsible for the attenuation of the thermomechanical impact (Ng, 2019). Thus, further studies need to be conducted to determine the effect of each phenomenon regarding this decrease in thermal loading induced effects.

2. Second centrifuge test

The second test takes place as follows: the group of piles is subjected to a centrifugal acceleration of 50g, and then three cycles of thermal loading are applied to one of the 4 piles. Afterwards, a flow of water is established in the model, and two thermal cycles are then applied always at 50g. Seen from above, the piles are located as below:

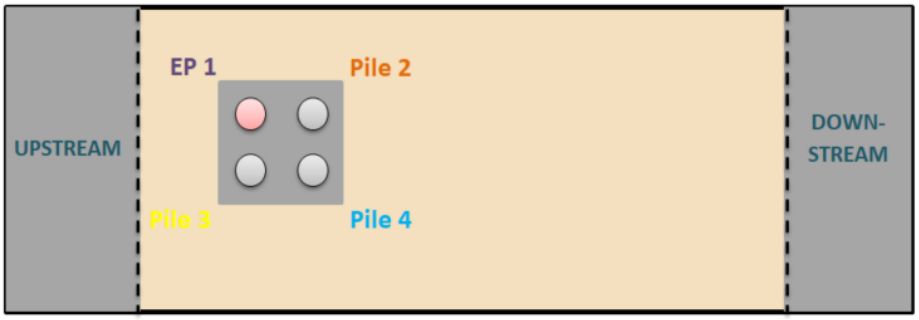

Figure IV. 10 - Schematic representation of piles group for first campaign tests (Top view)

2.1 Swing up

The swing up was realised in four steps reaching respectively 10, 20, 40 and 50g. This raise in acceleration appears in the increase of the loads above in pile (Figure IV. 11) and is also illustrated by the movements of the header (Figure IV. 12) and the increase of pore water pressures traduced by the increase in water height (Figure IV. 13). In all figures, the last values are constant and show the achievement of a permanent constant state at the end of the swing up. At this point, it is then possible to start applying the thermal load and analysing the results by attributing the variations of the head loads to thermal load. More particularly, in Figure IV. 3, it appears that at the end of the swing up, the loading above each pile is not identical for all four piles. The sum of the four mechanical loads reaches 850.3 N (2.1 MN at prototype scale). In theory, the centrifugal acceleration at the bottom of the box is 50g. It means that this acceleration reaches 45.6g on the top of the piles which are located 400mm closer to the rotation centre. Then a weight of 2.040kg should induce a total load of $45.6 \times g \times 2.04 = 912\ N$. Therefore, one can estimate an error of 7%. In addition, the g-raising induces a first settlement of the raft in a non-uniform way. As the Figure IV. 12 shows, three corners of the raft undergo a settlement while the corner of the header on the EP lifts. But, once again, no move is recorded at the end of the swing up and the header is therefore assumed static before thermal load application.

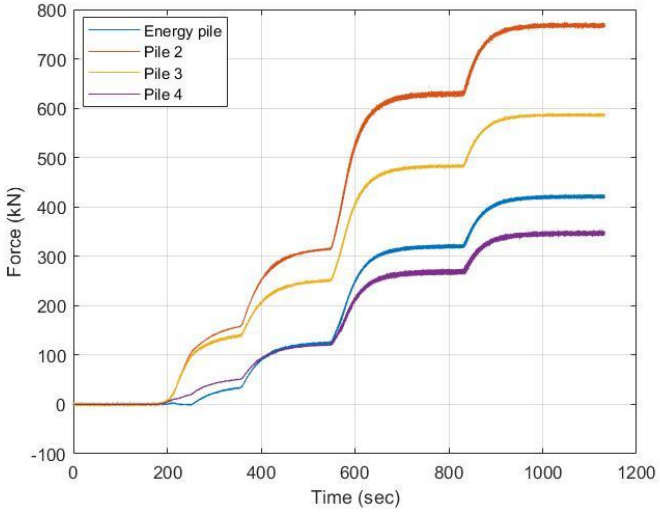

Figure IV. 11 - Increase in head load for all piles during swing up (Prototype scale)

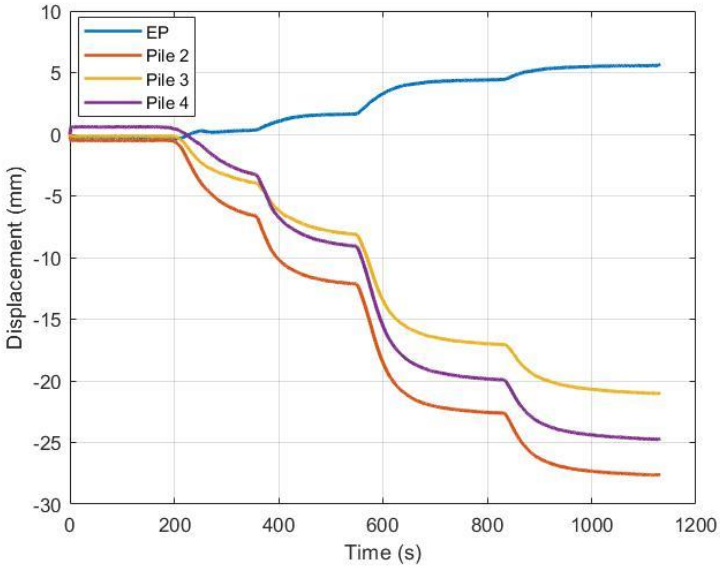

Figure IV. 12 - Displacement of the sensor above each pile during swing up (Prototype scale)

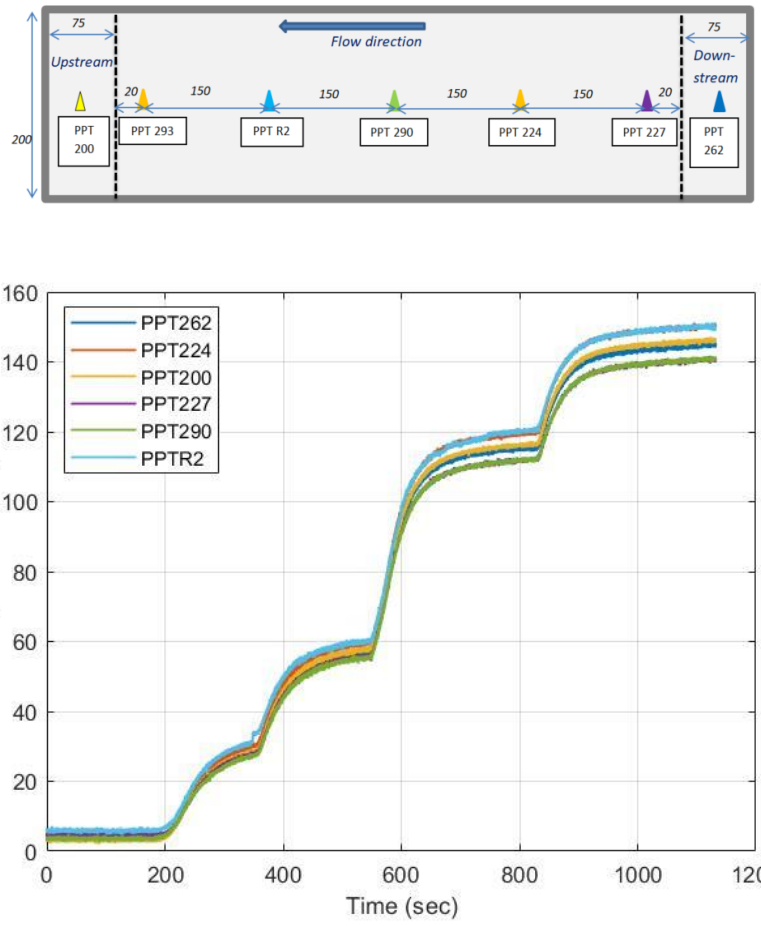

Figure IV. 13 - Water pressure evolution along the box during Swing Up (Model scale)

2.2 First thermal load: 3 cycles

The thermal cycles are monitored using the temperature of the water entering the energy model pile (EP1) and leaving it. The evolution of the temperatures are plotted in the Figure IV. 15. Each thermal cycle is around one hour. The Figure IV. 14 shows the voltage supplied to the Peltier module for one thermal cycle. This cycle is repeated as often as required: 2 or 3 times in this chapter, according to the experiment. To pass from a cooling mode to a heating one, the electrical current is handly inversed, in line with the operating principle of Peltier effect.

According to the scaling law, a thermal cycle of one hour corresponds to 3.5 months and not a year which would have been more realistic if one wants to model a balanced cycle over the year (6months of underfloor heating in summer and 6 months of cooling in winter). Nonetheless, a more realistic test (covering a one year range) should last longer or be carried out at a higher acceleration but will then be more difficult to setup. Figure IV. 15, it also appears that the temperature of the pile shows an increasing trend with cycles. This is due to the inertia of the soil which stores more and more heat with time as the pile is exchanging more heat than cold with soil along thermal cycles. Indeed, the heating device creates easily heat in comparison to cold. . That is why the voltage supplied to the Peltier module is higher in a cooling phase in order to obtain a sinusoidal centre temperature curve.

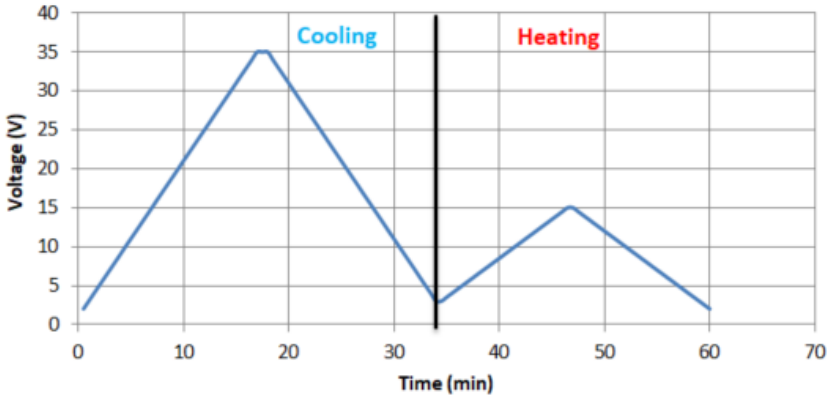

Figure IV. 14 - Voltage supplied to the Peltier module for one thermal cycle

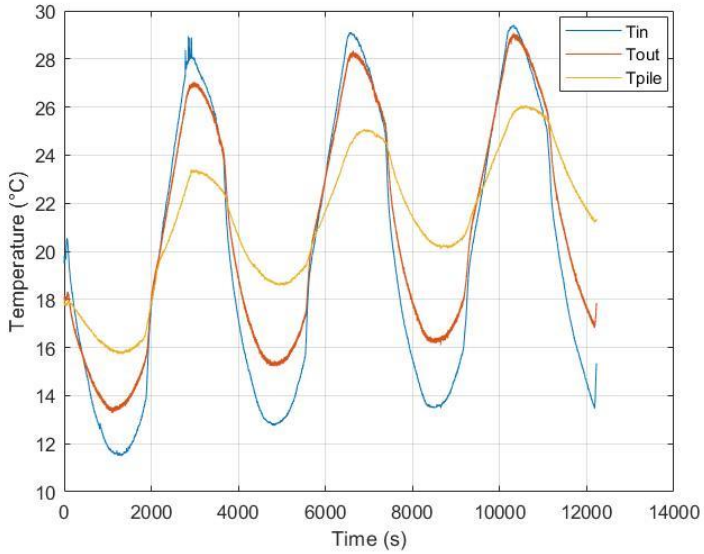

Figure IV. 15 - Temperatures of the pile and of the inlet and outlet water

The load variation at the head of each of the piles follows these cycles as shown below Figure IV. 16:

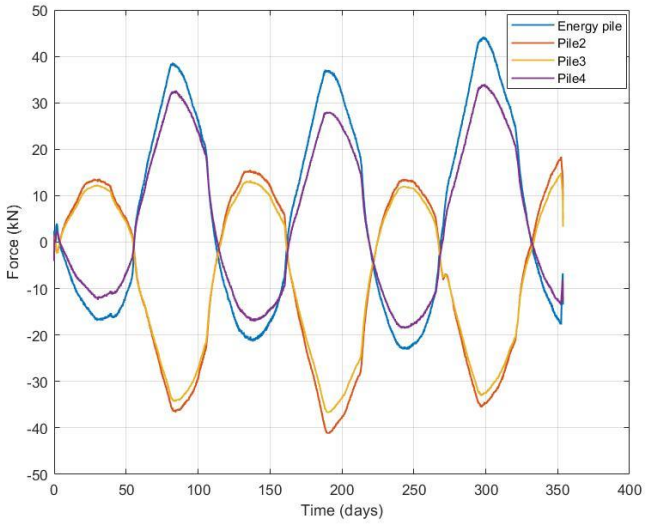

Figure IV. 16 - Increase in head load over each pile during thermal cycles without seepage (Prototype scale)

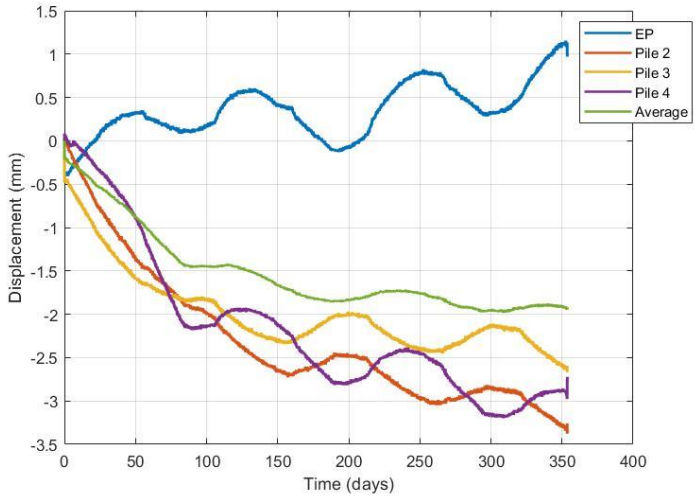

Figure IV. 17 - Displacement measures above each pile during thermal cycles without seepage (Prototype scale)

By focusing first on the behaviour of the model energy pile, it appears that its head load decreases during cooling period and increases during heating period. Moreover, the variations are bigger during the heating phases than during the cooling phases. This is due to the local increase of soil temperature around the pile along the cycles as explained previously.

If one focus now on the pile 4 located opposite on the diagonal to EP1, it appears that its head load variation follows the same evolution as for the model energy pile. This phenomenon was already observed in previous experimentation where the energy pile was only submitted to a heating phase. This phenomenon appears even more clearly here with thermal cycles. In parallel, the two other piles are undergoing the contrary effects. In fact, the cooling of the pile leads to a thermal contraction of the pile, which brings a diminution of the head load and a displacement of this latter towards the bottom. This displacement leads to an opposite move for the pile located at the opposite diagonal and so to the same diminution of the head load, as the header connecting the four piles is rigid. As the weight applied on the raft is constant during the test, the total load is constant as well.

Therefore, the diminution of head load for Energy Pile and Pile 2 are compensated by an increase in head load for Pile 2 and Pile 3. During a heating phase, the opposite phenomena occur. This opposition in behaviour between the piles located on different diagonals is also observable in the header movement. Indeed, the Figure IV. 17 shows that the corners of the header over EP and Pile 4 follows the same moves. From a general point of view and as it appears in Figure IV.17, the average settlment of the header (calculated as the avarge of the four displacements measure by the sensors in the four corners of the header) is positive and follows a ratechetting setllment trend.

2.3 Set up of groundwater flow in the model

To establish a horizontal water flow (seepage), running water is supplied to the upstream side of the box after a new swing up. With an in-flow of 1.5 l/min, and because of the permeability difference between gravels and sand, the water levels along the box change until reaching a steady state. The evolution of water levels along the box can be monitored by the PPTs which give the water pressures all along the box as plotted Figure IV. 18 in model scale. Once this steady state reached, the water flow is maintained and the water level is higher in the upstream part of the box than the downstream one. This results in a constant water table shap as it is shown in Figure IV. 19 where the water level is plotted along the box. The water level difference between the two extremities creates water flow in the sand.

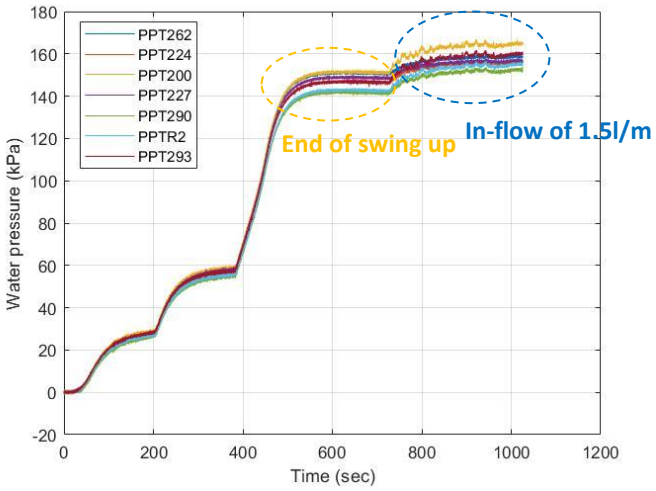

Figure IV. 18 - Evolution of water pressures during second swing up and opening of water tap (Model scale)

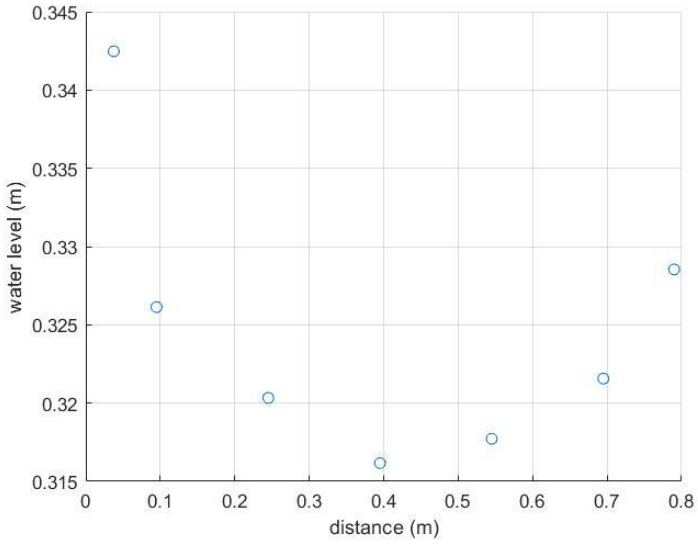

Figure IV. 19 - Water level along the box during seepage at steady state (Model scale)

To calculate the velocity of the water flow crossing the box, the two water pressures (respectively upstream and downstream) are considered, and the Darcy's law is used:

By considering that a water in-flow $Q^m = 1.5\ l/m$ supplies the model, the Darcy's law is written:

$$Q^m = k^m . i^m . S^m \quad \text{(IV.5)}$$

With k^m the hydraulic conductivity of the sand in the model, i^m the hydraulic gradient in the model, and S^m the cross section of the model. The dimensions of the box allow determining

$$S^m = W \times H_w = 0.2 \times 0.315 \text{ (IV.6)}$$

and the measure done by PPTs allow determining $i^m = \frac{\Delta h}{W} = \frac{0.343-0.323}{0.64}$.

Then,

$$k^m = 1.7 \times 10^{-2}\ m/s$$

The scaling law regarding the permeability of a soil states that $k^* = N$, and therefore the permeability of the sand used in this model (Hostun sand) is around $3.10^{-4}\ m/s$ (literatture gives $10^{-3}\ m/s$ as order of magnitude).Therefore, the water flow velocity in the model is:

$$V^m = k^m . i^m = 34\ m/day$$

This value corresponds to a seepage velocity of $0.7\ m/day$ in the prototype. Once this seepage established in the model, the monitoring of temperature located in the sand allow checking that the temperature field is homogeneous before starting again the heating system which creates the thermal load.

2.4 Second thermal load: two cycles in seepage

Two cycles of thermal load are applied to the model energy pile during seepage. The Figure IV. 20 shows the temperature of the energy pile interface with time with Pt100 stuck at midheight (Cf. figure 3). It also shows the temperature of the water entering (Tin) and leaving (Tout) the energy pile. Both temperatures make it possible calculating the thermal power P exchanged between the pile and the soil using the following formulation (already presented in previous chapters):

$$P = q.C_v.\Delta T$$

where q is the massic flow in the heat exchanger tube, C_v the heat capacity of the heat exchanger fluid and ΔT the difference between temperatures entering and leaving the energy pile. It is therefore possible to plot the exchanged thermal power as a function of time as in Figure IV. 21.

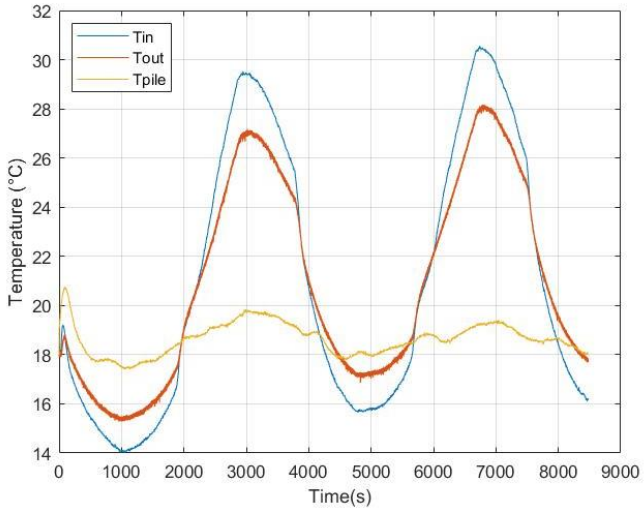

Figure IV. 20 - EP surface temperature and temperature of EP entering and leaving water

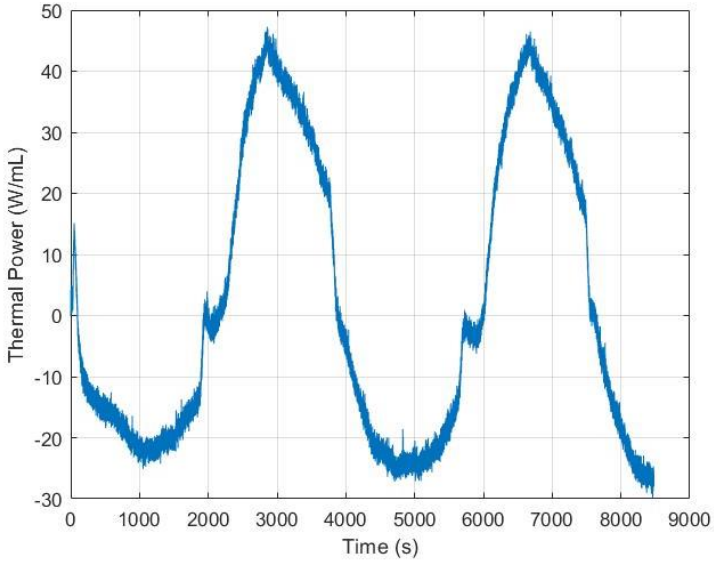

Figure IV. 21 - Exchanged thermal power between the ground and EP (Seepage case)

The load variation at the head of each of the piles follows these cycles as shown in Figure IV.22:

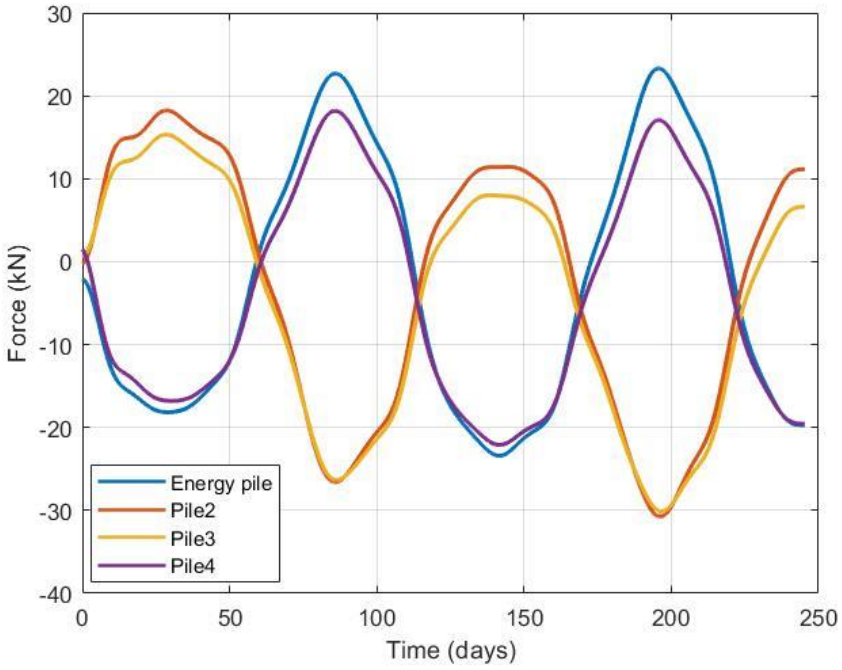

Figure IV. 22 - Head load variation over each pile during thermal cycles (seepage case, prototype scale)

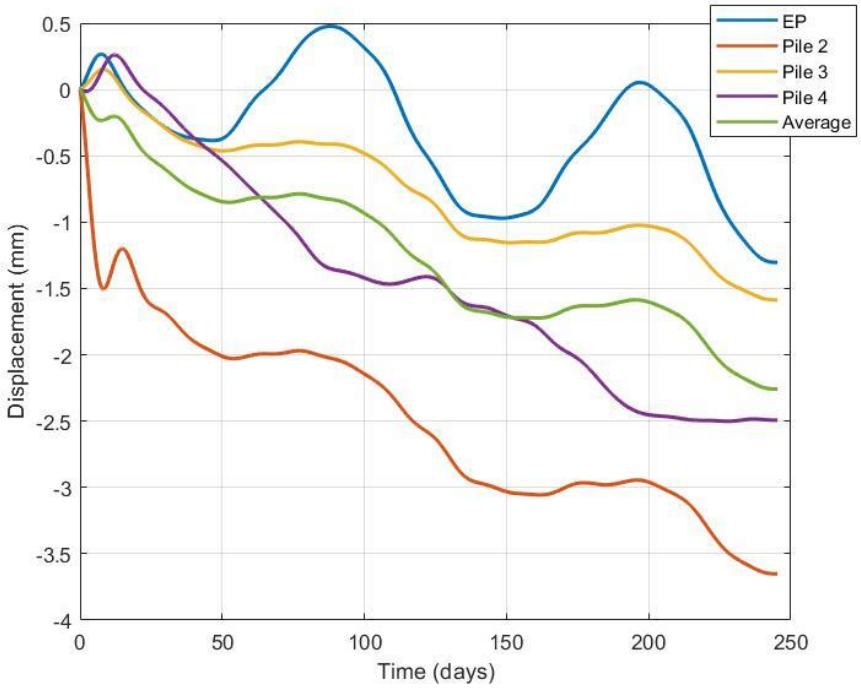

Figure IV. 23 - Displacement of the header at the level of each pile during thermal cycles (seepage case, prototype scale))

2.5 Discussion

From a thermo-mechanical point of view, it first appears that the pile subjected to positive thermal load undergoes an increase in the head load when it is heated and a decrease in this load when it is cooled. The pile 4 located on its diagonal undergoes the same effect because of the transmission of the displacement by the rigid header. Secondly, the two other piles (P2 and P3) undergo the contrary effects as the total load remains constant all along the test. Thirdly, seepage makes the temperature variations lower, so (a) the extreme temperatures are smaller (T_in_max and T_out_max), (b) the model energy pile reaches lower temperatures for an identical thermal loading, and (c), and the head load variations are then weaker.

As the piles did not initially support the same weight before the application of the thermal loading in the cases with and without seepage, it is not relevant to look at the absolute load variation but rather to focus on the relative variation according to what the pile was initially supporting (before the thermal load). Thus the normalized load variation is calculated as the load variation divided by the initial load supported. This work was carried out and the results are summarized in the following Figure IV. 24.

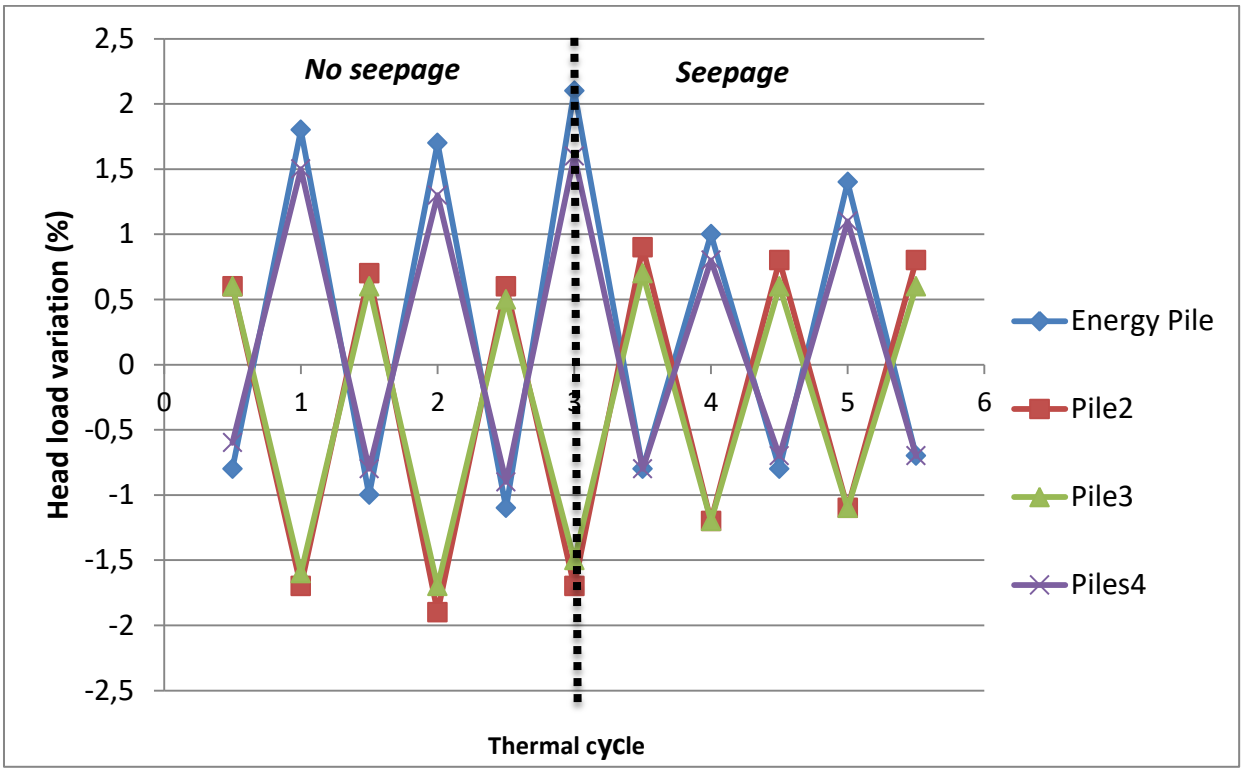

Figure IV. 24 - Evolution of relative head load variation of the piles with thermal cycles

It appears that the variation of the load relative to the load initially carried by a pile is higher in the case without flow. At the end of cycle 3, the flow in place clearly shows the break in behaviour (the amplitude of the variations are noticeably smaller). Moreover, the presence of this rupture after 3 cycles makes it possible to affirm that this weakening of the variations is not due to the succession of loading cycles which produces a “ratcheting” effect as shown in the literature (Ng, 2019).

From an energetic point of view, it appears in the Figure IV. 25 below that the thermal exchanged power is higher in the seepage case and seems to stay balanced along the cycles. Indeed, although

the voltage supplied to the Peltier module is identical in both cases, the energy pile temperature undergoes higher variations in the no seepage case and also a thermal drift. It seems that the water flow not only allows avoiding thermal drift but also increasing thermal exchanges, although these two points are linked between them, the double beneficial effect of seepage appears here. This effect would be even more beneficial in a case where the power demand is even more unbalanced. Indeed, in such a case, the thermal drift would be even greater without the thermal washing brought by underground water (Cf. chapter IV or V).

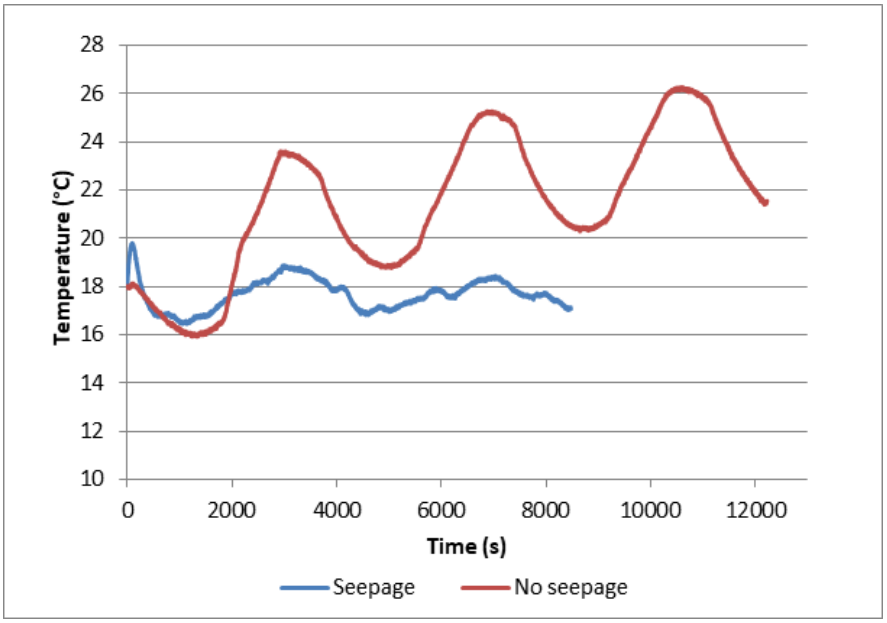

Figure IV. 25 - Temperature of EP without and with seepage

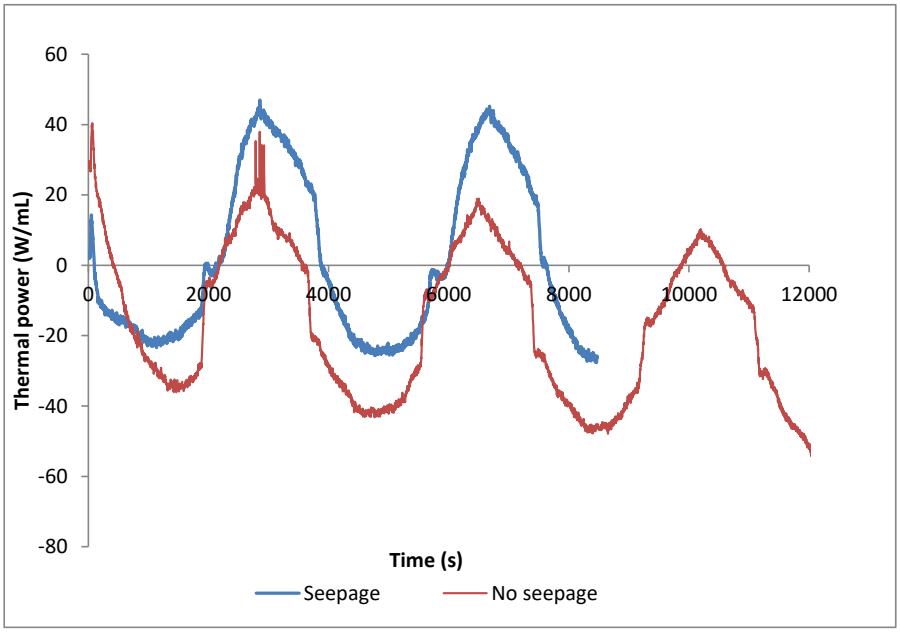

Figure IV. 26 - Exchanged thermal power between EP and soil for Seepage and No seepage cases

3. Third centrifuge test

The test is carried out as follows: the group of piles is subjected to an acceleration of 50g, then a flow of water in the model is established, three thermal cycles of 40min are applied to two model piles, the flow is stopped and three new cycles are applied to these same piles. Compared to the previous test, the experiment with seepage is carried out before the experience without seepage in order to avoid any confusion between the effect of seepage and the ratcheting effect mentioned in the literature about the energy piles submitted to cyclic thermal loadings.

This time, two aligned piles are subjected to thermal loading after reaching 50g. The configuration of the pile group, seen from above, is as follows in Figure IV. 27:

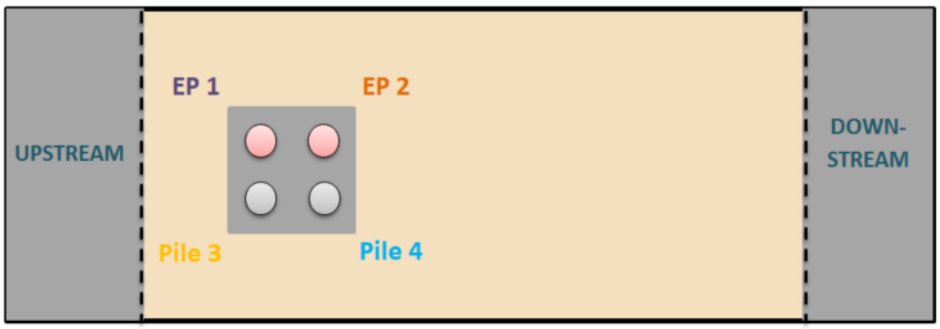

Figure IV. 27 - Schematic representation of piles group for third campaign tests (Top view)

To heat the two piles, a splitter tube is used in order to divide the flow of water leaving the Peltier module into two flows each going into a pile. At the output of the two piles, the same system is used to loop the heating system, the diagram of which is also shown in the Figure IV. 28 below:

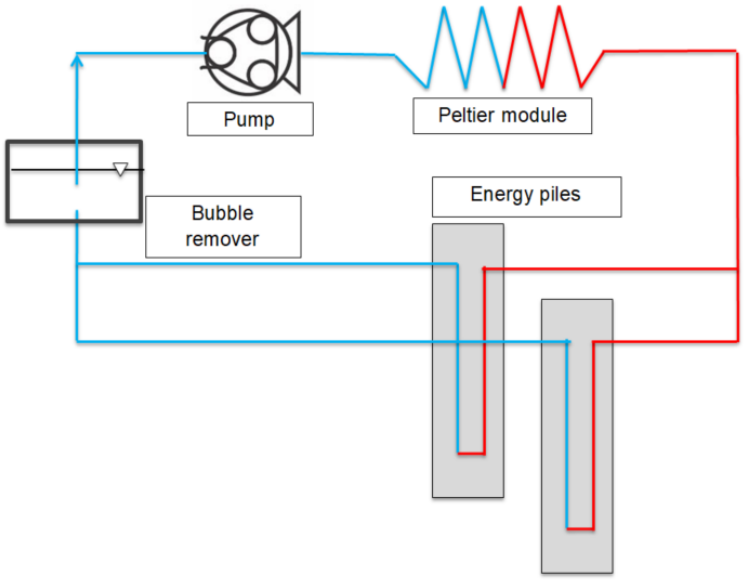

Figure IV. 28 - Schematic representation of the heating system for two energy piles

3.1 Seepage establishment

This time, seepage is established first, before any thermal loading and after the swing up. It is setup in the same way as previously, but with a higher flow $Q^m = 3\ l/min$. The evolution of the pore water pressures during seepage set up are plotted with time in Figure IV. 29. One can observe the pore water pressures increased with time. It corresponds to the opening of running water tap and to the model water supply. Figure IV. 29 shows well that the model was saturated before the flight and that at the end of seepage setup, the pore water pressures are all constant. It means that a steady state is reached and the water level in the box, plotted in Figure IV. 30, is now fixed. In this figure, the water level appears different from the one Figure IV. 19 because the flow is greater ($3\ l/min$).

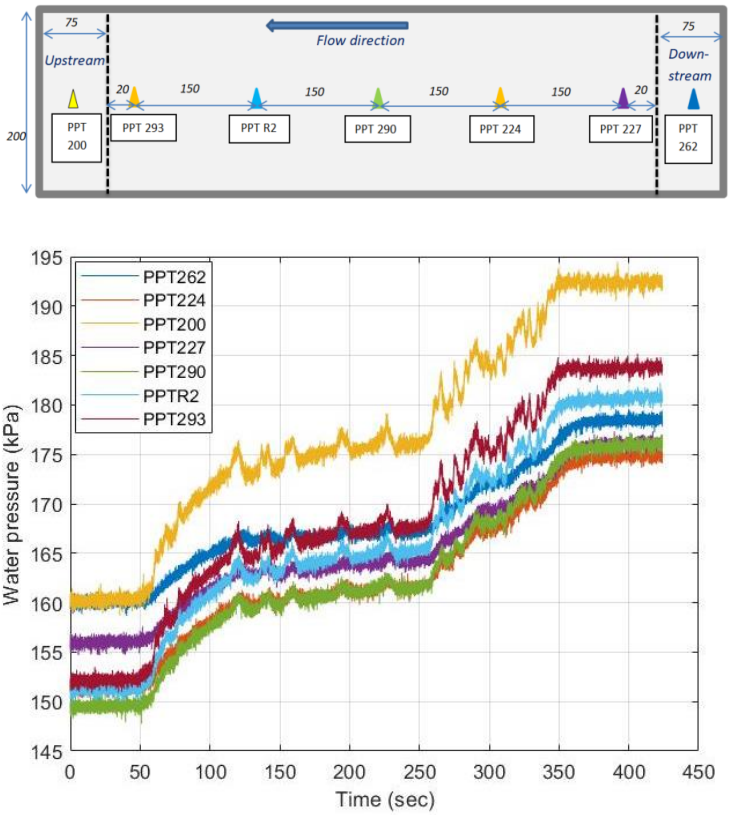

Figure IV. 29 - Water pressures evolution during seepage establishment (Model scale)

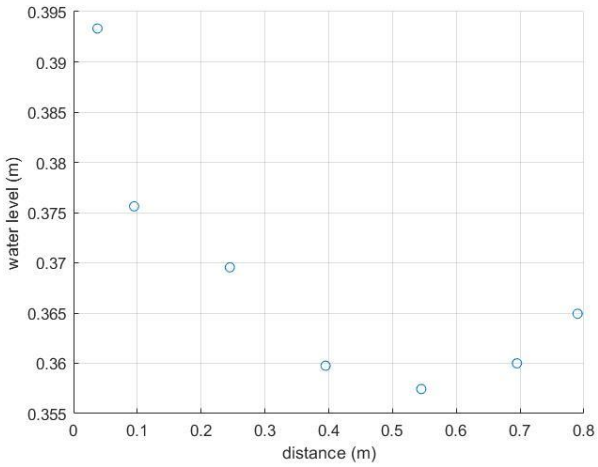

Figure IV. 30 - Water level shape once seepage established (Model scale)

3.2 First thermal load: 3 cycles in seepage

Once the water level is at the steady state, the heating system is switched on, and the two model energy piles are submitted to thermal loading. On Figure IV. 31 are presented the evolutions of the water temperatures entering and leaving the two active piles. In particular the temperature of the water at the outlet of the second energy (Tout2) pile undergoes smaller variations. It is very likely that the water flow is not equally separated before entering each of the piles. Concretely, the flow in the second pile might be lower, which leads to a weaker mass flow with, in addition, more time to exchange heat with the pile. Therefore, the water comes out of EP2 with a lower temperature. This difference of water flow between the two piles might be due to a different hydraulic head loss between the two loops that lead to the piles. Indeed, this heating system described Figure II. 6 was tested at 1g when the hydraulic head losses were negligible. However, it was not anymore the case at 50g, and it was easier for the pump to circulate water in one pile than in the other one. A temperature slip appears for all sensors around 2200 s. It corresponds to a command mistake and brings therefore none relevant analysis.

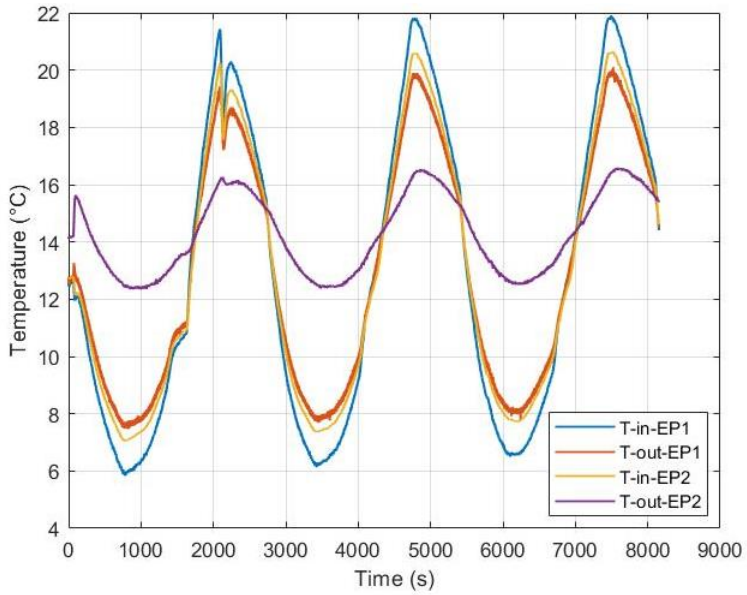

Figure IV. 31 - Temperature of water entering and leaving model energy piles

These thermal loading cycles induce, as seen previously, displacements of the header and load variations at the head of each pile. These displacements and head load variations are plotted respectively in Figure IV. 32 and Figure IV. 33. This time, a drift appears in the graph of head load variations. Indeed, Ep1 and Pile 4 seem to undergo an average increase over the cycles, and conversely a decrease for the two other piles. This suggests that the displacements induced by the dead weight are not stabilised during thermal loading. Thus, the cycle variations can be attributed to the thermal load and the linear trend increase to the mechanical load. In addition, it can be seen that the displacement sensors located above the active piles are subject to a ratcheting settlement in phase (they are lifting at the same time and settling at the same time). This seems logical since both piles follow the same heating and cooling phases. However, the cycles do not appear as clearer on Pile 4. The sensor above Pile 3 did not function during this test. The ratcheting settlement appears on the measures done by the LVDTs, with a lift during heating phases and a settlement during cooling phases. Although the two model energy piles did not undergo the same thermal load in terms of intensity, the magnitude of the displacements measured by the sensors above each of them appear

was found to be similar. Moreover, at approximately t=2000s (end of the first heating phase), EP1 shows an increase of the head load while EP2 shows a decrease in head load, although both of them are heated. As we explained previously, a heating phase should have led to an increase in head load. But, as EP2 is less heated, it seems that EP1 behaviour imposes the group behaviour. In other words, it is as if only EP1 is active.

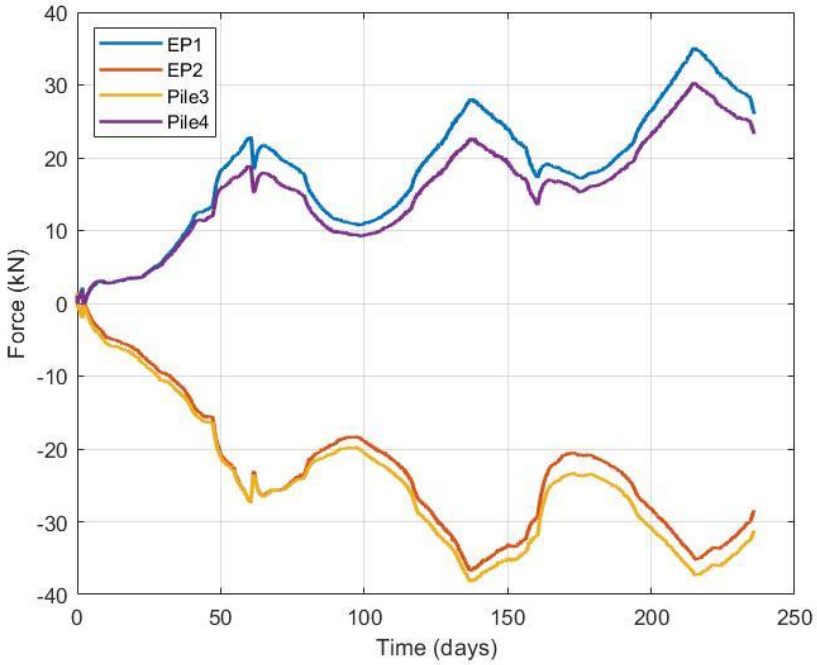

Figure IV. 32 - Increase in head load for each pile during thermal cycles (Seepage case, Prototype scale)

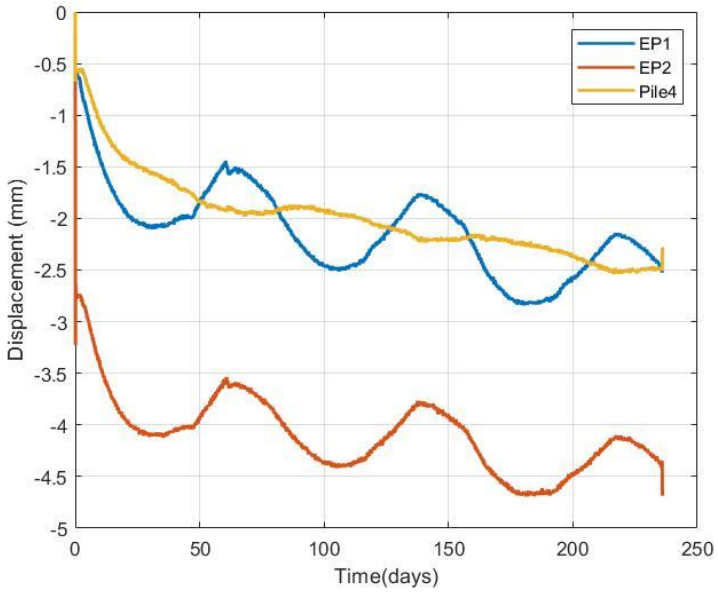

Figure IV. 33 - Displacement of the header during thermal cycles (Seepage case, Prototype scale))

3.3 Second thermal load: three cycles in saturated sand

After these three thermal loads, the heating system is switched off and seepage allows the soil regaining a homogeneous temperature field. Once the homogeneity is reached (checked by verifying the temperature curves), the flow is stopped and the water level returns to its normal curvature due to centrifugal acceleration as shown Figure IV. 34. The heating system can be started again to apply cyclic thermal loading to the two model energy piles for the case without seepage.

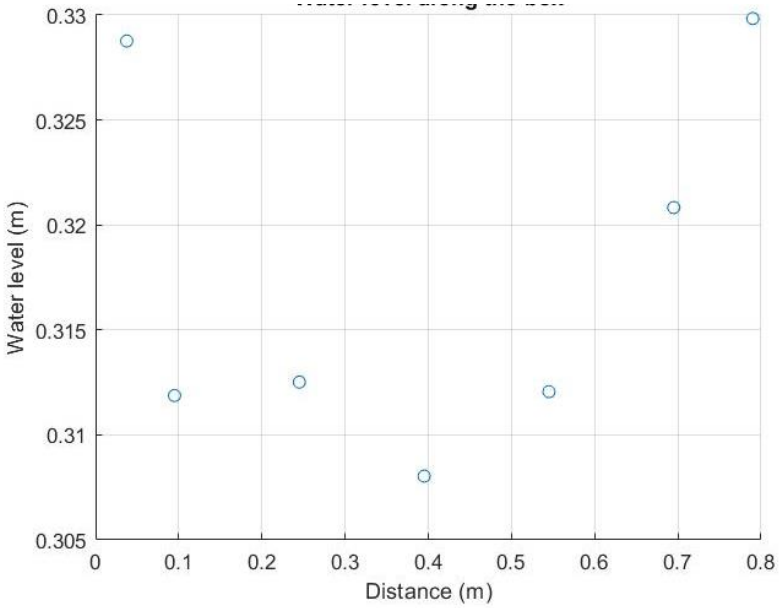

Figure IV. 34 - Water level along the box for saturated case (no seepage)

Once temperature field homogeneous and the water level stabilised, three thermal cycles are carried out.

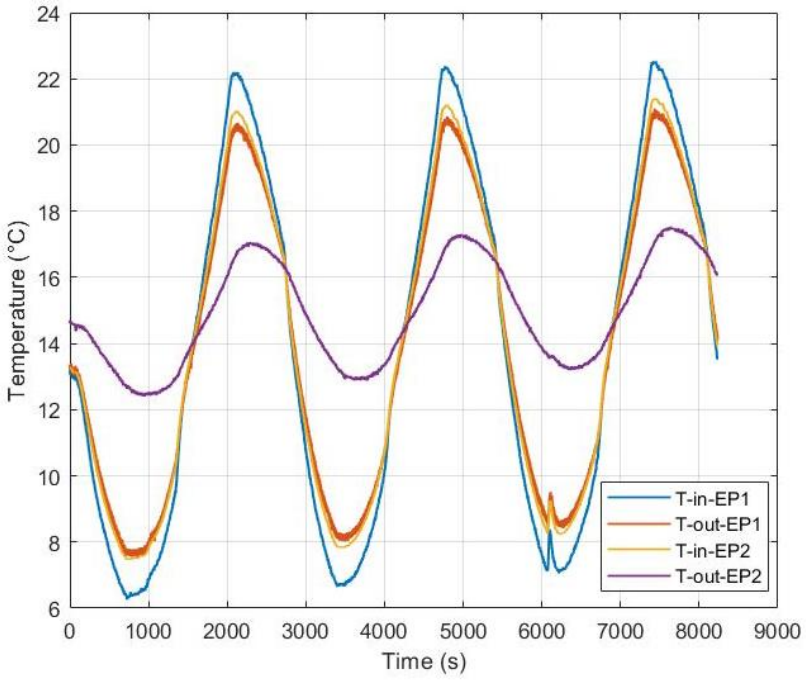

Figure IV. 35 - Temperature of water entering and leaving model energy piles (No seepage case)

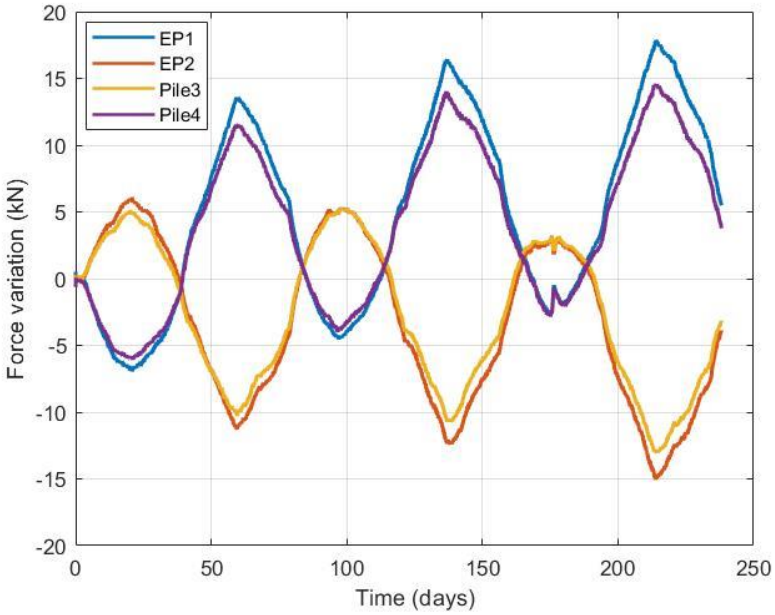

Figure IV. 36 - Increase in head load for each pile during thermal cycles (No seepage case, Prototype scale)

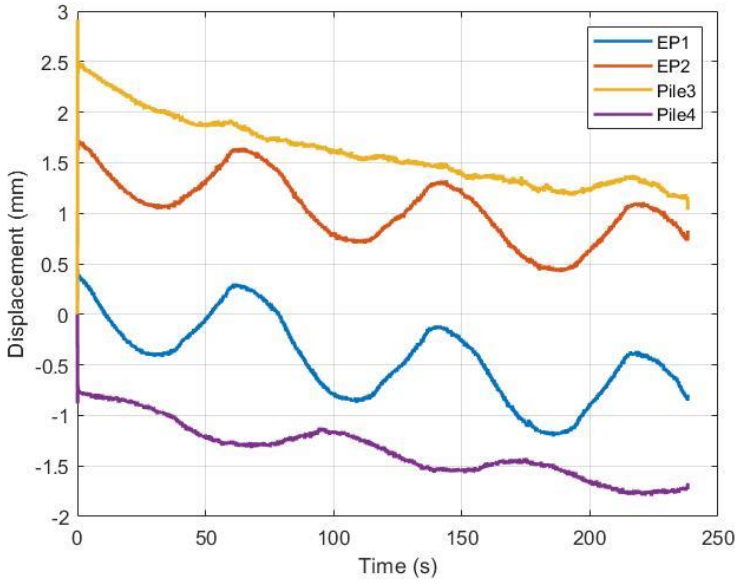

Figure IV. 37 - Displacement of the header above the piles during thermal cycles (No seepage case, Prototype scale)

It appears that the two model energy piles are not thermally loaded with the same intensity and that the pile which is more heated (or cooled) imposes the thermomechanical behaviour on the whole piles group. Namely, it is as if only Pile 1 is thermally loaded and the head load variations are similar to the first case. However, the header displacements are not identical in comparison to the first case. This time, the displacements at the head of both active piles showed cyclic variation and ratcheting settlements over cycles. Their evolutions are in phase and of the same amplitude.

As the flow rate of water through each pile is not known accurately, it is not possible to calculate the thermal power exchanged by each pile with the soil as in the previous test. However, as in the previous test, it can be seen that the temperature of the piles is logically lower in the case with flow.

The Figure IV. 38 shows that without the presence of flow the piles undergo temperature variations of 5° compared to 2° when there is flow. The thermal sensor on EP2 did not work for the Seepage case. It is also important to notice that, contrary to the No Seepage case, the temperature of the non-active piles did not vary during the experiment in the seepage case. Their head load variation is therefore exclusively due to thermally induced variations in the active piles.

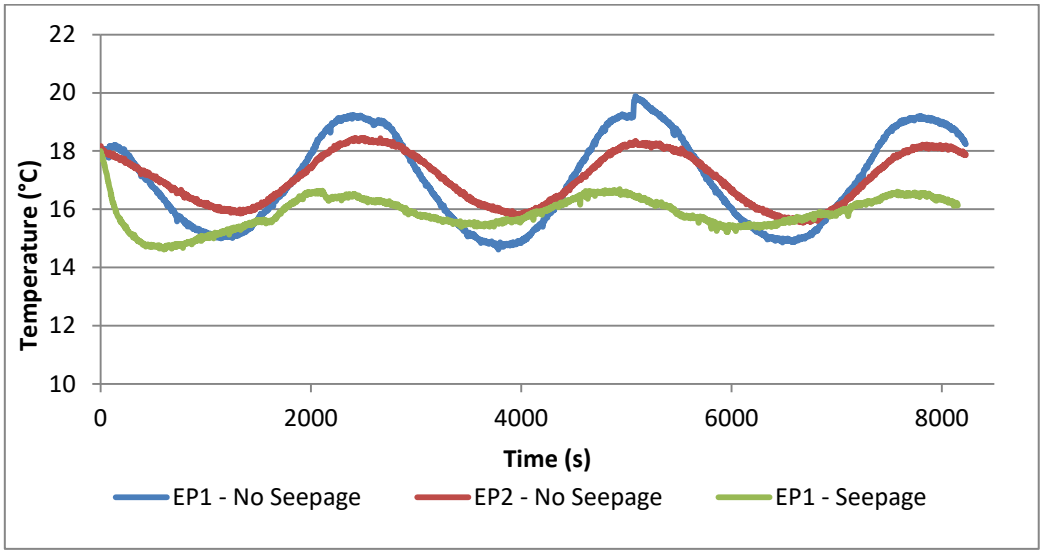

Figure IV. 38 - Temperature of the active piles during thermal cycles

The water flow attenuation effect is still visible and therefore confirmed. It is illustrated in the Figure IV. 39 where the variation of the head load is plotted as a function of the number of thermal loading cycles. It can be seen that from cycle 3 onwards, i.e. when the flow is stopped, that the head load variations are stronger. For this third test, the No seepage case was carried out after the seepage case and we know from literature review that the amplitude of head load variations due to the thermal ratcheting effect are decreasing with the number of cycles. The variations observed on Figure IV. 39 must therefore clearly be attributed to the effect of seepage.

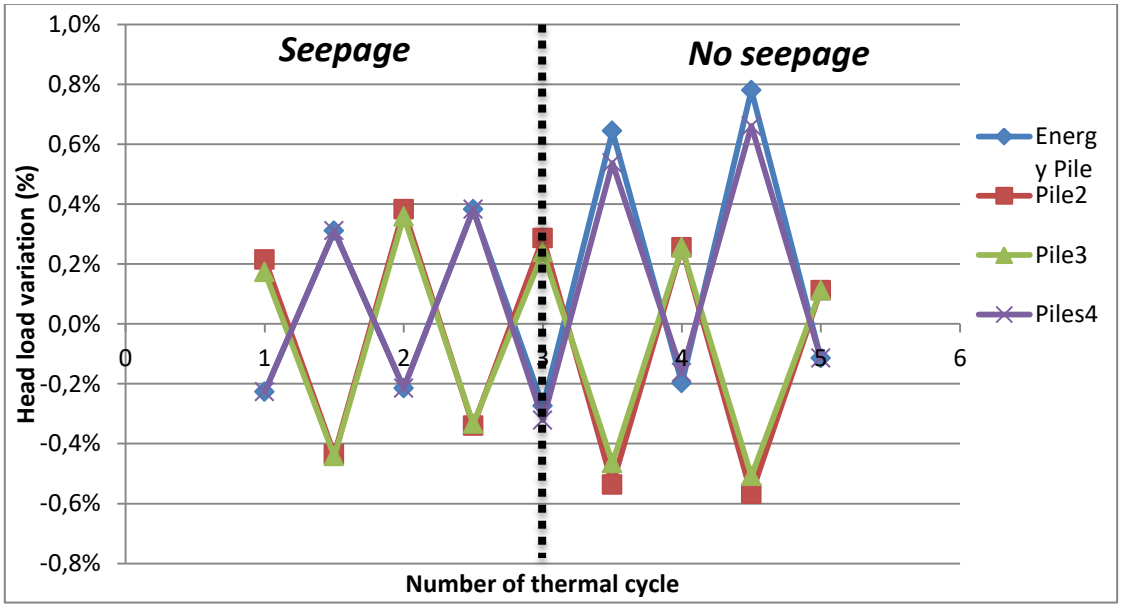

Figure IV. 39 - Evolution of relative head load variation of the piles with thermal cycles

4. Conclusion

Two centrifuge test campaigns carried out in saturated dense Hostun sand are presented in this chapter. The objective is to evaluate the impact of groundwater flow on the thermo-mechanical behaviour of a group of four energy piles. This group is subjected to a constant mechanical loading, and then one (two in the second test campaign) of the piles is/are subjected to cyclic thermal loading in the presence and absence of seepage. Two important and known points have been illustrated:

- Heating a pile leads to an upward movement of its head and conversely, cooling lead to a downward movement. The cycling of these thermal loads leads to ratcheting settlement as shown in literature. In the case of a group of piles linked by a rigid headframe where only one is active, tilting is observed but remains largely acceptable.
- The thermal loading therefore induces displacements that modify the load at the head of the piles. The latter increases during heating and decreases during cooling. When a rigid headframe connects a group of four piles, the pile located on the same diagonal as the active pile follows the same head load variations. The other two piles follow an opposite evolution in the sake of a mechanical balance.

From an energetic point of view, two main conclusions can be drawn from these tests are as follows:

- The presence of water flow in the model avoids the apparition of thermal anomaly, which occurs here despite the cyclical character of the thermal load because of the thermal inertia of the ground. Without mentioning the regulations specific to each region of the world concerning the use of the ground's energy, this thermal drift necessarily leads to a decline in the energy efficiency of the system and should then be avoided.
- In line with the previous point, the presence of water flow which recharges or thermally leaches it allows for a greater amount of energy exchange.

Finally, regarding the thermo-mechanical effect of seepage on energy pile group behaviour, it can be stated that seepage, by mitigating thermal variations, leads to lesser thermally induced head load variations.

Chapter V

NUMERICAL MODEL CALIBRATION AND ANALYSIS OF TYPICAL SCENARIOS

“All models are wrong, but some are useful”, James Clear

The work presented in this chapter aims to produce a numerical model that can reproduce the results obtained experimentally in a centrifuge. The ultimate aim is not merely to fit the data, but above all to provide a greater understanding of the phenomena and to highlight those that are important or decisive. Thus, an objective and critical approach is necessary to consider the model's limitations and validity to put in perspective the conclusions.

COMSOL Multiphysics software is used to carry out the simulations presented here. This is a finite element software package that allows the treatment of different physical problems (mechanical, thermal, electromagnetic, etc.) and the coupling phenomenon between them. As presented earlier, the behaviour of energy geostructures involves a problem of coupling between hydrology, thermics and mechanics. The diagram in Figure V.1 shows various links between these three branches of geotechnics, which are taken into account in the studies and which are not. In the models presented in this chapter, only simple coupling (as opposed to full coupling) is considered, as thermics does not influence hydrology and there is no direct link between hydrology and mechanics.

Initially, various models were produced, along with parametric studies to investigate the importance of modelling parameters. Once the model has been calibrated against the experimental results, the aim is to study several typical scenarios and draw overall conclusions. Indeed, the study of interactions between energy geostructures must be carried out on a case-by-case basis, given the many parameters involved (type of soil, type of structures, flow, thermal load, etc.). However, typical scenarios can be studied and give rise to some basic rules.

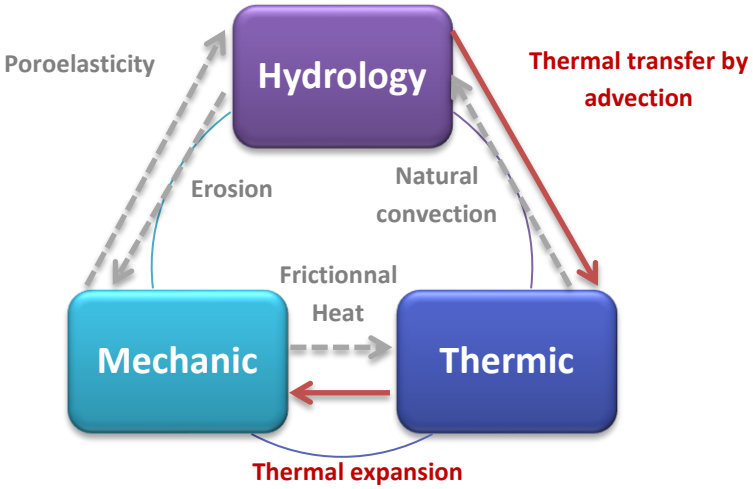

Figure V. 1 - Schematization of the couplings taken into consideration (red ones are the only one considered in our model)

1. Numerical model calibration

The main object of this first numerical work is the reduced model presented in the experimental studies. As a reminder, it is composed of these four piles made of cement supporting an aluminium head frame. The experimental test case considered is taken from the second centrifuge test (Chapter IV section 2). The figures presented in this section will be at model scale. Since the aim is simply to calibrate the numerical model on the experimental results, it is not necessary to convert the results to prototype scale.

1.1 First model: Thermo-mechanical

For this first model, the group of piles rests on a layer of soil modelling the dense sand of the centrifuge experiment. As shown in the Figure V.2 representing this first numerical model, only the supporting soil layer is modelled. The soil surrounding the piles is not modelled. Indeed, given the expansion coefficient of the pile and the temperature range considered, the thermally induced deformations are of a low order of magnitude and the interaction with the surrounding soil is therefore initially and for an initial modelling neglected. In the absence of specific conditions, the software assumes by default that the various blocks (piles, raft and soil) are rigidly linked.

1.1.1 Presentation of the model 1

Geometry

The dimensions of the numerical model are those of the reduced scale models used in the centrifuge tests: the piles are $300mm$ high and $20mm$ in diameter, the headframe is a parallelepiped of $100 \times 100 \times 40\ mm^3$ and the soil layer is assumed to be large enough to avoid mechanical boundaries effects (at least 4 times the diameter of a pile in depth and on the outside of each pile). The meshing is automatically done by the software. The user is merely asked for the fineness of the mehsing, ranging from very coarse to very fine. A fine mesh is used for all models.

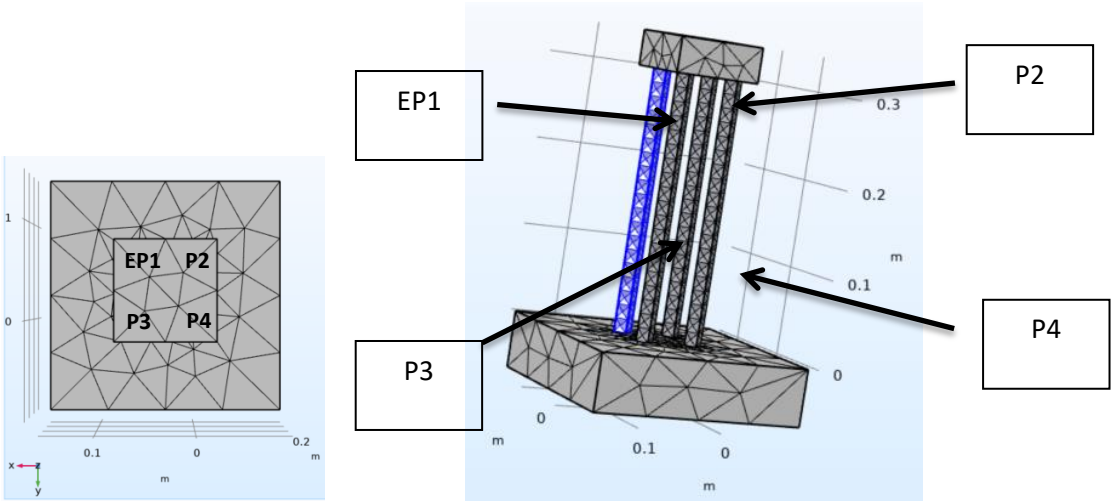

Figure V. 2 - Geometry of the numerical model 1

Parameters

The parameters assigned to the different materials that constitute the blocks are summarised in Table V. 1 and in line with the ground parameters characterisation done in Chapter I.

Table V. 1 - First model parameters

	Cement	Aluminium	Sand
Thermal conductivity (W/mK)	9000	/	/
Heat Capacity (J/K.kg)	1000	/	/
Density (kg/m3)	2200	4332	1800
Poisson's ratio	0.33	0.33	0.33
Young's Modulus (Pa)	12 500 000 000	70 000 000 000	100 000 000
Coef. of thermal expansion (1/K)	0.00001	/	/

The unit weight of the aluminium was modified so that its total weight includes the dead weight used in the centrifuge experiments.

Loading & boundary and limit conditions

Thermal

The energy pile named EP1 (coloured in blue in Figure V. 4) was subjected to the thermal variations measured during the centrifuge tests (second centrifuge test, IV.2). The temperature measured is shown in Figure IV. 3. Therefore, this temperature is imposed on the entire surface of the pile In order to apply the thermal load. The thermal conductivity of the energy pile is deliberately set at an unrealistic high value (see Table V. 1 - First model parameters) in order to ensure homogeneous temperature in the pile.

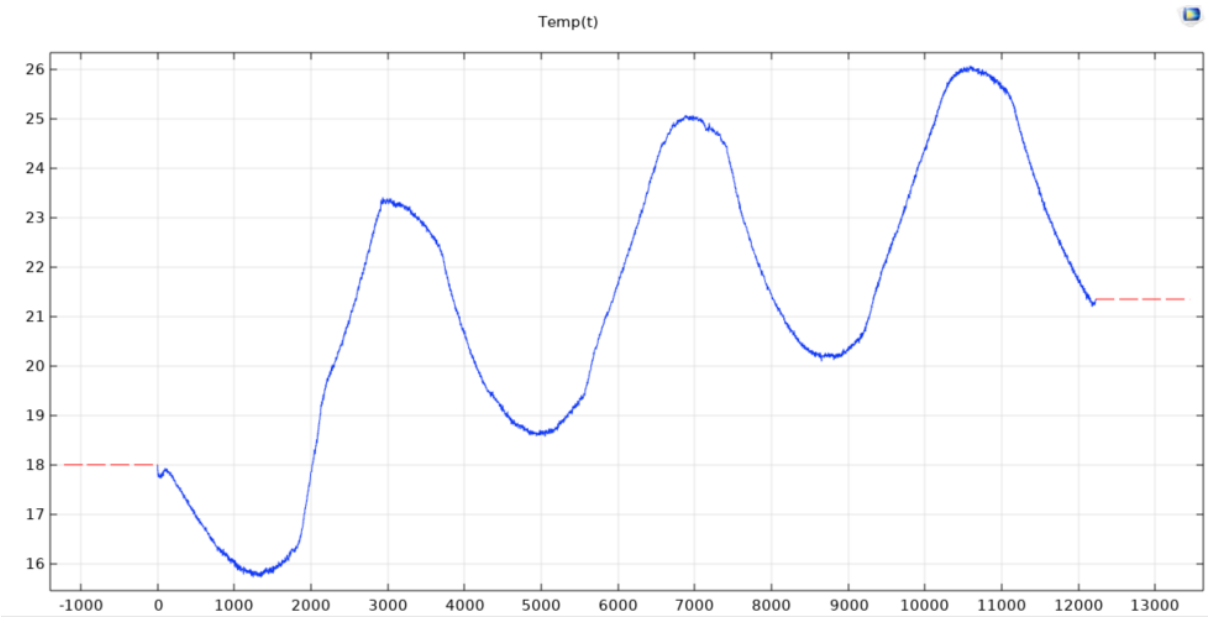

Figure V. 3 - Temperature (°C) applied to the model energy pile (EP1) with Time

The applied thermal variations induce thermal expansion of the pile in accordance with its arbitrarily fixed coefficient of expansion (value determined according to literature). The thermal expansion coefficient will be the subject of a further parametric study.

The initial temperature is set to 18°C throughout the pile ($T_{ref} = 18 + 273\ K$) consistently with the experimental measurements. This choice assumes that the temperature of the centrifuge room remains constant during the test even though this assumption is known to be false (see Figure II.26). However, due to the construction of the model not representing the container walls, nor the surrounding soil, the choice of the boundary condition as negligible effect. Indeed, the influence of this boundary condition has therefore been investigated. Within the duration of our experiment and for the given thermal load, it appeared that, by imposing complete insulation on the edges or an open edge condition or an imposed temperature, the temperature field the resulting from the modelling process were similar. The choice of an imposed temperature boundary condition is therefore maintained.

Mechanics

Linear elastic behaviour is assumed for the entire model. The initial conditions for displacements and velocities are zero and the outer edges (see Figure IV. 4) of the ground are fixed (zero displacement at all times). Finally, the entire model is subjected to normal gravity. This will be increased to 50g later in the study.

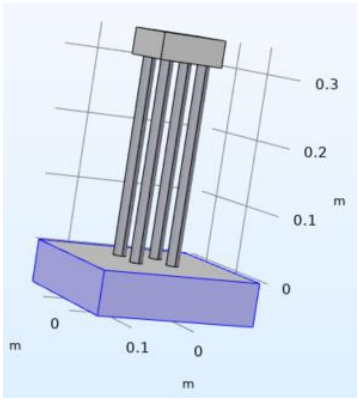

Figure V. 4 - Localisation of zero displacement condition in model 1

1.1.2 Results

The first case study on model 1 is deliberately simplistic in order to observe the effects of the elements that will make the model more complex. Thus, in the first case study, the pile does not rest on any soil and it is assumed that the piles are embedded at the foot (equivalent to a soil whose rigidity would be infinite). Two quantities are considered in this study, the variation in load and the displacement at the head of each pile. The load is calculated as the integral of the stresses calculated on Gauss points on a cross-section of the piles at a height of 0.298 m, i.e. 0.02 m below the pile head (see Figure IV. 5). This surface was chosen in order to avoid any artefact due to the fact that the surface at the head of the pile is an interface with the head frame. The displacement is calculated as the average of the displacements of the Gauss points on the same surface.

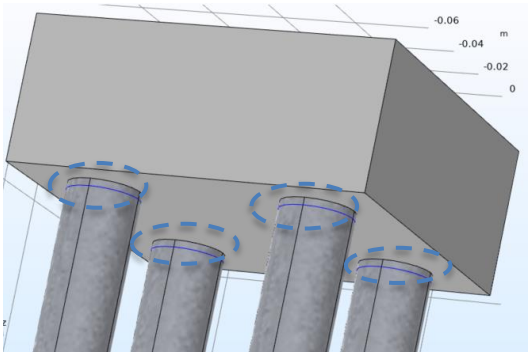

Figure V. 5 - Surfaces on which forces and displacements are calculated (coloured blue)

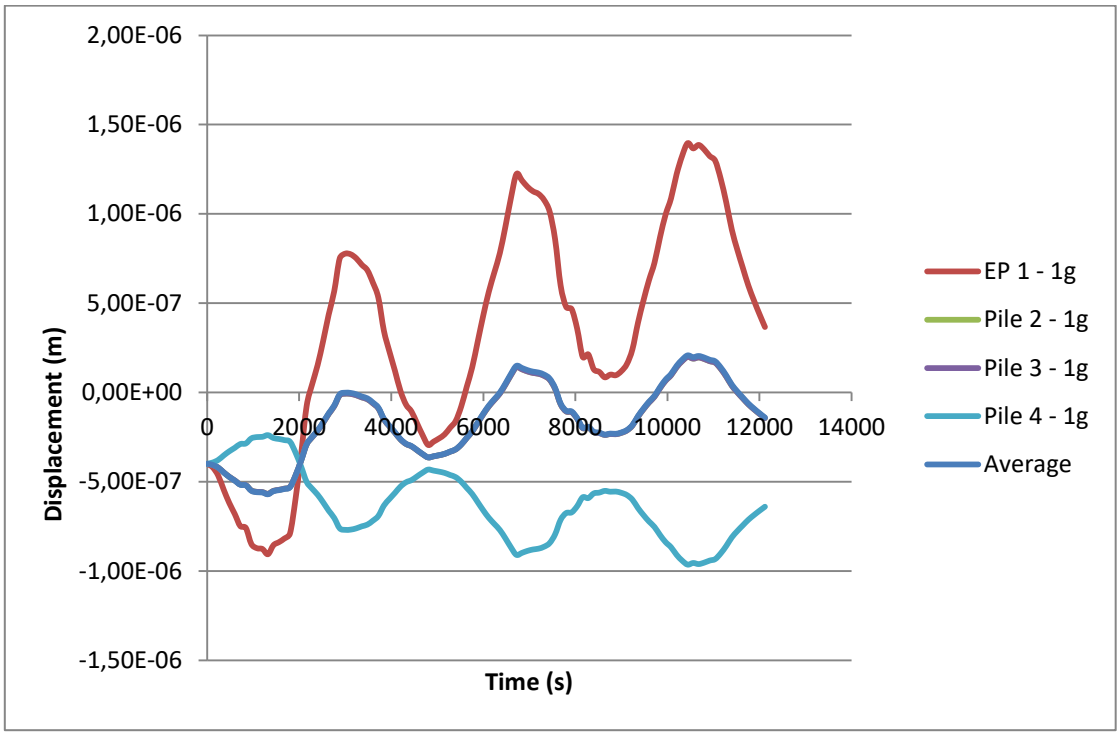

Figure V. 6 - Head piles displacement (model 1)

Figure IV. 6 shows an initial identical displacement for the four piles due to the dead weight (at t=0). Following this, EP 1 is subjected to cyclic thermal loading starting with a cooling phase which logically leads to thermal contraction according to the following equation:

$$\epsilon_{th} = \alpha(T - T_{ref}) \quad \text{(V.1)}$$

Again, according to this equation, the heating phase leads to thermal expansion, and this is indeed what can be seen on the displacement curve of the energy pile. In reaction to the thermally induced displacement of the energy pile, the other three piles show the opposite behaviour (settlement when EP1 is lifted and vice versa). Piles 2 and 3 show exactly the same behaviour. Pile 4, located on the diagonal of EP1, undergoes greater displacements due to the fact that it is further away from EP1. Looking at the average displacement of the group which is overlaid with the displacement curves for piles 2 and 3 (average of the displacements at the head of the 4 piles), we observe a movement that follows the thermal variations with a linear tendency towards uplift. Although this phenomenon is the opposite of that observed in reality (accumulative settlement), it follows logically from the assumption made about the elasticity of the materials. Since the thermal load is positive overall, this

results in positive expansion and hence in header uplift. This average displacement calculated numerically is equal to the displacements at the head of piles Pile 2 and Pile 3.

By looking at the load variations at the head of the piles without taking into account the first mechanical load due to the dead weight, we find the behaviour observed in reality:

- the energy pile experiences a decrease in its head load during cooling and an increase during heating
- Pile 4 (on the diagonal of EP1) is experiencing the same behaviour
- the other two piles (P2 and P3) behave in the opposite way

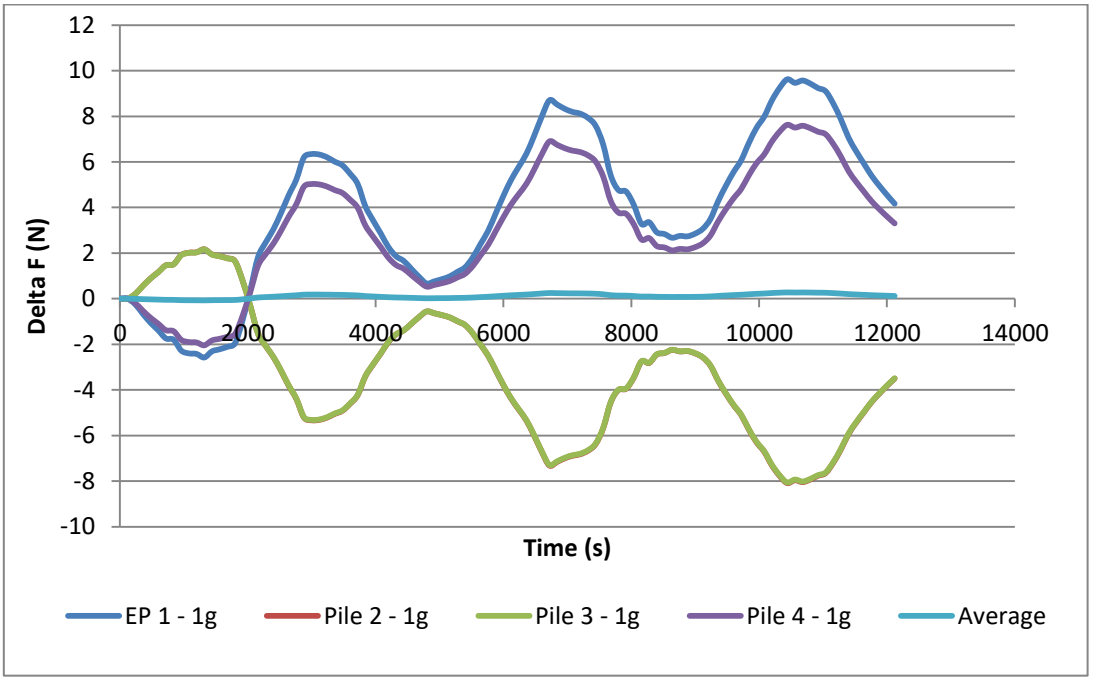

Figure V. 7 - Head load evolution with time (Study n°0)

However, two points are worth noting:

- The average of the load variations due to the thermal load is not perfectly constant over time, contrary to what was measured experimentally (although the variations are relatively small).
- While the shapes of the curves are consistent with the experimental observations, the numerical values are not exactly consistent with the experimental data, particularly during the cooling phases. A parametric study will then be carried out to investigate the influence of the coefficient of expansion, the level of macro-gravity and the rigidity of the soil.

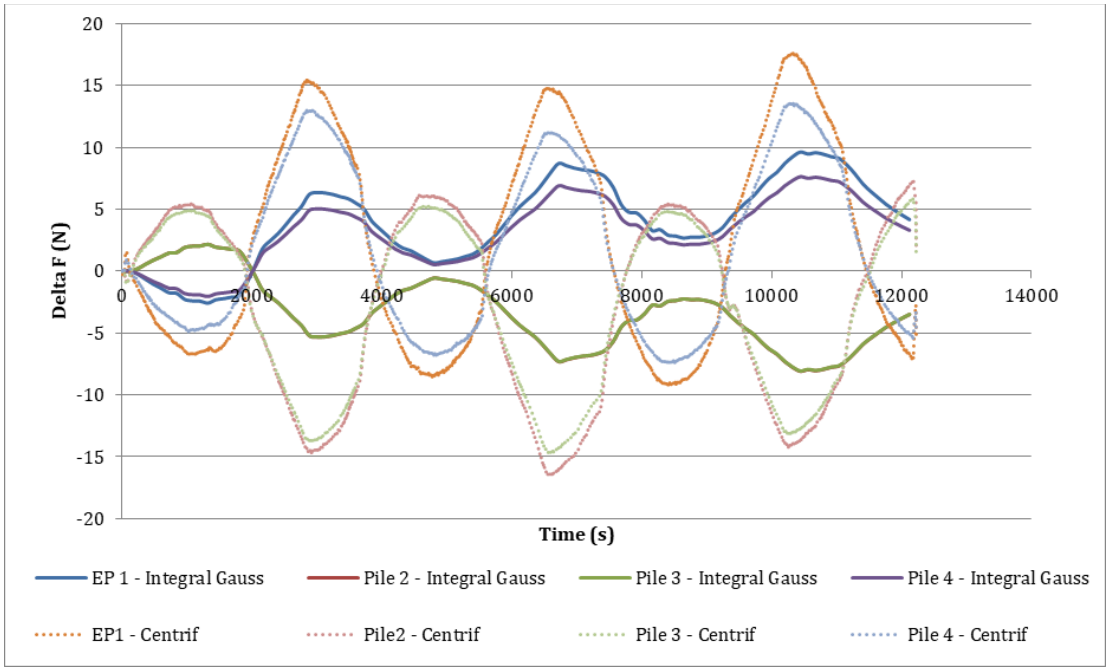

Figure V. 8 - Comparison of head load variation between experimental data and numerical model 1

A second study is thus carried out (Study 2). It is the same as Study 1, with the difference that the acceleration of gravity is 50g in Study 2 (rather than 1g in Study 1). Comparing the variations in load and displacements at the head of the piles for these two levels of gravity results in logical observations: the weight of the raft initially creates a head load and displacements 50 times greater (Figure IV. 9 and 10). However, focusing on the variations in thermally induced head load and displacement, the results at 1g and 50g are identical (Figure V. 11 and 12).

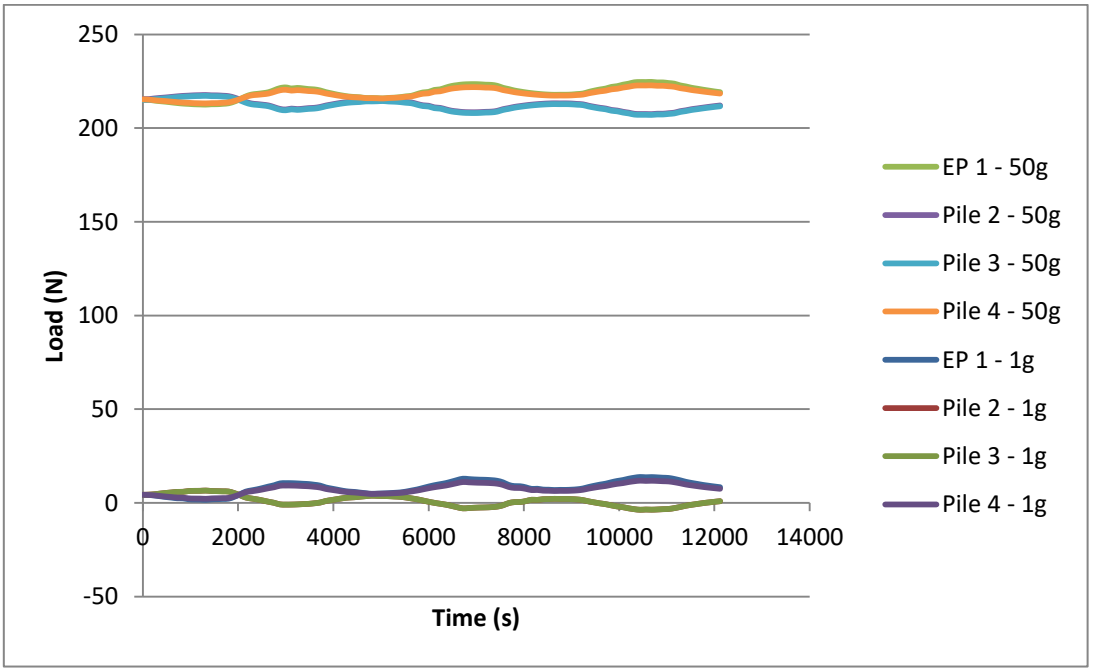

Figure V. 9 - Head load comparison between 1g case and 50g case

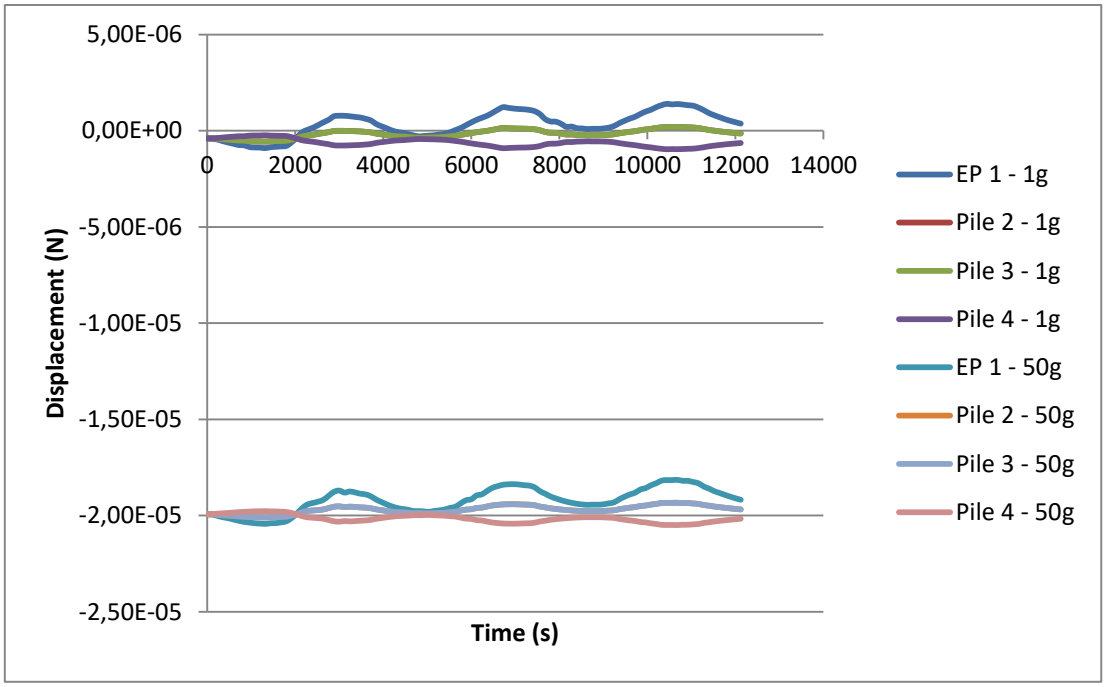

Figure V. 10 - Head displacements comparison between 1g case and 50g case

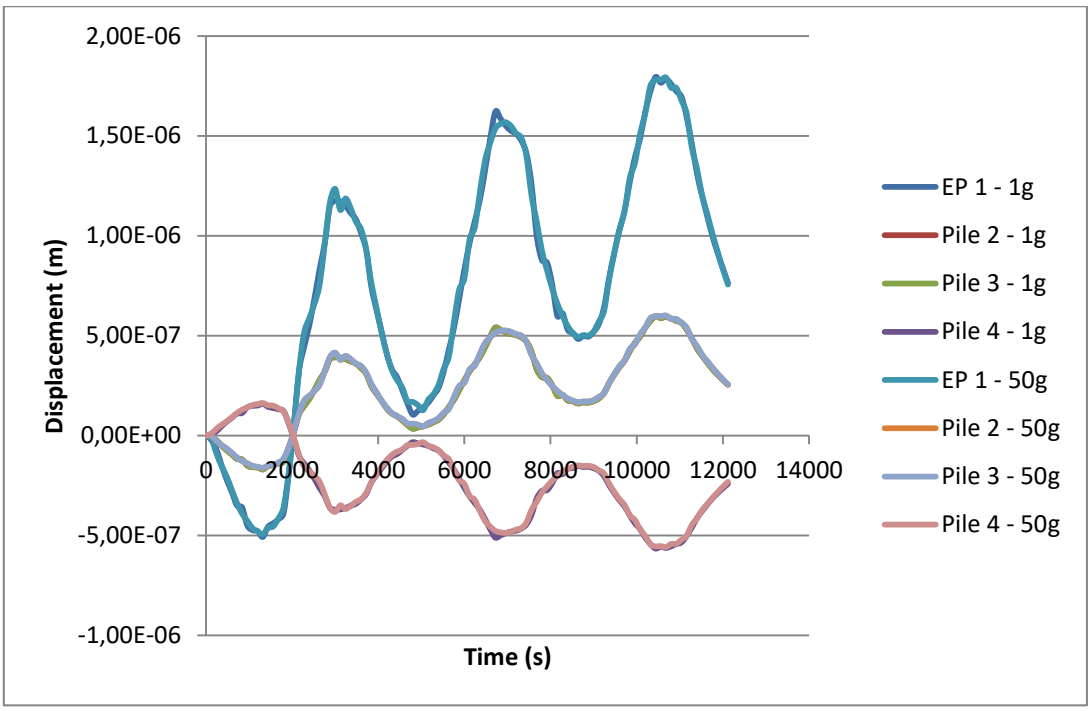

Figure V. 11 - Comparison of thermally induced head displacements 1g and 50g

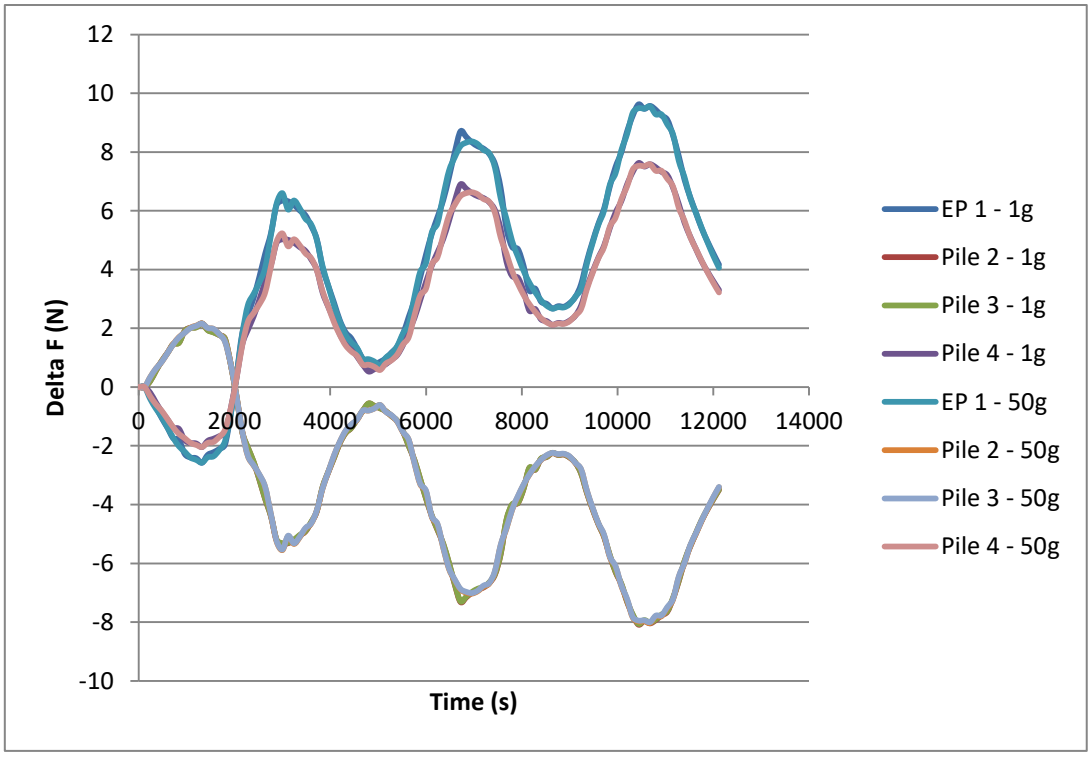

Figure V. 12 - Comparison of thermally induced head load variations 1g and 50g

1.1.3 Parametric study of the rigidity of the supporting soil

Changes in pile displacement and head load are calculated over time for several Young's moduli of the soil, ranging between 10 and 400 MPa. A case where the piles are built-in (infinite rigidity of the soil) is also considered. Here, only the model energy pile is affected by thermal phenomena as the heat transfer is numerically not allowed elsewhere. This means that the heat does not spread to either the head or the ground.

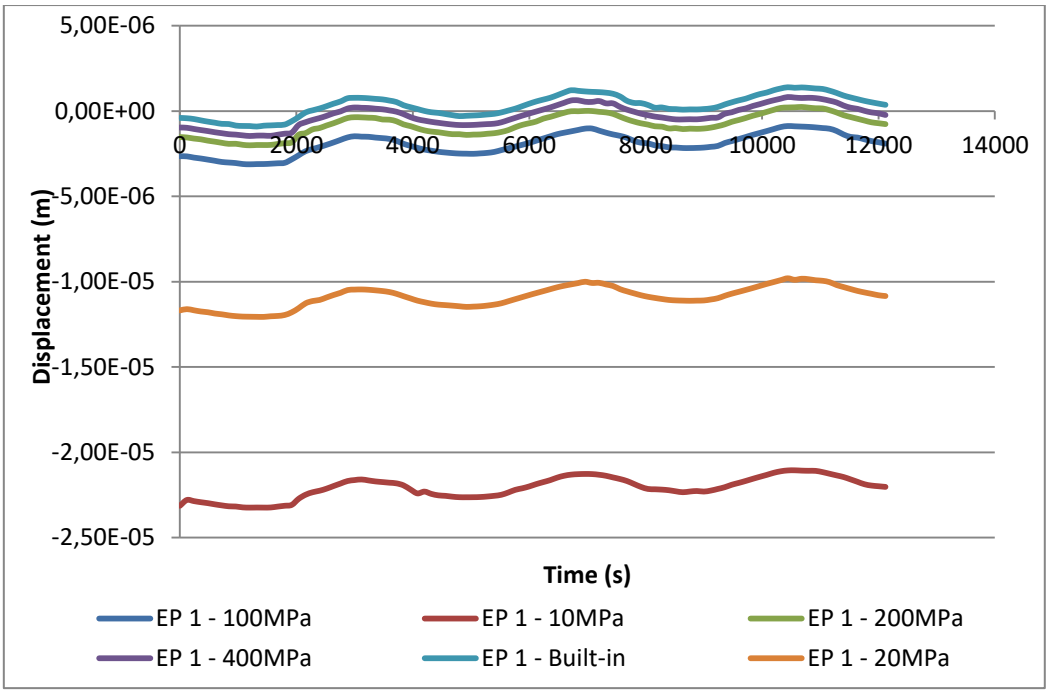

Figure V. 13 - EP1 head Displacement for different rigidity of the supporting soil

It can be seen from the Figure V. 13 above showing the displacement at the head of EP1 that the rigidity of the soil plays a role mainly in the first loading phase, which is purely mechanical in nature (when the weight of the raft is applied). Logically, the more rigid the soil, the less the pile group will sink into the soil when subjected to the weight of the raft. Once this mechanical loading phase is over, the thermal load induces exactly the same displacements.

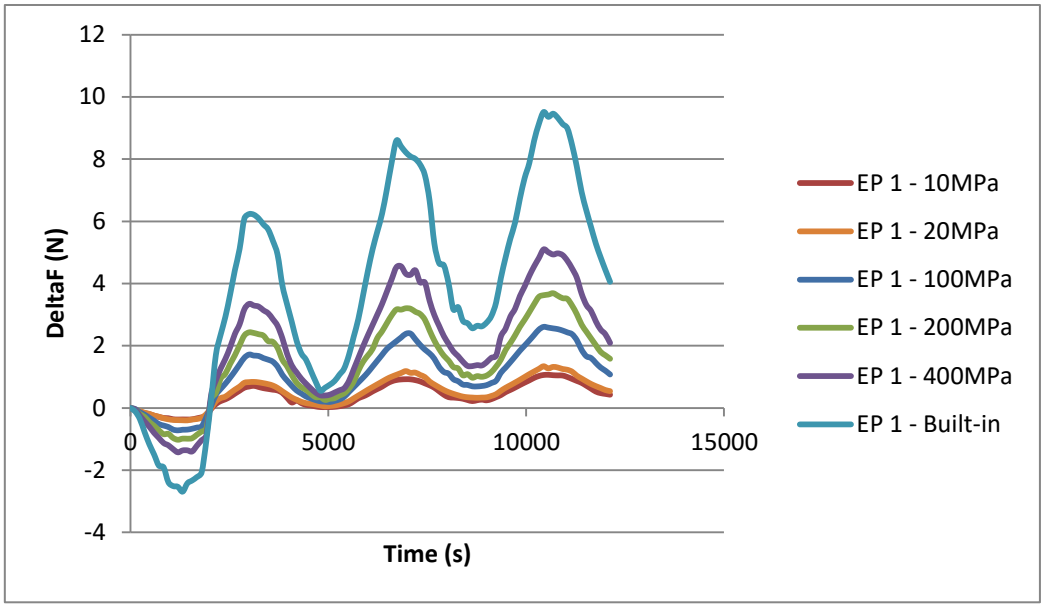

Figure V. 14 - Absolute variation in load at the head of EP1 for different stiffnesses of the supporting soil

By focusing on the variations in thermally induced head loads (Figure V. 14), one can see that the limit condition at the base plays a role in the behaviour of the pile group. Indeed, between a limit condition where the piles are blocked at the foot and a limit condition where the piles rest on a low stiffness soil (10MPa), the displacements, and therefore the thermally induced head load variations, show a clear difference. This result is easier to understand if we consider these load variations in relation to the initial load carried by a pile (approximately 200 N). For example, for EP1, a condition of embedment at the foot (close to a case where the soil is rocky) leads to a variation in head load of 5% of the initial load compared with 0.5% in the case where the pile rests on soft soil (10MPa).

For future studies, the soil rigidity is set at 100MPa, which corresponds to very dense sand according to the literature. This assumption corresponds well to the state of the soil in the centrifuge, given the method used to place the sand (rainfall favouring high density was set up during the experiments presented in chapter IV).

1.1.4 Parametric study of the coefficient of thermal expansion

The displacement of the piles and the head load are calculated over time for a soil stiffness of 100 MPa and a coefficient of thermal expansion of the concrete (for model piles) taking the values of $10^{-5}, 5.10^{-4}$ et 10^{-4} K^{-1}.

It can be seen on Figure V. 15 that by multiplying the coefficient of expansion by 10, the load variations at the head are also approximately multiplied by 10. This work has also been done for the displacements and there was also multiplied by 10. The same protocol was applied for a coefficient of multiplication of 50 and the results were also multiplied by 50. Thus, even more than the rigidity of the soil, the coefficient of thermal expansion is a major parameter in the behaviour of the pile group,

and this underlines the importance of estimating it correctly in the context of numerical modelling, but also when interpreting experimental results, and again in the choice of materials for real energy piles...

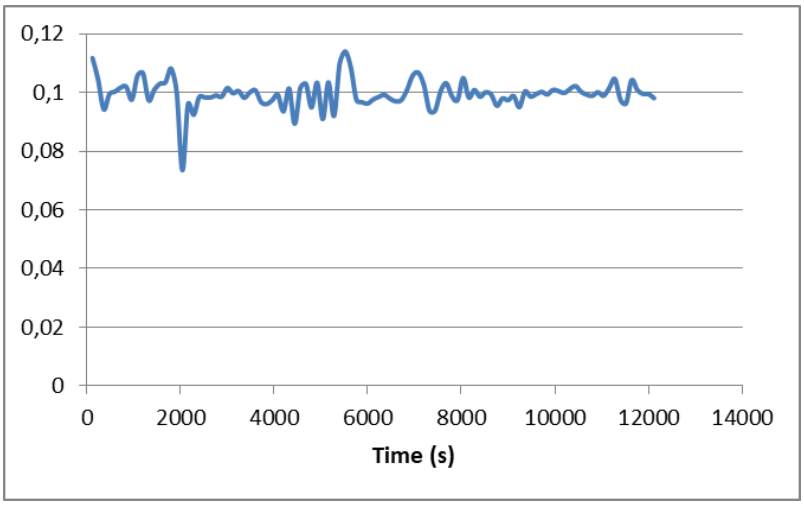

Figure V. 15 - Ratio between the force at the top of EP1 for a given coefficient of expansion and one 10 times smaller

Furthermore, by comparing the results obtained numerically and experimentally, stress and settlement magnitude are compatible for the case where the coefficient of thermal expansion is $10^{-5}\ K^{-1}$. This value is consistent with the literature. However, other parameters will influence magnitude of the variations in head load, and the linear trend observed during the succession of thermal cycles in the numerical calculations is not observed experimentally. In fact, for such coefficient of thermal expansion, the numerical results for the first cycle are close to those obtained experimentally, but the gap between the numerical and experimental results widens as the experiment progresses, particularly during the cooling phases (Figure V. 16 and 17).

It should be remembered that for the moment, there is no soil around the piles, so there is nothing around them to restrict movement. Lateral friction would limit displacements and therefore increase forces.

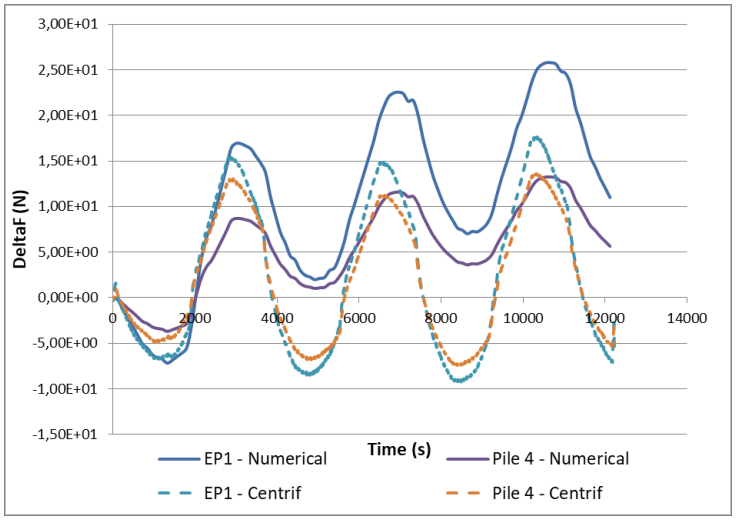

Figure V. 16 - Absolute variation in the head load of EP1 and Pile 4 - numerical/centrifuge comparison

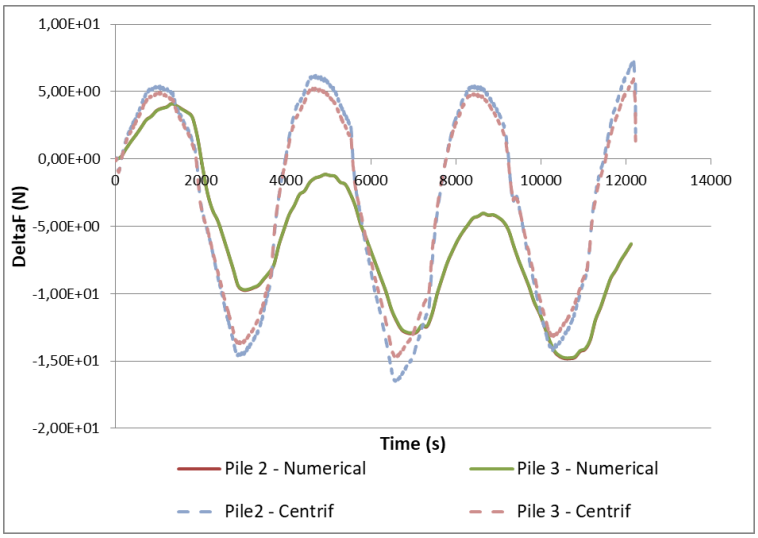

Figure V. 17 - Absolute variation of the charge at the head of Pile 2 and Pile 3 - Digital/centrifuge comparison - Model 1

1.2 Second model: Thermo-mechanical with elastic soil around the piles

In this model, the group of piles no longer rests solely on a supporting soil, but is buried in a block of soil 0.4m high (identical to the centrifuged model), 0.4m long (shorter than the centrifuged model to facilitate calculations) and 0.2m wide (identical to the centrifuged model). The 0.3 m high piles are buried to a height of 0.25 m.

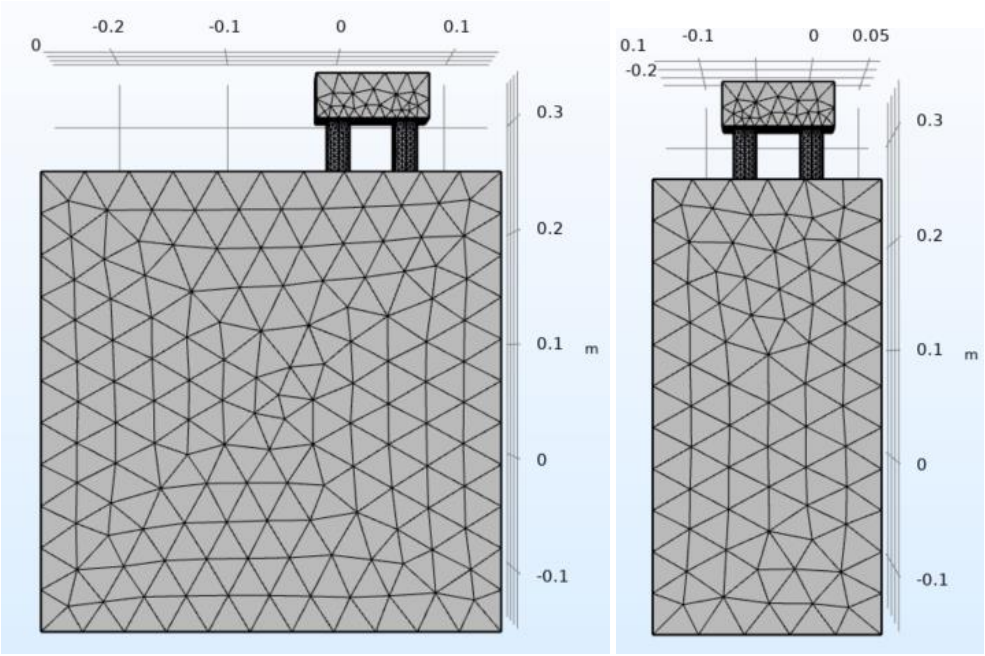

Figure V. 18 - Meshing and geometry of the numerical model 2

Parameters

As the group of piles is surrounded by soil, heat transfer no longer only affects the energy pile, but also the soil and the other piles. The raft is not affected by heat transfer. In fact, the heat from the

energy pile will diffuse into the ground (depending on its coefficient of thermal diffusivity) and the other piles, also resulting in thermal expansion (according to the coefficient of thermal expansion). It is therefore necessary to define thermal parameters for the soil and for the other piles. For the non-energy piles, the same parameters were chosen as for the energy pile, with the exception that the thermal conductivity is not artificially increased and is set at a realistic value of 0.9 W/mK. These new parameters are shown in red in the Table V. 2.

Table V. 2 - Thermal and Mechanical parameters for model 2

	Cement	Aluminium	Sand
Thermal conductivity (W/mK)	9000/**0.9**	/	**3**
Heat Capacity (J/K.kg)	1000	/	**1000**
Density (kg/m3)	2200	4332	1800
Poisson's ratio	0.33	0.33	0.33
Young's Modulus (Pa)	12 500 000 000	70 000 000 000	100 000 000
Coef. of thermal expansion (1/K)	0.00001	/	**0.00001**

Loading & Boundary and initial conditions

Thermal

As with the first model, only the energy pile is thermally loaded, with the exception that this time only the buried part of the pile is affected by this loading for the sake of realism. This thermal loading, which is the same as for the first model (see Figure V. 3), is also imposed in the same way, i.e. on the lateral surface of the pile as a boundary condition. As the energy pile has a high thermal conductivity, this temperature is homogeneous throughout the buried part of the pile.

The surfaces at the edge of the model have a boundary condition set at 18°C (291 K), with the exception of the top surfaces of the model, which has an isolated condition representing the contact with the ambient air. By default, the interfaces between the non-active piles and the ground allow the continuity of the temperature field and the heat flux, thus simulating perfect contact.

Mechanical

As in the first model, the external surfaces of the models have fixed boundary conditions (displacements prohibited in all three directions), except for the upper surfaces which is free to move. In addition, all the materials have linear elastic behaviour. The mechanical loading is only represented by the gravity applied on the raft at a 1g level as it appeared that macro gravity does not impact the thermal induced phenomena, which is applied to the entire model.

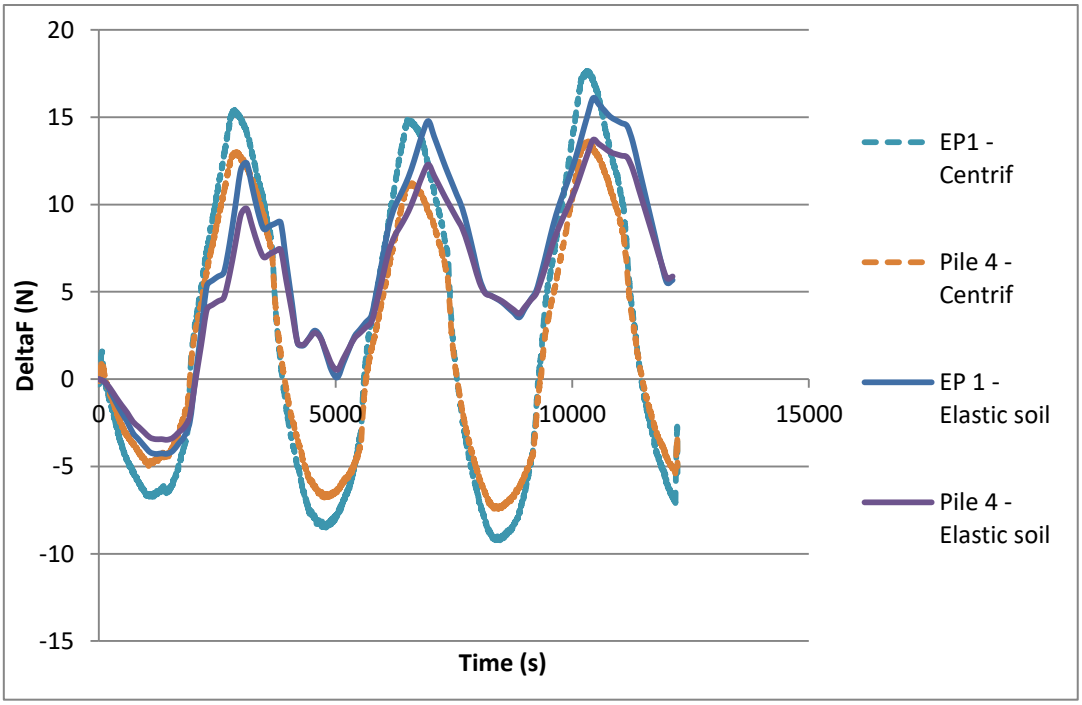

Figure V. 19 - Comparison of EP1 and Pile 4 head load variations between experimental results and model 2

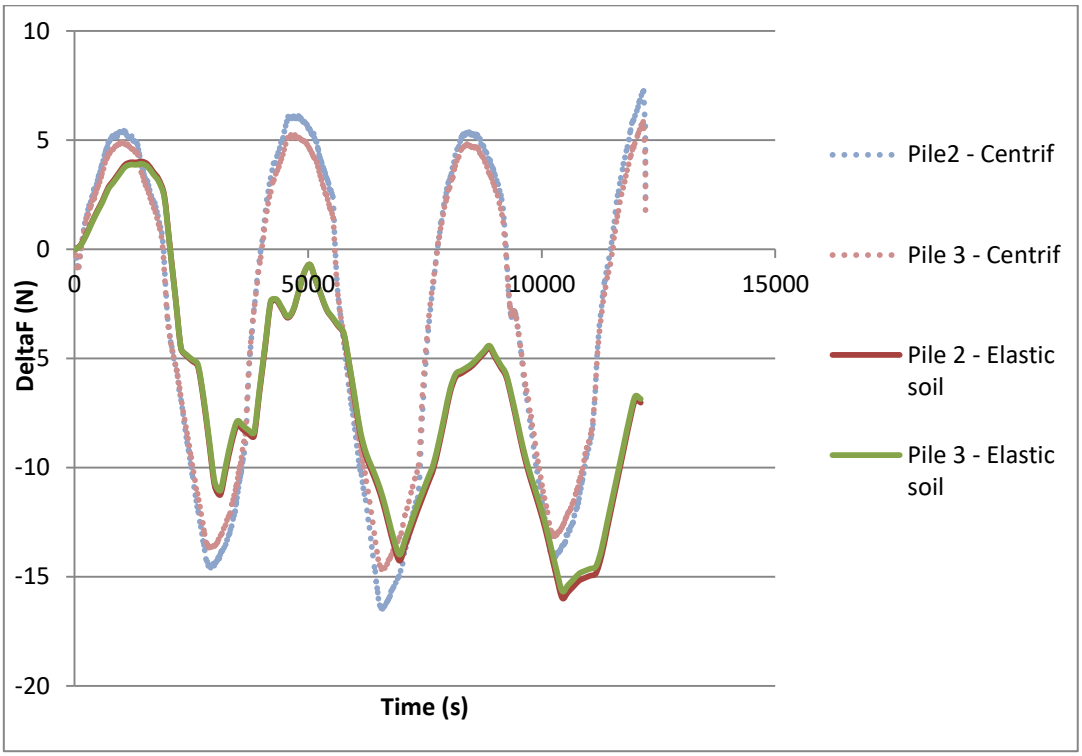

Figure V. 20 - Comparison of Pile 2 and 3 head load variations between experimental results and model 2

Figure V. 19 and 20, which compare the results obtained with the model 2 (presence of soil around the piles) and the experimental results, show that the curves overlap quite well during the heating phases, but much less during the cooling phases. One explanation for this is the assumption that the soil is elastic. In fact, this implies that during cooling phases, the pile contracts and the soil "swells". In reality, with plastic behaviour, contracting without the soil "swelling back" would mean that the pile would settle which would lead to tension at the head of the pile as it is "pulled" downwards. As a

result, we would have more tension in piles 1 and 4 and, by balancing the forces, more compression in piles 2 and 3.

To verify this hypothesis, a third model with elastic-plastic behaviour for the soil will be build. The hardening soil model theory has been selected for this purpose.

1.3 Third model: Thermo-mechanical with plastifying soil around piles

The geometry, thermal and mechanical loads, as well as the initial and boundary conditions of the model are the same as before. The only difference lies in the constitutive law governing the behaviour of the soil. Until now, the soil was considered to be linear isotropic elastic and therefore followed Hooke's law. In order to expose more complex behaviour, the Hardening soil model has been selected.

The Hardening Soil model is an elastoplastic model with a strain and stress path dependent stiffness. It is a so-called double stiffness model, meaning that its stiffness is different during the primary loading and unloading/reloading cases (Bergstrom, 2015). Namely, in the model, the total strains are determined by incorporating a stress-dependent stiffness, which varies for virgin loading and unloading/reloading. The calculation of plastic strains is achieved by employing a multi-surface yield criterion. Isotropic hardening is assumed, taking into account both the plastic shear and volumetric strain, (Schanz, 2000). Thus, rather than employing Hooke's single-stiffness model with linear elasticity in conjunction with ideal plasticity based on Mohr-Coulomb theory, a constitutive formulation is used and involves a double-stiffness model for elasticity along with isotropic strain hardening.

The physical parameters used include the initial stiffness of the soil before loading, the hardening deformation modulus (the soil's capacity to harden after several loadings), the hardening coefficient (which quantifies the amount of hardening) and the softening coefficient (which represents the loss of stiffness during unloading). The mathematical equations are summarized in the COMSOL documentation and presented in Annexe. The use of the Hardening soil model therefore requires the precision of the new parameters (see Table V. 3). The values of the void indices are those of the Hostun sand used in the experiments.

Table V. 3 - Soil parameters when using the HSM

Reference stiffness for primary loading [MPa]	E50Ref	**30**
Reference stiffness for unloading and reloading [MPa]	EurRef	**250**
Void ratio at reference pressure	evoidref	**0.4**
Stress exponent	m	**0.5**
Bulk modulus in compression [MPa]	Kc	**100**
Maximum void ratio	evoidmax	**1.01**

The ratio $E50ref/EeuRef$ is generally taken equal to 3 in the literature. However, with such a ratio the plasticity of the soil is not sufficiently apparent insofar as the results obtained are very close to

those obtained with an elastic soil. By varying this ratio, it appears that the greater the ratio, the more the numerical results tend towards the experimental results as long as the model does not diverge. This ratio is therefore chosen to be close to 8 and is still realistic in order of magnitude.

The results of force variations at the head of the piles are shown in Figures 20 and 21:

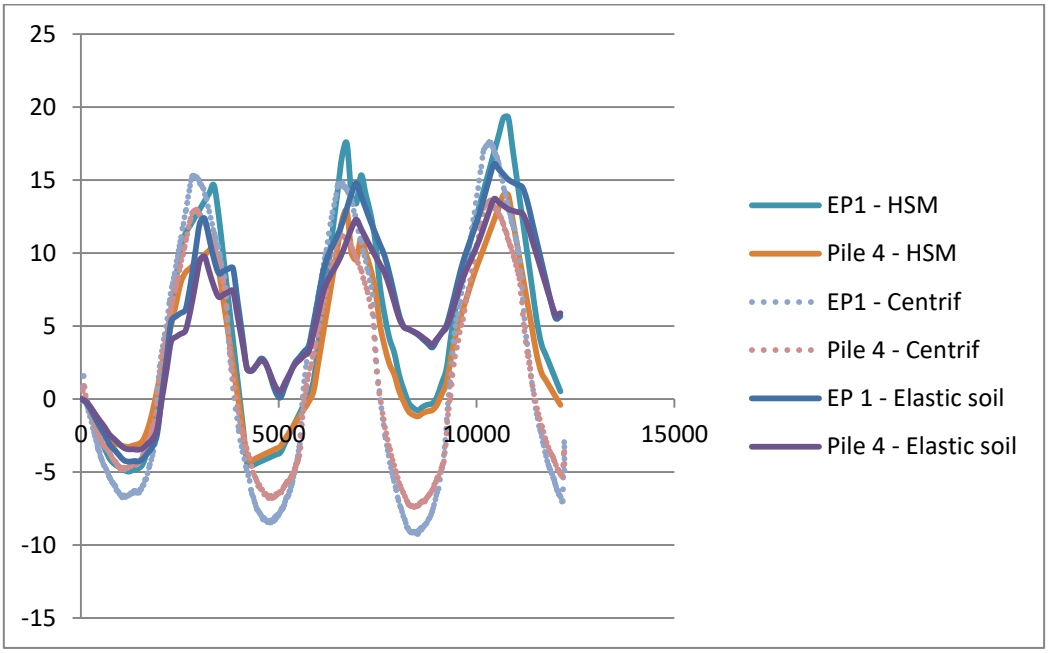

Figure V. 21 - Comparison of head load variations between experimental results, an elastic soil model and an HSM model for EP1 and Pile 4

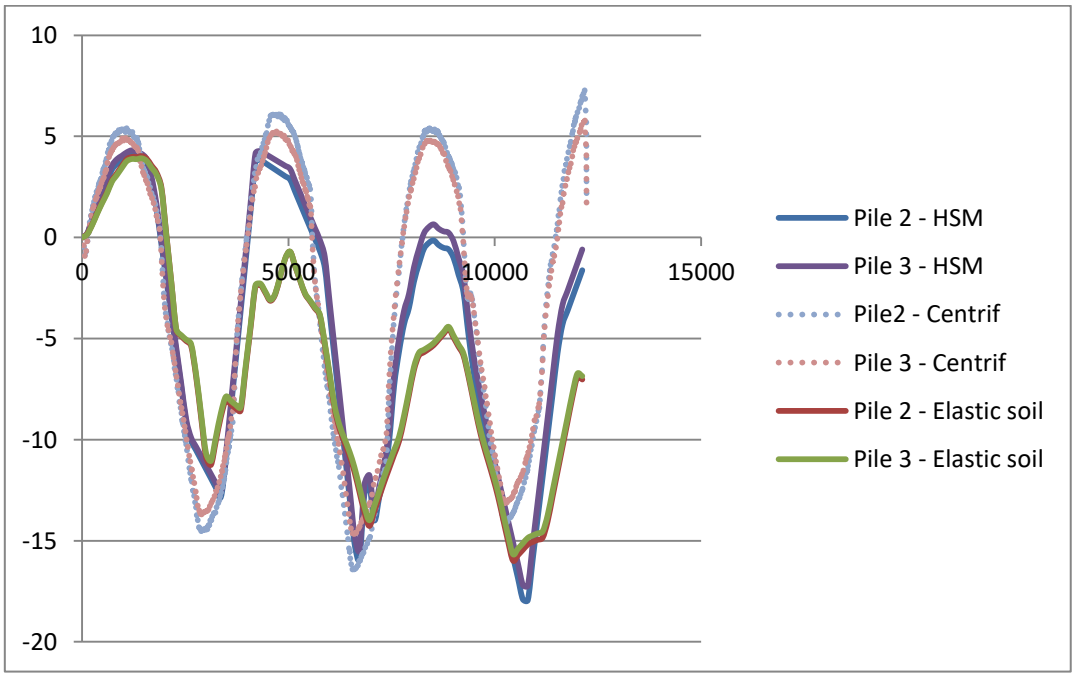

Figure V. 22 - Comparison of head load variations between experimental results, an elastic soil model and an HSM model for Pile 2 and Pile 3

It can be seen from these figures that, in accordance with the assumption stated earlier in this chapter, taking account of soil plasticisation enables variations in head load to be calculated which

are close to the experimental results, particularly during the cooling phases. The numerical results therefore correspond even more closely to the experimental results. The difference between the two is probably due to pile-soil friction, which is not modelled here.

1.4 Model 4: Hydro-thermo-mechanical

The previous model is used and hydraulic physics is added. The aim is to model longitudinal water flow in the model. This means that heat transfers no longer take place solely through diffusion, but also through advection. As a reminder, the Péclet number reflects the ratio between advection and conduction. More simply, a Péclet number ($Pe = \frac{LV}{\alpha}$) greater than 1 suggests that advection predominates and vice versa.

To add flow to the model, Darcy's law is used over the entire block representing the soil and the following boundary conditions are applied: zero flow on all walls except the two ends where a constant hydraulic load is applied to each of them (see Figure V. 23). These hydraulic loads do not correspond to those present during the experiment, but they have been arbitrarily imposed so that the resulting flow has a velocity of 34 m/year, the same velocity as that imposed in the corresponding centrifuge experiment.

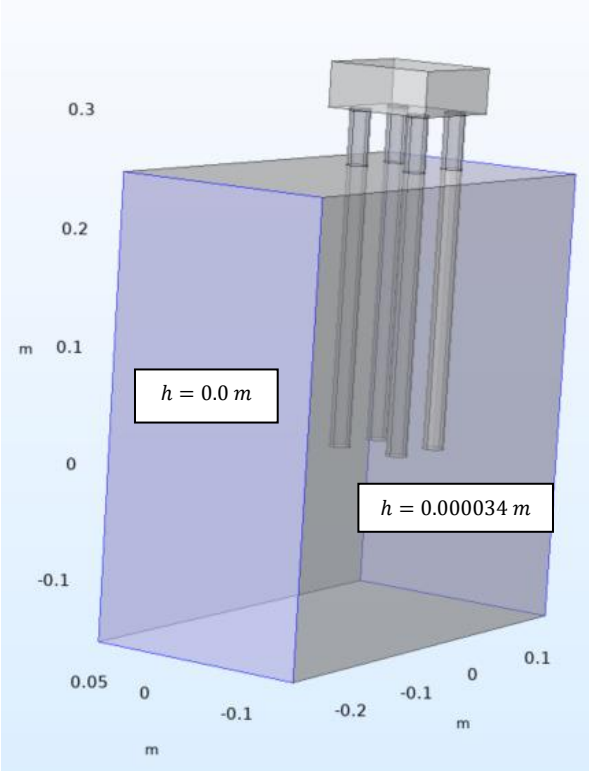

Figure V. 23 - Boundary conditions for Darcy's law implementation

In order to couple the flow with the heat transfer, it is no longer possible to use the physics of "heat transfer in solids" and so the physics of "heat transfer in porous media" is used. To achieve this, new physical parameters have been added, notably concerning the porosity of the soil (this is the porosity that was calculated for the centrifuge model) and the thermal properties of the water. These parameters are listed in the Table V. 4.

Table V. 4 - Soil parameters regarding the physics "heat transfer in porous media" in COMSOL

Porosity (-)	**0.45**
Ratio of specific heats (-)	1
Void ratio at reference pressure (-)	0.4
Dynamic viscosity (Pa.s)	0.001
Permeability (m^2)	10E-12
Maximum void ratio (-)	1.01

The thermal load between the flow case and the no-flow case is the same and correspond to the temperature measured in the no-flow experimental case. Here the aim is to confirm that the model allows observing the same impact of the flow on the piles group behaviour.

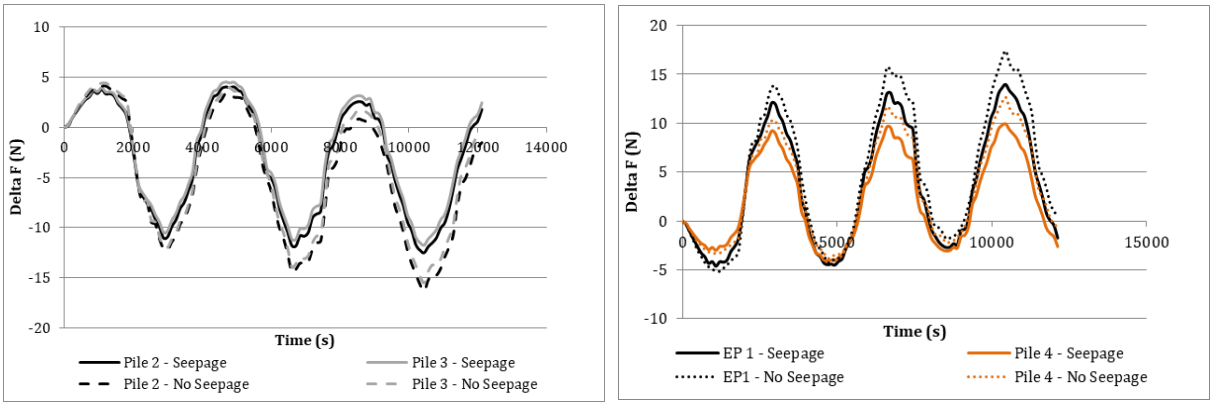

Figure V. 24 - Comparison of head load variation in seepage case and no seepage case a) Pile 2 and Pile 3, b) EP1 and Pile 4

Figure V.24 shows that the variations are slightly greater in the flow case, as might be expected. It should be remembered that in this numerical model, the hydraulics does not directly affect the mechanics, but they do influence the thermics, which in turn affect the mechanics (see Figure V.1). In this sense, it is clear that the heat dissipation due to the presence of a flow reduces the thermal expansion of the piles. As this is the phenomenon that governs head load variations, it follows that these are also less when there is a flow. Other simulations were carried out with higher flow velocities and no link was found between flow velocity and head load variation.

1.5 Limits of the model

The fourth model where soil with a plastic behaviour in line with the HSM is modelled around the piles group is the one which fits the best with the experimental results. Even that it does not take into account the friction between the soil and the piles group, nor the temperature dependence of the parameters, this model results from a number of numerical studies that have enabled us to choose the mechanical (modulus of elasticity, rigidity, etc.) and thermo-mechanical (coefficient of thermal expansion) parameters of the soil and the piles that gives results closest to the behaviour observed experimentally. This latter model can therefore be used for other numerical studies. Indeed, now that the model has been calibrated, the study of several scenarios will enable us to draw some general conclusions.

At this point, it is also worth to evocate the Courant number also well-known as CFL number for Courant-Friedrichs-Lewy stability criteria from its inventors names. It represents the fraction of the

cell that the fluid moves across in a time step. This number, often written Co is evaluated for every cell in the mesh. However to check the stability of the solution in most often case, it is recommended to check that $Co < 1$. In our simulation, although more complex algorithms can be used to calculate the Co field in the study model, a very simplistic initial estimate of stability (does not take into account the 3D aspect of the mesh) can be made by considering the Courant number in the smallest mesh present in the model. In our case study, the established mesh leads to a minimum mesh size of $dx = 0.009m$, the established velocity is $V_D = 34m/d$ay and the time step is $dt = 2s$. The current number is then $Co = \frac{V_D dt}{dx} = 0.087 < 1$. The calculated solution is therefore stable.

2. Analysis of typical scenarios

2.1 Presentation of the model and the problem

The most unfavourable case in mechanical terms is the case where only one pile is thermally loaded. A typical scenario analysis is then considered for this case study. The geometry of the model is now larger in order to avoid any possible boundaries effect. The piles group effect is still the same, but this time it is centred in a cubic soil mass (0.45 m square, i.e. 10 times larger than the group of piles). The boundary conditions and the behaviours laws are the same as in section 1.4 for all physics and the physical parameters are also identical except for the new case (Dry sand) where the density is lower (1600 kg/m3) and the thermal conductivity too (0.4 W/k/m).

The scenarios studied are as follows in Table V. 5:

Table V. 5 - Summary table of studied scenarios

Power demand \water status	Dry	Saturated	Seepage
Balanced	Bdry	Bsat	Bseep
Unbalanced	Udry	Usat	Useep

Regarding the thermal load, “Balanced” demand is an ideal case where the demand is such that no thermal drift is observed and the energy demand therefore imposes on the pile a sinusoidal temperature centred on the temperature of the environment (18°C) with amplitude of 4°C. Unbalanced demand is a case where the demand for energy would be higher in winter than in summer, creating a positive thermal drift (the heated pile and therefore the ground get colder and colder over the years). These two demands are represented in the Figure V. 25 and correspond to the temperature that will be imposed on the external surface of the energy pile by way of thermal loading (as in the previous cases). There are 5 temperature cycles, each lasting 52 minutes. Given the size of the model (50 times smaller than the prototype), this period of time represents 1 year at full scale. The simulation is therefore carried out over 5 years at prototype scale.

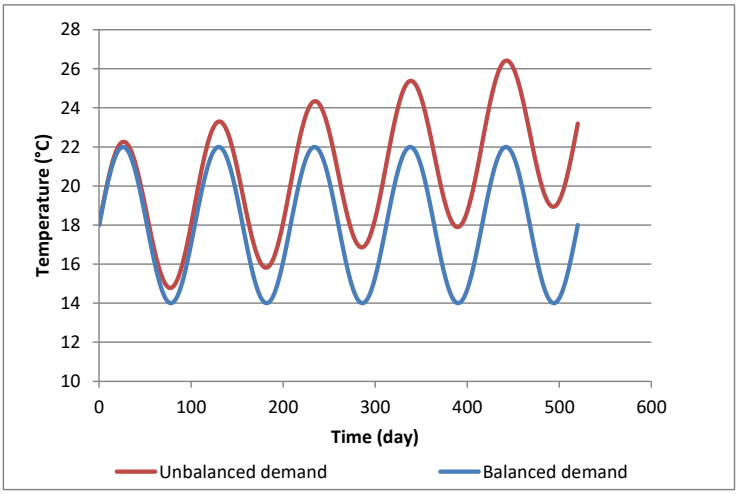

Figure V. 25 - Temperature imposed on the model energy pile as a thermal loading for two demand scenarios

Based on the results from previous chapters, we can expect that, from a mechanical point of view, the worst case must be Usat insofar as:

- Saturation increases heat transfer (better thermal properties)

- The absence of groundwater flow induces greater thermal anomaly

- The unbalanced demand prevents the thermal anomaly to be compensated

These three points mean that the Temperature should be higher, so thermal expansion higher and therefore variations in head load higher.

In this section, the results are presented on a prototype scale, since the aim of the analysis is to draw conclusions about the results obtained.

2.2 Results

2.2.1 Thermal transfers

During the numerical modelling, the temperature of each pile was recorded at a point on the pile surface located at mid-depth. Figure V.26 compares the temperature evolution of the non-energy piles for the cases with and without flow, when the demand is unbalanced (positive thermal drift). It can be seen that the three piles are not subjected to the same thermal variations, particularly Pile 2 and Pile 3, which are nevertheless at the same distance from the heat source (EP1). This observation makes it possible to appreciate the effect of the flow and the resulting thermal plume. In addition, it turns out that for the same pile, the amplitude of the temperature cycles is smaller in the flow case, but the overall increase in temperature over the entire duration of the modelling is identical. This is consistent with the results observed experimentally and presented in Chapter II, i.e. that the flow induces a plume that favours heat transfer in the direction of flow and also restricts thermal variations.

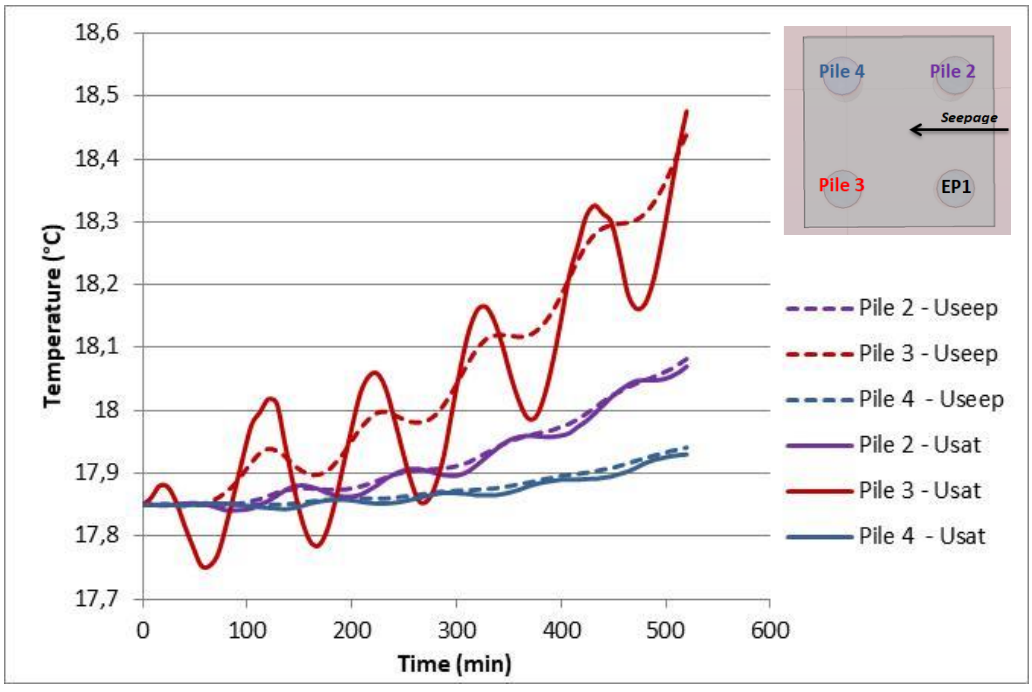

Figure V. 26 - Piles temperature evolution with time for unbalanced demand scenario

2.2.2 Head displacements

With regard to displacements, the results focus on those that are thermally induced. As a reminder, a mechanical load (the weight of the raft) is applied to the 4 piles before the thermal load is applied. Therefore, only the displacements induced by the thermal load are presented here, initial displacement is set to 0.

First of all, it seems sensible to compare the average displacement for an identical hydric state (saturated soil) in the case of balanced and unbalanced demand. This average displacement is calculated as the average of the head displacements of the four piles. It is expected that the unbalanced case will be more detrimental and we can focus on this later. This is shown in Figure V.27, where it can be seen that for a balanced application the induced displacements cause a slight cumulative settlement over the cycles, whereas the unbalanced case causes uplift, which can be explained by a mechanical load and a soil stiffness high enough for the heat accumulation to cause this overall uplift. In fact, these three points - mechanical load, stiffness (and more generally the behaviour) of the soil and thermal loading - always need to be put into perspective when analysing the behaviour of a group of energy piles. In particular, it appears here that the case where demand is unbalanced is obviously more detrimental (from a mechanical point of view). In the unbalanced case, there is a slight settlement of the header, so we can hope that the stresses induced in it will be lower than those generated by a greater uplift obtained in the unbalanced case.

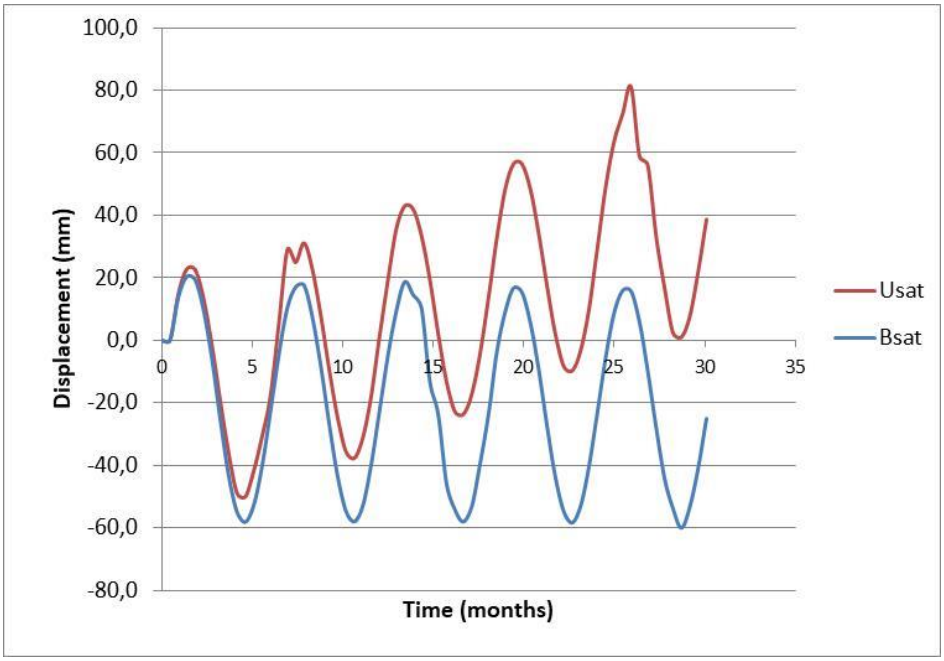

Figure V. 27 - Average displacement of the piles group in saturated soil for Balanced and Unbalanced scenarios

Thus, after comparing the results for different demands, Figure V.28 shows the evolution of the mean displacement of the pile group for the three cases where the demand is considered to be unbalanced (Udry, Usat, Useep) and where only the hydric state of the soil varies. It can be seen that in all three cases there is an accumulation of settlement due to the imbalance in the thermal load. However, there is a slight difference in that, in the case of saturated soil, this displacement seems to increase with each thermal cycle and there seems to be a gap between the Usat case and the others.

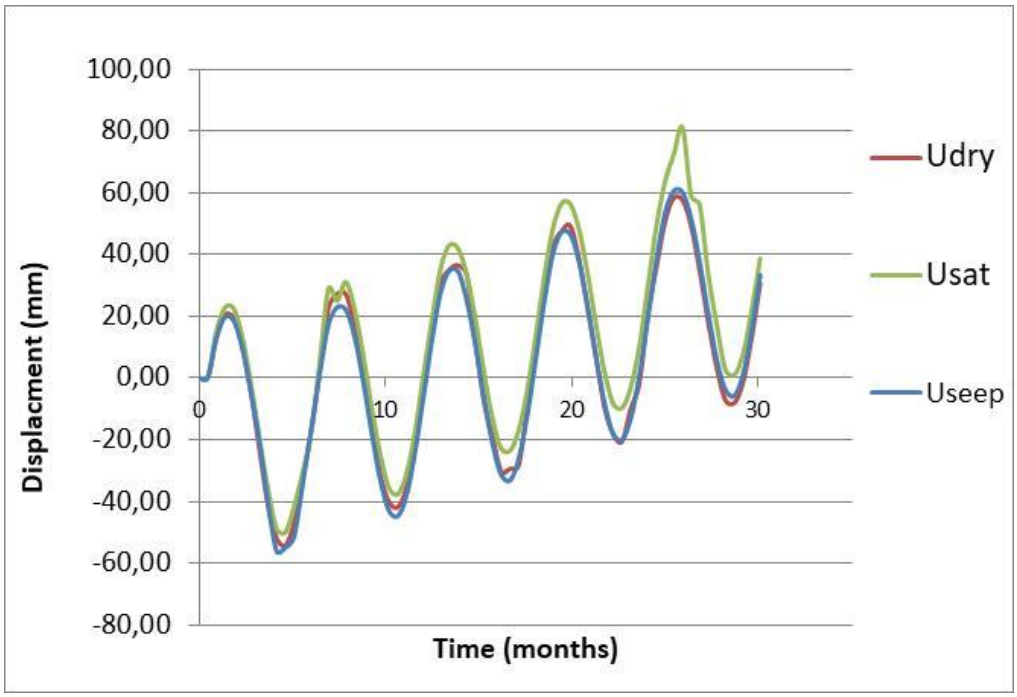

Figure V. 28 - Average displacement of the pile group for the unbalanced demand scenario

The greater accumulation of displacement in the case of saturated soil is explained by the fact that saturation improves the thermal parameters of the soil and therefore favours the accumulation of heat. This accumulation leads to greater thermal expansion and therefore greater displacement. The fact that the mechanical behaviours are similar in the Udry and Useep cases can be explained by heat dissipation, which comes from two different phenomena. In the case of dry sand, its lower density and the poor thermal parameters of the air in the pores of the soil (although the soil is modelled here as a homogeneous and continuous medium, its low thermal conductivity comes from the low thermal conductivity of the air, Cf. chapter I) mean that little heat is diffused and stored. The result is low thermally induced displacements. In the case of a flow, it is not the thermal parameters that prevent the accumulation of heat, but rather the advection that evacuates it progressively.

2.2.3 Head load variations

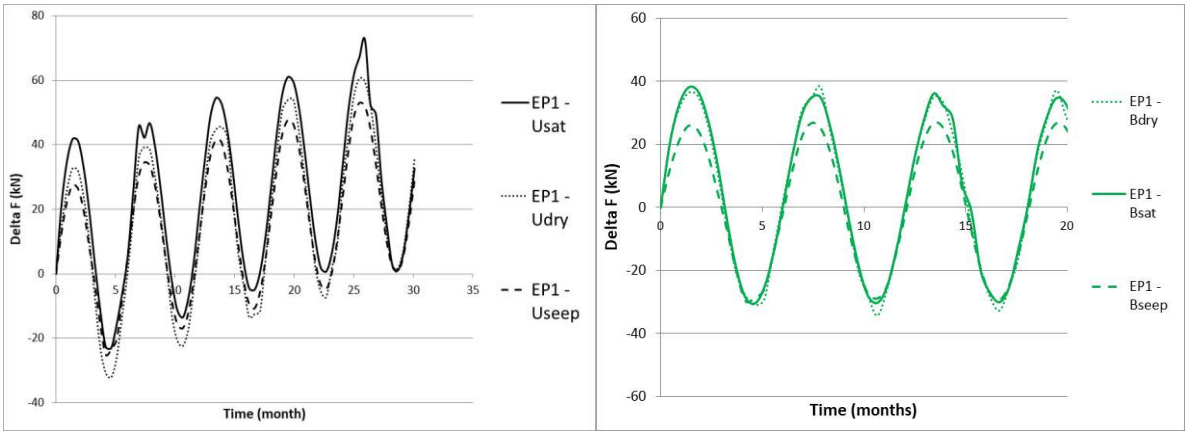

Figure V. 29 - Comparison of the EP1 head load variation for Balanced and Unbalanced scenarios

Figure V.29 shows the load variations at the head of the energy pile (EP1) thermally induced for the case of unbalanced (a) and balanced (b) demand. From an overall point of view, cyclic thermal

loading induces compression at the head of the energy pile. But the important point is to know in which case this compression is greatest. As predicted by the displacements, the figure shows that for unbalanced loading, the scenario that induces the greatest variation in head load is the case of saturated soil with no flow. And among the cases where demand is unbalanced, we again find that the saturated soil case generates the greatest variations in head load. Furthermore, this time we observe that the most favourable case from a mechanical point of view is the one where there is flow.

We know that the flow velocity will have an impact on the plume and therefore on the thermally induced mechanisms. Here, only one flow velocity is taken into account, but it is sufficiently high to consider that the impact is considerable. It should be remembered (see Chapter 1) that the impact of flow velocity on energy efficiency (available calories) is not linear but rather logarithmic (for low velocities, a variation creates a large difference, whereas for high velocities, the same variation does not produce a large difference).

3. Conclusion on the numerical model

The primary objective of this work was to obtain a numerical model that was sufficiently reliable in the sense that the results it provided matched the experimental ones. The link between the experimental and numerical models is that the temperature measured experimentally on the surface of the energetic pile was used as the thermal loading in the numerical model, and the concordance between these two models was achieved by comparing the load variations at the head of the pile. Several parameters were then studied in order to understand their impact on the HTM behaviour of the model. The main points that emerged were as follows:

- The rigidity of the soil and the structure are decisive factors in the mechanical response of the model, and it is therefore necessary to know them well and even to determine them experimentally before any numerical modelling.
- Thermal parameters (thermal conductivity and diffusivity of the soil) have less impact but can vary the mechanical response of the pile group. These parameters are generally well known (at least within a range) or easily found (see Chapter I).
- The coefficient of thermal expansion obviously has a direct impact, since it is according to this coefficient that thermal expansion (and therefore thermally induced stresses) will be generated.
- Finally, the constitutive law of the soil cannot be considered as purely elastic under conventional thermal loading conditions ($\Delta T<10°C$) in this study. Here, a Hardening Soil Model was used, and although the parameters are not always easy to access, this constitutive law makes it possible to approach the experimental observations, in particular the accumulation of settlements.

The second objective was to simulate typical scenarios in terms of demand balance and groundwater conditions in order to make an overall decision on the favourability of certain scenarios. As the results showed, and as expected, the presence of flow dissipates thermal variations and therefore thermally induced mechanical variations. This parameter (presence of flow), like the other parameters presented previously, was assessed from the point of view of its impact on the mechanical response. However, they could have a different impact on energy efficiency. Therefore, for the study of a real project, a more detailed study seems essential to grasp all the aspects (energetic and mechanical).

This model has therefore made it possible to simplify the problem while choosing parameters and constitutive equations that are in line with reality in order to provide certain keys to understanding the studied system. Although, not all the parameters have been mastered, the observed results match the experimental observations and the study of the different scenarios is therefore reliable insofar as the assumptions made do no present major risk.

General conclusion and perspectives

This doctoral investigation was dedicated to the examination of energy piles through laboratory-scale and macrogravity-based model experiments, coupled with numerical modelling.

The first chapter was devoted to a review of the literature, which identified the essential elements required for a thorough understanding of this subject. We recalled that energy piles are part of the energy geostructures, which are geotechnical structures that have a second role as heat exchangers, giving them an energetic and ecological utility. This dual role gives these elements, in interaction with the surrounding soil, a complexity resulting from various physical couplings involving hydrology, thermics and mechanics. Chapter I also outlined the intrinsic functioning of an energy pile, the impact of hydrology on thermics and the influence of thermics on mechanics. The complexity generated by these different couplings means that energy structures, and energy piles in particular, are studied using numerical models and small-scale experiments. The work presented in this dissertation is based on these two approaches, and it was therefore crucial to recall in this first chapter the predominant protocols and models as well as the remarkable results. In particular, numerical models are widely used to study the hydro-thermal coupling that takes place during the operation of an energy structure for energy efficiency purposes. Numerical models are also used to understand the mechanical aspects, but given the complexity of soil behaviour and soil-structure interactions, the mechanical aspect is more frequently studied experimentally on in situ sites or using scale models. It then became apparent that thermal loading, particularly cyclic loading due to the summer/winter operation of the pile, induced stresses and strains depend largely on the characteristics of the soil. Overall, it therefore appears that the thermal response was mainly studied for isolated piles and without taking into account the impact of groundwater flow. The thesis work was therefore carried out with the intention of providing elements of understanding regarding two issues which are the impact of the flow on the mechanical behaviour of a group of energy piles and on the impact of the flow on the energy efficiency of such a system.

Chapter II investigated the energy interactions present within a group of piles. To this end, a reduced model energetic pile was constructed, and the heat exchange between this model pile and a soil consisting of Hostun sand was characterised for different hydric conditions (dry, saturated, flow). To do this, a horizontal flow had to be set up in a mass of model soil. The method used and the characterisation of this flow showed that by maintaining two different hydraulic loads on either side of a soil model, a flow was established in accordance with Darcy's law. Thirdly, as the thermal loading of the model pile induced a variation in the temperature field in the soil, the heat transfer in the soil was characterised for the three hydric states and it can be emphasised that the presence of flow due to an advection phenomenon moves the thermal wave front further or faster depending on the point of view. Finally, the variation in the soil temperature field has an impact on the efficiency of the energy system. To study this phenomenon and see how the flow and the distance between the piles affected it, numerical work was carried out on CESAR-LCPC to simulate in 2D a group of 20 piles exchanging heat with the ground. The energy efficiency was calculated by simulating a heat pump using a Python program. This work once again highlights the importance of flow in maintaining the energy efficiency of a geothermal system. In the case of multi-year simulations with more or less balanced demands, it also emerges that not only the flow but also the nature of the demand can

maintain or even improve the efficiency of the system. Finally, it is clear that the distance between the piles is important and that, if this distance is too small, it can create a cluster effect and harm the system. Just as a group of piles suffers from the cluster effect due to the lack of soil with which to interact, a group of energy piles suffers from the cluster effect due to the lack of soil with which to exchange heat: too little capacity of friction in one case, too little reservoir of heat in the other. This work made it possible to fit a relation onto this interaction (see Equation II.4.14 and Figure II.39) which clearly shows the impact of distance between piles and flow speed on the COP of a heat pump.

Chapter III begins with theoretical work on the hydraulic, thermal and mechanical scaling laws involved in the study of energy piles through reduced scale models and, more specifically, in centrifuge tests. This theoretical work is essential for a proper understanding of the centrifuge tests and the interpretation of the results. The advection phenomenon presented in Chapter II and generated by the flow in the soil combines with the conduction naturally present in any material medium subjected to a thermal gradient. The study of scaling laws has shown that these two phenomena take place over characteristic times that follow the same similarity law ($1/N^2$), thus facilitating the analysis of heat transfer in the soil. From a thermomechanical point of view, the model piles must retain as many of the same properties as possible, particularly in terms of thermal conductivity, thermal expansion and mechanical strength. Secondly, the group of four piles on which the centrifuge tests will be carried out is presented. Particular emphasis is placed on the implementation of the model, the sensors used and data acquisition, as well as the heating system for the energy piles. Finally, in the third part, the flow set-up according to the method presented in Chapter III is characterised more particularly in the model box that will be used in the centrifuge (different dimensions from those used to test the 1g flow). In addition, since macro-gravity causes the flow velocity to be higher, as demonstrated by the scaling laws, a theoretical and numerical study was carried out to show that in a centrifuge, the flow set up does indeed take place in the Darcy domain, thus facilitating the interpretation of the results. The key result is that the two main phenomena through which heat transfer takes place in the ground (advection and conduction) follow the same law of similarity. Thus, the thermal results of reduced model tests are easily interpretable because it is not necessary to know which thermal phenomenon dominates.

Following on logically from Chapter III, Chapter IV presents the three centrifuge test campaigns. During each of the test campaigns, the objective is to evaluate the impact of the flow on the behaviour of the group of piles presented in Chapter III. To do this, the main indicator is the change in pile head load. The first campaign consists of heating one of the four piles in the group. This corresponds to a case where the energy piles are used in summer mode to evacuate heat from the building to the ground. This test enabled us to observe the uplift of the heated pile due to thermal expansion, which induced compression at the head of the energy pile and of the pile located on its diagonal, while the other two piles were subjected to tension at the head. The second test campaign consisted in using the same model but changing the thermal loading. This time, the loading was cyclic and represented a multi-year operation of the pile. During cooling, the opposite behaviour to that observed during heating was logically observed. In addition, the cyclic nature of the thermal loading made it possible to observe the evolution of load variations over the cycles and, in particular, the

accumulation of settlement. The third test campaign focused on imposing cyclic thermal loading, but on two piles aligned along the flow. The heating system meant that one of the two piles was subjected to a greater proportion of the load, and the results were therefore similar to those of the second test campaign. Finally, in all these tests, the flow appeared beneficial in the sense that load variations were less in its presence due to the thermal washing caused by advection.

Finally, Chapter V presents the calibration of a numerical model produced on COMSOL based on the experimental results in a centrifuge. We were then able to show the important role played by the structure's expansion coefficient, but also its rigidity and that of the soil. More generally, the complexity of the thermomechanical behaviour of the soil in interaction with a group of energy piles was highlighted and simulated using an HSM model. Calibration of the model then enabled us to study different scenarios based on cases that can be found in an energy pile project. In this case, it was necessary to consider a balanced energy demand (as much heat as cold over several years) and an unbalanced demand creating a positive thermal anomaly in the ground. For each of these scenarios, three soil water conditions were considered: dry, saturated and with significant runoff (around 1m/day as a prototype). The assumption that the unbalanced, saturated soil case would be the most unfavourable from a mechanical point of view was then confirmed insofar as the variations in head load were greater and the gap widened over time.

Overall findings and recommendations:

- The presence of flow further reduces the load variations at the head of the piles by approximately half

- The inter-pile distance and ground water velocity are two parameters that promote the energetic efficiency of an energy pile group system

- In practice, both from an energetic and mechanical point of view it can be wise to separate thermally active piles by activating every second pile for example

- The load variations and thermally induced deformations observed on both numerically and experimentally remain largely acceptable from a safety point of view and this demonstrates that energy piles can be installed without fear of mechanical problems arising from thermal loading.

- If the thermal diffusivity is low enough (dry sand for example), the thermal anomaly does not impact neighbouring piles over a time scale corresponding to realistic periods of use.

- For higher thermal diffusivity (saturated soil for instance), the other piles might be impacted and the asymmetric loading of the piles is reduced by approximately half.

- In terms of energy, the unbalanced scenario reduces significantly the efficiency of the system (Chapter II).

Perspectives

This thesis presents the innovative technique of flow establishment into ground model in centrifuge. This set-up is promising and could give rise to a large number of new studies, whereas the impact of hydrology was previously neglected in the experiments. These new results will provide an even more accurate characterisation of the behaviour of thermal geostructures.

Similarly, the numerical study of the impact of hydrology on the energy efficiency of an energy structure (through consideration of the evolution of the COP) is a promising approach with results that appear to be extrapolable. The study of more complex configurations (different number of piles, presence of a diaphragm wall, non-constant soil parameters, more accurate simulation of the heat pump, etc.) is undoubtedly a point that needs to be explored further in order to gain a broader view of the energy interactions between energy geostructures. This vision will undoubtedly be essential in the future if these technical solutions continue to develop, since they will have to share the common asset that is ground geothermal energy.

As the various results presented suggest, the scientific questions raised by energy geostructures are numerous and this PhD work could not embrace all of them. After a large state of the art, a focus has then been done on energy piles, leaving alone tunnels and energy diaphragm walls whose operation would present certain singularities in their study. Moreover, the centrifuge tests were carried out for a given type of soil and a given structure and were not generalised to other soils or other structures. In addition, head loads of piles have been considered, but results on the deformations along the entire pile would be a more accurate indicator of the response of the pile group, particularly for the peak load. Similarly, although the method has enabled conclusions to be drawn on certain parametric studies, the numerical models are far from having covered the various possible cases and the results obtained are difficult to extrapolate.

The many parameters involved mean that one energy geostructure project will be different from another, and therefore requires its own analysis. An energy geostructure project modifies the ground's temperature field both temporally and spatially. The ground temperature obviously depends on its nature (type of soil, saturation, density) but is also impacted by the type of energy demand made via the energy structure (more or less important and more or less balanced) and also the hydrology in place. Modification of the temperature field will influence the mechanics of the soil and therefore the mechanical response of the energy geostructure. Similarly, this change in the thermal field will have a direct impact on the energy efficiency of the system. The Figure GC. 1 illustrates these different interactions. It should be remembered that geotechnical structures are geometrically designed from a mechanical point of view only, and that the energy has to fit in the mechanical guidance.

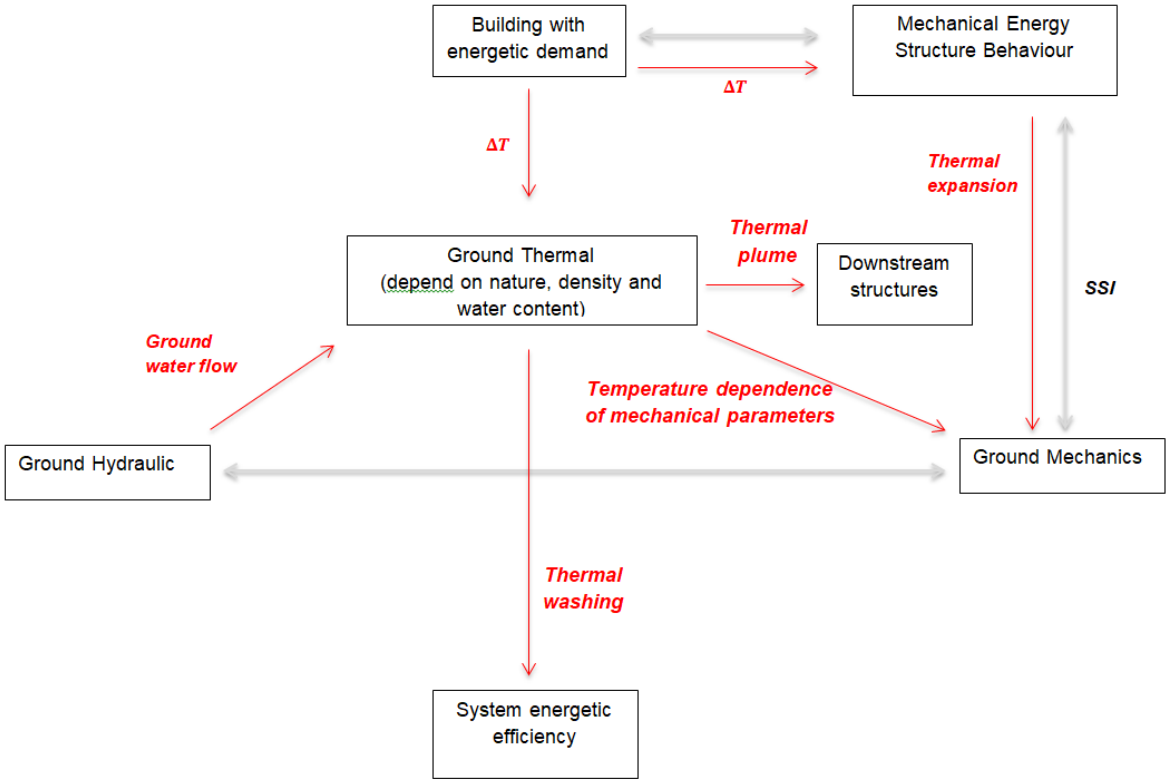

Figure GC. 1 – Interactions between the divers physics phenomenon involved in the HTM behaviour of an energy pile

More generally, the scientific contributions made in the course of this thesis shed light on certain technical points and promote energy geostructures as perfectly viable technical solutions. Of course, other key aspects have to be considered. In particular, one can think of the political choices that need to be made, taking into account the economic, financial and ecological aspects of such solutions. In Austria, these structures developed extensively in the 1980s as a political response to the aftermath of the oil crises, in particular to ensure a degree of energy independence. These issues are perhaps just as topical today.

Articles done during the thesis

In Chapter II, the numerical simulations that allow tackling the impact of ground water flow and inter-pile distance on the heat pump efficiency lead to the redaction of an article for Renewable Energy journal that is under reviewing:

- Badinier, T., Ouzzine, B., de Sauvage, J., Reiffsteck, P. (2023) Evaluation of heat pump efficiency within an energy pile group: effect of heat cluster and water flow and seasonal cycles. Renewable Energy

In Chapter II, the results of the first tests campaign in Centrifuge have been have been published in an IJPMG article:

- *Ouzzine, B., de Sauvage, J., Madabhushi, G., Viggiani, G., Reiffsteck, P., (2022). Centrifuge modelling of an energy pile group with ground water flow. International journal of physical modelling in geotechnics.*

In Chapter III, the different scaling laws related to the physical phenomenon involved in the energy pile behaviour been brought together in a paper for the IJPMG and is under reviewing.

- Ouzzine, B., de Sauvage, J., Hemmati, S., et al., (2023). Scaling laws for the modelling of energy geostructures. *International journal of physical modelling in geotechnics.*

Moreover, this thesis work has enabled me to contribute to two journal articles:

- *Badinier, T., de Sauvage, J., Ouzzine,B., Szymkiewicz,F., Reiffsteck,P., Delerablée,Y., Minatch, C., (2021). Energy Geostructure: experimental and numerical modelling of thermal behaviour and interaction within the city underground. Journal of Envrionmental and Civil Engineering*
- *Badinier, T., Ghandri, I., Grappe, T., Ouzzine, B., de Sauvage, J., (2022). Géostructures thermiques : verrous scientifiques et moyens d'étude. Revue Française de Géotechnique*

And also two conference papers:

- *Ouzzine, B., Badinier,T., de Sauvage, J., Szymkiewicz, F., Reiffsteck, F., (2022). Influence d'un écoulement souterrain sur les performances d'un système de fondation géothermiques. Congrès de la société française de thermique 2022.*
- *Ouzzine, B., Grappe, T., de Sauvage, J., Viggiani, G., Madabhushi, G., Reiffsteck, P., (2022). Centrifuge modelling of an energy pile group within seepage. ICPMG 2022,* 10th International Conference on Physical Modelling in Geotechnics

References

Abuel-Naga, H. M. D. T. B. a. A. B., 2007. Thermally induced volume change and excess pore water pressure of soft Bangkok clay. *Eng. Geol.,* p. 144–154. https://doi.org/10.1016/j.enggeo .2006.10.002.

Abu-Hamdeh, N., 2003. Thermal properties of soils as affected by density and water content.. *Biosystems Engineering,* pp. 97 - 102.

Abu-Hamdeh, N. R. R., 2000. Soil thermal conductivity: effects of density, moisture, salt concentration, and organic matter. *Soil Science Society of America Journal,* pp. 1285 - 1290.

Adam, D. M. R., 2009. Energy from earth-coupled structures, foundations, tunnels and sewers. *Géotechnique 59,* pp. 229-236.

ADEME, 2013. Géothermie sur champs de sondes: Le siège social Immobilier Picardie 80. *Les exemple à suivre,* p. EMR n° 4.

ADEME, 2017. La géothermie très basse énergie, chauffer et racfraichir avec une énergie renouvelable. *Ademe Editions,* p. 45.

AFNOR, 2000. NF P94-110-1, Sols : reconnaissance et essais Essai pressiométrique Ménard.

AFNOR, 2011. *NF EN 15411 Climatiseurs, groupes refroidisseurs de liquide et pompes à chaleur avec compresseur entrainé par moteur électrique pour le chauffage et la réfrigération des locaux.* La Plaine Saint-Denis: s.n.

AFPAC, 2007. *Pompe à Chaleur eau glycolée/eau sur plancher chauffant ou plancher chauffant-rafraichissant à capteurs verticaux.* s.l.:s.n.

Agar, J. C. R. S. J., 1986. Thermal expansion and pore pressure generation in oil sands. *Can Geotech J..*

Akrouch, G., 2014. Energy piles in cooling dominated climates. *Texas A&M University.*

Aljundi, K. V. A. M. J. e. a., 2020. Effects of Temperature, test duration and heat flux in thermal conductivity measurements under transient conditions in dry and fully saturated states. *E3S Web of conferences 195 ,* p. https://doi.org/10.1051/e3sconf/202019504007.

Anon., s.d. https://doc.comsol.com/6.0/doc/com.comsol.help.sme/sme_ug_theory.06.32.html#3677256.

Arairo, W. M. F. A. A. e. a., 2022. Temperature effects on the design parameters of a geothermal pile. *Magazine of Civil Engineering,* p. 116(8) .

ASTM, 2022. *Standard Test Method for Determination of Thermal Conductivity of Soil and Rock by Thermal Needle Probe Procedure,* s.l.: s.n.

Baralis, M. B. M., 2021. Development and testing of a novel geothermal wall system. *International Journal of Energy and Environmental Engineering.*

Barla et al., 2018. City-scale analysis of subsoil thermal conditions due to geothermal exploitation.. *Environmental Geotechnics,* p. https://doi.org/10.1680/jenge.17.00087.

Barla, 2023. Energy tunnels as an opportunity for sustainable development of urban areas. *Tunnelling and underground Space technology.*

Barla, M. & Di Donna, A., 2018. Energy tunnels: concept and design aspects. *Underground space 3,* pp. 268-276.

Barla, M., Di Donna, A. & Perino, A., 2016. Application of energy tunnels to an urban environment. *Geothermics,* pp. 104-113.

Batini, N. R. L. A. C. e. a., 2015. Energy and geotechnical behaviour of energy piles for different design solutions. *Appl Therm Eng.,* pp. 199-213.

Bergstrom, J., 2015. *Mechanics of solid polymers: Theroy and Computanional Modeling.* s.l.:Elsevier.

Borely, C. O. U., 2017. Structure énergétiques : Interaction Pieu-Sol-Strcuture. *Présentation pour la journée technique « Guide Géostructures énergétiques »* .

Bourne-Webb, P. A. B. A. T. e. a., 2009. "Energy pile test at Lambeth College, London: Geotechnical and thermodynamic aspects of pile response to heat cycles.". *Géotechnique,* p. 59 (3): 237–248.

Brandl, H., 2006. Energy foundations and other thermo-active ground structures. *Géotechnique,* pp. 81-122.

BRGM, 2012. *Protocale de test de réponse thermique - Rapport final,* s.l.: s.n.

BRGM, 2023. *L'eau souterraine : une ressource à protéger.* [En ligne].

Campanella, R. M. J., 1968. Influence of temperature variations on soil behavior. *J. Soil. Mech. Found. Div. ASCE 94, No. 3,,* p. 709–734..

Carotenuto, A. M. P. M. N. e. a., 2017. Energy piles for ground source heat pump applications: Comparison of heat transfer performance for different design and operating parameters. *Applied Thermal Engineering,* pp. 1492-1504.

Carslaw, H. J. J., 1959. *Conduction of heat in Solids, 2nd edn.* Oxford, UK: Oxford University Press.

Casarella, A. P. M. T. A. D. D. A., 2021. A critical review of the effect of temperature on clay inter-particle forces and its effect on macroscopic thermal behaviour of clay. *IACMAG ,* pp. 608-615.

Cekerevac, C. L. L., 2004. Experimental study of thermal effects on the mechanical behaviour of clay. *Int. Journal Numer. Anal. Methods Geomech.,* pp. 209-228.

CFMS, S. I. S.-F., 2017. Recommandation pour la conception, le dimensionnement et la mise en oeuvre des géostructures thermiques.

Charlwood, S. P., & Madabhushi, S. P. G. (2021). Experimental modelling of seasonal thermal energy storage within unconfined aquifer (ATES). Canadian Geotechnical Journal, 58(8), 1135-1147.

Comiti, J. e. a., 2000. Experimental characterization of flow regimes in various porous media - limit of Darcy's or creeping flow regime for Newtonian and purely viscous non-Newtonian fluids.. *Chemical Engineering Science 55,* pp. 3057-3061.

Coulibaly, J. R. L. A., 2022. Transient dynamics of the thermally induced deformation of sands. *International Journal for Numerical and Analytical Methods in Geomechanics.*

Darcy, H., 1856. *Les fontaines publiques de la ville de Dijon.* s.l.:Dalmont.

De Vries, D., 1963. Thermal properties of soils.. *Van Wijk, W.R. (ed) Physics of plant environment, Wiley, New York, ,* pp. 210 - 235..

Delerablee, Y., 2019. Intégration thermique et mécanique des géostructures thermiques : de l'échelle

Delerablee, Y. B. S. R. P., 2020. Long-term assessment of thermal sustainability of thermoactive geostructures. *Environmental Geotechnics.*

Di Donna A., F. A. e. L. L., 2016. Experimental investigations of the soil–concrete interface: Physical mechanisms, cyclic mobilization, and behaviour at different temperatures. *." Can. Geotech. J.,* pp. 659–672. https://doi.org/10.1139/cgj-2.

Di Donna et al., 2017. Energy geostructures: a collection of data from real applications. *15th IACMAG proceedings.*

Di Donna et al., 2020. Aspects géotechniques et énergétiques des géostructures thermoactives : application à un cas d'étude réel. *Revue Française de Géotechnique,* pp. 164, 4.

Di Donna, A., 2021. La géothermie, une source d'énergie verte sous nos bâtiments, Encyclopédie de l'Environnement,. *[en ligne ISSN 2555-0950] url : https://www.encyclopedie-environnement.org/sol/geothermie-source-energie-verte-batiments/.*

Di Donna, A. B. M. A. T., 2017. Energy geostructures: Analysis from research and systems installed around the World. *42nd DFI Conference.*

Di Donna, A. F. A. L. L., 2015. Experimental investigations of the soil–concrete interface: physical mechanisms, cyclic mobilization, and behaviour at different temperatures. *Canadian Geotechnical Journal.*

Ding, G. J. J. Z. D., 2008. Modelling study on the impat of deep building foundations on the groundwater system. *Hydrological Processes: An International Journal,* pp. 1857-1865.

Dong, S. e. a., 2019. Thermo-mechanical behavior of energy diaphragm wall: Physical and numerical modelling. *Appl Therm Eng,* pp. 243-251.

Fadejev, J. S. R. K. J. e. a., 2017. A review on energy piles design, sizing and modelling. *Energy ,* pp. 390-407.

Fang, J. K. G., 2022. Group performance of Energy piles under cyclic and variable thermal loading. *Journal of Geotechnical and Geoenvironmental Engineering,* pp. DOI: 10.1061/(ASCE)GT.1943-5606.0002840.

Farivar, A. J. F. L. A., 2023. Influence of pile head restraint on the performance of floating elevated energy pile groups in soft clay. *Computers and Geotechnics.*

Fetter, C., 1994. *Applied Hydrogeology.* 3rd ed éd. New York: Macmillan.

Forchheimer, P., 1901. *Wasserbewegung durch Boden.* Ing. 45, 1782-1788. éd. s.l.:Z. Ver. Deutsch. .

Fourier J., 1822. *Théorie analytique de la chaleur.* s.l.:Firmin Didot, père et fuls.

Freitas Murari, M. T. C. L. F., 2022. Investigation on the thermal response of steel pipe energy piles with different backfill materials.. *Renewable Energy.,* pp. 199:44-61..

Frodl, S. F. J. N. B. T., 2010. Design and construction of the tunnel geothermal system in Jenbach. *Geomechanics and tunnelling.*

Fromentin, A. P. D. L. L. e. a., 1999. Pieux échangeurs: concetption et règles de pré-dimensionnement. *Revue française de génie civil.*

Garnier, J. G. C. S. S. e. a., 2007. Catalogue of scaling laws and similitude questions in geotechnical centrifuge modeling. *IJPMG-International Journal of Physical Modelling in Geotechnics 3,* pp. 01-23.

Gehlin, S. S. J. D., 2015. Effects of ground Heat Exchanger Design Flow Velocities on System Performance of Ground Source Heat Pump Systems in Cold Climates. *ASHRAE Winter Meeting, Chicago, Illinois.*

Giraud, G. N. C., 2021. Actifs fossiles, les nouveaux subprimes ? Quand financer la crise climatique peut mener à la crise financière. *Institut Rousseau.*

Goode, J. M. J., 2015. Centrifuge Modeling on ende-restraint effects in energy foundations. *American Society of Civil Engineers.*

Guenneau, G., 2022. Modélisation des pieux géothermiques à échelle réduite en. *Master 2 Thermique Energétique.*

Haigh, S., 2012. Permeability and stiffness of sand at very low effective stresses. *Géotechnique,* pp. 69-75.

Healy, P. U. V., 1998. Performance and economic feasibility of gournd source heat pumps in cold climate. *International Journal of energy Research,* pp. 857-870.

Hirschberg, S. W. S., 2015. *nergy from the Earth. Deep geothermal as a resource for the future ?.* Zurich: Peter Brugberr eds.

Islam, M. S. F. T. W. H. e. a., 2006. Horizontal U-tube road heating system using tunnel ground heat. *J. of snow Eng. of Japan,* pp. 23-28.

Jannot, Y., 2012. *Transferts thermiques – Ecole des Mines Nancy.* s.l.:s.n.

Joao Diogo, J. B.-W. P. B. F. T., 2020. A novel approach to the evaluation of contact thermal resistance at soil-structure interfaces. *E3S Web of Conferences.*

Khalifa, A. G. J. T. P. R. G., 2000. Scaling laws of water flow in centrifuge models. *Int. Symp. On Physical Modelling and Testing in Environmental Geotechnics.*

Knappett, J. R. C. K. S. e. a., 2011. Small-Scale Modeling of Reinforced Concrete Structural Elements for Use in a Geotechnical Centrifuge. *Amercian Society of Civil Engineers.*

Lagrée, P.-Y., 2010. Coefficient d'échanges, Ailettes. Dans: s.l.:http://www.lmm.jussieu.fr/~lagree/COURS/MECAVENIR/cours5_echange.pdf.

Lahoori, M. R.-P. S. M. F., 2021. Effect of monotonic and cyclic temperature variations on the mechanical behavior of a compacted soil. *Engineering Geology.*

Laloui, L., Cekerevac, C., 2008. Non-isothermal plasticity model for cyclic behaviour of soils. International Journal for Numerical and Analytical Methods in Geomechanics. Volume 32, Issue 5. p.437-460

Laloui, L. N. M. &. V. L., 2006 . Experimental and numerical investigations of the behaviour of a heat exchanger pile. *Int. J. Numer. Anal. Methods Geomech. ,* pp. 30, No. 8, 763–781.

Lee, J. K. Y. K. H. K. J. &. B. G., 2011. Evaluation of methods for predicting thermal conductivity of saturated unfrozen Kaolinite. *Proceedings of the 21st International Offshore and Polar Engineering Conference,* pp. 1193 - 1198 .

Lesquel, E., 2021. Un entrepôt déclare son indépendance énergétique. *Le moniteur.*

Leung, A., 2019. *Innovations in the centrifuge modelling of energy pile behaviour in unsaturated soil.* s.l., s.n.

Leung, A. V. M. M. L. Z. R., 2019. *Innovations in the centrifuge modelling of energy pile behaviour in unsaturated soil.* s.l., s.n.

Lingnau, B. G. J. Y. D. e. a., 1996. Effects of temperature on strength and compressibility of sand bentoninte buffer. *Engineering geology,* pp. 103-115.

Liu, H. X. Y. M. J., 2018. Influence of temperature on the volume change behavior of saturated sand. *Geotech Test J..*

Loveridge, F. C. F., 2016. Thermal performance of thermoactive continuous flight auger piles. *Environmental Geotechnics,* pp. 265-279.

Loveridge, F. P. W., 2012. Pile heat exchangers: thermal behaviour and interactions. *Geotechnical Engineering,* pp. 178-196.

Loveridge, F. P. W., 2014. 2D thermal resistance of pile heat exchangers. *Geotechniques,* pp. 122-135.

Madabhushi, G., 2017. *Centrifuge Modelling for civil Engineers.* s.l.:s.n.

Maghsoodi, S. C. F., 2020. Thermal effects on mechanical behaviour of strcuture interface. *Canadian Geotech. journal,* pp. 32-47.

Magnan, J.-P., 2008. *Mécanique des sols et des roches.* s.l.:s.n.

Makasis, N. N. G. B. A. e. a., 2020. The importance of boundary conditions on the modelling of energy retaining walls. *Comput Geotech.*

Maragna, C. L. F., 2019. A resistive-capacitive model of pile heat exchangers with an application to thermal response tests interpretation. *Renewable Energy,* pp. 891-910.

Marcotte, D. a. P. P., 2008. On the estimation of thermal resistance in borehole thermal conductivity test. *Renewable Energy,* p. 2407–2415 . https://doi.org/10.1016/j.renene.2008.01.021..

McCartney, J. M. K., 2012. Strain Distribution in Full-Scale Energy foundations (DFI younf professor paper competition). *DFI J J Deep Found Insr,* pp. 6:26-38.

Morais, T. T. C. N. L. S. R., 2020 . Effects of seasonal variations on the thermal response of energy piles in an unsaturated Brazilian tropical soil. *Energy and Buildings ,* p. 216:109971..

MTES, 2022. *Chiffres clés de l'énergie 2022,* s.l.: s.n.

Murphy, K. M. J. H. K. F. L., 2014. Thermo-mechanical characterization of a sull-scale energy foundation. In: from Soil behav. Fudam. to Innov.. *Geotech. Eng.,* pp. 617-628.

Nagano, K. K. T. T. S. e. a., 2005. Thermal characteristics of steel foundation piles as ground heat exchangers. *IEA Heat Pump Conference.*

Nakajima, H. H. A. T. J. a. M. M. A., 1998. *Centrifuge Modeling of One-Dimensional.* s.l.:s.n.

Ng., C. Z. C. F. A. e. a., 2016. Centrifuge modelling of displacement and replacement energy piles constructed in saturated sand: a comparative study. *Géotechnique letters,* pp. 34-38.

Ng, 2019. Energy pile group subjected to non-symmetrical cyclic thermal loading in centrifuge. *Géotechnique letters,* pp. 73-177.

Ng, C. S. C. G. A. e. a., 2014. Centrifuge modelling of energy piles subjected to heating and cooling cycles in clay. *Géotechnique Letters,* pp. 310-316.

Ng, C. W. W. e. a., 2019. Scaling effects on the centrifuge modelling of energy piles in saturated sand. *Géotechnique Letters,* pp. 9,1-6.

Nguyen VT, W. N. G. Y. P. J. a. T. A. (., 2020. Long-term thermo-mechanical behaviour of energy piles in clay. *Environmental Geotechnics,* pp. 237-248.

Nguyen, V. T. A. P. J., 2017. Long-term thermo-mechanical behavior of energy pile in dry sand. *Acta Geotech. 12, No. 4,,* pp. 729-737.

Pannike, S. K. M. P. B. R. J. S. V. &. S. H., 2006. Auswirkung hydrogeologischer Kenngrössen auf die Kältefahnen von Erdwärmesondenanlagen in Lockersedimenten. *Grundwasser,* p. 6 – 18. .

Pasten, C. S. J. C., 2014. Thermally induced longterm displacement of thermoactive piles.. *J. Geotech. Geoenviron. Engng 140, No. 5,,* p. 06014003.

Phillips, E., 1869. *Mémoire sur l'équilibre des corps solides élastiques semblables.* s.l.:s.n.

Pilot, G., 1975. Centrifugation de modèles réduits d'ouvrages en terre et de fondations. *Rapport de recherche n°48, Laboratoires des ponts et chaussées.*

Polubarinova-Kochina, 1951. *Advances in Applied Mechanics Advances in Applied Mechanics Volume 2.* s.l.:s.n.

Qi, L. N. G., 2019. Cost effectiveness of Energy Piles in Residential Dwellings in Australia. *Current trends in civil & structural engineering.*

Ramadan, M. I. B. S. D. a. P. R., 2013. Offshore anchor piles under mooring forces: Numerical modeling. *Can. Geotech.,* p. J. 50 (2): 189–199.

Robert Chapuis, M. A., 2003. On the use of the Kozeny-Carman equation to predict the hydraulic conductivity of soils. *Can. Geotech.,* pp. 616-628.

Rotta Loria, A. D. D. A. Z. M., 2022. Stresses and deformations induced by geothermal operations of energy tunnels. *Tunnelling and undreground space technology incorporating trenchless technology research,* p. https://doi.org/10.1016/j.tust.2022.104438.

Salciarini, D. R. F. C. E. e. a., 2013. Thermomechanical Effects Induced by Energy Piles Operation in a Small Piled Raft. *International Journal of Geomechanics,* pp. https://doi.org/10.1061/(ASCE)GM.1943-5622.0000375.

Salim, R., 2016. Extent of capillary rise in sands and silts. *Thesis submitted to the Graduate College in partial fulfilment of the requirements for the degree of Master of Science Geosciences,* Issue Western Michigan University.

Salomone L.H., M. J., 1989. Soil and Rock Classification for the Design of Ground Coupled Heat Pump Systems.

Salomone, L. Y. F. W. H., 1984. The influence of soil type and gradation on the thermal resistivity of soils. *National Bureau of Standards.*

Sani, A. K. S. R. T. C. C. I., 2019. Pipe–pipe thermal interaction in a geothermal energy pile. *Geothermics,* pp. 209-23.

Schanz, T. V. P. B. P., 2000. The hardening soil model: Formulation and verification. *Computational Geotechnics.*

Schneebeli, G., 1966. *Hydraulique souterraine Volume 12 de Collection de la Direction des études et recherches d'électricité de France, ISSN 0399-4198.* Eyrolles éd. s.l.:s.n.

Schoflied, A. N., 1980. Cambridge geotechnical centrifuge operations. *Géotechnique,* pp. 227-268.

SIA, 2005. Utilisation de la chaleur du sol par des ouvrages de fondation et de soutènement en béton. *Guide pour la conseption, la réalisation et la maintenance.*

Staffell, 2012. A review of domestic heat pumps. *Energy and environmental sciences.*

Sterpi, D. T. G. A. A., 2018. Energy performance of ground heat exchangers embedded in diaphragm walls: Field observations and opmization by numerical modelling. *Renewable Energy.*

Stewart, M. M. J., 2013. Centrifuge modeling of Soil-Structure Interaction in energy foundations. *Amercian Society of Civil Engineers.*

Tarnawski, V. M. T. &. L. W., 2009. Assessing the impact of quartz content on the prediction of soil thermal conductivity. *Géotechnique,* pp. 331 - 338.

Tidfors M, S. S., 1989. Temperature effect on preconsolidation pressure. *Geotechnical Testing Journal,* p. 93–97.

Uchaipichat, A. K. N., 2009. Experimental investigation of thermo-hydro-mechanical behaviour of an unsaturated silt. *Géotechnique,* pp. 339-353.

Usowicz, B. L. J. M. W., 2013. Effects of aggregate size on soil thermal conductivity: Comparison of measuredand model-predicted data. *International Journal of Heat and Mass transfer,* pp. 536-541.

Vasilescu, R., 2019. *Design and execution of energu piles : Validation by in-situ and laboratory.* s.l.:ECN.

Vasilescu, R. K. P. D. C., 2020. Retour d'expérience sur le comportement thermomecanique des pieux énergétiques dans des conditions réelles d'exploitation. *Jounrée Nationales de Géotechnique et de Géologie de l'Ingénieur.*

Viggiani, C. M. A. R. G., 2011. *Piles and Pile foundations.* s.l.:PBShop.

Wang, W. R. R. M. J., 2015. Long-term performance of heat exchanger piles. *Acta Geotch,* pp. 10:553-569.

Wang, Y. Z. F. L. F. e. a., 2023. Full-scale in situ experimental study on the bearing capacity of energy piles under varying temperature and multiple mechanical load levels. *Acta Geotechnica,* pp. https://doi.org/10.1007/s11440-023-01904-6.

Yavari, N. T. A. P. J.-M. e. a., 2013. Experimental study on the mechanical behaviour of a heat exchanger pile using physical modelling. *Acta Geotechnica,* pp. 385-398.

Zhao, R. L. A. K. V. D. e. a., 2020. Small-Scale modeling of thermomechanical behavior of reinforced concrete energy piles in soil.. *American Society of Civil Engineers.*

Annexes

Appendix A: *Calculation of the load capacity of the piles group*

Two main approaches to the calculation of the pile capacity: one using fundamental soil properties and another one using in situ tests.

Using the approach using fundamental soil properties, the ultimate bearing capacity Q_s of a single pile with length L and diameter d is written:

$$Q_s = \pi d \int_0^L s dz + \frac{\pi d^2}{4} p - W$$

Where p and s are respectively the unit base resistance and the average skin friction, and W the weight of the pile.

On one hand, in general:

$$p = N_q \sigma_{VL} + N_c c + \frac{N_\gamma \gamma d}{2}$$

But, considering that d/2 << L, the term with N_γ is neglected. Moreover, it is considered that in sandy soils, one can consider to be in drained conditions. Therefore, the cohesion term is zero and the analysis is carried out in terms of effective stress. Thus:

$$p = N_q \sigma_{VL}{}'$$

N_q is the bearing capacity coefficient. Abacuses where the evolution of this coefficient according to the friction angle is plotted for different pile slenderness have been made by Berezantzev (1965). For a pile slenderness of 15 and a friction angle of 35 (considered for Hostun sand), one can read $N_q = 25$.

Then: $p = 25 \times (\gamma - \gamma_w) \times N \times L = 25 \times (15 - 10) \times 50 \times 0.250 = 1562\ kPa$

NB: N is the scaling factor, here the experiment has been run at 50g, then $N = 50$

On the other hand: $s = a + \sigma_h \mu$

Where μ is the pile-soil friction coefficient and a the cohesive term.

Likewise, in sandy soils, one can consider that, at the middle of the pile, the average skin friction is:

$$s_a = K_0 \sigma_v' \tan(\delta) = K_0 \times \frac{(\gamma - \gamma_w) N L}{2} \times \tan(\delta) = (1 - \sin(35)) \times (15 - 10) \times 50 \times \frac{0.250}{2} \times \tan(35)$$
$$= 21.1\ kPa$$

In addition, $W = m_{pile} \times 50 \times g = 0.19 \times 50 \times 9.81 = 93.2\ N$

Finally,

$$Q_s = \pi d s_a L + \frac{\pi d^2}{4} p - W = 0.331 + 0.490 - 0.0932 = 0.73\ kN$$

And with a safety factor of 2, $Q_{s_{FS}} = 0.365\ kN$

The weight of the mass has then to be $\frac{Q_{S_{FS}}}{50g} = \frac{1000}{50 \times 9.81} = 0.73\ kg$

Annexe B: Hardening soil model equations

(Anon., s.d.)

The stiffness moduli for primary loading, denoted by E_{50}, and for unloading/reloading, denoted by E_{ur}, are given by

$$E_{50} = E_{50}^{\mathrm{ref}}\left(\frac{c\cot(\phi) - \sigma_1}{c\cot((\phi) + p_{\mathrm{ref}})}\right)^m$$

and

$$E_{\mathrm{ur}} = E_{\mathrm{ur}}^{\mathrm{ref}}\left(\frac{c\cot(\phi) - \sigma_1}{c\cot(\phi) + p_{\mathrm{ref}}}\right)^m$$

Here E_{50}^{ref} and $E_{\mathrm{ur}}^{\mathrm{ref}}$ are reference stiffness for primary loading and for unloading and reloading at reference pressure, c is the cohesion, ϕ is the angle of internal friction, and m is the stress exponent. The ultimate deviatoric stress q_f and the stress to failure q_a are derived from the Mohr–Coulomb criterion

$$q_{\mathrm{f}} = \frac{2c\cos(\phi) - 2\sigma_1\sin(\phi)}{1 - \sin(\phi)} \quad \text{and} \quad q_{\mathrm{a}} = \frac{q_{\mathrm{f}}}{R_{\mathrm{f}}}$$

where R_f is the failure ratio. Consider the stress invariants $q = \sqrt{3J_2}$ and $p = -I_1/3$, the yield function and plastic potential for the shear hardening cone are given by

$$F_{\mathrm{y}} = q_{\mathrm{a}}\left(\frac{q_{\mathrm{a}}q}{E_{50}(q_{\mathrm{a}} - q)} - \frac{2q}{E_{\mathrm{ur}}} - \gamma_{\mathrm{p}}\right)$$

$$Q_{\mathrm{p}} = \frac{q}{2} - \left(p + \frac{q}{6}\right)\sin(\psi_{\mathrm{m}})$$

where γ_p is the accumulated plastic shear strain and ψ_m is the mobilized dilatancy angle.

	The definition of the shear strain measure γ_p in the original *Hardening Soil* model is not compatible with pure volumetric loading as it does not vanish during pure volumetric straining. Therefore, the shear strain measure γ_p is defined as $\gamma_{\mathrm{p}} = 2\sqrt{J_2(\varepsilon_{\mathrm{pl}})}$, see Nonlinear Elastic Materials.

The yield function for the elliptic cap, and the associated plastic potential, are also defined in terms of stress invariants, and given by

$$F_{\mathrm{y}} = Q_{\mathrm{p}} = \frac{(R_{\mathrm{c}}\bar{q})^2}{p_{\mathrm{c}}} + \frac{p^2}{p_{\mathrm{c}}} - p_{\mathrm{c}}$$

Here, R_c is the ellipse aspect ratio, and it can directly entered, or given as the inverse of the *coefficient of earth pressure at rest* k_0^{nc}

$$R_c = \frac{1}{k_0^{nc}}$$

The coefficient of earth pressure at rest k_0^{nc} is computed from the angle of internal friction ϕ

$$k_0^{nc} = 1 - \sin(\phi)$$

The special deviatoric stress $\bar{q}$ is defined as

$$\bar{q} = \delta\sigma_1 - (\delta - 1)\sigma_2 - \sigma_3$$

where

$$\delta = \frac{3 + \sin(\phi)}{3 - \sin(\phi)}$$

The internal variables p_c and γ_p depend on the volumetric plastic strain $\varepsilon_{pl,vol}$ and the plastic strain invariant $J_2(\varepsilon_{pl})$, and their evolution is defined as

$$\dot{p}_c = -H\dot{\varepsilon}_{pl,vol}$$

$$\dot{\gamma}_p = 2\sqrt{J_2(\dot{\varepsilon}_{pl})}$$

where H is the hardening modulus which depends on the bulk modulus in compression K_c and the bulk modulus in swelling K_s

$$\frac{1}{H} = \frac{1}{K_c} - \frac{1}{K_s} \quad \text{where} \quad K_s = \frac{E_{ur}^{ref}}{3(1 - 2\nu_{ur})}$$

The dilatancy cutoff is implemented by setting the mobilized dilatancy angle ψ_m equal to zero when the void ratio reaches the critical void ratio e_{max}.

Cauchy's stress tensor is then written as

$$\sigma - \sigma_0 = \mathbf{C}:(\varepsilon - \varepsilon_{inel})$$

where $\mathbf{C}$ is a function of the stiffness modulus E_{ur} and Poisson's ratio ν.